Physics Theses & Dissertations   Physics

Summer 2015

Studies of Two-Nucleon Interactions and Few-Body Electromagnetic Structure in Chiral Effective Field Theory

Maria Piarulli
Old Dominion University

STUDIES OF TWO-NUCLEON INTERACTIONS AND FEW-BODY ELECTROMAGNETIC STRUCTURE IN CHIRAL EFFECTIVE FIELD THEORY

by

Maria Piarulli
B.S. February 2006, Univerità degli Studi di Pisa, Italy
M.S. March 2009, Univerità degli Studi di Pisa, Italy
M.S. December 2011, Old Dominion University, Norfolk, Virginia

A Dissertation Submitted to the Faculty of
Old Dominion University in Partial Fulfillment of the
Requirements for the Degree of

DOCTOR OF PHILOSOPHY

PHYSICS

OLD DOMINION UNIVERSITY
August 2015

Approved by:

Rocco Schiavilla (Director)

Craig A. Bayse (Member)

Jozef Dudek (Member)

Sebastian Kuhn (Member)

Leposava Vušković (Member)

ABSTRACT

STUDIES OF TWO-NUCLEON INTERACTIONS AND FEW-BODY ELECTROMAGNETIC STRUCTURE IN CHIRAL EFFECTIVE FIELD THEORY

Maria Piarulli
Old Dominion University, 2015
Director: Dr. Rocco Schiavilla

A coordinate-space nucleon-nucleon potential is constructed in chiral effective field theory (χEFT) retaining pions, nucleons and Δ-isobars as explicit degrees of freedom. The calculation of the potential is carried out by including one- and two-pion-exchange contributions up to next-to-next-to-leading order (N2LO) and contact interactions up to next-to-next-to-next-to-leading order (N3LO). The low-energy constants multiplying these contact interactions are fitted to the 2013 Granada database in the laboratory-energy range 0–300 MeV. Three versions of this chiral potential, corresponding to three different cutoffs, have been developed. The cutoff regularizes the one- and two-pion exchange as well as the contact part of the potential. A study of the electromagnetic structure of $A = 2$ and 3 nuclei is also presented in this thesis. The calculation of the static properties and elastic form factors of the deuteron and trinucleons (^{3}He and ^{3}H) is implemented in momentum-space, by utilizing nuclear wave functions obtained either from chiral or realistic potentials, in combination with chiral electromagnetic operators derived up to one loop. Predictions for these physical observables are in a satisfactory agreement with the experimental data.

ACKNOWLEDGEMENTS

There are many people who have supported and helped me during these years of graduate studies that I would like to thank. I hope I will mention all of them, without forgetting anybody.

Foremost, I would like to express my deepest gratitude to my advisor Prof. Rocco Schiavilla without whom this research would not have been possible. I would like to thank him for his patient guidance, dedication, perseverance, and for providing me with a wonderful atmosphere for doing research. His knowledge, competence and commitment to constantly accomplish excellent results inspired and motivated me.

I am thankful to all of the faculty and staff of the Old Dominion University Physics Department for promoting a stimulating and welcoming academic and social environment. In particular, I would like to thank my committee members, Craig A. Bayse, Jozef Dudek, Sebastian Kuhn, Leposava Vušković for guiding me through all these years. Their advise, suggestions and feedback have been absolutely valuable.

In these years, I spent some of my time at Jefferson Lab: I would like to thank the members of the Theory Group for their hospitality and for the possibility of interacting with them and listening to the talks they organized.

My time at Old Dominion University and Jefferson Lab was made enjoyable in large part due to many friends and colleagues. In particular, I would like to thank Saori Pastore, Valentina Sorbera, and Marco Versace for literally taking care of me when I landed for the first time at the Newport News airport and for their effort to make me feel at home. My deepest gratitude goes to Tosca Ballerini, Federico Casprini, Gianluca De Leo, Mary Goldburg, Trinity Massey, and Paolo Pezzulo for being such excellent friends. I have enjoyed every single moment spent with you all. A special thanks goes to my officemates, both past (Ivan Koralt and Mike Mayer) and current (Alessandro Baroni and Christian Shultz) for providing such a fun work environment that I thought I would never get any work done.

As last, but also as most important, I would like to thank my amazing family and my boyfriend Stetson for the love, support, and constant encouragement I have gotten over these years.

To everybody else who accompanied me in this beautiful PhD journey: THANK YOU!

TABLE OF CONTENTS

LIST OF TABLES

LIST OF FIGURES

1

CHAPTER 1

INTRODUCTION

The force responsible for binding protons and neutrons (nucleons) in atomic nuclei, also known as the nuclear interaction, has been the subject of intense study since the beginning of the twentieth century. Although the existence of nuclei and their constituents has been known for a century, nuclear forces are not understood very well at a fundamental level. The nuclear force is now understood as a residual effect of the even more powerful force, or strong interaction, that binds particles called quarks together, to form the nucleons themselves. This more powerful force is mediated by particles called gluons. Quantum chromodynamics (QCD), established to be the theory describing the interactions between these fundamental degrees of freedom, *i.e.* quarks and gluons, does not have a simple solution in the low-energy regime characteristic of nuclear physics. At these energies the strong coupling constant becomes too large and perturbative techniques cannot be applied to solve low-energy QCD. Therefore a direct derivation of nuclear forces from QCD is not yet available. It is for this reason that the relevant degrees of freedom in which nuclei are described are bound states of QCD, called hadrons, such as nucleons, pions and Δ-isobars.

The recent history of nuclear physics has witnessed the tremendous development of nuclear chiral effective field theory (χEFT), originally proposed by Weinberg in a series of papers in the early 1990's [1]. The (approximate) chiral symmetry exhibited by the underlying theory of QCD in the low-energy regime severely restricts the form of the interactions of pions among themselves and with other particles. In particular, pions couple to baryons, such as nucleons and Δ-isobars, by powers of their momenta Q, and the Lagrangian describing these interactions can be expanded in powers of Q/Λ_χ, where $\Lambda_\chi \sim 1$ GeV specifies the chiral-symmetry breaking scale. As a result, classes of Lagrangians emerge, each characterized by a given power of Q/Λ_χ and each involving a certain number of unknown coefficients, so called low-energy constants (LEC's), which are then determined by fits to experimental data. Thus, χEFT provides, on the one hand, a direct connection between QCD and its symmetries, in particular chiral symmetry, and the strong (and electroweak) interactions in nuclei,

and, on the other hand, a practical calculational scheme amenable, in principle, to systematic improvement. In this sense, it can be justifiably argued to have put low-energy few-nucleon physics on a more fundamental basis.

Within the nuclear χEFT approach, a variety of studies have been carried out in the strong-interaction sector dealing with the derivation of not only two-nucleon potentials (2N or NN) [2–15] but also three-nucleon potentials (3N or NNN) [16–19] and accompanying isospin symmetry-breaking corrections [20–26]. Current chiral 2N (3N) potentials commonly used in calculations include up to next-to-next-to-next-to leading order, N3LO or Q^4 for 2N (next-to-next-to leading order, N2LO or Q^3 for 3N) corrections in the chiral expansions.

In parallel to these developments in the strong interaction sector, much effort has been devoted to electroweak interactions. Among the great advantages of the χEFT framework is the possibility of deriving nuclear electroweak currents consistently with the nuclear interactions. In the present thesis, the focus is on nuclear electromagnetic (EM) charge and current operators. These were originally derived up to one loop level in the heavy baryon formulation of covariant perturbation theory by Park *et al.* [27], where the baryons are treated as heavy static sources, and the perturbative expansion is performed in terms of the involved momenta over the baryon mass. More recently, χEFT EM charge and current operators up to one loop have been derived within two different implementations of time ordered perturbation theory (TOPT): one is by the Jlab-Pisa group (see [28–31]) and the other one is by the Bochum-Bonn group (see [32, 33]). In this study we adopt the formalism developed in Refs. [28–31] in which the NN potential and the electromagnetic charge and current operators are derived by considering suitable transition amplitudes for the processes $NN \longrightarrow NN$ and $NN\gamma \longrightarrow NN$ based on TOPT [34, 35]. These amplitudes are conveniently represented by time-ordered diagrams scaling as a power of Q/Λ_χ. The power of Q/Λ_χ associated with each diagram in the perturbative expansion follow the rule of the so-called power counting. The Hamiltonians employed in the calculation are derived from the chiral Lagrangians formulated in Refs. [4, 36–39], describing the interaction between pions, nucleons and Δ-isobars. Only terms entering the two-nucleon potential and electromagnetic charge and current operators up to one loop are considered here. In particular, integrals entering the loop contributions are ultraviolet divergent and are regularized via dimensional regularization [40, 41]. The divergent part of these loop integrals are absorbed in the redefinition of the relevant

LEC's, which are then fixed by fits to experimental data. However, the resulting renormalized operators have power-law behavior for large momenta, and must be further regularized before they can be used for solving the Schrödinger equation and for the calculation of the current matrix elements. This is accomplished by the inclusion of a cutoff function.

Following the formalism described above, two calculations are presented in this thesis. The first one deals with the construction of a coordinate-space NN potential derived up to next-to-next-to-next-to leading order (N3LO or Q^4) in the chiral expansion, including pions, nucleons and Δ-isobars degrees of freedom. At this order, it consists of the venerable one-pion exchange (OPE) potential at leading order (LO or Q^0), the two pion-exchange (TPE) potential at next-to leading (NLO or Q^2) and next-to-next-to-leading order (N2LO or Q^3), derived from leading and sub-leading pion-nucleon (πN) and pion-nucleon-delta ($\pi N\Delta$) couplings, and also contact interactions entering at LO, NLO, and N3LO. While the OPE and TPE potentials represent the long-range part of the NN interaction, the contact terms, instead, encode the short-range physics, and their strength are specified by unknown LEC's. The inclusion of Δ-isobars in the TPE component of the NN interaction is dictated from phenomenological considerations which explain the important role of Δ isobars in nuclear structure and reactions. An illustration of this are the important role that the Δ plays in πN scattering and the relevance of electroweak N-to-Δ transition currents in radiative and weak capture processes involving few-nucleon systems [42], specifically the radiative captures of thermal neutrons on deuteron and ^{3}He [43, 44] or the weak capture of protons on ^{3}He (the so-called *hep* process) [45].

The necessity to derive a coordinate-space chiral potential, whose natural formulation is in momentum-space, is related to the fact that many computational techniques utilized to calculate properties of nuclei and nuclear matter such as Quantum Monte Carlo (QMC) methods [46] require a local coordinate-space representation of the nuclear interactions. However, available momentum-space chiral potentials have the feature of being strongly non-local meaning that, upon Fourier transformation, they lead to non-local interactions (or **p**-dependent interactions, where $\mathbf{p} \longrightarrow -i\nabla$ is the relative momentum operator) in coordinate-space. The sources of non-localities in χEFT are mostly due to contact interactions that depend not only on the momentum transfer $\mathbf{k} = \mathbf{p}' - \mathbf{p}$ but also on $\mathbf{K} = (\mathbf{p}' + \mathbf{p})/2$ (**p** and $\mathbf{p}'$ are the initial and final relative momenta of the two nucleons), and also to

specific choices of cutoff functions. It is for this reason that we construct a chiral potential as local as possible by minimizing the number of non-localities due to contact interactions and removing those due to the choice of regulator functions. In order to make the short-range part as local as possible, we use Fierz identities [47] to remove terms which in coordinate-space would lead to powers higher than two in the relative momentum operator **p**. However, while this chiral potential is local at N2LO, terms proportional to p^2 still persist at N3LO. To avoid non-localities due to regulators, we choose cutoff functions that depend only on the relative distance between the two nucleons.

The second calculation, presented in this thesis, deals with the study of the electromagnetic structure of $A = 2$ and $A = 3$ nuclei based on χEFT approach. Electromagnetic form factors as well as static properties (such as the deuteron quadrupole moment and charge and magnetic radii for $A = 2$ and 3) of these few-nucleon systems are interesting observables, since they are known to be sensitive to both the nuclear potentials used to generate the wave functions and the nuclear electromagnetic charge and current operators. The goal of this study is to investigate the validity of the χEFT approach to describe the strong interaction dynamics in these few-nucleon systems, and their response to electromagnetic probes.

The calculation of the electromagnetic observables is carried out in momentum-space by utilizing nuclear wave functions derived from both chiral and phenomenological two- and three-body potentials, in combination with the charge and current operators obtained up to one loop within the χEFT formalism. In particular, the $A = 2$ calculations use either the Argonne v_{18} (AV18) [48] or the chiral N3LO potentials [5, 6]. Of course, the $A = 3$ calculations also include three nucleon potentials—the Urbana IX model [49] in combination with the AV18 and the chiral local N2LO potential [16] in combination with the chiral N3LO two-nucleon potentials. One could ask why the calculation of these observables has not been performed with nuclear wave functions obtained from the NN potential developed in this thesis. This would require a program of its momentum-space representation, which has yet to be implemented, and also the inclusion of Δ-isobars in the three-body potential and in the electromagnetic charge and current operators, respectively discussed in Refs. [50] and [28], but not yet revised and implemented.

The thesis is organized into five chapters and six appendices. In Chapter 2, we discuss the formalism used to derive the chiral NN potential and the electromagnetic

charge and current operators, and define the power counting rule adopted here. In Chapter 3, we present the momentum- and coordinate-space representation of the renormalized NN potential up to order Q^4 (N3LO) in the chiral expansion, including Δ-isobar degree of freedom in its TPE component. In that chapter particular attention is given to the solution of the Schrödinger equation and also to fits of the nuclear potential to the pp, np phase shifts, deuteron binding energy, as well as to the NN scattering data. In Chapter 4 the discussion of the chiral charge and current operators up to the order $e\,Q$ is carried out. We present the calculation of the electromagnetic form factors of $A = 2$ and 3 nuclei as well as their static properties. Finally, in Chapter 5 we summarize our conclusions. A number of details are relegated to the Appendices, including: notation and conventions adopted in this work as well as a list of the strong and electromagnetic interaction Hamiltonians required in our calculations (Appendix A); dimensional regularization of loop integrals at order Q^2 (NLO) involving Δ-isobar intermediate states (Appendix B); a list of the relevant expressions for the coordinate-space representation of TPE and contact interaction entering the present NN potential (Appendix C); the calculation of the pp phase shifts and effective range expansion with inclusion of the full electromagnetic potential (Appendix D); the pp and np phase shifts and the various components of the long-range and short-range potentials corresponding to three different cutoff functions (Appendix E); and finally details on the evaluations of the loop contributions to the charge operators (Appendix F).

CHAPTER 2

FORMALISM

This introductory Chapter is devoted to describing the formalism and the scheme adopted to construct the nuclear two-body (NN) potential up to Q^4 in the power counting, discussed in detail in Chapter 3, and the electromagnetic (EM) charge and current operators up to eQ needed for the calculation of the EM form factors of $A = 2$ and 3 nuclei, presented in Chapter 4.

The NN potential and the EM charge and current operators are derived by considering suitable transition amplitude, T and T_γ, for the processes $NN \longrightarrow NN$ and $NN\gamma \longrightarrow NN$ based on time-ordered perturbation theory (TOPT) [34, 35]. In Sec. 2.1, we start off our discussion by introducing the conventional perturbative expansion for the NN scattering amplitude, and we specify the power counting adopted in this work. In Sec. 2.2 we introduce the prescription used to derive the nuclear two-body potential v from the quantum field theory transition amplitude T. Finally, in Sec. 2.3, we generalize the scheme to the inclusion of the EM interaction in the perturbative series, defining in this way the transition amplitude T_γ and the corresponding EM potential v_γ.

2.1 NN SCATTERING AMPLITUDE IN TIME ORDERED PERTURBATION THEORY

In the present work the nuclear two-body potential is obtained by considering pions, nucleons and also Δ-isobar degrees of freedom. In particular, pions are treated relativistically while nucleons and Δ's are considered in the non-relativistic limit.

The conventional perturbative expansion of the NN scattering amplitude T reads as

$$T_{fi} \equiv \langle f|T|i \rangle = \langle f|H_1 \sum_{n=1}^{\infty} \left(\frac{1}{E_i - H_0 + i\eta} H_1 \right)^{n-1} |i \rangle \,, \qquad (1)$$

where $|i\rangle$ and $|f\rangle$ are the initial and final two-nucleon states of energies $E_i = E_f$, respectively, and η is a positive infinitesimal quantity, inserted to give meaning to the reciprocal of $E_i - H_0$.

In Eq. (1) the Hamiltonian H_0 describes free pions, nucleons, and Δ-isobars, while H_1 represents the interactions. The interaction Hamiltonians are derived, in the canonical formalism, from the effective chiral Lagrangian $\mathcal{L}_{\text{eff}}$ of type

$$\mathcal{L}_{\text{eff}} = \mathcal{L}_{\pi\pi} + \mathcal{L}_{\pi N} + \mathcal{L}_{\pi N \Delta} + \mathcal{L}_{NN} \, , \tag{2}$$

where $\mathcal{L}_{\pi\pi}$ [3, 36, 38] deals with the dynamics of pions, and $\mathcal{L}_{\pi N}$ [3, 36, 38] and $\mathcal{L}_{\pi N\Delta}$ [3, 37, 38] describe the interactions between pions and nucleons and between pions, nucleons and Δ-isobars, respectively. The two-nucleon contact Lagrangian $\mathcal{L}_{NN}$ [3, 4, 39] involves only nucleons. This type of Lagrangian features contact terms that encode the short-range dynamics of the nuclear force. Their strengths are specified by the unknown LEC's of the theory which are determined by a fit to the NN data. This point will be more extensively discussed in Chapter 3. In principle, the Lagrangians in Eq. (2) contain an infinite number of interactions compatible with the QCD symmetries. However, they can be organized in powers of Q/Λ_χ, where $Q \ll \Lambda_\chi$ is not only the momentum of the pion, but also the generic value of the momentum of other particles, and $\Lambda_\chi \sim 1\,\text{GeV}$ is the chiral symmetry breaking scale. As a result, the transition amplitude defined in Eq. (1) can be arranged in powers of $(Q/\Lambda_\chi)^m$, where m is determined by power counting. The evaluation of the scattering amplitude in Eq. (1) is performed by introducing complete sets of H_0 eigenstates $|I_n\rangle$ between successive terms of H_1, such that

$$\langle f|T|i\rangle = \langle f|H_1|i\rangle + \sum_{I_1} \langle f|H_1|I_1\rangle \frac{1}{E_i - E_1 + i\eta} \langle I_1|H_1|i\rangle$$
$$+ \sum_{I_1,I_2} \langle f|H_1|I_2\rangle \frac{1}{E_i - E_2 + i\eta} \langle I_2|H_1|I_1\rangle \frac{1}{E_i - E_1 + i\eta} \langle I_1|H_1|i\rangle + \dots , \tag{3}$$

where E_1, E_2,....,E_n are the energies of the intermediate states $|I_1\rangle$, $|I_2\rangle$,...,$|I_n\rangle$, respectively. Terms in this expansion are conveniently represented by time-ordered diagrams. In particular, we can distinguish between reducible and irreducible diagrams. The reducible ones have at least in one of their intermediate states only nucleons (see panel (a) of Fig. 1), while the irreducible ones have at least one pion or Δ-isobar in each intermediate state (see panels (b), (c), (d), (e), and (f) of Fig. 1). A generic (reducible and irreducible) contribution is characterized by a certain number, say n, of vertices represented by $\langle I_j|H_1|I_k\rangle$, each one scaling as $Q^{\alpha_i - \beta_i/2}$ $(i = 1, ..., n)$, where α_i is the Q-power implied by the relevant interaction Hamiltonian and β_i is the number of pions in and/or out of this vertex (this is related to the normalization
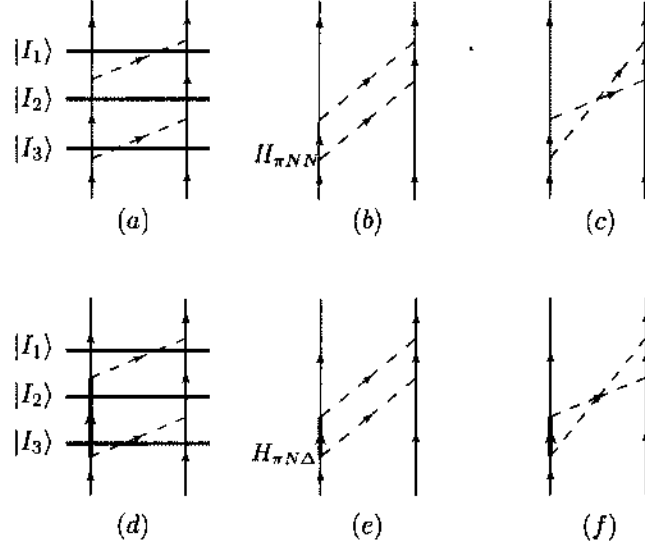
FIG. 1: Examples of time-ordered contributions to the NN transition amplitude involving pions, nucleons and Δ-isobars: panel (a) represents a reducible diagram while panels (b)–(f) represent irreducible diagrams. Pions are denoted by dashed lines, nucleons by solid lines, and Δ-isobars by thick solid lines.

factor in the definition of pion fields as discussed in Appendix A), the corresponding $n-1$ energy denominators $(E_i - E_k + i\eta)^{-1}$ with $k = 1, ..., (n-1)$, and possibly L loops. Out of those $n-1$ energy denominators, n_K will involve only nucleonic kinetic energies (these enter only the reducible diagrams), which scale as Q^{-2}, and the remaining $n - n_K - 1$ will involve, in addition, pion energies ω_π and/or the $N - \Delta$ mass splitting, considered as being of order Q. From now on, we define the $N - \Delta$ mass splitting as $\Delta \equiv m_\Delta - m_N = 293\,\mathrm{MeV}$ where m_N and m_Δ are the nucleon and Δ-isobar masses, respectively. Loops, on the other hand, contribute a factor Q^3 each, since they imply integrations over the intermediate three momenta. Hence, the power counting which determines the chiral index m associated with each contribution in the perturbative series is given by

$$m = \prod_{i=1}^{n} Q^{\alpha_i - \beta_i/2} \times Q^{-(n-n_K-1)} Q^{-2n_K} \times Q^{3L} \ . \tag{4}$$

Clearly, each of the $n - n_K - 1$ denominators can be further expanded as

$$\frac{1}{E_i - E_j + i\eta} \equiv \frac{1}{E_i - E_{I_j} - \Omega + i\eta} = -\frac{1}{\Omega}\Big[1 + \frac{E_i - E_{I_j}}{\Omega} + \frac{(E_i - E_{I_j})^2}{\Omega^2} + ...\Big] , \quad (5)$$

where, depending on the topology of the diagram under consideration, E_{I_j} denotes the kinetic energy of the intermediate two-nucleon, or one-nucleon and one-Δ, or two-Δ states with corresponding $\Omega \equiv \omega_\pi$ (if one or more than one pion are involved), $\Omega \equiv \omega_\pi + \Delta$ (if one or more than one pion and a Δ-isobar are involved) or $\Omega \equiv \Delta$ (if only a Δ-isobar is involved), $\Omega \equiv \omega_\pi + 2\Delta$ (if one or more than one pion and two Δ-isobars are involved) or $\Omega \equiv 2\Delta$ (if only two Δ-isobars are involved). The ratio $(E_i - E_{I_j})/\Omega$ is of order of Q. The first order of the Eq. (5) is called the static limit, which means that the nucleon and Δ-isobar masses $m_N, m_\Delta \to \infty$, while the subsequent terms represent corrections to the static limit, named non-static corrections. In particular, the first non-static correction is suppressed by a factor Q with respect to the static limit. As an example of power counting, consider panel (a) of Fig. 1. Each of the $n = 4$ vertices, implied from the $H_{\pi NN}$ interaction Hamiltonian listed in Appendix A, scales as Q, i.e. $\alpha_i = 1$, and there is only one pion in and/or out of each vertex, i.e. $\beta_i = 1$. The intermediate state $|I_2\rangle$ has only nucleons ($n_K = 1$) while the remaining ($n - n_K - 1 = 2$) intermediate states, $|I_1\rangle$ and $|I_3\rangle$, include also one pion. Obviously $L = 1$ since there is only one loop. Using Eq. (4) we find that diagram (a), in the static limit, scales as Q. All the other diagrams in Fig. 1 scale as Q^2 since $n_K = 0$. Note that the vertices, as implied from the $H_{\pi N\Delta}$ Hamiltonian given in Appendix A, also scale as Q.

Finally, the Q-scaling of the interaction vertices and the considerations above show that the NN transition amplitude T admits the following expansion

$$T_{fi} = T_{fi}^{(0)} + T_{fi}^{(1)} + ... T_{fi}^{(m)} , \quad (6)$$

where $T_{fi}^{(m)} \sim Q^m$.

At this point it is worthwhile making a few considerations. Reducible diagrams are enhanced compared to the irreducible ones by a factor Q for each purely nucleonic intermediate states. In addition, in the static limit, these contributions are infrared-divergent (since reducible diagrams involve nucleonic kinetic energy denominators which lead to infinities for $m_N \to \infty$). According to the prescription proposed by Weinberg [1] the nuclear potentials (and current operators) are given by the irreducible contributions only. Reducible contributions, instead, are generated

by solving the Lippmann-Schwinger (or Schrödinger) equation iteratively with the nuclear potential (and currents) arising from the irreducible amplitudes. However, the omission of reducible contributions from the definition of nuclear operators needs to be dealt with carefulness when the irreducible amplitudes are evaluated under an approximation. For example, if the irreducible amplitude is evaluated under the static limit approximation then the iterative process will generate only part of the reducible amplitude (i.e. the one which includes the approximate static nuclear operators). The reducible part of the amplitude which is not generated by iteration (i.e. the one that is obtained going beyond the static limit) needs to be incorporated order by order—along with the irreducible amplitude— in the definition of the nuclear operators.

2.2 FROM THE AMPLITUDE TO THE POTENTIAL

The perturbative series discussed in Eq. (3) is not very useful to describe nuclei and nuclear properties. For example, it cannot treat bound states. Thus, in nuclear physics a potential v is introduced, and the bound state and continuum two-nucleon states are derived from solutions of the Lippmann-Schwinger (LS) equation (or Schrödinger equation). We then face the problem of how to obtain the potential v entering the LS equation from the field theory amplitude (T-matrix). We solve this problem by requiring that this v, when iterated in the LS equation,

$$v + vG_0v + vG_0vG_0v + \cdots \,, \tag{7}$$

leads to the on-the-energy-shell ($E_i = E_f$) T-matrix in Eq. (6) order by order in the power counting. Here $G_0 = 1/(E_i + E_I + i\eta)$ denotes the free two-nucleon propagator. We assume that the potential v has an expansion like

$$v = v^{(0)} + v^{(1)} + v^{(2)} + v^{(3)} + \dots \,, \tag{8}$$

where $v^{(m)}$ is of order $\mathcal{Q}^m$. By matching the iterated v in Eq. (7) with the field theory

amplitude T order by order in the power counting, we find that

$$v^{(0)} = T^{(0)}, \tag{9}$$

$$v^{(1)} = T^{(1)} - \left[v^{(0)} G_0 v^{(0)} \right], \tag{10}$$

$$v^{(2)} = T^{(2)} - \left[v^{(0)} G_0 v^{(0)} G_0 v^{(0)} \right] - \left[v^{(1)} G_0 v^{(0)} + v^{(0)} G_0 v^{(1)} \right], \tag{11}$$

$$v^{(3)} = T^{(3)} - \left[v^{(0)} G_0 v^{(0)} G_0 v^{(0)} G_0 v^{(0)} \right] - \left[v^{(1)} G_0 v^{(0)} G_0 v^{(0)} + \text{permutations} \right]$$
$$- \left[v^{(1)} G_0 v^{(1)} \right] - \left[v^{(2)} G_0 v^{(0)} + v^{(0)} G_0 v^{(2)} \right], \tag{12}$$

$$\text{.......} \tag{13}$$

where terms like $v^{(l)} G_0 v^{(n)}$ are of order Q^{l+n+1}, since G_0 is of order Q^{-2} and the implicit loop integration brings in a factor Q^3. The relations above allow us to construct $v^{(m)}$ from the field theory amplitude $T^{(m)}$.

The leading-order (LO or Q^0) $v^{(0)}$ term consists of the (static) one-pion-exchange (OPE) potential and two (non-derivative) contact terms arising from the interaction Hamiltonians given in Appendix A in Eq. (276). The term $v^{(1)}$ vanishes [30], since the leading non-static corrections (of order Q) in $T^{(1)}$ to the (static) OPE amplitude add up to zero on-the-energy-shell, while the remaining diagrams in $T^{(1)}$ represent iterations of $v^{(0)}$ whose contributions are exactly canceled by $\left[v^{(0)} G_0 v^{(0)} \right]$ terms. The next-to-leading order (NLO or Q^2) and non-vanishing term $v^{(2)}$ follows from Eq. (11), and contains two-pion-exchange (TPE) and contact terms. These latter contributions involve two gradients of the nucleon fields and arise from the interaction Hamiltonians listed in Appendix A in Eq. (277). The next-to-next-to leading order (N2LO or Q^3) will include sub-leading contributions to the TPE potential obtained from higher order interaction Hamiltonians (see Chapter 3).

2.3 $NN\gamma$ SCATTERING AMPLITUDE

Because of the smallness of the coupling $\sqrt{\alpha}$, where α is the fine structure constant, electromagnetic interactions are treated in first order in the perturbative expansion of Eq. (1). The electromagnetic transition amplitude includes disconnected and connected contributions schematically represented by panels (a) and (b) of Fig. 2, respectively. Disconnected contributions involve a δ-function in the initial and final three-momenta of one of the two particles, for example the contribution of panel (a) is $\propto \delta(\mathbf{p}_2' - \mathbf{p}_2)$ and will be enhanced by a factor Q^3 relative to the connected diagram in panel (b). The power counting is not affected by the
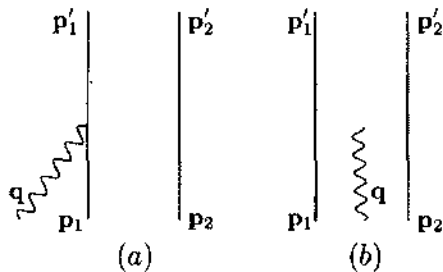
FIG. 2: Schematic representation of the contributions to the $NN\gamma$ transition amplitude: panels (a) and (b) represent the disconnected and connected diagrams, respectively. Solid and wavy lines denote nucleons and photons, respectively.

introduction of the electromagnetic field and follows Eq. (4). The photon's energy denoted as ω_q is considered to be of order Q^2. This scaling follows from the conservation of energy between final and initial states where $E_f - E_i = \Delta E + \omega_q = 0$, ΔE is the difference between the final and initial nucleonic kinetic energies. The electromagnetic interaction Hamiltonians are derived from the $\pi\pi$, $N\pi$ and NN chiral Lagrangians in Eq. (2) by gauging the derivative of nucleon and pion fields, such that

$$\partial_\mu N(\mathbf{r}) \to [\partial_\mu + i\,e\,e_N\,A_\mu(\mathbf{r})]N(\mathbf{r}) , \qquad \partial_\mu \pi_\pm(\mathbf{r}) \to [\partial_\mu \pm i\,e\,A_\mu(\mathbf{r})]\pi_\pm(\mathbf{r}) , \qquad (14)$$

where $e(> 0)$ is the electric charge, $N(\mathbf{r})$ and $\pi_\pm(\mathbf{r})$ are the nucleon and charged pion fields, respectively, defined in Appendix A, $A^\mu \equiv (A^0, \mathbf{A})$ is the external electromagnetic field and $e_N = (1 + \tau_z)/2$ is the isospin project operator. We refer to these Hamiltonians obtained by gauging the derivative couplings as "minimal" Hamiltonians. The LEC's involved here are the same as those entering the strong interaction.

However, gauging the derivatives is not sufficient to generate all the electromagnetic interactions compatible with the symmetries of the underlying theory. In addition, one has to account interactions involving the gauge invariant electromagnetic field tensor $F_{\mu\nu} = \partial_\mu A_\nu - \partial_\nu A_\mu$. The interactions obtained in this way are called "non-minimal" and involve additional LEC's which are not constrained from the strong-interaction sector. In Appendix A we list the electromagnetic interactions involved in the calculation of the charge and current operators up to one loop presented in Chapter 4.

The vertices associated with the electromagnetic interactions scale as $e\,\mathcal{Q}^{\alpha_i}$ and inspection of $\mathcal{Q}$ scaling of the various interaction terms shows that field theory electromagnetic amplitude has the expansion [30]

$$T_\gamma = T_\gamma^{(-3)} + T_\gamma^{(-2)} + T_\gamma^{(-1)}\dots\,, \tag{15}$$

where $T_\gamma^{(m)}$ is of order $e\,\mathcal{Q}^m$. In the context of the LS equation, we assume that the potential v_γ has the same expansion as in Eq. (15), and then determine the potential $v_\gamma^{(m)}$ by matching the field theory amplitude $T_\gamma^{(m)}$ order by order in the power counting obtaining the following relations

$$v_\gamma^{(-3)} = T_\gamma^{(-3)} \tag{16}$$

$$v_\gamma^{(-2)} = T_\gamma^{(-2)} - \left[v_\gamma^{(-3)}\,G_0\,v^{(0)} + v^{(0)}\,G_0\,v_\gamma^{(-3)} \right]\,, \tag{17}$$

$$\begin{aligned} v_\gamma^{(-1)} = {}& T_\gamma^{(-1)} - \left[v_\gamma^{(-3)}\,G_0\,v^{(0)}\,G_0\,v^{(0)} + \text{permutations} \right] \\ & - \left[v_\gamma^{(-2)}\,G_0\,v^{(0)} + v^{(0)}\,G_0\,v_\gamma^{(-2)} \right]\,, \end{aligned} \tag{18}$$

$$\begin{aligned} v_\gamma^{(0)} = {}& T_\gamma^{(0)} - \left[v_\gamma^{(-3)}\,G_0\,v^{(0)}\,G_0\,v^{(0)}\,G_0\,v^{(0)} + \text{permutations} \right] \\ & - \left[v_\gamma^{(-2)}\,G_0\,v^{(0)}\,G_0\,v^{(0)} + \text{permutations} \right] \\ & - \left[v_\gamma^{(-1)}\,G_0\,v^{(0)} + v^{(0)}\,G_0\,v_\gamma^{(-1)} \right] \\ & - \left[v_\gamma^{(-3)}\,G_0\,v^{(2)} + v^{(2)}\,G_0\,v_\gamma^{(-3)} \right]\,, \end{aligned} \tag{19}$$

$$\begin{aligned} v_\gamma^{(1)} = {}& T_\gamma^{(1)} - \left[v_\gamma^{(-3)}\,G_0\,v^{(0)}\,G_0\,v^{(0)}\,G_0\,v^{(0)}\,G_0\,v^{(0)} + \text{permutations} \right] \\ & - \left[v_\gamma^{(-2)}\,G_0\,v^{(0)}\,G_0\,v^{(0)}\,G_0\,v^{(0)} + \text{permutations} \right] \\ & - \left[v_\gamma^{(-1)}\,G_0\,v^{(0)}\,G_0\,v^{(0)} + \text{permutations} \right] \\ & - \left[v_\gamma^{(0)}\,G_0\,v^{(0)} + v^{(0)}\,G_0\,v_\gamma^{(0)} \right] \\ & - \left[v_\gamma^{(-3)}\,G_0\,v^{(2)}\,G_0\,v^{(0)} + \text{permutations} \right] \\ & - \left[v_\gamma^{(-2)}\,G_0\,v^{(2)} + v^{(2)}\,G_0\,v_\gamma^{(-2)} \right] \\ & - \left[v_\gamma^{(-3)}\,G_0\,v^{(3)} + v^{(3)}\,G_0\,v_\gamma^{(-3)} \right]\,, \end{aligned} \tag{20}$$

where $v_\gamma^{(m)} = A^0\rho^{(m)} - \mathbf{A}\cdot\mathbf{j}^{(m)}$ (ρ and $\mathbf{j}$ are the charge and current operators, respectively) and $v^{(m)}$ are the NN potentials constructed in Eq. (9) (12). In Eqs. (16)–(20) the use of the fact that $v^{(1)}$ vanishes has been made. Finally, in the propagator G_0 the intermediate energy E_I may include, in addition to the kinetic energies of the intermediate nucleons, also the photon energy, depending on the specific time ordering being considered.

CHAPTER 3

MINIMALLY NON-LOCAL NUCLEON-NUCLEON POTENTIAL WITH CHIRAL TWO-PION EXCHANGE INCLUDING Δ-ISOBAR

The objectives of the present chapter are twofold. The first is to construct a minimally non-local chiral NN potential up to N3LO (or Q^4) in the power counting including Δ-isobars in its TPE component. The second objective is to determine the LEC's entering the strong Hamiltonians, in particular the contact interactions. These LEC's are determined by fits to the NN scattering data and deuteron binding energy.

In our formalism, where nucleons are treated in a non-relativistic approach, the Hamiltonian describing the two-nucleon system in the center-of-mass (COM) is given by

$$H = -\frac{\nabla^2}{2\mu} + v_{NN} , \tag{21}$$

where the first term represents the non-relativistic kinetic energy of the two nucleons, μ is the reduced mass and v_{NN} is the two-body potential. Natural units $\hbar = c = 1$ are used throughout the present work. The NN potential is written as a sum of a strong interaction component derived with the formalism described in Chapter 2 and denoted as v_{12}, and an electromagnetic interaction component v_{12}^{EM}, including up to terms quadratic in the fine structure constant α (first and second order Coulomb, Darwin-Foldy, vacuum polarization, and magnetic moment interactions). The v_{12}^{EM} component is the same as that adopted in the AV18 potential [48] and will not be discussed further in the present work. The component induced by the strong interaction is conveniently separated into long- and short-range parts, labeled, respectively, v_{12}^L and v_{12}^S. The v_{12}^L part includes the one pion-exchange (OPE) and two pion-exchange (TPE) contributions up to N2LO (or Q^3), illustrated in Fig. 3: panel (b) represents the static OPE contribution at leading order (LO or Q^0); panels (d)–(i) represent the TPE contributions at NLO (or Q^2) without and with Δ-isobars in the
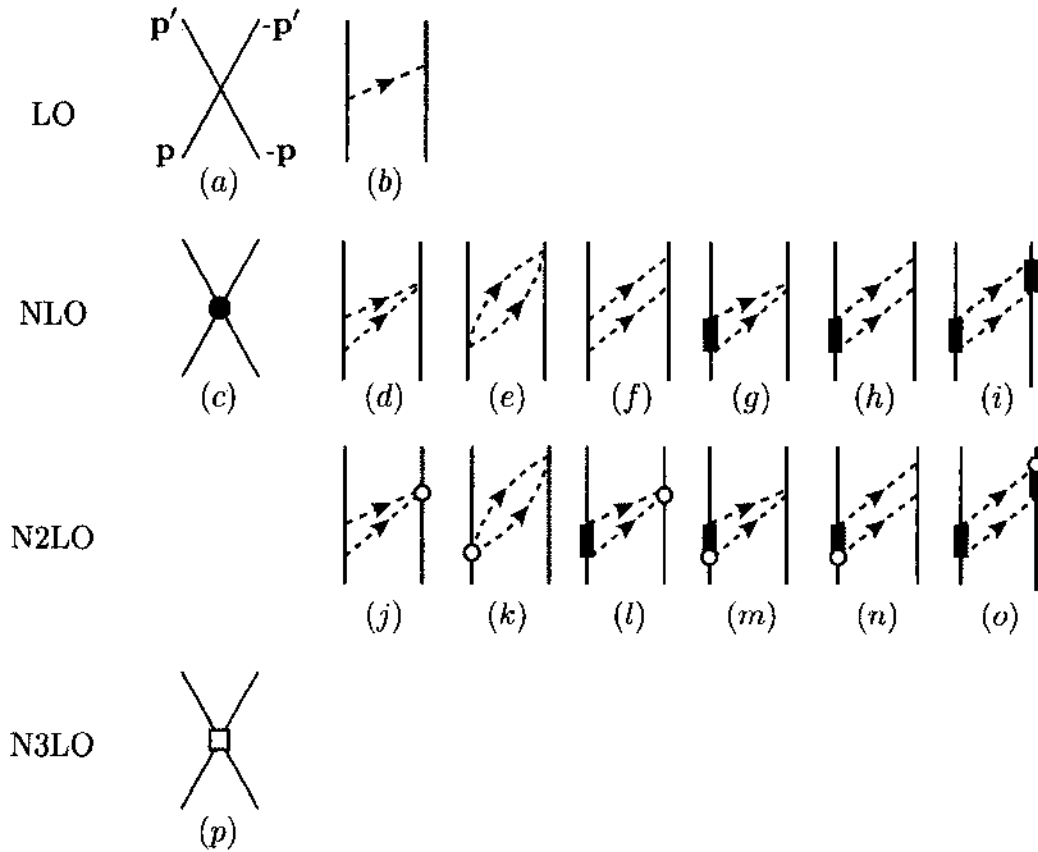
FIG. 3: Diagrams illustrating contributions to the NN potential entering LO (Q^0), panels (a) and (b), NLO (Q^2), panels (c)–(i), N2LO (Q^3), panels (j)–(o), and N3LO (Q^4), panel (p). Nucleons, Δ isobars, and pions are denoted by the solid, thick-solid, and dashed lines, respectively. The filled circle in panel (c) represent the vertex from the contact Hamiltonian containing two gradients of the nucleons' fields. The open circles in panels (j)–(o) denote the $\pi\pi NN$ and $\pi N\Delta$ couplings from the sub-leading Hamiltonians $H^{(2)}_{\pi\pi NN}$ and $H^{(2)}_{\pi N\Delta}$, respectively. The open square in panel (p) represent the vertex from the contact Hamiltonian involving four gradients of the nucleons' fields.

intermediate states; lastly, panels (j)–(o) represent sub-leading TPE contributions at N2LO. The open circles denote the $\pi\pi NN$ and $\pi N\Delta$ couplings from the sub-leading interaction Hamiltonians $H^{(2)}_{\pi\pi NN}$ and $H^{(2)}_{\pi N\Delta}$, respectively, given in Appendix A. Note that in Fig. 3 only one among all possible time-ordered diagrams is displayed. The short-range part, v^S_{12}, consists of nucleon contact interactions up to N3LO. At LO the contact interactions (panel (a) of Fig. 3) have no derivatives of the nucleons' field, while the contact terms at NLO (panel (c) of Fig. 3) and N3LO (panel (p) of Fig. 3), denoted with a solid dot and open square, involve two and four gradients acting on the nucleons' fields, respectively.

The momentum-space representation of the OPE and TPE components as well as the contact interactions is discussed in Sec. 3.1. The evaluation of transition amplitudes associated with those contributions are obtained using the approach outlined in Chapter 2. In Sec. 3.2 we construct the coordinate-space potential v_{12} starting from its momentum-space representation, while in Sec. 3.3 the fitting procedure is laid out. Special attention is given to the discussion of the Schrödinger equation for single and coupled-channels in order to obtain phase shifts. In Sec. 3.4 we report the χ^2 values obtained in the fits as well as the values for the low-energy constants that characterize the potential, and show the calculated phase shifts for the lower partial waves (S, P, and D waves) and compare them to those from recent partial-wave-analyses (PWA's). There, we also provide tables of the pp, np and nn effective range parameters and deuteron properties, including a figure of the deuteron S and D waves. A number of details are relegated to Appendices B–E.

3.1 MOMENTUM-SPACE REPRESENTATION OF THE NN POTENTIAL

In following section, the momentum-space potential is derived in the COM frame where the initial and final relative momenta of the two nucleons are $\mathbf{p}$ and $\mathbf{p}'$, respectively. We also define $\mathbf{k} = \mathbf{p}' - \mathbf{p}$ and $\mathbf{K} = (\mathbf{p}' + \mathbf{p})/2$.

3.1.1 ONE-PION-EXCHANGE

The well-known static one-pion-exchange (OPE) potential illustrated in panel (b)

of Fig. 3 can be written in the form

$$
v^{\pi,\text{LO}}(\mathbf{k}) = \left[v_{\sigma\tau}^{\pi,\text{LO}}(k)\,\boldsymbol{\sigma}_1 \cdot \boldsymbol{\sigma}_2 + v_{t\tau}^{\pi,\text{LO}}(k)\,S_{12}(\mathbf{k}) \right] \boldsymbol{\tau}_1 \cdot \boldsymbol{\tau}_2
$$
$$
+ \left[v_{\sigma T}^{\pi,\text{LO}}(k)\,\boldsymbol{\sigma}_1 \cdot \boldsymbol{\sigma}_2 + v_{tT}^{\pi,\text{LO}}(k)\,S_{12}(\mathbf{k}) \right] T_{12} \,, \tag{22}
$$

where we include the isospin-symmetry breaking induced by the mass difference between charged and neutral pions. The operator $S_{12}(\mathbf{k})$ is defined as

$$
S_{12}(\mathbf{k}) = 3\,\boldsymbol{\sigma}_1 \cdot \mathbf{k}\,\boldsymbol{\sigma}_2 \cdot \mathbf{k} - k^2\,\boldsymbol{\sigma}_1 \cdot \boldsymbol{\sigma}_2 \,, \tag{23}
$$

and

$$
T_{12} = 3\,\tau_{1z}\tau_{2z} - \boldsymbol{\tau}_1 \cdot \boldsymbol{\tau}_2 \,, \tag{24}
$$

is the isotensor operator. The σ_i (τ_i) are the usual spin (isospin) Pauli matrices. The OPE functions, $v_{\sigma\tau}^{\pi,\text{LO}}(k)$, $v_{t\tau}^{\pi,\text{LO}}(k)$, $v_{\sigma T}^{\pi,\text{LO}}(k)$, and $v_{tT}^{\pi,\text{LO}}(k)$ are defined as

$$
v_{\sigma\tau}^{\pi,\text{LO}}(k) = \frac{Y_0(k) + 2\,Y_+(k)}{3} \,, \tag{25}
$$

$$
v_{t\tau}^{\pi,\text{LO}}(k) = \frac{T_0(k) + 2\,T_+(k)}{3} \,, \tag{26}
$$

$$
v_{\sigma T}^{\pi,\text{LO}}(k) = \frac{Y_0(k) - Y_+(k)}{3} \,, \tag{27}
$$

$$
v_{tT}^{\pi,\text{LO}}(k) = \frac{T_0(k) - T_+(k)}{3} \,, \tag{28}
$$

with $Y_\alpha(k)$ and $T_\alpha(k)$ given by

$$
Y_\alpha(k) = -\frac{g_A^2}{3\,F_\pi^2}\frac{k^2}{k^2 + m_{\pi_\alpha}^2} \,, \tag{29}
$$

$$
T_\alpha(k) = -\frac{g_A^2}{3\,F_\pi^2}\frac{1}{k^2 + m_{\pi_\alpha}^2} \,, \tag{30}
$$

where g_A and F_π are respectively the nucleon axial coupling constant and the pion decay amplitude (see Table 1) and m_{π_α} denotes the neutral (m_{π_0}) and charged (m_{π_+}) pion masses. The charged and neutral pion masses as well as other masses and physical constants adopted in this study are given in Table 2.

3.1.2 LOOP CORRECTIONS TO THE NN POTENTIAL

The two-pion-exchange (TPE) loop diagrams entering the NLO and N2LO NN potential can be separated into three categories: i) contributions without Δ-isobar intermediate state (panels (d)–(f) and (j)–(k) of Fig. 3), denoted with the symbol $\Delta\!\!\!/$;

TABLE 1: Values of (fixed) low energy constants (LEC's): g_A and $h_A = 3\,g_A/\sqrt{2}$ are dimensionless, $F_\pi = 2\,f_\pi$ is in MeV, and the remaining LEC's are in GeV^{-1}.

g_A	h_A	F_π	c_1	c_2	c_3	c_4	$b_3 + b_8$
1.29	2.74	184.80	−0.57	−0.25	−0.79	1.33	1.40

TABLE 2: Values of neutral (m_{π_0}) and charged (m_{π_+}) pion masses, neutron (M_n) and proton (M_p) masses, Δ-nucleon (Δ) mass difference, and electron (m_e) mass (all in MeV), and of the (dimensionless) fine structure constant α. Note that $\hbar c$ is taken as 197.32697 MeV fm.

m_{π_0}	m_{π_+}	M_n	M_p	Δ	m_e	α^{-1}
134.9766	139.5702	939.56524	938.27192	293.1	0.510999	137.03599

ii) contributions with one Δ-isobar intermediate states (panels (g)–(h) and (l)–(n) of Fig. 3), labeled as 1Δ, and iii) contributions involving two intermediate Δ's (panels (i) and (o) of Fig. 3), denoted as 2Δ.

3.1.2.1 Δ-LESS LOOP CORRECTIONS

We start the discussion considering diagrams that do not include isobars in the intermediate states. The TPE potential at NLO, given by the sum of diagrams (d)–(f) in Fig. (3), reads as [29]

$$
v^{2\pi,\mathrm{NLO}}(\mathbf{k};\Delta) = \frac{g_A^2}{F_\pi^4}\tau_1\cdot\tau_2\int_l \frac{l^2-k^2}{\omega_+\omega_-(\omega_++\omega_-)} - \frac{1}{8F_\pi^4}\tau_1\cdot\tau_2\int_l \frac{(\omega_+-\omega_-)^2}{\omega_+\omega_-(\omega_++\omega_-)}
$$
$$
- \frac{g_A^4}{2F_\pi^4}\int_l \frac{\omega_+^2+\omega_-^2\omega_+^2+\omega_-^2}{\omega_+^3\omega_-^3(\omega_++\omega_-)}\left[\tau_1\cdot\tau_2(l^2-k^2)^2\right.
$$
$$
\left. +6\,\sigma_1\cdot(\mathbf{k}\times\mathbf{l})\,\sigma_2\cdot(\mathbf{k}\times\mathbf{l})\right]\,,
\tag{31}
$$

where $\omega_\pm = \sqrt{(l\pm k)^2 + 4\,m_\pi^2}$. The first and second term in Eq. (31) represent the irreducible diagrams in panels (d) and (e) of Fig. 3, respectively, denoted as "triangle-like" and "football-like" diagrams. The last term in Eq. (31) is the contribution arising from the TPE "box-like" diagrams in panel (f) of Fig. 3.

The sub-leading (N2LO) TPE potential, given by panels (j)–(k) of Fig. 3, reads

as [9]

$$v^{2\pi,\text{N2LO}}(\mathbf{k};\cancel{\Delta}) \;=\; \frac{3\,g_A^2}{F_\pi^4} \int_l \frac{l^2 - k^2}{\omega_+^2\omega_-^2}[8\,c_1\,m_\pi^2 + c_3\,(l^2 - k^2)]$$
$$-\frac{4\,c_4\,g_A^2}{F_\pi^4}\,\boldsymbol{\tau}_1\cdot\boldsymbol{\tau}_2\int_l\frac{1}{\omega_+^2\omega_-^2}\,[\boldsymbol{\sigma}_1\cdot(\mathbf{k}\times\mathbf{l})\,\boldsymbol{\sigma}_2\cdot(\mathbf{k}\times\mathbf{l})]\;,\qquad(32)$$

where here the whole contribution is due to diagram (j) in Fig. 3. Note that the "football-like" diagrams in panel (k) of Fig. 3 vanishes because the loop integrals involve odd powers of the loop momentum. The parameters c_i are the LEC's entering the second order $\pi\pi NN$ Hamiltonian $H^{(2)}_{\pi\pi NN}$ specified in Appendix A. Their values, as determined by fits to πN scattering data [11], are given in Table 1. Before investigating all the other contributions to the NN potential, a couple of comments are in order. The first is that loop diagrams contain ultraviolet divergencies ($l \to \infty$) which need to be removed by using a proper renormalization scheme. Consider as an example the first term in Eq. (31): it has a quadratic divergence for $l \to \infty$. In order to isolate these divergencies, loop integrals have been regularized with dimensional regularization (DR) [40, 41] as outlined in Appendix B. In DR a generic TPE contribution, $v^{2\pi}(\mathbf{k})$, can be decomposed as

$$v^{2\pi}(\mathbf{k}) = \bar{v}^{2\pi}(\mathbf{k}) + v^{2\pi}(\mathbf{k})_{\text{pol}}\;,\qquad(33)$$

where $\bar{v}^{2\pi}(\mathbf{k})$ represents the renormalized (finite) part and $v^{2\pi}(\mathbf{k})_{\text{pol}}$ polynomial terms in powers of $\mathbf{k}$ which include the removed divergencies. In the present chapter we only give the relevant expressions for the renormalized loop integrals. However, in Appendix B we sketch the renormalization procedure using as examples diagrams (g)–(i) which are presented in the next section.

The renormalized (finite) part of TPE at NLO, given in Eq. (31), reads:

$$\bar{v}^{2\pi,\text{NLO}}(\mathbf{k};\cancel{\Delta}) \;=\; v_\sigma^{2\pi,\text{NLO}}(k;\cancel{\Delta})\,\boldsymbol{\sigma}_1\cdot\boldsymbol{\sigma}_2 + v_t^{2\pi,\text{NLO}}(k;\cancel{\Delta})\,S_{12}(\mathbf{k})$$
$$+v_\tau^{2\pi,\text{NLO}}(k;\cancel{\Delta})\boldsymbol{\tau}_1\cdot\boldsymbol{\tau}_2\;,\qquad(34)$$

where the funtions, $v_\sigma^{2\pi,\text{NLO}}(k;\cancel{\Delta})$, $v_t^{2\pi,\text{NLO}}(k;\cancel{\Delta})$, and $v_\tau^{2\pi,\text{NLO}}(k;\cancel{\Delta})$, are defined as

follow

$$v_\sigma^{2\pi,\text{NLO}}(k;\cancel{\Delta}) = \frac{g_A^4}{4\pi^2 F_\pi^4} G(k) \, k^2 \, , \tag{35}$$

$$v_t^{2\pi,\text{NLO}}(k;\cancel{\Delta}) = -\frac{1}{8\pi^2}\frac{g_A^4}{F_\pi^4} G(k) \, , \tag{36}$$

$$v_\tau^{2\pi,\text{NLO}}(k;\cancel{\Delta}) = \frac{1}{48\pi^2 F_\pi^4} G(k) \left[4m_\pi^2(1 + 4g_A^2 - 5g_A^4) + k^2(1 + 10g_A^2 - 23g_A^4) \right.$$
$$\left. - \frac{48\, g_A^4 m_\pi^4}{4\, m_\pi^2 + k^2} \right] \, , \tag{37}$$

and the logarithmic loop function $G(k)$ is given by

$$G(k) \equiv 2 \, \frac{\sqrt{k^2 + 4\, m_\pi^2}}{k} \ln \frac{\sqrt{k^2 + 4\, m_\pi^2} + k}{2\, m_\pi} \, . \tag{38}$$

The finite part of the TPE at N2LO, represented by Eq. (32), reads:

$$\bar{v}^{2\pi,\text{N2LO}}(\mathbf{k};\cancel{\Delta}) = v_c^{2\pi,\text{N2LO}}(k;\cancel{\Delta}) + [v_{\sigma\tau}^{2\pi,\text{N2LO}}(k;\cancel{\Delta}) \, \boldsymbol{\sigma}_1 \cdot \boldsymbol{\sigma}_2$$
$$+ v_{t\tau}^{2\pi,\text{N2LO}}(k;\cancel{\Delta}) \, S_{12}(\mathbf{k})] \, \boldsymbol{\tau}_1 \cdot \boldsymbol{\tau}_2 \, , \tag{39}$$

where

$$v_c^{2\pi,\text{N2LO}}(k;\cancel{\Delta}) = -\frac{3g_A^2}{\pi F_\pi^4} \left[2m_\pi^2 \left(2c_1 - c_3 \right) - c_3 k^2 \right] \left(2m_\pi^2 + k^2 \right) A(k) \, , \tag{40}$$

$$v_{\sigma\tau}^{2\pi,\text{N2LO}}(k;\cancel{\Delta}) = \frac{g_A^2}{3\pi F_\pi^4} c_4 k^2 \left(4m_\pi^2 + k^2 \right) A(k) \, , \tag{41}$$

$$v_{t\tau}^{2\pi,\text{N2LO}}(k;\cancel{\Delta}) = -\frac{g_A^2}{6\pi F_\pi^4} c_4 \left(4m_\pi^2 + k^2 \right) A(k) \, , \tag{42}$$

and the loop function $A(k)$ is defined as

$$A(k) = \frac{1}{2k} \arctan \frac{k}{2m_\pi} \, . \tag{43}$$

3.1.2.2 Δ-FULL LOOP CORRECTIONS

In what follows, we focus our attention on contributions involving Δ-isobar intermediate states. The TPE loop diagrams involving one and two Δ's intermediate states (panels (g)–(i) of Fig. 3), entering the NLO NN potential, can be written as

$$v^{2\pi,\text{NLO}}(\mathbf{k};\Delta) = v_{\text{tr}}^{2\pi,\text{NLO}}(k;1\Delta) + v_{\text{box}}^{2\pi,\text{NLO}}(\mathbf{k};1\Delta) + v_{\text{box}}^{2\pi,\text{NLO}}(\mathbf{k};2\Delta) \, , \tag{44}$$

where $v_{\text{tr}}^{2\pi,\text{NLO}}(k; 1\Delta)$ refers to contributions associate with "triangle-like" diagrams (panel (g) in Fig. 3) while $v_{\text{box}}^{2\pi,\text{NLO}}(\mathbf{k}; 1\Delta)$ and $v_{\text{box}}^{2\pi,\text{NLO}}(\mathbf{k}; 2\Delta)$ represent the "box-like" contributions with 1Δ and 2Δ's in the intermediate states (panels (h)–(i) in Fig. 3), respectively. The evaluation of the corresponding amplitudes lead to the following expressions

$$v_{\text{tr}}^{2\pi,\text{NLO}}(k; 1\Delta) = \frac{2\,h_A^2}{9\,F_\pi^4}\,\tau_1 \cdot \tau_2 \int_1 \frac{k^2 - l^2}{(\omega_+ + 2\,\Delta)(\omega_- + 2\,\Delta)(\omega_+ + \omega_-)}\,, \tag{45}$$

$$v_{\text{box}}^{2\pi,\text{NLO}}(\mathbf{k}; 1\Delta) = -\frac{g_A^2\,h_A^2}{9\,\Delta\,F_\pi^4} \int_1 \left[\frac{1}{\omega_+^2\,\omega_-^2}\left[3\left(k^2 - l^2\right)^2 + 2\,\tau_1 \cdot \tau_2\,(\boldsymbol{\sigma}_1 \times \mathbf{k}) \cdot \mathbf{l} \right. \right.$$
$$\left. \times (\boldsymbol{\sigma}_2 \times \mathbf{k}) \cdot \mathbf{l}\right] + \frac{2\,\Delta + \omega_+ + \omega_-}{\omega_+\,\omega_-\,(\omega_+ + 2\,\Delta)\,(\omega_- + 2\,\Delta)\,(\omega_+ + \omega_-)}$$
$$\left. \times \left[6\,(\boldsymbol{\sigma}_1 \times \mathbf{k}) \cdot \mathbf{l}\,(\boldsymbol{\sigma}_2 \times \mathbf{k}) \cdot \mathbf{l} + \tau_1 \cdot \tau_2\left(k^2 - l^2\right)^2\right] \right]\,, \tag{46}$$

$$v_{\text{box}}^{2\pi,\text{NLO}}(\mathbf{k}; 2\Delta) = -\frac{h_A^4}{81\,F_\pi^4} \int_1 \left[\frac{\omega_+^2 + \omega_-^2 + \omega_+\omega_- + 4\,\Delta\,(\omega_+ + \omega_- + \Delta)}{\omega_+\,\omega_-\,(\omega_+ + 2\,\Delta)^2\,(\omega_- + 2\,\Delta)^2\,(\omega_+ + \omega_-)} \right.$$
$$\times (6 + \tau_1 \cdot \tau_2)\left[\left(k^2 - l^2\right)^2 + (\boldsymbol{\sigma}_1 \times \mathbf{k}) \cdot \mathbf{l}\,(\boldsymbol{\sigma}_2 \times \mathbf{k}) \cdot \mathbf{l}\right]$$
$$+ \frac{2\,\Delta + \omega_+ + \omega_-}{2\,\Delta\,\omega_+\,\omega_-\,(\omega_+ + 2\,\Delta)\,(\omega_- + 2\,\Delta)\,(\omega_+ + \omega_-)}$$
$$\left. \times (6 - \tau_1 \cdot \tau_2)\left[\left(k^2 - l^2\right)^2 - (\boldsymbol{\sigma}_1 \times \mathbf{k}) \cdot \mathbf{l}\,(\boldsymbol{\sigma}_2 \times \mathbf{k}) \cdot \mathbf{l}\right] \right]\,, \tag{47}$$

where Δ is the Δ-nucleon mass difference and h_A is the N-to-Δ axial coupling constant taken as $h_A = 3\,g_A/\sqrt{2}$ (this value for h_A is take from strong-coupling model [51], and is in good agreement with the value inferred from the empirical Δ-width [52]). The value for Δ is given in Table 2 while the value for h_A is give in Table 1. The DR procedure of these loop diagrams and the relevant integration formulas are discussed in Appendix B. In particular, the finite parts of Eqs. (45)–(46) (47) are summarized in Eqs. (343)–(400)–(423), respectively. Their expressions involve parametric integrals that one can evaluate numerically.

The inclusion of Δ-isobar degree of freedom in the TPE amplitude has also been derived by Kaiser et al. [7, 8, 11]. These authors use covariant perturbation theory (Feynman diagrams) combined with dimensional regularization to evaluate diagrams (g)–(i) as well as those in panels (l)–(o) of Fig. 3. The authors derive compact expressions for the corresponding non-polynomial pieces. The expressions, particularly for diagrams (g)–(i) in Fig. 3, obtained in the two formalisms have been

compared numerically observing an agreement between the results. We list these expressions in what follows. At NLO the TPE potential corresponding to diagrams (g)–(h) in Fig. 3 reads

$$
\begin{aligned}
\bar{v}^{2\pi,\mathrm{NLO}}(\mathbf{k};1\Delta) &= v_c^{2\pi,\mathrm{NLO}}(k;1\Delta) + v_\sigma^{2\pi,\mathrm{NLO}}(k;1\Delta)\,\boldsymbol{\sigma}_1\cdot\boldsymbol{\sigma}_2 \\
&\quad + v_t^{2\pi,\mathrm{NLO}}(k;1\Delta)\,S_{12}(\mathbf{k}) + [v_\tau^{2\pi,\mathrm{NLO}}(k;1\Delta) \\
&\quad + v_{\sigma\tau}^{2\pi,\mathrm{NLO}}(k;1\Delta)\,\boldsymbol{\sigma}_1\cdot\boldsymbol{\sigma}_2 + v_{t\tau}^{2\pi,\mathrm{NLO}}(k;1\Delta)\,S_{12}(\mathbf{k})]\,\boldsymbol{\tau}_1\cdot\boldsymbol{\tau}_2\ ,\quad(48)
\end{aligned}
$$

where the functions depending on the momentum k are given by

$$
v_c^{2\pi,\mathrm{NLO}}(k;1\Delta) = -\frac{g_A^2 h_A^2}{3\pi F_\pi^4 \Delta}\left(2m_\pi^2 + k^2\right)^2 A(k)\ ,
\tag{49}
$$

$$
v_\sigma^{2\pi,\mathrm{NLO}}(k;1\Delta) = \frac{g_A^2 h_A^2}{18\pi^2 F_\pi^4}\,k^2\left[-2L(k) + \left(\omega^2 - 4\Delta^2\right)D(k)\right]\ ,
\tag{50}
$$

$$
v_t^{2\pi,\mathrm{NLO}}(k;1\Delta) = -\frac{g_A^2 h_A^2}{36\pi^2 F_\pi^4}\left[-2L(k) + \left(\omega^2 - 4\Delta^2\right)D(k)\right]\ ,
\tag{51}
$$

$$
\begin{aligned}
v_\tau^{2\pi,\mathrm{NLO}}(k;1\Delta) &= -\frac{h_A^2}{54\pi^2 F_\pi^4}\left[\left(6\Sigma - \omega^2\right)L(k) + 12\Delta^2\Sigma D(k)\right] \\
&\quad - \frac{g_A^2 h_A^2}{54\pi^2 F_\pi^4}\left[\left(12\Delta^2 - 20m_\pi^2 - 11k^2\right)L(k) + 6\Sigma^2 D(k)\right]\ ,\quad(52)
\end{aligned}
$$

$$
v_{\sigma\tau}^{2\pi,\mathrm{NLO}}(k;1\Delta) = \frac{g_A^2 h_A^2}{54\pi F_\pi^4 \Delta}\,k^2\omega^2 A(k)\ ,
\tag{53}
$$

$$
v_{t\tau}^{2\pi,\mathrm{NLO}}(k;1\Delta) = -\frac{g_A^2 h_A^2}{108\pi F_\pi^4 \Delta}\omega^2 A(k)\ .
\tag{54}
$$

The quantities Σ, $L(k)$, $A(k)$, $D(k)$, and $H(k)$ are defined as

$$
\Sigma = 2m_\pi^2 + k^2 - 2\Delta^2\ ,\qquad \omega = \sqrt{k^2 + 4m_\pi^2}\ ,
\tag{55}
$$

$$
L(k) = \frac{\omega}{k}\ln\frac{\omega + k}{2m_\pi}\ ,
\tag{56}
$$

$$
A(k) = \frac{1}{2k}\arctan\frac{k}{2m_\pi}\ ,
\tag{57}
$$

$$
D(k) = \frac{1}{\Delta}\int_{2m_\pi}^\infty \frac{d\mu}{\mu^2 + k^2}\arctan\frac{\sqrt{\mu^2 - 4m_\pi^2}}{2\Delta}\ ,
\tag{58}
$$

$$
H(k) = \frac{2\Sigma}{\omega^2 - 4\Delta^2}\left[L(k) - L(2\sqrt{\Delta^2 - m_\pi^2})\right]\ .
\tag{59}
$$

The TPE "box-like" contribution corresponding to diagram (i) in Fig. 3 reads as

$$
\begin{aligned}
\bar{v}^{2\pi,\mathrm{NLO}}(\mathbf{k};2\Delta) &= v_c^{2\pi,\mathrm{NLO}}(k;2\Delta) + v_\sigma^{2\pi,\mathrm{NLO}}(k;2\Delta)\,\boldsymbol{\sigma}_1\cdot\boldsymbol{\sigma}_2 \\
&\quad + v_t^{2\pi,\mathrm{NLO}}(k;2\Delta)\,S_{12}(\mathbf{k}) + [v_\tau^{2\pi,\mathrm{NLO}}(k;2\Delta) \\
&\quad + v_{\sigma\tau}^{2\pi,\mathrm{NLO}}(k;2\Delta)\,\boldsymbol{\sigma}_1\cdot\boldsymbol{\sigma}_2 + v_{t\tau}^{2\pi,\mathrm{NLO}}(k;2\Delta)\,S_{12}(\mathbf{k})]\,\boldsymbol{\tau}_1\cdot\boldsymbol{\tau}_2\ ,\quad(60)
\end{aligned}
$$

where

$$v_c^{2\pi,\text{NLO}}(k;2\Delta) = -\frac{h_A^4}{27\,\pi^2\,F_\pi^4}\left[-4\Delta^2 L(k) + \Sigma\left[H(k) + \left(\Sigma + 8\Delta^2\right)D(k)\right]\right] ,\quad(61)$$

$$v_\sigma^{2\pi,\text{NLO}}(k;2\Delta) = \frac{h_A^4}{324\,\pi^2\,F_\pi^4}k^2\left[6L(k) + \left(12\Delta^2 - \omega^2\right)D(k)\right] ,\quad(62)$$

$$v_t^{2\pi,\text{NLO}}(k;2\Delta) = -\frac{h_A^4}{648\,\pi^2\,F_\pi^4}\left[6L(k) + \left(12\Delta^2 - \omega^2\right)D(k)\right] ,\quad(63)$$

$$v_\tau^{2\pi,\text{NLO}}(k;2\Delta) = -\frac{h_A^4}{486\,\pi^2\,F_\pi^4}\left[\left(12\Sigma - \omega^2\right)L(k) + 3\Sigma[H(k)\right.$$
$$\left. + \left(8\Delta^2 - \Sigma\right)D(k)\right] ,\quad(64)$$

$$v_{\sigma\tau}^{2\pi,\text{NLO}}(k;2\Delta) = \frac{h_A^4}{1944\,\pi^2\,F_\pi^4}k^2\left[2L(k) + \left(4\Delta^2 + \omega^2\right)D(k)\right] ,\quad(65)$$

$$v_{t\tau}^{2\pi,\text{NLO}}(k;2\Delta) = -\frac{h_A^4}{3888\,\pi^2\,F_\pi^4}\left[2L(k) + \left(4\Delta^2 + \omega^2\right)D(k)\right] .\quad(66)$$

Moving on to the loop corrections at N2LO, the contribution corresponding to diagrams (l)–(n) in Fig. 3 is

$$\begin{aligned}\bar{v}^{2\pi,\text{N2LO}}(\mathbf{k};1\Delta) = &\ v_c^{2\pi,\text{N2LO}}(k;1\Delta) + v_\sigma^{2\pi,\text{N2LO}}(k;1\Delta)\,\boldsymbol{\sigma}_1\cdot\boldsymbol{\sigma}_2\\ &+ v_t^{2\pi,\text{N2LO}}(k;1\Delta)\,S_{12}(\mathbf{k}) + [v_\tau^{2\pi,\text{N2LO}}(k;1\Delta)\\ &+ v_{\sigma\tau}^{2\pi,\text{N2LO}}(k;1\Delta)\,\boldsymbol{\sigma}_1\cdot\boldsymbol{\sigma}_2 + v_{t\tau}^{2\pi,\text{N2LO}}(k;1\Delta)\,S_{12}(\mathbf{k})]\,\boldsymbol{\tau}_1\cdot\boldsymbol{\tau}_2 ,\end{aligned}$$
$$(67)$$

where

$$\begin{aligned}v_c^{2\pi,\text{N2LO}}(k;1\Delta) = &-\frac{2h_A^2\Delta}{9\pi^2 F_\pi^4}\left[6\Sigma\left[4c_1 m_\pi^2 - 2c_2\Delta^2 - c_3\left(2\Delta^2 + \Sigma\right)\right]D(k)\right.\\ &\left. + \left[-24c_1 m_\pi^2 + c_2(\omega^2 - 6\Sigma) + 6c_3(2\Delta^2 + \Sigma)\right]L(k)\right] ,\quad(68)\end{aligned}$$

$$v_\sigma^{2\pi,\text{N2LO}}(k;1\Delta) = \frac{2(b_3 + b_8)g_A^2 h_A\Delta}{9\pi^2 F_\pi^4}k^2\left[(\omega^2 - 4\Delta^2)D(k) - 2L(k)\right] ,\quad(69)$$

$$v_t^{2\pi,\text{N2LO}}(k;1\Delta) = -\frac{(b_3 + b_8)g_A^2 h_A\Delta}{9\pi^2 F_\pi^4}\left[(\omega^2 - 4\Delta^2)D(k) - 2L(k)\right] ,\quad(70)$$

$$\begin{aligned}v_\tau^{2\pi,\text{N2LO}}(k;1\Delta) = &-\frac{2(b_3 + b_8)h_A\Delta}{27\pi^2 F_\pi^4}\left[12\Delta^2\Sigma D(k) + (-\omega^2 + 6\Sigma)L(k)\right]\\ &-\frac{2(b_3 + b_8)g_A^2 h_A\Delta}{27\pi^2 F_\pi^4}\left[6\Sigma^2 D(k) + \left[\omega^2 - 12(\Delta^2 + \Sigma)\right]\right] ,\quad(71)\end{aligned}$$

$$v_{\sigma\tau}^{2\pi,\text{N2LO}}(k;1\Delta) = \frac{c_4 h_A^2\Delta}{27\pi^2 F_\pi^4}k^2\left[(\omega^2 - 4\Delta^2)D(k) - 2L(k)\right] ,\quad(72)$$

$$v_{t\tau}^{2\pi,\text{N2LO}}(k;1\Delta) = -\frac{c_4 h_A^2\Delta}{54\pi^2 F_\pi^4}\left[(\omega^2 - 4\Delta^2)D(k) - 2L(k)\right] .\quad(73)$$

The expressions above depend also on the new combination of LEC's $(b_3 + b_8)$ arising from the second order Hamiltonian $H^{(2)}_{\pi N\Delta}$ given in Appendix A. The value of this combination of LEC's is also taken by fits to πN scattering data [11], and is given in Table 1.

Finally, the TPE contribution corresponding to diagram (o) in Fig. 3 reads

$$
\begin{aligned}
\bar{v}^{2\pi,\text{N2LO}}(\mathbf{k};2\Delta) &= v^{2\pi,\text{N2LO}}_c(k;2\Delta) + v^{2\pi,\text{N2LO}}_\sigma(k;2\Delta)\,\boldsymbol{\sigma}_1 \cdot \boldsymbol{\sigma}_2 \\
&\quad + v^{2\pi,\text{N2LO}}_t(k;2\Delta)\,S_{12}(\mathbf{k}) + [v^{2\pi,\text{N2LO}}_\tau(k;2\Delta) \\
&\quad + v^{2\pi,\text{N2LO}}_{\sigma\tau}(k;2\Delta)\,\boldsymbol{\sigma}_1 \cdot \boldsymbol{\sigma}_2 + v^{2\pi,\text{N2LO}}_{t\tau}(k;2\Delta)\,S_{12}(\mathbf{k})]\,\boldsymbol{\tau}_1 \cdot \boldsymbol{\tau}_2 ,
\end{aligned}
$$
(74)

where

$$
\begin{aligned}
v^{2\pi,\text{N2LO}}_c(k;2\Delta) &= -\frac{8(b_3+b_8)h_A^3\Delta}{81\pi^2 F_\pi^4}\Big[3\,(8\Delta^2 - \Sigma)\,\Sigma\,D(k) + \\
&\quad 3\Sigma\,H(k) + (-\omega^2 + 12\Sigma)\,L(k)\Big] ,
\end{aligned}
$$
(75)

$$
v^{2\pi,\text{N2LO}}_\sigma(k;2\Delta) = \frac{2(b_3+b_8)h_A^3\Delta}{81\pi^2 F_\pi^4}k^2\Big[(-\omega^2 + 12\Delta^2)D(k) + 6L(k)\Big] ,
$$
(76)

$$
v^{2\pi,\text{N2LO}}_t(k;2\Delta) = -\frac{(b_3+b_8)h_A^3\Delta}{81\pi^2 F_\pi^4}\Big[(-\omega^2 + 12\Delta^2)D(k) + 6L(k)\Big] ,
$$
(77)

$$
\begin{aligned}
v^{2\pi,\text{N2LO}}_\tau(k;2\Delta) &= -\frac{4(b_3+b_8)h_A^3\Delta}{243\pi^2 F_\pi^4}\Big[3\,(8\Delta^2 - \Sigma)\,\Sigma\,D(k) + \\
&\quad 3\Sigma\,H(k) + (-\omega^2 + 12\Sigma)L(k)\Big] ,
\end{aligned}
$$
(78)

$$
v^{2\pi,\text{N2LO}}_{\sigma\tau}(k;2\Delta) = \frac{(b_3+b_8)h_A^3\Delta}{243\pi^2 F_\pi^4}k^2\Big[(-\omega^2 + 12\Delta^2)D(k) + 6L(k)\Big] ,
$$
(79)

$$
v^{2\pi,\text{N2LO}}_{t\tau}(k;2\Delta) = -\frac{(b_3+b_8)h_A^3\Delta}{486\pi^2 F_\pi^4}\Big[(-\omega^2 + 12\Delta^2)D(k) + 6L(k)\Big] .
$$
(80)

In conclusion, the long-range part of the NN potential is defined as the sum of the OPE and renormalized TPE without and with Δ-isobars:

$$
\begin{aligned}
v^{\text{L}}_{12}(\mathbf{k}) &\equiv v^{\pi,\text{LO}}(\mathbf{k}) + \bar{v}^{2\pi,\text{NLO}}(\mathbf{k};0\Delta) + \bar{v}^{2\pi,\text{N2LO}}(\mathbf{k};0\Delta) + \bar{v}^{2\pi,\text{NLO}}(\mathbf{k};1\Delta) \\
&\quad + \bar{v}^{2\pi,\text{NLO}}(\mathbf{k};2\Delta) + \bar{v}^{2\pi,\text{N2LO}}(\mathbf{k};1\Delta) + \bar{v}^{2\pi,\text{N2LO}}(\mathbf{k};2\Delta) ,
\end{aligned}
$$
(81)

which can be written, in a compact way, as

$$
v^{\text{L}}_{12}(\mathbf{k}) = \sum_{l=1}^{6} v^l_{\text{L}}(k)\,O^l_{12}(\mathbf{k}) + v^{\pi,\text{LO}}_{\sigma T}(k)\,O^{\sigma T}_{12} + v^{\pi,\text{LO}}_{tT}(k)\,O^{tT}_{12}(\mathbf{k}) ,
$$
(82)

where

$$O_{12}^{i=1,\dots,6}(\mathbf{k}) = [1\,,\,\boldsymbol{\sigma}_1\cdot\boldsymbol{\sigma}_2\,,S_{12}(\mathbf{k})]\otimes[1\,,\,\boldsymbol{\tau}_1\cdot\boldsymbol{\tau}_2]\,, \tag{83}$$

$$O_{12}^{\sigma T} = \boldsymbol{\sigma}_1\cdot\boldsymbol{\sigma}_2\,T_{12}\,, \tag{84}$$

$$O_{12}^{tT}(\mathbf{k}) = S_{12}(\mathbf{k})\,T_{12}\,, \tag{85}$$

and the functions $v_{\rm L}^i(k)$ are given by

$$v_{\rm L}^c(k) = v_c^{2\pi,\rm N2LO}(k;\slashed{\Delta}) + v_c^{2\pi,\rm NLO}(k;1\Delta) + v_c^{2\pi,\rm NLO}(k;2\Delta) + v_c^{2\pi,\rm N2LO}(k;1\Delta)$$
$$+ v_c^{2\pi,\rm N2LO}(k;2\Delta)\,, \tag{86}$$

$$v_{\rm L}^\sigma(k) = v_\sigma^{2\pi,\rm NLO}(k;\slashed{\Delta}) + v_\sigma^{2\pi,\rm NLO}(k;1\Delta) + v_\sigma^{2\pi,\rm NLO}(k;2\Delta) + v_\sigma^{2\pi,\rm N2LO}(k;1\Delta)$$
$$+ v_\sigma^{2\pi,\rm N2LO}(k;2\Delta)\,, \tag{87}$$

$$v_{\rm L}^t(k) = v_t^{2\pi,\rm NLO}(k;\slashed{\Delta}) + v_t^{2\pi,\rm NLO}(k;1\Delta) + v_t^{2\pi,\rm NLO}(k;2\Delta) + v_t^{2\pi,\rm N2LO}(k;1\Delta)$$
$$+ v_t^{2\pi,\rm N2LO}(k;2\Delta)\,, \tag{88}$$

$$v_{\rm L}^\tau(k) = v_\tau^{2\pi,\rm NLO}(k;\slashed{\Delta}) + v_\tau^{2\pi,\rm NLO}(k;1\Delta) + v_\tau^{2\pi,\rm NLO}(k;2\Delta) + v_\tau^{2\pi,\rm N2LO}(k;1\Delta)$$
$$+ v_\tau^{2\pi,\rm N2LO}(k;2\Delta)\,, \tag{89}$$

$$v_{\rm L}^{\sigma\tau}(k) = v_{\sigma\tau}^{\pi,\rm LO}(k) + v_{\sigma\tau}^{2\pi,\rm N2LO}(k;\slashed{\Delta}) + v_{\sigma\tau}^{2\pi,\rm NLO}(k;1\Delta) + v_{\sigma\tau}^{2\pi,\rm NLO}(k;2\Delta)$$
$$+ v_{\sigma\tau}^{2\pi,\rm N2LO}(k;1\Delta) + v_{\sigma\tau}^{2\pi,\rm N2LO}(k;2\Delta)\,, \tag{90}$$

$$v_{\rm L}^{t\tau}(k) = v_{t\tau}^{\pi,\rm LO}(k) + v_{t\tau}^{2\pi,\rm N2LO}(k;\slashed{\Delta}) + v_{t\tau}^{2\pi,\rm NLO}(k;1\Delta) + v_{t\tau}^{2\pi,\rm NLO}(k;2\Delta)$$
$$+ v_{t\tau}^{2\pi,\rm N2LO}(k;1\Delta) + v_{t\tau}^{2\pi,\rm N2LO}(k;2\Delta)\,. \tag{91}$$

It is worthwhile noting that terms proportional to T_{12} (retained in the OPE potential at LO) are ignored in the NLO and N2LO loop corrections which are evaluated with the average pion mass $m_\pi = (2\,m_{\pi^+} + m_{\pi^0})/3$. Additional loop contributions, such as those represented in Fig. 4, are not considered here, since they only lead to renormalization of OPE (and also contact interactions) [4, 53]. In other words, these contributions do not affect the renormalized potential since they are absorbed in the definition of the LEC's g_A, C_S and C_T (the constants C_S and C_T will be introduced in the next subsection). Furthermore additional one-loop as well as two-loop TPE and three-pion exchange contributions at order Q^4 are not considered in the present work. These contributions have been neglected, since they are known to be small (see, for example, Ref. [6]) and are not crucial for obtaining a good χ^2 fit to NN data.
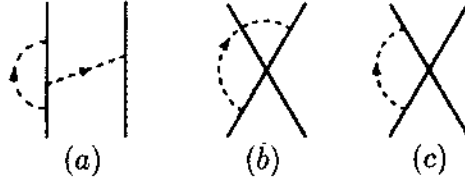
FIG. 4: Loop corrections to OPE, panel (a), and to contact interactions, panels (b) and (c). Notation is as in Fig. 3

3.1.3 CONTACT INTERACTIONS

In this section we focus our attention on the short-range part of the NN interaction, denoted $v_{12}^S(\mathbf{k}, \mathbf{K})$. The potential $v_{12}^S(\mathbf{k}, \mathbf{K})$ includes charge-independent (CI) contact interactions at LO, NLO and N3LO, and charge-dependent (CD) ones at LO and NLO such that

$$v_{12}^S(\mathbf{k}, \mathbf{K}) = v_{12}^{S,\text{CI}}(\mathbf{k}, \mathbf{K}) + v_{12}^{S,\text{CD}}(\mathbf{k}, \mathbf{K}) \ . \tag{92}$$

These contributions are represented in panels (a), (c) and (p) of Fig. 3, respectively. We start off from the charge-independent contribution. The amplitude resulting from the contact interaction Hamiltonians H_{CT0} of Eq. (276) gives rise to the LO contact potential v^{CT0} which is expressed in terms of two LEC's, C_S and C_T, as

$$v^{\text{CT0}} = C_S + C_T\, \boldsymbol{\sigma}_1 \cdot \boldsymbol{\sigma}_2. \tag{93}$$

Next we consider the contribution implied by the contact Hamiltonian involving two gradients acting on the nucleons' field given in Eq. (277). The corresponding potential $\tilde{v}^{\text{CT2}}(\mathbf{k}, \mathbf{K})$ in the COM is expressed in terms of seven independent operatorial structures [3, 4, 39]:

$$\tilde{v}^{\text{CT2}}(\mathbf{k}, \mathbf{K}) = \tilde{C}_1\, k^2 + \tilde{C}_2\, K^2 + (\tilde{C}_3\, k^2 + \tilde{C}_4\, K^2)\, \boldsymbol{\sigma}_1 \cdot \boldsymbol{\sigma}_2 + i\, \tilde{C}_5\, \mathbf{S} \cdot (\mathbf{K} \times \mathbf{k})$$
$$+ \tilde{C}_6\, S_{12}(\mathbf{k}) + \tilde{C}_7\, S_{12}(\mathbf{K}) \ , \tag{94}$$

where $\mathbf{S} = (\boldsymbol{\sigma}_1 + \boldsymbol{\sigma}_2)/2$ is the total spin of the two nucleons and $S_{12}(\mathbf{K}) = 3\,\boldsymbol{\sigma}_1 \cdot \mathbf{K}\, \boldsymbol{\sigma}_2 \cdot \mathbf{K} - K^2 \boldsymbol{\sigma}_1 \cdot \boldsymbol{\sigma}_2$. The coefficients $\tilde{C}_i$ used here are related, of course, to the coefficients C_i' that occur in the Hamiltonian H_{CT2} in Eq. (277). These relations, which are irrelevant for the purpose of this work, can be found in [4, 39]. Finally the

contact potential at order N3LO, $\tilde{v}^{\mathrm{CT4}}(\mathbf{k}, \mathbf{K})$, which involves four gradients acting on the nucleons' field is epressed in terms of 15 independent operators [6] as

$$
\begin{aligned}
\tilde{v}^{\mathrm{CT4}}(\mathbf{k}, \mathbf{K}) = {} & \tilde{D}_1\, k^4 + \tilde{D}_2\, K^4 + \tilde{D}_3\, k^2\, K^2 + \tilde{D}_4\, (\mathbf{K} \times \mathbf{k})^2 + \left[\tilde{D}_5\, k^4 + \tilde{D}_6\, K^4 \right. \\
& \left. + \tilde{D}_7\, k^2 K^2 + \tilde{D}_8\, (\mathbf{K} \times \mathbf{k})^2 \right] \boldsymbol{\sigma}_1 \cdot \boldsymbol{\sigma}_2 + i\, (\tilde{D}_9\, k^2 + \tilde{D}_{10}\, K^2)\, \mathbf{S} \cdot (\mathbf{K} \times \mathbf{k}) \\
& + (\tilde{D}_{11}\, k^2 + \tilde{D}_{12}\, K^2)\, S_{12}(\mathbf{k}) + (\tilde{D}_{13}\, k^2 + \tilde{D}_{14}\, K^2)\, S_{12}(\mathbf{K}) \\
& + \tilde{D}_{15}\left[\boldsymbol{\sigma}_1 \cdot (\mathbf{K} \times \mathbf{k})\, \boldsymbol{\sigma}_2 \cdot (\mathbf{K} \times \mathbf{k}) \right].
\end{aligned}
\tag{95}
$$

Available versions of NN potentials derived up to N3LO in the chiral expansion, such those in Refs. [5, 6, 10], implement the parametrizations of contact interactions at NLO and N3LO given in Eqs. (94) and (95), respectively. However terms proportional to K^2 and K^4 in those expressions, upon Fourier transformation, would lead to p^2 and p^4 operators in coordinate-space ($\mathbf{p} \longrightarrow -i\boldsymbol{\nabla}$ is the relative momentum operator), making the NN potential strongly non-local. It is for this reason that it is desirable to replace the non-local contact interactions by local ones. In particular, these non-local terms can be partially removed by using Fierz identities [47]. These identities are obtained by considering that a generic operator ($\mathcal{O}$) in Eqs. (94) and (95) needs to be evaluated between initial and final two-nucleon states that are antisymmetric

$$
P^{\mathrm{exc}}\,|i\rangle = -\,|i\rangle\,, \qquad P^{\mathrm{exc}}\,|f\rangle = -\,|f\rangle\,.
\tag{96}
$$

The space-spin-isospin exchange operator, P^{exc}, is given by

$$
P^{\mathrm{exc}} = \frac{1 + \boldsymbol{\tau}_1 \cdot \boldsymbol{\tau}_2}{2} \frac{1 + \boldsymbol{\sigma}_1 \cdot \boldsymbol{\sigma}_2}{2}\, P^{\mathrm{space}}\,, \qquad P^{\mathrm{exc}\dagger} = P^{\mathrm{exc}}\,,
\tag{97}
$$

where P^{space} is the exchange operator for the momenta (or coordinates) variables so that $\mathbf{k} \to -2\,\mathbf{K}$ and $\mathbf{K} \to -1/2\,\mathbf{k}$. It follows that the matrix element for an operator $\mathcal{O}$ satisfies

$$
\langle f|\mathcal{O}|i\rangle = -\langle f|P^{\mathrm{exc}}\,\mathcal{O}|i\rangle\,.
\tag{98}
$$

Consider, for example, terms proportional to K^2 and K^4 in Eqs. (94) and (95), respectively. Applying Eq. (98) to these operators, we find that they can be completely removed by using the following Fierz relation

$$
K^m \longrightarrow -\frac{1 + \boldsymbol{\tau}_1 \cdot \boldsymbol{\tau}_2}{2} \frac{1 + \boldsymbol{\sigma}_1 \cdot \boldsymbol{\sigma}_2}{2} \frac{k^m}{2^m}
\tag{99}
$$

with $m = 2$ or 4. Mixed terms of the type $k^2\, K^2$ or $\mathbf{K} \times \mathbf{k}$ cannot be Fierz-transformed

away since

$$k^2 K^2 \quad \longrightarrow \quad -\frac{1 + \boldsymbol{\tau}_1 \cdot \boldsymbol{\tau}_2}{2} \frac{1 + \boldsymbol{\sigma}_1 \cdot \boldsymbol{\sigma}_2}{2} K^2 k^2 \; , \tag{100}$$

$$\mathbf{K} \times \mathbf{k} \quad \longrightarrow \quad -\frac{1 + \boldsymbol{\tau}_1 \cdot \boldsymbol{\tau}_2}{2} \frac{1 + \boldsymbol{\sigma}_1 \cdot \boldsymbol{\sigma}_2}{2} \mathbf{k} \times \mathbf{K} \; . \tag{101}$$

The use of these identities leads to the following choices of contact interactions at NLO

$$
\begin{aligned}
v^{\mathrm{CT2}}(\mathbf{k}, \mathbf{K}) \; = \; & C_1 \, k^2 + C_2 \, k^2 \, \boldsymbol{\tau}_1 \cdot \boldsymbol{\tau}_2 + C_3 \, k^2 \, \boldsymbol{\sigma}_1 \cdot \boldsymbol{\sigma}_2 + C_4 \, k^2 \, \boldsymbol{\sigma}_1 \cdot \boldsymbol{\sigma}_2 \, \boldsymbol{\tau}_1 \cdot \boldsymbol{\tau}_2 \\
& + C_5 \, S_{12}(\mathbf{k}) + C_6 \, S_{12}(\mathbf{k}) \, \boldsymbol{\tau}_1 \cdot \boldsymbol{\tau}_2 + i \, C_7 \, \mathbf{S} \cdot (\mathbf{K} \times \mathbf{k}) \; ,
\end{aligned}
\tag{102}
$$

and at N3LO

$$
\begin{aligned}
v^{\mathrm{CT2}}(\mathbf{k}, \mathbf{K}) \; = \; & D_1 \, k^4 + D_2 \, k^4 \, \boldsymbol{\tau}_1 \cdot \boldsymbol{\tau}_2 + D_3 \, k^4 \, \boldsymbol{\sigma}_1 \cdot \boldsymbol{\sigma}_2 + D_4 \, k^4 \, \boldsymbol{\sigma}_1 \cdot \boldsymbol{\sigma}_2 \, \boldsymbol{\tau}_1 \cdot \boldsymbol{\tau}_2 \\
& + D_5 \, k^2 \, S_{12}(\mathbf{k}) + D_6 \, k^2 \, S_{12}(\mathbf{k}) \, \boldsymbol{\tau}_1 \cdot \boldsymbol{\tau}_2 + i D_7 \, k^2 \, \mathbf{S} \cdot (\mathbf{K} \times \mathbf{k}) \\
& + i \, D_8 \, k^2 \, \mathbf{S} \cdot (\mathbf{K} \times \mathbf{k}) \, \boldsymbol{\tau}_1 \cdot \boldsymbol{\tau}_2 + D_9 \left[\mathbf{S} \cdot (\mathbf{K} \times \mathbf{k}) \right]^2 + D_{10} \, (\mathbf{K} \times \mathbf{k})^2 \\
& + D_{11} \, (\mathbf{K} \times \mathbf{k})^2 \, \boldsymbol{\sigma}_1 \cdot \boldsymbol{\sigma}_2 + D_{12} \, k^2 K^2 + D_{13} \, k^2 K^2 \boldsymbol{\sigma}_1 \cdot \boldsymbol{\sigma}_2 \\
& + D_{14} \, K^2 \, S_{12}(\mathbf{k}) + D_{15} \, K^2 \, S_{12}(\mathbf{k}) \, \boldsymbol{\tau}_1 \cdot \boldsymbol{\tau}_2 \; .
\end{aligned}
\tag{103}
$$

The coefficients $C_{i=1,\dots,7}$ and $D_{i=1,\dots,15}$ are related to $\tilde{C}_{i=1,\dots 7}$ and $\tilde{D}_{i=1,\dots,15}$, respectivelly, via Fierz identities. Therefore, the charge-independent contact interaction, including terms at LO, NLO and N3LO, can be written as

$$
\begin{aligned}
v^{\mathrm{S,CI}}_{12}(\mathbf{k}, \mathbf{K}) \; \equiv \; & v^{\mathrm{CT0}} + v^{\mathrm{CT2}}(\mathbf{k}, \mathbf{K}) + v^{\mathrm{CT4}}(\mathbf{k}, \mathbf{K}) \\
= \; & \left(C_S + C_1 \, k^2 + D_1 \, k^4 \right) + \left(C_2 \, k^2 + D_2 \, k^4 \right) \boldsymbol{\tau}_1 \cdot \boldsymbol{\tau}_2 \\
& + \left(C_T + C_3 \, k^2 + D_3 \, k^4 \right) \boldsymbol{\sigma}_1 \cdot \boldsymbol{\sigma}_2 + \left(C_4 \, k^2 + D_4 \, k^4 \right) \boldsymbol{\sigma}_1 \cdot \boldsymbol{\sigma}_2 \, \boldsymbol{\tau}_1 \cdot \boldsymbol{\tau}_2 \\
& + \left(C_5 + D_5 \, k^2 \right) S_{12}(\mathbf{k}) + \left(C_6 + D_6 \, k^2 \right) S_{12}(\mathbf{k}) \, \boldsymbol{\tau}_1 \cdot \boldsymbol{\tau}_2 \\
& + i \left(C_7 + D_7 \, k^2 \right) \mathbf{S} \cdot (\mathbf{K} \times \mathbf{k}) + i \, D_8 \, k^2 \, \mathbf{S} \cdot (\mathbf{K} \times \mathbf{k}) \, \boldsymbol{\tau}_1 \cdot \boldsymbol{\tau}_2 \\
& + D_9 \left[\mathbf{S} \cdot (\mathbf{K} \times \mathbf{k}) \right]^2 + D_{10} \, (\mathbf{K} \times \mathbf{k})^2 + D_{11} \, (\mathbf{K} \times \mathbf{k})^2 \, \boldsymbol{\sigma}_1 \cdot \boldsymbol{\sigma}_2 \\
& + D_{12} \, k^2 K^2 + D_{13} \, k^2 K^2 \boldsymbol{\sigma}_1 \cdot \boldsymbol{\sigma}_2 + D_{14} \, K^2 \, S_{12}(\mathbf{k}) \\
& + D_{15} \, K^2 \, S_{12}(\mathbf{k}) \, \boldsymbol{\tau}_1 \cdot \boldsymbol{\tau}_2 \; .
\end{aligned}
\tag{104}
$$

Finally, we also consider a charge-dependent component of the short-range NN parametrized as

$$
\begin{aligned}
v^{\mathrm{S,CD}}_{12}(\mathbf{k}, \mathbf{K}) \; = \; & \left[C_0^{\mathrm{IT}} + C_1^{\mathrm{IT}} \, k^2 + C_2^{\mathrm{IT}} \, k^2 \, \boldsymbol{\sigma}_1 \cdot \boldsymbol{\sigma}_2 + C_3^{\mathrm{IT}} \, S_{12}(\mathbf{k}) + i \, C_4^{\mathrm{IT}} \mathbf{S} \cdot (\mathbf{K} \times \mathbf{k}) \right] T_{12} \\
& + [C_0^{\mathrm{IV}} + C_1^{\mathrm{IV}} \, k^2 + C_2^{\mathrm{IV}} \, k^2 \, \boldsymbol{\sigma}_1 \cdot \boldsymbol{\sigma}_2 + C_3^{\mathrm{IV}} \, S_{12}(\mathbf{k}) \\
& + i \, C_4^{\mathrm{IV}} \mathbf{S} \cdot (\mathbf{K} \times \mathbf{k})] (\tau_{1z} + \tau_{2z}) \; .
\end{aligned}
\tag{105}
$$

In the potential $v_{12}^{S,CD}(\mathbf{k},\mathbf{K})$ only terms up to NLO, involving charge-independence breaking (proportional to T_{12}) and charge-symmetry breaking (proportional to $\tau_{1z}+\tau_{2z}$), are accounted for. The associated LEC's, labeled with the superscript IT and IV, while providing some additional flexibility in the data fitting discussed in Sec. 3.4 (especially C_0^{IV} in reproducing the singlet nn scattering length), are not well constrained.

3.2 COORDINATE-SPACE REPRESENTATION OF THE NN POTENTIAL

In this section we derive the coordinate-space NN potential starting from its momentum-space representation discussed in Sec. 3.1. In particular the coordinate-space of the OPE potential as well as contact interactions is carried out via Fourier transformation, while the coordinate-space expressions for the TPE potential are obtained via spectral function representation [9]. In what follows we define $\mathbf{r}$ as the relative separation between the two nucleons and $\hat{\mathbf{r}}$ the unit vector $\mathbf{r}/r$.

3.2.1 OPE AND TPE IN COORDINATE-SPACE

After Fourier transforming the expressions in Eq. (22), the OPE potential reads:

$$v^{\pi,LO}(\mathbf{r}) = \left[v_{\sigma\tau}^{\pi,LO}(r)\,\boldsymbol{\sigma}_1\cdot\boldsymbol{\sigma}_2 + v_{t\tau}^{\pi,LO}(r)\,S_{12}\right]\boldsymbol{\tau}_1\cdot\boldsymbol{\tau}_2$$
$$+ \left[v_{\sigma T}^{\pi,LO}(r)\,\boldsymbol{\sigma}_1\cdot\boldsymbol{\sigma}_2 + v_{tT}^{\pi,LO}(r)\,S_{12}\right]T_{12}\,, \tag{106}$$

where the tensor operator S_{12} is defined as $S_{12}=3\,\boldsymbol{\sigma}_1\cdot\hat{\mathbf{r}}\,\boldsymbol{\sigma}_2\cdot\hat{\mathbf{r}}-\boldsymbol{\sigma}_1\cdot\boldsymbol{\sigma}_2$. The OPE functions are given by

$$v_{\sigma\tau}^{\pi,LO}(r) = \frac{Y_0(r)+2Y_+(r)}{3}\,, \tag{107}$$

$$v_{t\tau}^{\pi,LO}(r) = \frac{T_0(r)+2T_+(r)}{3}\,, \tag{108}$$

$$v_{\sigma T}^{\pi,LO}(r) = \frac{Y_0(r)-Y_+(r)}{3}\,, \tag{109}$$

$$v_{tT}^{\pi,LO}(r) = \frac{T_0(r)-T_+(r)}{3}\,, \tag{110}$$

where the dimensionless functions $Y_\alpha(r)$ and $T_\alpha(r)$ are defined as

$$Y_\alpha(r) = \frac{g_A^2}{12\pi}\frac{m_{\pi_\alpha}^3}{F_\pi^2}\frac{e^{-x_\alpha}}{x_\alpha}\,, \tag{111}$$

$$T_\alpha(r) = Y_\alpha(r)\left(1+\frac{3}{x_\alpha}+\frac{3}{x_\alpha^2}\right)\,. \tag{112}$$

and $x_\alpha = m_{\pi_\alpha} r$, with m_{π_α} denoting the neutral (m_{π_0}) and charged (m_{π_1}) pion masses. Note that Eq. (106) only holds in the case $r > 0$, and a δ-function singularity at the origin has been dropped, since it can be reabsorbed in the contact terms at LO.

Coordinate-space expressions for the TPE terms at NLO and N2LO are obtained by using the spectral function representation [9] (with no spectral cutoff) since the TPE potential satisfies a dispersion relation based on $\overline{N}N \to 2\pi$ amplitude. For $r > 0$, one has the representations

$$v_c^{2\pi}(r) = \frac{1}{2\pi^2 r} \int_0^\infty d\mu\, \mu\, e^{-\mu r} \rho_c(\mu) ,\tag{113}$$

$$v_t^{2\pi}(r) = -\frac{1}{6\pi^2 r^3} \int_0^\infty d\mu\, \mu\, e^{-\mu r}(3 + 3\mu r + \mu^2 r^2)\rho_t(\mu) ,\tag{114}$$

$$v_\sigma^{2\pi}(r) = -\frac{1}{6\pi^2 r} \int_0^\infty d\mu\, \mu\, e^{-\mu r}\left[\mu^2 \rho_t(\mu) - 3\rho_\sigma(\mu)\right] ,\tag{115}$$

and similarly for $v_\tau^{2\pi}(r)$, $v_{\sigma\tau}^{2\pi}(r)$, and $v_{t\tau}^{2\pi}(r)$. The spectral functions $\rho_l(\mu)$ are given [9]

$$\rho_l(\mu) = \mathrm{Im}\left[\tilde{v}_l^{2\pi}(0^+ - i\mu)\right] ,\tag{116}$$

in terms of the left-cut discontinuity at $k = 0^+ - i\mu$, and the functions $\tilde{v}_l^{2\pi}(k)$ are the momentum-space TPE components of the potential at NLO and N2LO written using the following basis

$$\tilde{v}_{12}^{I,2\pi}(\mathbf{k}) = \sum_{l=1}^{6} \tilde{v}_l^{2\pi}(k)\,\tilde{O}_{12}^l ,\tag{117}$$

with $\tilde{O}_{12}^{l=1,\cdots,6} = [1\,,\,\boldsymbol{\sigma}_1 \cdot \boldsymbol{\sigma}_2\,,\,\boldsymbol{\sigma}_1 \cdot \mathbf{k}\,\boldsymbol{\sigma}_2 \cdot \mathbf{k}] \otimes [1\,,\,\boldsymbol{\tau}_1 \cdot \boldsymbol{\tau}_2]$ instead of the basis $O_{12}^{l=1,\cdots,6} = [1\,,\,\boldsymbol{\sigma}_1 \cdot \boldsymbol{\sigma}_2\,,\,S_{12}(\mathbf{k})] \otimes [1\,,\,\boldsymbol{\tau}_1 \cdot \boldsymbol{\tau}_2]$, adopted in the previous section. Consider the TPE at NLO given in Eq. (34). We can rewrite this expression in the following way:

$$\begin{aligned}\tilde{v}^{2\pi,\mathrm{NLO}}(\mathbf{k};\Delta) &= v_\sigma^{2\pi,\mathrm{NLO}}(k;\Delta)\,\boldsymbol{\sigma}_1 \cdot \boldsymbol{\sigma}_2 + v_t^{2\pi,\mathrm{NLO}}(k;\Delta)\,\boldsymbol{\sigma}_1 \cdot \mathbf{k}\,\boldsymbol{\sigma}_1 \cdot \mathbf{k}\\ &\quad + v_\tau^{2\pi,\mathrm{NLO}}(k;\Delta)\boldsymbol{\tau}_1 \cdot \boldsymbol{\tau}_2 ,\end{aligned}\tag{118}$$

where now the TPE functions, in the new basis, read as

$$v_\sigma^{2\pi,\mathrm{NLO}}(k;\Delta) = \frac{3\,g_A^4}{8\pi^2\,F_\pi^4}\,G(k)\,k^2 ,\tag{119}$$

$$v_t^{2\pi,\mathrm{NLO}}(k;\Delta) = -\frac{3\,g_A^4}{8\pi^2\,F_\pi^4}\,G(k) ,\tag{120}$$

$$v_\tau^{2\pi,\mathrm{NLO}}(k;\Delta) = \frac{1}{48\pi^2 F_\pi^4}\,G(k)\Bigg[4m_\pi^2(1 + 4g_A^2 - 5g_A^4) + k^2(1 + 10g_A^2 - 23g_A^4)$$
$$- \frac{48\,g_A^4 m_\pi^4}{4\,m_\pi^2 + k^2}\Bigg] ,\tag{121}$$

and the loop function $G(k)$ is defined in Eq. (38). In order to calculate the coordinate-space representation of $v_\sigma^{2\pi,\mathrm{NLO}}(k; \Delta)$, for example, we first evaluate the spectral functions $\rho_t(\mu)$ and $\rho_\sigma(\mu)$,

$$\rho_\sigma(\mu) \equiv \mathrm{Im}[v_\sigma^{2\pi,\mathrm{NLO}}(0^+ - i\mu; \Delta)] = \frac{3\,g_A^4}{8\pi^2\,F_\pi^4}\,\mu\,\sqrt{\mu^2 - 4\,m_\pi^2}\ , \qquad (122)$$

$$\rho_t(\mu) \equiv \mathrm{Im}[v_t^{2\pi,\mathrm{NLO}}(0^+ - i\mu; \Delta)] = \frac{3\,g_A^4}{8\pi^2\,F_\pi^4}\,\frac{\sqrt{\mu^2 - 4\,m_\pi^2}}{\mu}\ , \qquad (123)$$

where we used

$$\mathrm{Im}[G(0^+ - i\mu)] = -\frac{\pi}{\mu}\,\sqrt{\mu^2 - 4\,m_\pi^2}\ . \qquad (124)$$

The integral in Eq. (115) is then carried out by using the substitution $\mu \to \mu/(2\,m_\pi)$ obtaining the final analytical expression

$$v_\sigma^{2\pi,\mathrm{NLO}}(r; \Delta) = \frac{1}{2\pi^3 r^4}\frac{g_A^4}{F_\pi^4}\,m_\pi \left[3x\,K_0(2x) + (3 + 2x^2)K_1(2x)\right]\ , \qquad (125)$$

where $x = m_\pi r$ (m_π is the average pion mass) and K_n are modified Bessel functions of the second kind. We provide in Appendix C a list of all the coordinate-space TPE components. In particular those corresponding to diagrams (d)–(f) and (j)–(k) in Fig. 3 are expressed in closed form and are given in Eqs. (430)–(432) and Eqs. (445)–(447), respectively; the remaining ones corresponding to diagrams (g)–(i) and (l)–(o) are obtained in terms of a parametric integral, and they are given in Eqs. (433)–(444) and Eqs. (448)–(459).

The radial functions $v_L^i(r)$ are singular at the origin (they behave as $1/r^n$ with n taking on values up to $n = 6$); therefore they need a further regularization. Indeed, each TPE component in Appendix C is regularized by a cutoff of the form

$$C_{R_L}(r) = 1 - \frac{1}{(r/R_L)^6\,e^{(r - R_L)/a_L} + 1}\ , \qquad (126)$$

where in the present work three values for the radius R_L are considered $R_L = (0.8, 1.0, 1.2)$ fm with the diffuseness a_L fixed at $a_L = R_L/2$ in each case. This ensures that the short-distance part of the long-range potential at r smaller that R_L is smoothly cut off and that the singularities at the origin are removed since

$$C_{R_L}(r \to 0) \propto \left(\frac{r}{R_L}\right)^6\ . \qquad (127)$$

The potential v_{12}^{L}, including the well known OPE components at LO regularized also by the cutoff in Eq. (126), then reads in coordinate space

$$v_{12}^{L} = \left[\sum_{l=1}^{6} v_{L}^{l}(r)\, O_{12}^{l}\right] + v_{L}^{\sigma T}(r)\, O_{12}^{\sigma T} + v_{L}^{tT}(r)\, O_{12}^{tT} \,, \tag{128}$$

where

$$O_{12}^{l=1,\ldots,6} = [\mathbf{1}\,,\, \boldsymbol{\sigma}_1 \cdot \boldsymbol{\sigma}_2\,,\, S_{12}] \otimes [\mathbf{1}\,,\, \boldsymbol{\tau}_1 \cdot \boldsymbol{\tau}_2]\,, \tag{129}$$

$O_{12}^{\sigma T} = \boldsymbol{\sigma}_1 \cdot \boldsymbol{\sigma}_2\, T_{12}$ and $O_{12}^{tT} = S_{12}\, T_{12}$. The radial functions $v_{L}^{l}(r)$ are summarized in Eqs. (460)–(465) while the charge-dependent functions $v_{L}^{\sigma T}(r)$ and $v_{L}^{tT}(r)$ are given in Eqs. (109)–(110), respectively.

3.2.2 CONTACT INTERACTIONS IN COORDINATE-SPACE

In this section we perform the coordinate-space representation of the short-range part of the potential, $v_{12}^{S}(\mathbf{k},\mathbf{K})$, defined in Eq. (92). The Fourier transformation of the single contact terms in Eqs. (104) and (105) is carried out with a Gaussian regulator, depending only on the momentum transfer k, such that

$$\widetilde{C}_{R_S}(k) = e^{-R_S^2 k^2/4} \longrightarrow C_{R_S}(r) = \frac{1}{\pi^{3/2} R_S^3} e^{-(r/R_S)^2}, \tag{130}$$

which leads to a coordinate-space representation only mildly non-local, containing at most terms quadratic in the relative momentum operator as will become clear below. The coordinate-space representation of a (regularized) term $O(\mathbf{K},\mathbf{k})$ in Eqs. (104) and (105) follows from

$$O(\mathbf{r}) = \int \frac{d\mathbf{k}}{(2\pi)^3} \int \frac{d\mathbf{K}}{(2\pi)^3} e^{i\,\mathbf{k}\cdot(\mathbf{r}'+\mathbf{r})/2}\, O(\mathbf{K},\mathbf{k})\, e^{i\,\mathbf{K}\cdot(\mathbf{r}'-\mathbf{r})}\,, \tag{131}$$

where $\mathbf{r}$ is the relative position and $\mathbf{K} \to \mathbf{p} = -i\,\boldsymbol{\nabla}'\delta(\mathbf{r}'-\mathbf{r})$, the relative momentum operator. For the momentum-space operator structures present in Eqs. (104)

and (105) one finds the following relations:

$$1 \longrightarrow C_{R_S}(r) \,, \tag{132}$$

$$k^2 \longrightarrow -C_{R_S}^{(2)}(r) - \frac{2}{r} C_{R_S}^{(1)}(r) \,, \tag{133}$$

$$k^4 \longrightarrow C_{R_S}^{(4)}(r) + \frac{4}{r} C_{R_S}^{(3)}(r) \,, \tag{134}$$

$$S_{12}(\mathbf{k}) \longrightarrow -\left[C_{R_S}^{(2)}(r) - \frac{1}{r} C_{R_S}^{(1)}(r) \right] S_{12} \,, \tag{135}$$

$$i\,\mathbf{S} \cdot (\mathbf{K} \times \mathbf{k}) \longrightarrow -\frac{1}{r} C_{R_S}^{(1)}(r)\,\mathbf{L} \cdot \mathbf{S} \,, \tag{136}$$

$$\mathbf{K}^2 \longrightarrow \left\{ \mathbf{p}^2 \,, C_{R_S}(r) \right\} \,, \tag{137}$$

$$(\mathbf{K} \times \mathbf{k})^2 \longrightarrow -\frac{1}{r^2} \left[C_{R_S}^{(2)}(r) - \frac{1}{r} C_{R_S}^{(1)}(r) \right] \mathbf{L}^2 - \left\{ \mathbf{p}^2 \,, \frac{1}{r} C_{R_S}^{(1)}(r) \right\}$$
$$-\frac{1}{r} C_{R_S}^{(3)}(r) \,, \tag{138}$$

$$[\mathbf{S} \cdot (\mathbf{K} \times \mathbf{k})]^2 \longrightarrow -\frac{1}{r^2} \left[C_{R_S}^{(2)}(r) - \frac{1}{r} C_{R_S}^{(1)}(r) \right] (\mathbf{L} \cdot \mathbf{S})^2$$
$$-\left\{ \mathbf{p}^2 \frac{(1 + \boldsymbol{\sigma}_1 \cdot \boldsymbol{\sigma}_2)}{2} - \boldsymbol{\sigma}_1 \cdot \mathbf{p}\, \boldsymbol{\sigma}_2 \cdot \mathbf{p} \,, \frac{1}{r} C_{R_S}^{(1)}(r) \right\} \,, \tag{139}$$

where

$$C_{R_S}^{(n)}(r) = \frac{d^n C_{R_S}(r)}{dr^n} \,. \tag{140}$$

Finally v_{12}^S in coordinate-space reads as

$$v_{12}^S = \left[\sum_{l=1}^{19} v_S^l(r)\, O_{12}^l \right] + \left\{ v_S^p(r) + v_S^{p\sigma}(r)\, \boldsymbol{\sigma}_1 \cdot \boldsymbol{\sigma}_2 \right.$$
$$\left. + v_S^{pt}(r)\, S_{12} + v_S^{pt\tau}(r)\, S_{12}\, \boldsymbol{\tau}_1 \cdot \boldsymbol{\tau}_2 \,, \mathbf{p}^2 \right\} \,, \tag{141}$$

where $O_{12}^{l=1,\dots,6}$ have been defined in the previous section,

$$O_{12}^{l=7,\dots,11} = \mathbf{L} \cdot \mathbf{S}\,, \mathbf{L} \cdot \mathbf{S}\, \boldsymbol{\tau}_1 \cdot \boldsymbol{\tau}_2\,, (\mathbf{L} \cdot \mathbf{S})^2\,, \mathbf{L}^2\,, \mathbf{L}^2 \boldsymbol{\sigma}_1 \cdot \boldsymbol{\sigma}_2 \,, \tag{142}$$

referred to as b, $b\tau$, bb, q, $q\sigma$, and

$$O_{12}^{l=12,\dots,19} = [\mathbf{1}\,, \boldsymbol{\sigma}_1 \cdot \boldsymbol{\sigma}_2\,, S_{12}\,, \mathbf{L} \cdot \mathbf{S}] \otimes [T_{12}\,, \tau_1^z + \tau_2^z] \,, \tag{143}$$

referred to as T, τz, σT, $\sigma \tau z$, tT, $t\tau z$, bT, $b\tau z$. The four additional terms, denoted as p, $p\sigma$, pt, and $pt\tau$, in the anti-commutator of Eq. (141) are $\mathbf{p}^2$-dependent. The radial functions $v_S^l(r)$ as well as those multiplying the $\mathbf{p}^2$-terms are listed in Appendix C. We consider, in combination with $R_L = (0.8, 1.0, 1.2)$ fm, $R_s = (0.6, 0.7, 0.8)$ fm,

corresponding to typical momentum-space cutoffs $\Lambda_S = 2/R_S$ from about 660 MeV down to 500 MeV. While the use of a Gaussian cutoff mixes up orders in the power counting—for example, the LO contact interactions proportional to C_S and C_T in Eq. (104) generate contributions at NLO and N3LO—such a choice nevertheless leads to smooth functions for the potential components $v_S^i(r)$ and the resulting deuteron waves. Sharper cutoffs, like those $\propto \exp\left[-(r/R)^n\right]$ with $n = 4$, as suggested in Ref [14], or $n = 6$, as in one of the earlier versions of the present model, generate wiggles in the deuteron waves at $r \sim R$ (as well as mixing of power-counting orders).

3.3 DATA ANALYSIS

The NN potential discussed in Sec. 3.2 involves 34 unknown LEC's associated with the charge-independent contact interactions entering at LO (C_S and C_T), NLO (C_i, $i = 1, ..., 7$) and N3LO (D_i, $i = 1, ..., 15$), and the charge-dependent contact interactions entering the LO (C_0^{IT} and C_0^{IV}) and NLO (C_i^{IT} and C_i^{IV}, $i = 1, ..., 4$). One goal of this thesis is to determine these contact parameters by fitting the 2013 Granada database [54], consisting of 2309 pp and 2982 np data in the laboratory-energy range $E_{\text{lab}} = 0 - 300\,\text{MeV}$, as well as the deuteron binding energy. In the optimization procedure, as described in detail in Sec. 3.3.3, we fit first phase shifts, then we refine the fit by minimizing the χ^2 obtained from a direct comparison with the database. To this end we need first to formulate the NN scattering problem in coordinate-space.

3.3.1 NN SCATTERING PROBLEM: PHASE SHIFTS

In the following section, we discuss the solution of the Schrödinger equation with the strong-component potential (v_{12}) discussed in Sec. 3.2, which contains $\mathbf{p}^2$-dependent central and tensor terms. For simplicity, we ignore the electromagnetic and charge-dependent parts of v_{12}—the treatment in the presence of v_{12}^{EM} is discussed in Appendix D. In spin S and isospin T channel, the potential v_{12} reads

$$
\begin{aligned}
v_{12}^{TS} &= v_{TS}^c(r) + v_T^t(r)\, S_{12} + v_T^b(r)\, \mathbf{L} \cdot \mathbf{S} + v_{TS}^q(r)\, \mathbf{L}^2 + v_T^{bb}(r)\,(\mathbf{L} \cdot \mathbf{S})^2 \\
&\quad + \left\{ v_{TS}^p(r) + v_T^{pt}(r)\, S_{12}\, , \, \mathbf{p}^2 \right\}\,,
\end{aligned}
\tag{144}
$$

with

$$
\mathbf{p}^2 = \frac{\mathbf{L}^2}{r^2} - \frac{2}{r}\frac{d}{dr} - \frac{d^2}{dr^2}\,.
\tag{145}
$$

For single channels ($J = L$, where L and J are the orbital and total angular momenta, except for the $^3P_0$ channel), the scattering total wave function can be written as

$$\Psi_{JST}(\mathbf{r}) = \frac{1}{r} u_{LSJ,T}(r) \mathcal{Y}_{LSJ}(\hat{\mathbf{r}}) \eta_T , \tag{146}$$

where $u(r)$ is the reduced radial wave function (the subscription LSJ, T is removed for brevity) and η_T represent the total isospin state of the nucleon-nucleon system. The "spin-angle" functions $\mathcal{Y}_{LSJ}(\hat{\mathbf{r}})$ are convenient to use in order to express two-nucleon partial waves. They are defined as

$$
\begin{aligned}
\mathcal{Y}_{LSJ}(\hat{\mathbf{r}}) &\equiv \left[Y_{LM_L}(\hat{\mathbf{r}}) \otimes \chi_{SM_S} \right]_{JM} \\
&= \sum_{M_L, M_S} Y_{LM_L}(\hat{\mathbf{r}}) \chi_{SM_S} \langle LM_L; SM_S | JM \rangle ,
\end{aligned}
\tag{147}
$$

where $Y_{LM_L}(\hat{\mathbf{r}})$ are spherical harmonics, and $\hat{\mathbf{r}}$ represent the θ and ϕ polar angles of the relative position vector $\mathbf{r} = \mathbf{r}_1 - \mathbf{r}_2$ and $\langle LM_L; SM_S | JM \rangle$ are the Clebsch-Gordon coefficients, χ_{SM_S} represent the spin state of the nucleon-nucleon system. The Schrödinger equation for the reduced radial function $u(r)$ reads

$$- (1 + \overline{v}) u'' - \overline{v}' u' + \left[v - \frac{\overline{v}''}{2} - k^2 \right] u = 0 , \tag{148}$$

where

$$
\begin{aligned}
v_{TSJ} &= 2\mu \left[v_{TS}^c + \delta_{S,1} \left(2 v_T^t - v_T^b \right) + J(J+1) \left(v_{TS}^q + 2 \frac{v_{TS}^p}{r^2} + \delta_{S,1} 4 \frac{v_T^{pt}}{r^2} \right) \right. \\
&\quad \left. + \delta_{S,1} v_T^{bb} \right] + \frac{J(J+1)}{r^2} ,
\end{aligned}
\tag{149}
$$

$$\overline{v}_{TS} = 4\mu \left(v_{TS}^p + \delta_{S,1} 2 v_T^{pt} \right) , \tag{150}$$

μ is the reduced mass, and the subscripts in Eq. (148) have been dropped for brevity. The dependence on the first derivative u' is removed by setting

$$u = \lambda w , \tag{151}$$

and by requiring that terms proportional to w' vanish. One finds that λ must satisfy

$$2 (1 + \overline{v}) \lambda' + \overline{v}' \lambda = 0 , \tag{152}$$

which has the solution

$$\lambda = (1 + \overline{v})^{-1/2} . \tag{153}$$

The function w then satisfies

$$w'' = f\,w\ ,\qquad (1+\overline{v})f = v - \frac{(\overline{v}'/2)^2}{1+\overline{v}} - k^2\ ,\qquad (154)$$

with the boundary condition (reinstating the appropriate superscripts and subscripts for the case under consideration)

$$\frac{w_{JSJ,T}(r)}{r} \simeq \frac{1}{2}\left[h_J^{(2)}(kr) + S_{JJ}^{JS,T}(k)\,h_J^{(1)}(kr)\right]\ ,\qquad (155)$$

where the Hankel functions are defined as $h_L^{(1,2)}(kr) = j_L(kr) \pm i\,n_L(kr)$, $j_L(kr)$ and $n_L(kr)$ being the regular and irregular spherical Bessel functions, respectively, and $S_{L'L}^{JS,T}$ are S-matrix elements. Denoting phase shifts as $\delta_{L'L}^{JS,T}$, the S-matrix in single channels ($L = L' = J$) is simply given by

$$S_{JJ}^{JS,T} = e^{2i\delta^{JS,T}}\ .\qquad (156)$$

The differential equation above is solved with the standard Numerov method. In the case of $^3P_0$ ($T = S = 1$) the same equation above holds but

$$v_{110} = 2\mu\left[v_{11}^c - 4\,v_1^t - 2\,v_1^b + 2\left(v_{11}^q + 2\,\frac{v_{11}^p}{r^2} - 8\,\frac{v_1^{pt}}{r^2}\right) + 4\,v_1^{bb}\right] + \frac{2}{r^2}\ ,\qquad (157)$$

$$\overline{v}_{11} = 4\mu\left(v_1^p - 4\,v_1^{pt}\right)\ ,\qquad (158)$$

For the coupled channels ($L = J \pm 1$ and $S = 1$), the wave function is represented by

$$\Psi_{J1T}(\mathbf{r}) = \left[\frac{1}{r}u_{(J-1)1J,T}(r)\mathcal{Y}_{(J-1)1J}(\hat{\mathbf{r}}) + \frac{1}{r}u_{(J+1)1J,T}(r)\mathcal{Y}_{(J+1)1J}(\hat{\mathbf{r}})\right]\eta_T\ .\qquad (159)$$

It is convenient to introduce the vector U with components $u_{(J-1)1J,T}(r) = u_-$ and $u_{(J+1)1J,T}(r) = u_+$, and the 2×2 matrices V and $\overline{V}$ with matrix elements given respectively by

$$v_{T1J}^{--} = 2\mu\left[v_{T1}^c - 2\,\frac{J-1}{2J+1}\,v_T^t + (J-1)v_T^b + J(J-1)\left(v_{T1}^q + 2\,\frac{v_{T1}^p}{r^2} - 4\,\frac{J-1}{2J+1}\,\frac{v_T^{pt}}{r^2}\right)\right.$$
$$\left. + (J-1)^2 v_T^{bb}\right] + \frac{J(J-1)}{r^2}\ ,\qquad (160)$$

$$v_{T1J}^{++} = 2\mu\left[v_{T1}^c - 2\,\frac{J+2}{2J+1}\,v_T^t - (J+2)v_T^b + (J+1)(J+2)\left(v_{T1}^q + 2\,\frac{v_{T1}^p}{r^2}\right.\right.$$
$$\left.\left. - 4\,\frac{J+2}{2J+1}\,\frac{v_T^{pt}}{r^2}\right) + (J+2)^2 v_T^{bb}\right] + \frac{(J+1)(J+2)}{r^2}\ ,\qquad (161)$$

$$v_{T1J}^{-+} = 12\mu\,\frac{\sqrt{J(J+1)}}{2J+1}\left(v_T^t + 2\,\frac{J^2+J+1}{r^2}\,v_T^{pt}\right)\ ,\qquad v_{T1J}^{+-} = v_{T1J}^{-+}\ ,\qquad (162)$$

and

$$\overline{v}_{T1J}^{--} = 4\mu \left(v_{T1}^{p} - 2\frac{J-1}{2J+1} v_T^{pt} \right) , \tag{163}$$

$$\overline{v}_{T1J}^{++} = 4\mu \left(v_{T1}^{p} - 2\frac{J+2}{2J+1} v_T^{pt} \right) , \tag{164}$$

$$\overline{v}_{T1J}^{-+} = 24\mu \frac{\sqrt{J(J+1)}}{2J+1} v_T^{pt} , \qquad \overline{v}_{T1J}^{+-} = \overline{v}_{T1J}^{-+} . \tag{165}$$

where the script $-$ or $+$ specifies the orbital angular momentum $L = J - 1$ or $L = J + 1$. With these definitions, the coupled-channel Schrödinger equation can be written as

$$-\left(I + \overline{V}\right) U'' - \overline{V}' U' + \left[V - \frac{\overline{V}''}{2} - k^2 \right] U = 0 , \tag{166}$$

where I is the 2×2 identity matrix. Introducing the 2×2 matrix Λ with

$$U = \Lambda W , \tag{167}$$

and requiring that terms proportional to W' vanish lead to

$$2\left(I + \overline{V}\right) \Lambda' + \overline{V}' \Lambda = 0 . \tag{168}$$

The set of first order differential equations above is solved with the Runge-Kutta method [55]. Note that in the limit $r \to \infty$, Λ reduces to the identity matrix (and hence the asymptotic behavior of $w_{\mp}$ is the same as that of $u_{\mp}$). Straightforward manipulations allow one to cast the Schrödinger equation for W in the standard form

$$W'' = F W , \qquad \left(1 + \overline{V}\right) \Lambda F \Lambda^{-1} = V - \frac{1}{4}\overline{V}'(1+\overline{V})^{-1}\overline{V}' - k^2 , \tag{169}$$

with the boundary conditions (again, reinstating superscripts and subscripts)

$$\frac{w_{L'L}^{TSJ}(r)}{r} \simeq \frac{1}{2}\left[\delta_{L'L} h_{L'}^{(2)}(kr) + S_{L'L}^{JST} h_{L'}^{(1)}(kr) \right] , \tag{170}$$

where $L, L' = J \pm 1$ are the orbital angular momenta of the incoming and outgoing waves and the $\delta_{L'L}$ are Kronecker deltas, and the S-matrix is given by

$$S_{L'L}^{JST} \equiv S^J = \left[\begin{array}{cc} e^{2i\delta_-^J} \cos 2\epsilon_J & i\,e^{i(\delta_-^J+\delta_+^J)} \sin 2\epsilon_J \\ i\,e^{i(\delta_-^J+\delta_+^J)} \sin 2\epsilon_J & e^{2i\delta_+^J} \cos 2\epsilon_J \end{array} \right] , \tag{171}$$

where ϵ_J is the mixing angle.

In particular the low-energy scattering can be expressed in terms of an effective range function such that

$$F(k^2) \equiv k \cot \delta_N = -\frac{1}{a} + \frac{1}{2} r_0 k^2 + O(k^4) \,, \tag{172}$$

where a is the scattering length and r_0 is the effective range and δ_N indicates S-wave phase shifts without the electromagnetic interaction. In the presence of the electromagnetic interaction we have to use a more complicated effective range function (see Appendix D), where the phase shifts are with respect to the full range-electromagnetic interaction. In the Sec. 3.4, we present the results of the nn, pp and np scattering length and effective range calculated both with and without electromagnetic interaction.

3.3.2 FROM PHASE SHIFTS TO OBSERVABLES

Setting aside electromagnetic (EM) contributions (Coulomb and higher order ones) for the time being, the invariant on-shell scattering amplitude M for the NN system can be expressed in terms of five independent complex functions—the Wolfenstein parametrization—as

$$M(\mathbf{p}', \mathbf{p}) = a + m\,\boldsymbol{\sigma}_1 \cdot \hat{\mathbf{n}}\,\boldsymbol{\sigma}_2 \cdot \hat{\mathbf{n}} + (g - h)\,\boldsymbol{\sigma}_1 \cdot \hat{\mathbf{m}}\,\boldsymbol{\sigma}_2 \cdot \hat{\mathbf{m}} + (g + h)\,\boldsymbol{\sigma}_1 \cdot \hat{\mathbf{l}}\,\boldsymbol{\sigma}_2 \cdot \hat{\mathbf{l}} + c\,(\boldsymbol{\sigma}_1 + \boldsymbol{\sigma}_2) \cdot \hat{\mathbf{n}} \,,$$
$$\tag{173}$$

where $\hat{\mathbf{l}}$, $\hat{\mathbf{m}}$, $\hat{\mathbf{n}}$ are three orthonormal vectors along the directions of $\mathbf{p}' + \mathbf{p}$, $\mathbf{p}' - \mathbf{p}$, and $\mathbf{p} \times \mathbf{p}'$, and $\mathbf{p}'$, $\mathbf{p}$ are the final and initial relative momenta, respectively. The functions $a, m, g, h,$ and c are taken to depend on the energy in the laboratory (lab) frame and the scattering angle θ in the center-of-mass frame. Any scattering observable can be constructed out of these amplitudes [56, 57].

The NN amplitude is diagonal in pair spin S, and pair isospin and isospin projection TM_T, and is expanded in partial waves as

$$M_{M_S' M_S}^{S, T M_T}(E, \theta) = \sqrt{4\pi} \sum_{JLL'} i^{L-L'} \sqrt{2L + 1} \frac{1 - (-1)^{L+S+T}}{2} \langle L'(M_S - M_S'), S M_S' \mid J M_S \rangle$$
$$\langle L0, S M_S \mid J M_S \rangle Y_{L'}^{M_S - M_S'}(\theta, 0) \frac{S_{L'L}^{JS, T M_T}(p) - \delta_{L'L}}{i\,p} \,. \tag{174}$$

Hereafter, for notational simplicity we drop from the phase shifts unnecessary subscripts as well as the superscripts TM_T, with $T = 1$ and $M_T = 1, 0, -1$ for respectively pp, np, and nn. The S-matrix elements and phase shifts are obtained

from solutions of the Schrödinger equation with suitable boundary conditions, as discussed in the previous section. In terms of the amplitudes $M^S_{M'_S M_S}$, the functions $a, m, g, h,$ and c then read

$$a = \left(M^1_{11} + M^1_{00} + M^0_{00} + M^1_{-1-1} \right)/4 , \tag{175}$$

$$c = i \left(M^1_{10} - M^1_{01} + M^1_{0-1} - M^1_{-10} \right)/(4\sqrt{2}) , \tag{176}$$

$$m = \left(-M^1_{1-1} + M^1_{00} - M^0_{00} - M^1_{-11} \right)/4 , \tag{177}$$

$$g = \left(M^1_{11} + M^1_{1-1} + M^1_{-11} + M^1_{-1-1} - 2\,M^0_{00} \right)/8 , \tag{178}$$

$$h = \cos\theta \left(M^1_{11} - M^1_{1-1} - M^1_{-11} + M^1_{-1-1} - 2\,M^1_{00} \right)/8$$
$$+ \sqrt{2} \sin\theta \left(M^1_{10} + M^1_{01} - M^1_{0-1} - M^1_{-10} \right)/8 , \tag{179}$$

and this can be further simplified by noting that $M^1_{0-1} = -M^1_{01}$, $M^1_{1-1} = M^1_{-11}$, $M^1_{-10} = -M^1_{10}$, and $M^1_{11} = M^1_{-1-1}$.

When EM interactions are included, the full scattering amplitudes M are conveniently separated into a part due to nuclear interactions and another one stemming from EM interactions,

$$M = M_{\text{EM}} + M_{\text{N}} . \tag{180}$$

The pp EM amplitudes contain Coulomb with leading relativistic corrections, vacuum polarization, and magnetic moments contributions, whereas the np ones contain magnetic moment contributions only (see Ref. [54] for a compendium of formulas for these EM contributions). For completeness, however, the determination of the pp phase shifts relative to EM functions and of the pp effective range expansion is summarized in Appendix D. Due to the finite range of the NN force, the nuclear part of the scattering amplitudes, M_{N}, converges with a maximum total angular momentum of $J = 15$. In contrast, EM scattering amplitudes, M_{EM}, require a summation of about a thousand partial waves due to the long range and tensor character of the dipolar magnetic interactions. While these corrections are numerically tiny, they are nevertheless indispensable for an accurate description of the data [58].

3.3.3 FITTING PROCEDURE

We use the database developed by the Granada group [54], where a selection of the large collection of np and pp scattering data taken from 1950 till 2013 was made.

References to these data are listed in Ref. [54]. The criterium adopted in this latter work was to represent the NN interaction with a general and flexible parametrization, based on a minimal set of theoretical assumptions so as to avoid any systematic bias in the selection process. The aim of the method, first suggested by Gross and Stadler [59], was to obtain a 3σ-self-consistent database. This entails removing 3σ outliers and re-fitting iteratively until convergence. The procedure results in a database with important statistical features [60] and therefore amenable to statistical analysis, and leads to the identification of a consistent subset among the large body of 6713 np and pp experimental cross sections and polarization observables. In the present study we are concerned with a subset of this 3σ-self-consistent database, namely data below 300 MeV lab energy. This database is organized in the following way: there are N sets of data, each one corresponding to a different experiment. Each data set contains measurements at fixed E_{lab} and different scattering angles θ. However a few observables are measured at different E_{lab} and fixed θ, like, for example, total cross sections since their measurement does not involve the scattering angle. An experiment may have a specified systematic error (normalized data), no systematic error (absolute data), or an arbitrarily large systematic error (floated data).

We briefly describe the fitting procedure. The total figure of merit is defined as the usual χ^2 function

$$\chi^2 = \sum_{t=1}^{N} \chi_t^2 \, , \tag{181}$$

where χ_t^2 refers to the corresponding contribution from each data set, which we explain next. In all cases, the χ_t^2 for a data set is given by

$$\chi_t^2 = \sum_{i=1}^{n} \frac{(o_i/Z_t - t_i)^2}{(\delta o_i/Z_t)^2} + \frac{(1 - 1/Z_t)^2}{(\delta_{\text{sys}}/Z_t)^2} \, , \tag{182}$$

where o_i and t_i are the measured and calculated values of the observable at point i, δo_i and δ_{sys} are the statistical and systematic errors, respectively, and Z_t is a scaling factor chosen to minimize the χ_t^2 ($\partial \chi_t^2 / \partial Z_t = 0$),

$$Z_t = \left(\sum_i^n \frac{o_i t_i}{\delta o_i^2} + \frac{1}{\delta_{\text{sys}}^2} \right) \bigg/ \left(\sum_i^n \frac{t_i^2}{\delta o_i^2} + \frac{1}{\delta_{\text{sys}}^2} \right) \, . \tag{183}$$

The last term in Eq. (182) is denoted χ_{sys}^2. For absolute data $Z_t = 1$ and $\chi_{\text{sys}}^2 = 0$, while for floated data use of Eq. (183) is made with $\delta_{\text{sys}} = \infty$ so that $\chi_{\text{sys}}^2 = 0$.

Normalized data have in most cases $Z_t \neq 1$ such that $\chi^2_{\text{sys}} \neq 1$ and the normalization is counted as an extra data point. For some normalized data the systematic error can give a rather large χ^2_{sys} due to an underestimation of δ_{sys}. In order to account for this, we float data that have $\chi^2_{\text{sys}} > 9$ and no extra normalization data is counted. This is in line with the criterion used to build the pp and np database. Finally, the total χ^2 is the sum of all the χ^2_t for each pp and np data set.

The minimization of the objective function χ^2 with respect to the LEC's in Eqs. (104) and (105) is carried out with the "Practical Optimization Using no Derivatives (for Squares)", POUNDerS [61]. This derivative-free algorithm is designed for minimizing sums of squares and uses interpolation techniques to construct residuals at each point. In the optimization procedure, we fit first phase shifts and then refine the fit by minimizing the χ^2 obtained from a direct comparison with the database. In fact, sizable changes in the total χ^2 are found when passing from phase shifts to observables, so this refining is absolutely necessary to claim reasonable fits to data. This is a general feature which is often found, and reflects the different weights in the χ^2 contributions of the two different fitting schemes. Indeed, the initial guiding fit to phase shifts chooses a prescribed energy grid arbitrarily, which *does not* correspond directly to measured energies, nor necessarily samples faithfully the original information provided by the experimental data. Moreover, there are different partial-wave-analyses (PWA's) which describe the same data but yield different phase shifts with significantly larger discrepancies than reflected by the inferred statistical uncertainties [54, 60, 62].

3.4 RESULTS

We report results for the potentials $v_{12} + v_{12}^{\text{EM}}$ corresponding to three different choices of cutoffs $(R_{\text{L}}, R_{\text{S}})$: model a with $(1.2, 0.8)$ fm, model b with $(1.0, 0.7)$ fm, and model c with $(0.8, 0.6)$ fm. Models a, b, and c were fitted to the Granada database of pp and np cross sections, polarization observables, and normalizations up to lab energies of 300 MeV, to the pp, np, and nn singlet scattering lengths, and to the deuteron binding energy. We list the number of pp and np data (including normalizations) and corresponding total χ^2 for the three models in Table 3, where we also report for comparison the χ^2 corresponding to the AV18 [48] (of course, without a refit of it) and the same database. The total number of data points changes slightly for each of the various models because of fluctuations in the number

TABLE 3: Total χ^2 for model a with $(R_L, R_S) = (1.2, 0.8)$ fm, model b with $(1.0, 0.7)$ fm, and model c $(0.8, 0.6)$ fm, and the AV18; N_{pp} (N_{np}) denotes the number of pp (np) data, including observables and normalizations.

Lab Energy (MeV)	N_{pp}^{a}	N_{pp}^{b}	N_{pp}^{c}	N_{pp}^{18}	$\chi^2(pp)$			
					v_{12}^{a}	v_{12}^{b}	v_{12}^{c}	v_{18}
0–300	2262	2260	2258	2269	3353	3345	3430	4191

Lab Energy (MeV)	N_{np}^{a}	N_{np}^{b}	N_{np}^{c}	N_{np}^{18}	$\chi^2(np)$			
					v_{12}^{a}	v_{12}^{b}	v_{12}^{c}	v_{18}
0–300	2957	2954	2949	2961	3548	3523	3636	3391

of normalizations included in the database according to the criterion discussed at the end of the previous section. In the range (0–300) MeV, the $\chi^2(pp)$/datum and $\chi^2(np)$/datum are about 1.48, 1.48, 1.52 and 1.20, 1.19, 1.23 for models a, b, and c, respectively; the corresponding global $\chi^2(pp + np)$/datum are 1.33, 1.33, 1.37. For the AV18, the $\chi^2(pp)$/datum, $\chi^2(np)$/datum, and global $\chi^2(pp+np)$/datum are 1.84, 1.14, and 1.46, respectively. Note that the global χ^2 values above have been evaluated by taking into account the number of fitting parameters characterizing these models (34 in the case of models a, b, and c). Errors for pp data are significantly smaller than for np, thus explaining the consistently higher $\chi^2(pp)$/datum. The quality of the fits deteriorates slightly as the (R_L, R_S) cutoffs are reduced from the values (1.2,0.8) fm of model a down to (0.8,0.6) fm of model c.

The fitted values of the LEC's in Eqs. (104) and (105) corresponding to models a, b, and c are listed in Table 4. The values for the πN LEC's in the OPE and TPE terms of these models have already been given in Tables 1 and 2.

The S-wave, P-wave, and D-wave phase shits for np (in $T = 0$ and $T = 1$) and pp are displayed in Figs. 5–7 up to 300 MeV lab energies. The phases calculated with the full models a, b, and c including strong and electromagnetic interactions are represented by the band. The np phases are relative to spherical Bessel functions, while the pp phases are with respect to electromagnetic functions (see Appendix D). The cutoff sensitivity, as represented by the width of the shaded band, is very weak for pp, and generally remains modest for np, except for the $T = 0$ $^3D_3$ phase and ϵ_1 mixing angle, particularly for energies larger than 150 MeV. The calculated phases

are compared to those obtained in PWA's by the Nijmegen [63, 64], Granada [54], and Gross-Stadler [59] groups. Note that the recent Gross and Stadler's PWA was limited to np data only. We also should point out that, since the Nijmegen's PWA of the early nineties which was based on about 1780 pp and 2514 np data in the lab energy range 0–350 MeV, the NN elastic scattering database has increased very significantly. Indeed, in the same energy range the 2013 Granada database contains a total of 2972 pp and 4737 np data. Especially for the higher partial waves in the np sector and at the larger energies there are appreciable differences between these various PWA's. It is also interesting to observe that these differences are most significant for the $T = 0$ $^3D_3$ phase and ϵ_1 mixing angle, and therefore correlate with the cutoff sensitivity displayed in these cases by models a, b, and c.
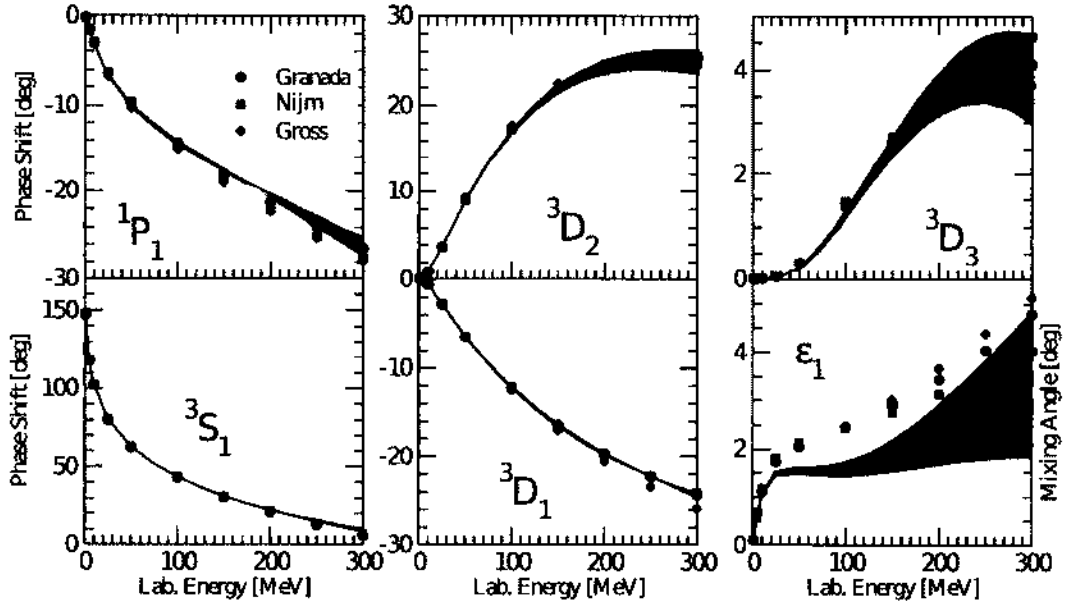
FIG. 5: S-wave, P-wave, and D-wave phase shifts in the np $T=0$ channel, obtained in the Nijmegen [63, 64], Gross and Stadler [59], and Navarro Pérez et $al.$ [54] partial-wave analysis, are compared to those of models a, b, and c, indicated by the band. For the mixing angle ϵ_1 (phase shift $^3D_3$) the lower limit of the band corresponds to model a (model b) and the upper limit to model c (model c).

The low-energy scattering parameters are listed in Table 5, where they are compared to experimental results. The singlet and triplet np, and singlet pp and nn,

scattering lengths are calculated with and without the inclusion of electromagnetic interactions. Without the latter, the effective range function is given in Eq. (172). In the presence of electromagnetic interactions, a more complicated effective range function must be used; it is reported in Appendix D, along with the relevant references. The latest determinations of the empirical values for the singlet scattering lengths and effective ranges, obtained by retaining only strong interactions (hence the superscript N), are [65-68] (as reported in Ref. [6]):

$$^1a_{pp}^N \ = \ -17.3 \pm 0.4 \text{ fm} \ , \qquad ^1r_{pp}^N = 2.85 \pm 0.04 \text{ fm} \ , \tag{184}$$

$$^1a_{np}^N \ = \ -23.74 \pm 0.02 \text{ fm} \ , \qquad ^1r_{np}^N = 2.77 \pm 0.05 \text{ fm} \ , \tag{185}$$

$$^1a_{nn}^N \ = \ -18.95 \pm 0.40 \text{ fm} \ , \qquad ^1r_{nn}^N = 2.75 \pm 0.11 \text{ fm} \ , \tag{186}$$

which imply that charge symmetry (meaning that pp and nn interactions are identical after removing all the electromagnetic contributions) and charge independence (meaning that the three nucler forces pp, nn and np are identical after again removing all the electromagnetic contributions) are broken respectively by [6]

$$\Delta a_{\text{CSB}} \ = \ a_{pp}^N - a_{nn}^N = 1.65 \pm 0.60 \text{ fm} \ , \tag{187}$$

$$\Delta r_{\text{CSB}} \ = \ r_{pp}^N - r_{nn}^N = 0.10 \pm 0.12 \text{ fm} \ , \tag{188}$$

and

$$\Delta a_{\text{CIB}} \ = \ (a_{pp}^N + a_{nn}^N)/2 - a_{np}^N = 5.6 \pm 0.6 \text{ fm} \ , \tag{189}$$

$$\Delta r_{\text{CIB}} \ = \ (r_{pp}^N + r_{nn}^N)/2 - r_{np}^N = 0.03 \pm 0.13 \text{ fm} \ . \tag{190}$$

The more significant values for Δa_{CSB} and Δa_{CIB} can be compared to those inferred from Table 5: $(\Delta a_{\text{CSB}}, \Delta a_{\text{CIB}}) = (2.13, 5.11)$ fm for model a, $(2.34, 5.12)$ fm for model b, and $(1.90, 5.08)$ fm for model c.

In the left upper panel of Fig. 8 we show the $^1S_0$ phase shifts for pp, np and nn calculated with and without the inclusion of electromagnetic interactions (only model b is considered). There is excellent agreement between these phases and those obtained in the the Granada, Gross and Stadler, and Nijmegen PWA's, when electromagnetic effects are fully accounted for. Particularly at low energies (see Fig. 9), the latter provide most of the splitting between the pp and np phases, with remaining differences originating from isospin symmetry breaking due to the OPE term in v_{12}^L and the central terms in $v_{12}^{S,CD}$, proportional to the LEC's C_i^{IT} and C_i^{IV}

with $i = 0$–2. In the absence of electromagnetic interactions, the splitting between the pp and nn $^1S_0$ phases is induced by the charge-symmetry breaking terms of $v_{12}^{S,CD}$ proportional to the LEC's C_i^{IV} with $i = 0$–2; it is smaller than that between pp and np $^1S_0$ phases.

The effects of isospin symmetry breaking are also seen in the pp and np ^3P_J phases with $J = 0, 1, 2$ in the upper right and lower panels of Fig. 8, especially at the higher energies. The calculated phases, which correspond again to model b, include electromagnetic effects, but the latter are negligible beyond 100 MeV. The splitting between the pp and np ^3P_J phases is mostly due to the isotensor and isovector terms of $v_{12}^{S,CD}$, in particular those proportional to the LEC's C_i^{IV} and C_i^{IT} with $i = 3$ and 4 associated respectively with the tensor and spin-orbit components of $v_{12}^{S,CD}$. There is no evidence on the basis of the Granada and Nijmegen PWA's for such a large splitting, and so the latter is likely to be an artifact of the parametrization adopted for $v_{12}^{S,CD}$.
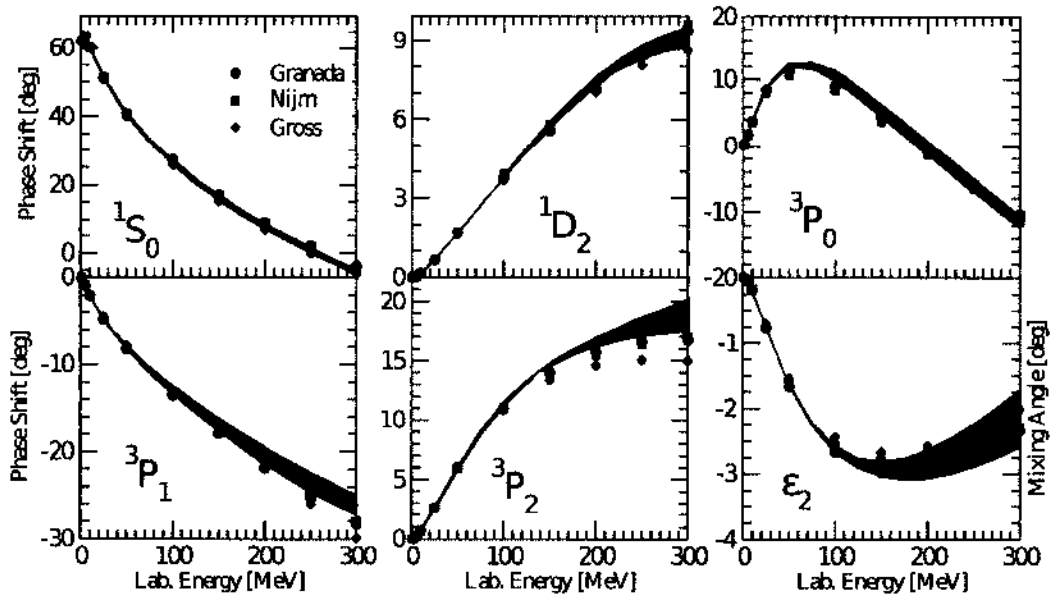
FIG. 6: Same as in Fig. 5, but for the S-wave, P-wave, and D-wave phase shifts in the np T=1 channel. For the mixing angle ϵ_2 the lower limit of the band corresponds to model c and the upper limit to model b.

The static deuteron properties are shown in Table 6 and compared to experimental values [69–73]. The binding energy E_d is fitted exactly and includes the contributions
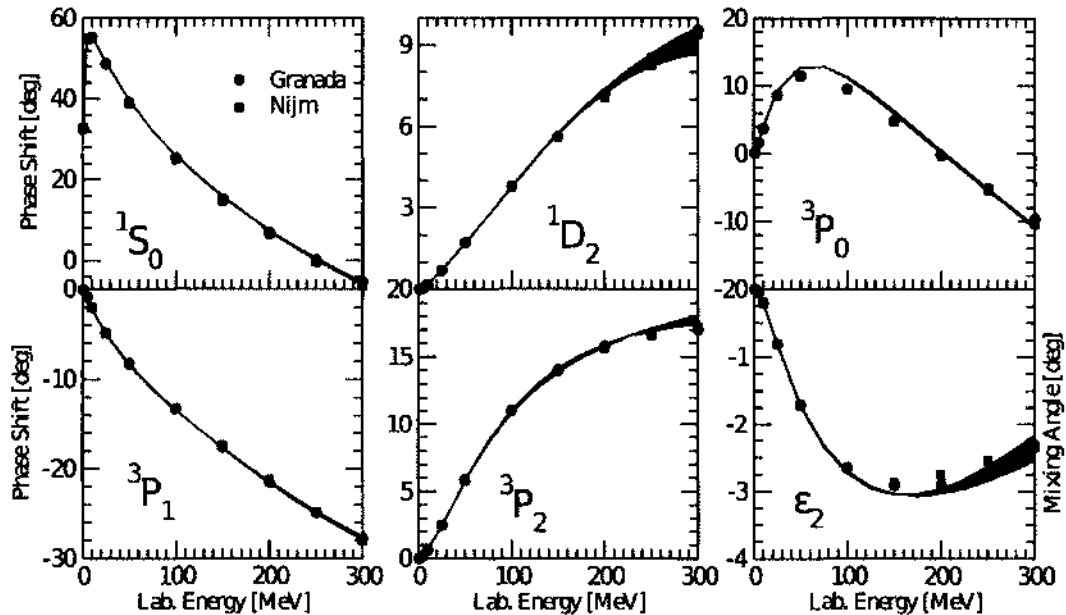
FIG. 7: S-wave, P-wave, and D-wave phase shifts in the pp $T=1$ channel, obtained in the Nijmegen [63, 64] and Navarro Pérez *et al.* [54] partial-wave analysis, are compared to those of models a, b, and c, indicated by the band.

(about 20 keV) of electromagnetic interactions, among which the largest is that due to the magnetic moment term. The asymptotic S-state normalization, A_S, and the D/S ratio, η, are both ~ 2 standard deviations from experiment for all models considered. The deuteron (matter) radius, r_d, is exactly reproduced with model b, but is under-predicted (over-predicted) by about 1.4% (0.7%) with model a (model c). It should be noted that this observable has negligible contributions due to two-body electromagnetic operators as discussed in the next chapter. The magnetic moment, μ_d, and quadrupole moment, Q_d, experimental values are underestimated by all three models, but these observables are known to have significant corrections from (isoscalar) two-body terms in nuclear electromagnetic charge and current (see next chapter). Their inclusion would bring the calculated values considerably closer to, if not in agreement with, experiment. Finally, the S- and D-wave components of the deuteron wave function are displayed in Fig. 10, where they are compared to those of the Argonne v_{18} (AV18) model. There is significant cutoff dependence as
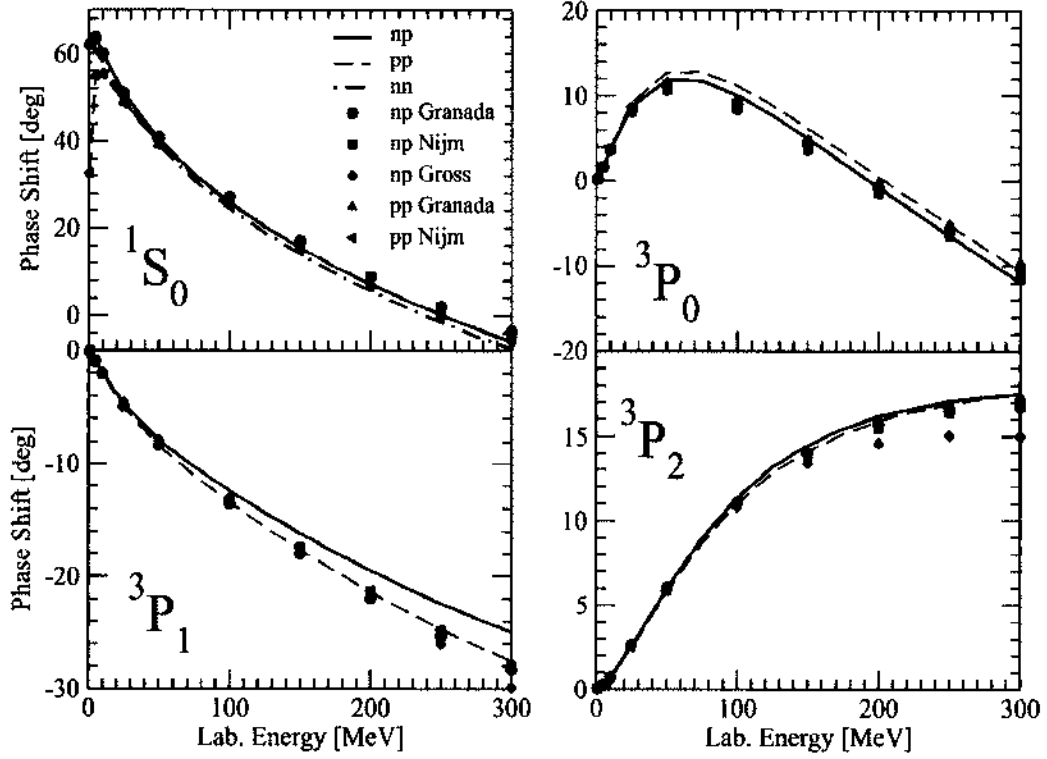
FIG. 8: The pp, np, and nn $^1S_0$ and the pp and np $^3P_0$, $^3P_1$, and $^3P_2$ phase shifts obtained with potential model b, including the full electromagnetic component.

(R_L, R_S) are reduced from the values (1.2, 0.8) fm of model a down to (0.8, 0.6) fm of model c. For $r \lesssim 1$ fm, the S-wave becomes smaller (is pushed out), while the D-wave becomes larger (is pushed in) in going from model a to model c. The D-state percentage increases correspondingly (see Table 6).

We note in closing that in Appendix E we provide figures of the various components of potential models a, b, and c (their charge-independent parts only) as well as tables of numerical values for the pp and np S, P, D, F, and G phase shifts obtained with model b.
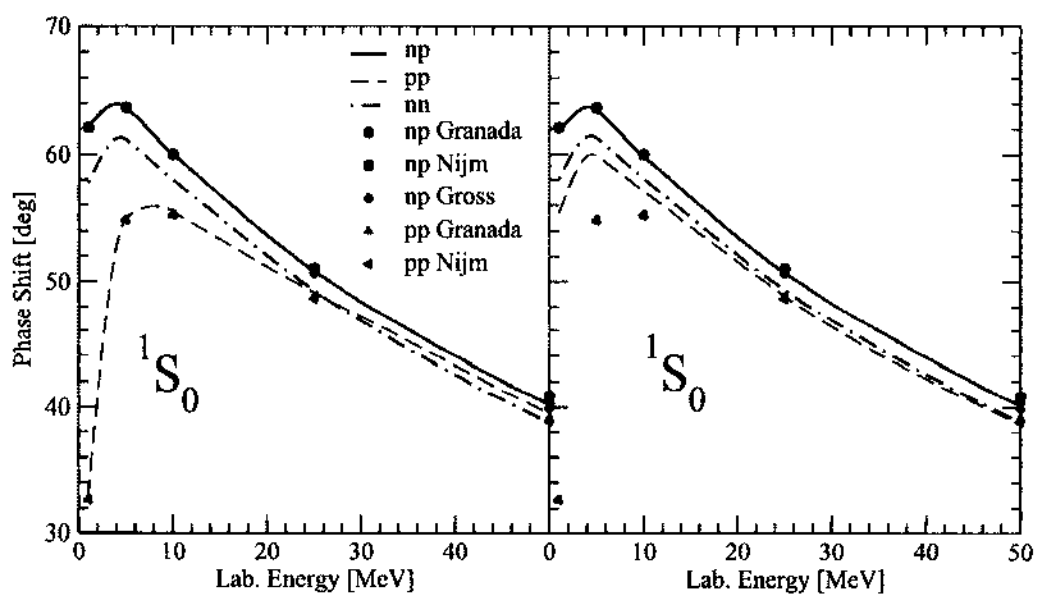
FIG. 9: The pp, np, and nn $^1S_0$ up to lab energy of 50 MeV including (panel left) and ignoring (panel right) the full electromagnetic component of potential model b.

TABLE 4: Fitted values of the LEC's corresponding to potential models a, b, and c. The notation $(\pm n)$ means $10^{\pm n}$.

LEC's	Model a	Model b	Model c
C_S (fm^2)	0.2003672(+1)	0.8841864(+1)	0.2588776(+2)
C_T (fm^2)	-0.1660743(+1)	-0.4168038(+1)	-0.9160861(+1)
C_1 (fm^4)	-0.1759574	-0.9367926(-1)	-0.4455626(-3)
C_2 (fm^4)	-0.2029026	-0.2520756	-0.3082608
C_3 (fm^4)	-0.1856897	-0.2589016	-0.3222661
C_4 (fm^4)	-0.5745498(-1)	-0.2453381(-1)	0.3773411(-1)
C_5 (fm^4)	-0.8813877(-1)	-0.4685034(-1)	-0.5156581(-2)
C_6 (fm^4)	-0.5857848(-1)	-0.2804770(-1)	-0.2762013(-1)
C_7 (fm^4)	-0.1140923	0.7338611	0.7568732
D_1 (fm^6)	-0.9498379(-1)	-0.6986704(-1)	-0.2565252(-1)
D_2 (fm^6)	-0.7149729(-2)	0.1681828(-3)	0.4909682(-2)
D_3 (fm^6)	-0.6502509(-2)	-0.6355876(-2)	-0.1721433(-1)
D_4 (fm^6)	-0.3217370(-2)	-0.1153354(-2)	0.2592172(-2)
D_5 (fm^6)	0.2692050(-2)	0.2258031(-2)	0.2101464(-2)
D_6 (fm^6)	-0.6654712(-2)	-0.2757790(-2)	-0.4252508(-2)
D_7 (fm^6)	-0.2318069(-1)	0.1451856(-1)	0.4247406(-1)
D_8 (fm^6)	-0.2899833(-1)	-0.2897869(-1)	-0.1122591(-1)
D_9 (fm^6)	0.2634392(-2)	0.3909073(-1)	0.4966263(-1)
D_{10} (fm^6)	-0.1787025	-0.2061108	-0.1628166
D_{11} (fm^6)	0.1758785(-1)	0.3667628(-2)	-0.2316157(-1)
D_{12} (fm^6)	0.1126531	0.1023936	0.5361795(-1)
D_{13} (fm^6)	-0.1649902(-1)	-0.9890485(-2)	0.1744601(-2)
D_{14} (fm^6)	0.1989863(-2)	0.3066270(-2)	0.7219031(-2)
D_{15} (fm^6)	0.4540768(-2)	0.2426771(-2)	0.2979197(-2)
C_0^{IV} (fm^2)	-0.8730299(-1)	-0.1162192	0.6195324
C_0^{IT} (fm^2)	0.5804662(-1)	0.6669167(-1)	0.7020630(-1)
C_1^{IV} (fm^4)	0.6961072(-1)	0.5088496(-1)	0.2174468(-1)
C_2^{IV} (fm^4)	0.3507986(-1)	0.2288370(-1)	-0.8112580(-2)
C_3^{IV} (fm^4)	0.3862077(-1)	-0.7707131(-2)	-0.6115902(-1)
C_4^{IV} (fm^4)	-0.7617836	-0.1581137(+1)	-0.1533212(+1)
C_1^{IT} (fm^4)	-0.2382471(-1)	-0.2373048(-1)	0.7623486(-2)
C_2^{IT} (fm^4)	-0.1325513(-1)	-0.1013726(-1)	0.1205547(-2)
C_3^{IT} (fm^4)	-0.1399371(-1)	-0.1098114(-3)	0.2109716(-1)
C_4^{IT} (fm^4)	0.2582607	0.5180368	0.4955952

TABLE 5: The singlet and triplet np, and singlet pp and nn, scattering lengths and effective ranges corresponding to the three potential models with $(R_L, R_S)=(1.2,0.8)$ fm (model a), $(1.0,0.7)$ fm (model b), and $(0.8,0.6)$ fm (model c).

	Experiment	v_{12}^a	w/o v_{12}^{EM}	v_{12}^b	w/o v_{12}^{EM}	v_{12}^c	w/o v_{12}^{EM}
$^1a_{pp}$	-7.8063(26)	-7.766	-17.014	-7.766	-16.956	-7.763	-17.137
	-7.8016(29)						
$^1r_{pp}$	2.794(14)	2.742	2.818	2.743	2.820	2.730	2.802
	2.773(14)						
$^1a_{nn}$	-18.90(40)	-18.867	-19.148	-19.025	-19.301	-18.719	-19.039
$^1r_{nn}$	2.75(11)	2.831	2.827	2.799	2.795	2.738	2.732
$^1a_{np}$	-23.740(20)	-23.752	-23.196	-23.755	-23.248	-23.745	-23.167
$^1r_{np}$	2.77(5)	2.665	2.670	2.672	2.677	2.638	2.644
$^3a_{np}$	5.419(7)	5.408	5.391	5.404	5.389	5.412	5.396
$^3r_{np}$	1.753(8)	1.741	1.740	1.737	1.734	1.740	1.745

TABLE 6: Same as in Table 5 but for the deuteron static properties; experimental values are form Refs. [69–73].

	Experiment	v_{12}^a	v_{12}^b	v_{12}^c
E_d (MeV)	2.224575(9)	2.224575	2.224574	2.224575
$A_S(\mathrm{fm}^{-1/2})$	0.8781(44)	0.8777	0.8904	0.8964
η	0.0256(4)	0.0245	0.0248	0.0246
r_d (fm)	1.97535(85)	1.948	1.975	1.989
μ_d (μ_0)	0.857406(1)	0.852	0.850	0.848
Q_d (fm^2)	0.2859(3)	0.257	0.268	0.269
P_d (%)		4.94	5.29	5.55
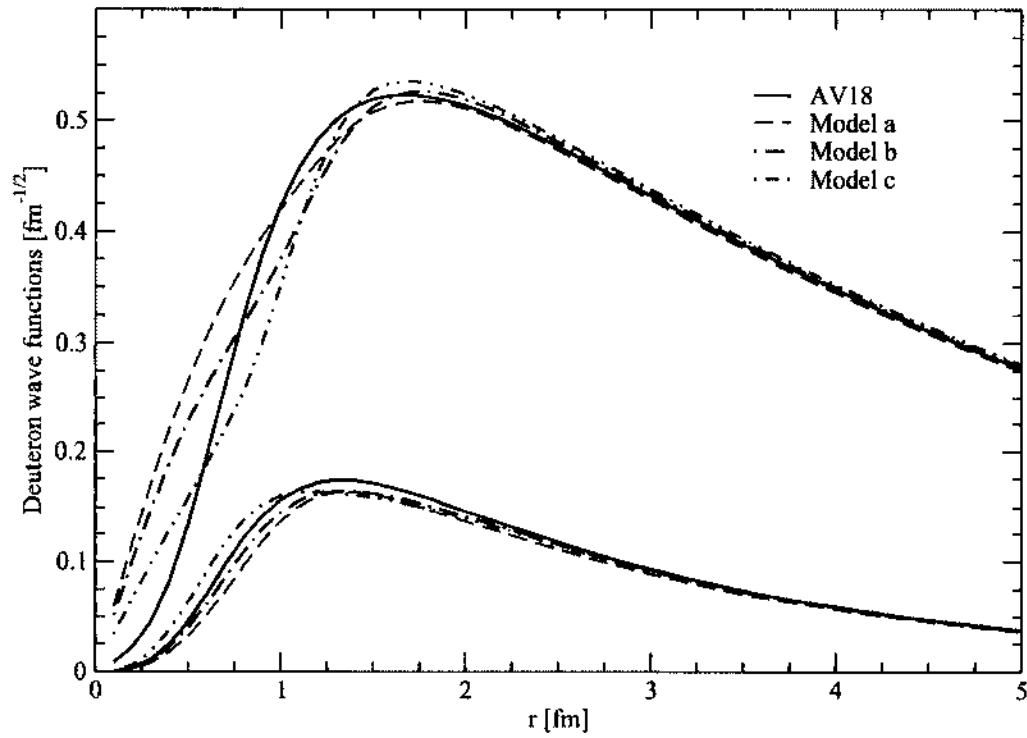
FIG. 10: The S-wave and D-wave components of the deuteron wave function corresponding to models a (dashed lines), b (dotted-dashed lines) and c (dotted-dashed-dotted lines) are compared with those corresponding to the AV18 (solid lines).

CHAPTER 4

ELECTROMAGNETIC STRUCTURE OF A=2 AND 3

NUCLEI IN χEFT

In this Chapter we provide a complete set of χEFT predictions for the structure functions and tensor polarization of the deuteron ($A = 2$), for the charge and magnetic form factors of the ^{3}He and ^{3}H ($A = 3$) as well as for the static properties of these few-nucleon systems. Electromagnetic form factors of these light nuclei are among the observables of choice for testing models of nuclear interactions and associated electromagnetic charge and current operators. Therefore the goal of this study is to investigate the validity of the χEFT approach to describe strong-interaction dynamics in these few-nucleon systems and their response to electromagnetic probes. These calculations are carried out by utilizing nuclear wave functions derived either from chiral or realistic potentials, in combination with the charge and current operators discussed here. In particular, the wave functions for $A = 2$ are obtained from solutions of the Schrödinger equation with the Argonne v_{18} (AV18) [48] or chiral Idaho N3LO [5, 6] two-nucleon potential. Both these nuclear models describe the long-range component of the NN interaction via OPE. In the case of the AV18 potential, the intermediate-range part is parametrized in terms of TPE with intermediate nucleons and Δ isobars [74], while its short-range part is represented by spin-isospin (and momentum-dependent) operators multiplied by Woods-Saxon radial functions [48]. The AV18 potential is directly fit to the Nijmegen NN scattering database [63], which contains 1787 pp and 2514 np data up to laboratory-energy of 350 MeV. With 40 adjustable parameters it gives a χ^2/datum of 1.09 relative to that database which was assembled in the early nineties. The Idaho N3LO potentials are derived within a χEFT formulation with pions and nucleons up to order Q^4. It involves 24 LEC's, which are fixed so as to reproduce the Nijmegen NN scattering database up to laboratory-energy of 290 MeV with a χ^2/datum of 1.3. Wave functions for $A = 3$ nuclei are obtained from a Hamiltonian including, in addition to the AV18 or N3LO two-nucleon, a three-nucleon potential, the Urbana-IX (UIX) [49] or the chiral N2LO [16] model. The UIX model describes

the three-nucleon potential in terms of a TPE three-nucleon term involving the excitation of an intermediate Δ-resonance and a short-range term. Their strengths are adjusted to reproduce the triton binding energy and the saturation density of nuclear matter. The N2LO three-nucleon potential is derived in a χEFT approach involving pions and nucleons up to leading order. It depends on two LEC's, which are constrained to reproduce the binding energy of $A = 3$ nuclei and the tritium Gamow-Teller matrix elements.

The charge and current operators, discussed in Sec. 4.1, are obtained up to one loop ($e\,\mathcal{Q}$ in the power counting) using the formulation based on TOPT as outlined in Chapter 2. In Sec. 4.2 we discuss the methods used to carry out the calculations, and the analysis of the results is presented in Sec. 4.3. Details of loop integrals entering the charge operators are relegated in Appendix F.

4.1 NUCLEAR CHARGE AND CURRENT OPERATORS UP TO ONE LOOP

Nuclear electromagnetic charge (ρ) and current ($\mathbf{j}$) operators—that is the time and vector component of the four-vector current $J^{\mu} = (\rho, \mathbf{j})$—are expressed as an expansion in many-body operators that act on the nucleonic degrees of freedom

$$\rho(\mathbf{q}) = \sum_i \rho_i(\mathbf{q}) + \sum_{i<j} \rho_{ij}(\mathbf{q}) + \cdots , \tag{191}$$

$$\mathbf{j}(\mathbf{q}) = \sum_i \mathbf{j}_i(\mathbf{q}) + \sum_{i<j} \mathbf{j}_{ij}(\mathbf{q}) + \cdots , \tag{192}$$

where ρ_i ($\mathbf{j}_i$) represents the one-body charge (current) operators in which the probing photon, with associated momentum $\mathbf{q}$, interacts with individual nucleons; ρ_{ij} ($\mathbf{j}_{ij}$) are the two-body charge (current) operators, and the ellipsis stands for higher many-body operators.

In the present work we discuss one- and two-body charge and current operators up to one loop ($e\,\mathcal{Q}$) which have been derived in Refs. [29] and [30], respectively. In the following we define

$$\mathbf{k}_i = \mathbf{p}'_i - \mathbf{p}_i , \qquad \mathbf{K}_i = (\mathbf{p}'_i + \mathbf{p}_i)/2 , \tag{193}$$

$$\mathbf{k} = (\mathbf{k}_1 - \mathbf{k}_2)/2 , \qquad \mathbf{K} = \mathbf{K}_1 + \mathbf{K}_2 , \tag{194}$$

where $\mathbf{p}_i$ ($\mathbf{p}'_i$) is the initial (final) momentum of nucleon i. We further define

$$\rho = \sum_{m=-3}^{+1} \rho^{(m)} , \qquad \mathbf{j} = \sum_{m=-2}^{+1} \mathbf{j}^{(m)} , \tag{195}$$

54

(a)   (b)   (c)   (d)   (e)
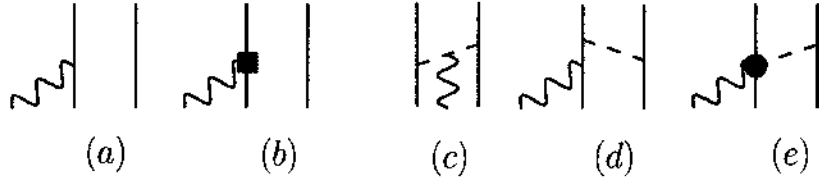
FIG. 11: Diagrams illustrating one- and two-body charge operators entering at $e\, \mathcal{Q}^{-3}$ (LO), $e\, \mathcal{Q}^{-1}$ (N2LO), $e\, \mathcal{Q}^0$ (N3LO). Nucleons, pions, and photons are denoted by solid, dashed, and wavy lines, respectively. The square in panel (b) represents the $(\mathcal{Q}/m_N)^2$ relativistic correction to the LO one-body charge operator, whereas the solid circle in panel (e) is associated with a $\gamma\pi NN$ charge coupling of order $e\,\mathcal{Q}$. Only one among the possible time orderings is shown for the N3LO.

The superscript m in $\rho^{(m)}$ and $\mathbf{j}^{(m)}$, which include both one- and two-body operators, specifies the order $e\, \mathcal{Q}^m$ in the power counting. They follow from the interaction Hamiltonians listed in Appendix A and the perturbative expansion for $v_\gamma^{(m)}$ discussed in Chapter 2.

4.1.1 CHARGE OPERATORS UP TO ONE LOOP

Contributions to the charge operators up to N3LO ($e\, \mathcal{Q}^0$) and N4LO ($e\, \mathcal{Q}$) are represented in Fig. 11 and Fig. 12, respectively. According to the power counting, the LO ($e\, \mathcal{Q}^{-3}$) charge operator results from the coupling of the external photon to the individual nucleons (panel (a) of Fig. 11) and reads:

$$\rho^{(-3)} = e\, e_{N,1}(q^2) + (1 \rightleftharpoons 2) \,, \tag{196}$$

where

$$e_{N,i}(q^2) = \frac{G_E^S(q^2) + G_E^V(q^2)\, \tau_{i,z}}{2} \,, \tag{197}$$

and $G_E^{S/V}$ denote the isoscalar/isovector combinations of the proton and neutron electric (E) form factors, normalized as $G_E^S(0) = G_E^V(0) = 1$. The power counting $e\, \mathcal{Q}^{-3}$ follows from the product of a factor $e\, \mathcal{Q}^0$ associated with the Hamiltonian $H_{\gamma NN}$ in Appendix A, and a factor $\mathcal{Q}^{-3}$ due to the momentum-conserving δ-function implicit in this type of disconneted terms. Of course, this counting ignores the fact that the
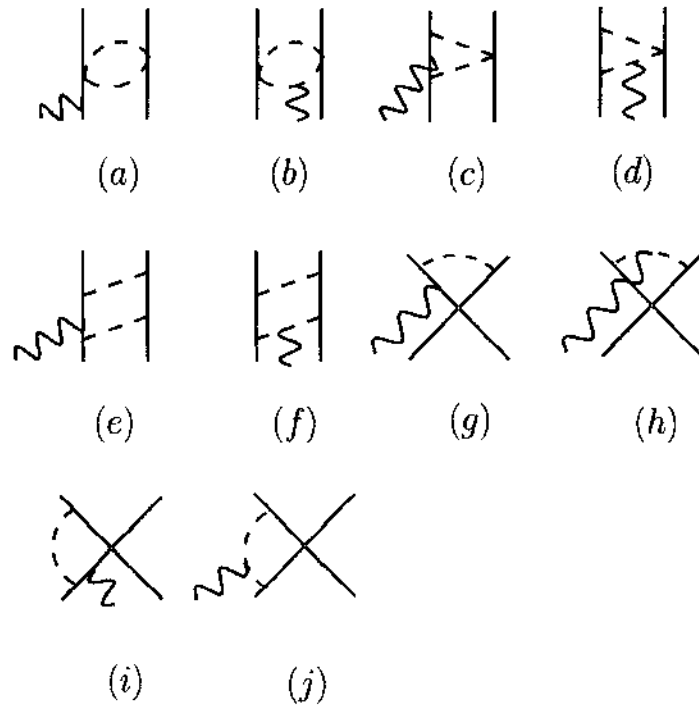
FIG. 12: Diagrams illustrating two-body charge operators entering at order $e\,Q$ (N4LO). Nucleons, pions, and photons are denoted by the solid, dashed, and wavy lines, respectively. Only one among the possible time orderings is shown.

nucleon electric form factors (as well as the magnetic form factors below) themselves also have a power series expansion in Q. Here, they are taken from fits to elastic electron scattering data off the proton and deuteron [75]—specifically, the Höhler parametrization [76]—rather than derived consistently in chiral perturbation theory (χPT) [77]. The calculations of the $A = 2$ and 3 nuclei elastic form factors that follow are carried out in the Breit frame, in which the electron-energy transfer vanishes. Hence, the hadronic electromagnetic form factors are evaluated at four-momentum transfer $Q_\mu^2 \equiv -q^\mu q_\mu = q^2$.

At NLO ($e\,Q^{-2}$) there are no contributions to the charge operators, while at N2LO ($e\,Q^{-1}$) we can distinguish three types of diagrams: i) a relativistic correction to the LO charge operator (panel (b) of Fig. 11); ii) a pion-in-flight term (panel (c) of Fig. 11); and iii) a one-pion-exchange (OPE) contribution (panel (d) of Fig. 11). The relativistic correction of order $(Q/m_N)^2$ to the LO charge operators, coming from the second order γNN Hamiltonian $H_{\gamma NN}^{(2)}$, is given by

$$\rho^{(-1)} = -\frac{e}{8\,m_N^2} \left[2\,\mu_{N,1}(q^2) - e_{N,1}(q^2) \right] \left(q^2 + 2\,i\,\mathbf{q} \cdot \boldsymbol{\sigma}_1 \times \mathbf{K}_1 \right) + (1 \rightleftharpoons 2) \,, \quad (198)$$

where $\mu_{N,i}(q^2)$ is defined as

$$\mu_{N,i}(q^2) = \frac{G_M^S(q^2) + G_M^V(q^2)\,\tau_{i,z}}{2} \,, \quad (199)$$

and $G_M^{S/V}$ denote the isoscalar/isovector combinations of the proton and neutron magnetic (M) form factors, normalized as $G_M^S(0) = \mu^S$, and $G_M^V(0) = \mu^V$ with μ^S and μ^V denoting the isoscalar and isovector combinations of the proton and neutron magnetic moments, $\mu^S = 0.88$ and $\mu^V = 4.706$ in units of nuclear magnetons μ_N. The pion-in-flight term, panel (c) of Fig. 11, vanishes when all the six time-ordered diagrams, evaluated in the static limit, are summed up. The OPE contribution, panel (d) of Fig. 11, has reducible and irreducible diagrams. The reducible ones are not considered since they are generated by iterations of the Lippman-Schwinger equation as discussed in Chapter 2, while the static irreducible contributions are exactly cancelled from the first non-static corrections to the reducible terms [30]. Note that, hereafter, momentum conserving δ-functions ($\mathbf{q} = \mathbf{k}_i$) for the $\rho^{(-3)}$ and $\rho^{(-1)}$, and ($\mathbf{k}_1 + \mathbf{k}_2 = \mathbf{q}$) for the following expressions of the two-body operators, have been dropped for brevity.

The N3LO ($e\,Q^0$) contribution illustrated in panel (e) of Fig. 11 is associated with the Hamiltonian $H_{\gamma\pi NN}$ in Appendix A. The evalution of the corresponding

amplitude gives rise to the following expression

$$\rho_e^{(0)} = \frac{e}{2\,m_N}\frac{g_A^2}{F_\pi^2}[G_E^S(q^2)\,\boldsymbol{\tau}_1\cdot\boldsymbol{\tau}_2 + G_E^V(q^2)\tau_{2,z}]\frac{\boldsymbol{\sigma}_1\cdot\mathbf{q}\,\boldsymbol{\sigma}_2\cdot\mathbf{k}_2}{\omega_{k_2}^2} + (1\rightleftharpoons 2)\,, \qquad (200)$$

with $\omega_{k_i}^2 = k_i^2 + m_\pi^2$. In the present χEFT contest, $\rho_e^{(0)}$ was first derived in Ref. [78]. At this order, there are also contributions originating from non-static terms in the diagrams in panels (c) and (d) of Fig. 11, obtained by expanding the energy denominators involving pions as in Eq. (5). They are given, respectively, by

$$\rho_c^{(0)} = i\,\frac{e}{m_N}\frac{g_A^2}{F_\pi^2}\,G_\pi(q^2)\,(\boldsymbol{\tau}_1\times\boldsymbol{\tau}_2)_z\,\frac{\boldsymbol{\sigma}_1\cdot\mathbf{k}_1\boldsymbol{\sigma}_2\cdot\mathbf{k}_2}{\omega_{k_1}^2\,\omega_{k_2}^2}\,\mathbf{k}_1\cdot\mathbf{K}_1 + (1\rightleftharpoons 2)\,, \qquad (201)$$

$$\begin{aligned}
\rho_d^{(0)}(\nu) = &-\frac{e}{4\,m_N}\frac{g_A^2}{F_\pi^2}\frac{\boldsymbol{\sigma}_1\cdot\mathbf{k}_2\boldsymbol{\sigma}_2\cdot\mathbf{k}_2}{\omega_{k_2}^4}\Bigg[(1-\nu)\,[G_E^S(q^2)\,\boldsymbol{\tau}_1\cdot\boldsymbol{\tau}_2 + G_E^V(q^2)\tau_{z,1}]\,\mathbf{q}\cdot\mathbf{k}_2 \\
&+2\,i\,G_E^V(q^2)\,(\boldsymbol{\tau}_1\times\boldsymbol{\tau}_2)_z\,\mathbf{k}_2\cdot\Big[(1+\nu)\,\mathbf{K}_2 + (1-\nu)\mathbf{K}_1\Big]\Bigg] + (1\rightleftharpoons 2)\,,
\end{aligned}$$
$$\qquad (202)$$

where $G_\pi(q^2)$ is the pion form factor, which we parametrize in vector-meson dominance and consistently with experimental data at low momentum transfers as

$$G_\pi(q^2) = \frac{1}{1+q^2/m_\rho^2}\,, \qquad (203)$$

where m_ρ is the ρ-meson mass. The operator of panel (d) of Fig. 11 depends on the off-energy-shell extrapolation, specified by the parameter ν, adopted for the non-static corrections of order $m = 2$ (Q^2) to the OPE potential, retained in Eq. (11), which is parametrized by [79]

$$v_\pi^{(2)}(\mathbf{k},\mathbf{K};\nu) = (1-2\,\nu)\,\frac{v_\pi^{(0)}(\mathbf{k})}{\omega_k^2}\,\frac{(\mathbf{k}\cdot\mathbf{K})^2}{4\,m_N^2}\,, \qquad (204)$$

where $v_\pi^{(0)}(\mathbf{k})$ is the static OPE potential

$$v_\pi^{(0)}(\mathbf{k}) = -\frac{g_A^2}{F_\pi^2}\,\boldsymbol{\tau}_1\cdot\boldsymbol{\tau}_2\,\frac{\boldsymbol{\sigma}_1\cdot\mathbf{k}\,\boldsymbol{\sigma}_2\cdot\mathbf{k}}{\omega_k^2}\,. \qquad (205)$$

As shown in Ref. [79] (and within the present approach in Refs. [30] and [31]), different off-shell prescriptions for $v^{(2)}(\nu)$ and $\rho^{(0)}(\nu)$ are unitarily equivalent:

$$\begin{aligned}
\rho^{(-3)}+\rho_d^{(0)}(\nu) &= \mathrm{e}^{-i\,U(\nu)}\left[\rho^{(-3)} + \rho_d^{(0)}(\nu=0)\right]\mathrm{e}^{+i\,U(\nu)} \\
&\simeq \rho^{(-3)}+\rho_d^{(0)}(\nu=0)+\left[\rho^{(-3)},i\,U^{(0)}(\nu)\right]\,, \qquad (206)
\end{aligned}$$

where the hermitian operator $U(\nu)$ admits the expansion

$$U(\nu) = U^{(0)}(\nu) + U^{(1)}(\nu) + \ldots \, , \qquad (207)$$

and $U^{(0)}(\nu)$ and $U^{(1)}(\nu)$ have been constructed, respectively, in Refs. [79] and [30]. A common choice for this parametrization is given by $\nu = 1/2$ in Eq. (204), which removes non-static corrections to the OPE potential (these corrections are typically ignored in chiral and realistic potentials).

The two-body charge operators at one loop (N4LO, $e\,Q$) are illustrated in Fig. 12, and have been discussed in Ref. [30]. In particular, the contribution arising from diagram of type (a) in Fig. 12 vanishes due to an exact cancellation between the static irreducible terms and the non-static corrections associated with the reducible ones, while the pion-in-flight contributions, illustrated in panel (b) of Fig. 12, vanishes (in the static limit) when all the contributions of time-ordered diagrams are summed up. The contributions of diagrams in panels (g)–(h) of Fig. 12 also vanish. After carrying out the loop integrations (discussed in App. F), the contributions from diagrams of type (c)–(f) and (i)–(j) in Fig. 12 read

$$\rho_{\mathrm{c}}^{(1)} = -e\,\frac{1}{2\,\pi}\,\frac{g_A^2}{F_\pi^4}\,G_E^V(q^2)\,\tau_{2,z}\,\int_0^{1/2} \mathrm{d}x\,\left[4\,L(x,k_2) - \frac{m_\pi^2}{L(x,k_2)}\right] + (1 \rightleftharpoons 2)\,, \quad (208)$$

$$\rho_{\mathrm{d}}^{(1)} = e\,\frac{1}{2\,\pi}\,\frac{g_A^2}{F_\pi^4}\,G_\pi(q^2)\,\tau_{2,z}\,\int_0^{1/2} \mathrm{d}x\,\left[4\,L(x,k_1) - \frac{m_\pi^2}{L(x,k_1)}\right] + (1 \rightleftharpoons 2)\,, \qquad (209)$$

$$\rho_{\mathrm{e}}^{(1)}(\nu) = -e\,\frac{1}{16\,\pi}\,\frac{g_A^4}{F_\pi^4}\,G_E^V(q^2)\,\int_0^{1/2} \mathrm{d}x\,\left[\,[4\,\tau_{2,z} + \nu\,(\tau_1 \times \tau_2)_z]\left[-24\,L(x,k_2)\right.\right.$$

$$+\frac{k_2^2 + 8\,m_\pi^2}{L(x,k_2)} + \frac{m_\pi^4}{L^3(x,k_2)}\right] + [4\,\tau_{1,z} - \nu\,(\tau_1 \times \tau_2)_z]\,\frac{(\sigma_2 \times \mathbf{k}_2) \cdot (\sigma_1 \times \mathbf{k}_2)}{L(x,k_2)}\right]$$

$$+(1 \rightleftharpoons 2)\,, \qquad (210)$$

$$
\begin{aligned}
\rho_{\mathrm{f}}^{(1)} \;=\; & -e\frac{1}{8\,\pi}\frac{g_A^4}{F_\pi^4}\,G_\pi(q^2)\int_0^1 \mathrm{d}x\,x\int_{-1/2}^{1/2}\mathrm{d}y\Bigg[-2\,\tau_{1,z}\Bigg[-15\,\lambda(x,y)+\frac{1}{\lambda(x,y)} \\
& \times\Big[3\,\mathbf{A}\cdot(\mathbf{B}+\mathbf{C})+(\mathbf{A}+\mathbf{B})\cdot(\mathbf{A}+\mathbf{C})+(\boldsymbol{\sigma}_1\times\mathbf{A})\cdot(\boldsymbol{\sigma}_2\times\mathbf{A}) \\
& -(\boldsymbol{\sigma}_1\times\mathbf{A})\cdot(\boldsymbol{\sigma}_2\times\mathbf{C})-(\boldsymbol{\sigma}_1\times\mathbf{B})\cdot(\boldsymbol{\sigma}_2\times\mathbf{A})+(\boldsymbol{\sigma}_1\times\mathbf{B})\cdot(\boldsymbol{\sigma}_2\times\mathbf{C})\Big] \\
& +\frac{1}{\lambda^3(x,y)}\Big[(\mathbf{A}\cdot\mathbf{B})(\mathbf{A}\cdot\mathbf{C})+\boldsymbol{\sigma}_1\cdot(\mathbf{A}\times\mathbf{B})\,\boldsymbol{\sigma}_2\cdot(\mathbf{A}\times\mathbf{C})\Big]\Big] \\
& +\frac{1}{\lambda(x,y)}\,(\boldsymbol{\tau}_1\times\boldsymbol{\tau}_2)_z\Big[-3\,\boldsymbol{\sigma}_2\cdot(\mathbf{A}\times\mathbf{C})-\mathbf{B}\cdot(\boldsymbol{\sigma}_2\times\mathbf{A}) \\
& +(\mathbf{A}+\mathbf{B})\cdot(\boldsymbol{\sigma}_2\times\mathbf{C})-\frac{1}{\lambda^2(x,y)}\mathbf{A}\cdot\mathbf{B}\,\boldsymbol{\sigma}_2\cdot(\mathbf{A}\times\mathbf{C})\Big]\Bigg]+(1\rightleftharpoons 2)\,, \quad (211)
\end{aligned}
$$

$$
\rho_{\mathrm{i}}^{(1)} \;=\; e\,\frac{1}{\pi}\frac{g_A^2}{F_\pi^2}\,C_T\,G_V^E(q^2)\,\tau_{1,z}\,\boldsymbol{\sigma}_1\cdot\,\boldsymbol{\sigma}_2\,m_\pi+(1\rightleftharpoons 2)\,, \quad (212)
$$

$$
\begin{aligned}
\rho_{\mathrm{j}}^{(1)} \;=\; & -e\,\frac{1}{\pi}\frac{g_A^2}{F_\pi^2}\,C_T\,G_\pi(q^2)\,\tau_{1,z}\int_0^{1/2}\mathrm{d}x\Bigg[\frac{3\,L^2(x,q)-m_\pi^2}{L(x,q)}\boldsymbol{\sigma}_1\cdot\boldsymbol{\sigma}_2 \\
& -\frac{1/4-x^2}{L(x,q)}\,\boldsymbol{\sigma}_1\cdot\mathbf{q}\,\boldsymbol{\sigma}_2\cdot\mathbf{q}\Bigg]+(1\rightleftharpoons 2)\,, \quad (213)
\end{aligned}
$$

where

$$
L^2(x,p)=(1/4-x^2)\,\mathbf{p}^2+m_\pi^2\,, \quad (214)
$$

$$
\lambda^2(x,y)=x\,\mathbf{q}^2/4-\big[x\,y\,\mathbf{q}-(1-x)\,\mathbf{k}\big]^2+(1-x)\,\mathbf{k}^2+m_\pi^2\,, \quad (215)
$$

$$
\mathbf{A}\;=\;-x\,(y\,\mathbf{q}+\mathbf{k})\,, \quad (216)
$$

$$
\mathbf{B}\;=\;(1-2\,x\,y)\,\mathbf{q}/2+(1-x)\,\mathbf{k}\,, \quad (217)
$$

$$
\mathbf{C}\;=\;-(1+2\,x\,y)\,\mathbf{q}/2+(1-x)\,\mathbf{k}\,. \quad (218)
$$

Note that, due to global charge conservation, contributions beyond the LO term vanish at $\mathbf{q}=0$. The loop integrals entering the expressions of charge operators at $e\,Q$ are ultraviolet divergent. However the charge operator at N4LO is finite since the divergencies associated with diagrams (c) and (d), (e) and (f), and (i) and (j) in Fig. 12 cancel out [30]. This is in line with the fact that there are no counter terms at this order. Finally, we note that the form of the operator (e) in Fig. 12 depends on the off-the-energy-shell prescription adopted for the non-static corrections to the TPE potential. As in the OPE case, however, these different forms for the TPE non-static potential and accompanying charge operator are unitarily equivalent [30].
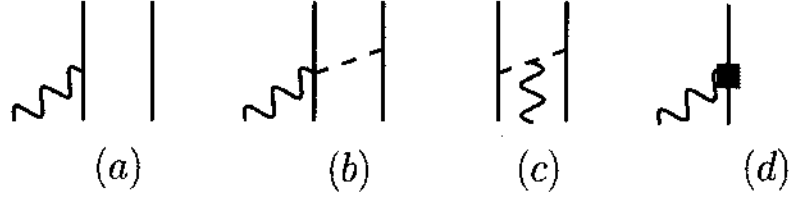
FIG. 13: Diagrams illustrating one- and two-body current operators entering at $e\,\mathcal{Q}^{-2}$ (LO), $e\,\mathcal{Q}^{-1}$ (NLO), $e\,\mathcal{Q}^{0}$ (N2LO). Nucleons, pions, and photons are denoted by solid, dashed, and wavy lines, respectively. The square in panel (d) represents the $(\mathcal{Q}/m_N)^2$ relativistic correction to the LO one-body current operator. Only one among the possible time orderings is shown for the NLO.

4.1.2 CURRENTS OPERATORS UP TO ONE LOOP

The contributions to the electromagnetic current operator up to N2LO $(e\,\mathcal{Q}^0)$ and N3LO $(e\,\mathcal{Q})$ are illustrated diagrammatically in Fig. 13 and Fig. 14, respectively.

The lowest order $e\,\mathcal{Q}^{-2}$ (LO) consists of the single-nucleon convection and spin-magnetization currents

$$\mathbf{j}_a^{(-2)} \;=\; \frac{e}{2\,m_N}\left[\,2\,e_{N,1}(q^2)\,\mathbf{K}_1 + i\,\mu_{N,1}(q^2)\,\boldsymbol{\sigma}_1\times\mathbf{q}\right] + (1 \rightleftharpoons 2)\;,\tag{219}$$

where $e_{N,i}(q^2)$ and $\mu_{N,i}(q^2)$ have been defined in Eqs. (197)–(199), respectively.

At order $e\,\mathcal{Q}^{-1}$ (NLO) there are contributions arising from panels (b) and (c) of Fig. 13. The evaluation of these diagrams in the static limit leads to

$$\mathbf{j}_b^{(-1)} \;=\; -i\,e\frac{g_A^2}{F_\pi^2}\,G_E^V(q^2)\,(\boldsymbol{\tau}_1\times\boldsymbol{\tau}_2)_z\boldsymbol{\sigma}_1\frac{\boldsymbol{\sigma}_2\cdot\mathbf{k}_2}{\omega_{k_2}^2} + (1\rightleftharpoons 2)\;,\tag{220}$$

$$\mathbf{j}_c^{(-1)} \;=\; i\,e\frac{g_A^2}{F_\pi^2}\,G_E^V(q^2)\,(\boldsymbol{\tau}_1\times\boldsymbol{\tau}_2)_z\frac{\mathbf{k}_1-\mathbf{k}_2}{\omega_{k_1}^2\,\omega_{k_2}^2}\,\boldsymbol{\sigma}_1\cdot\mathbf{k}_1\,\boldsymbol{\sigma}_2\cdot\mathbf{k}_2\;,\tag{221}$$

where a δ-function representing the overall momentum conservation has been dropped.

The $e\,\mathcal{Q}^0$ (N2LO) current is represented by the one-body operator in panel (d) of
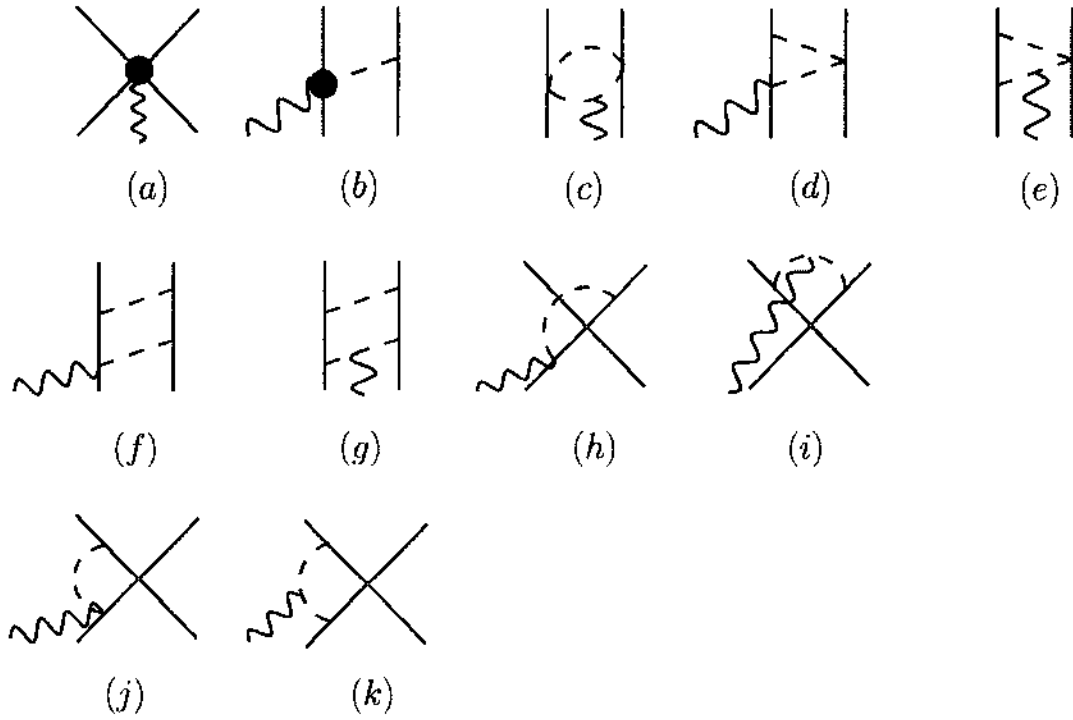
FIG. 14: Diagrams illustrating two-body current operators entering at order $e\,\mathcal{Q}$ (N3LO). Nucleons, pions, and photons are denoted by the solid, dashed, and wavy lines, respectively. The solid circle in panel (b) is associated with the $\gamma\pi N$ current coupling of order $e\,\mathcal{Q}$, involving the LEC's d'_8, d'_9, and d'_{21}; the solid circle in panel (a) denotes two-body contact terms of minimal and non-minimal nature, the latter involving the LEC's C'_{15} and C'_{16}.

Fig. 13, due to the relativistic correction of order $(Q/m_N)^2$ to the LO. It reads:

$$\mathbf{j}_d^{(0)} = -\frac{e}{8\,m_N^3} e_{N,1}(q^2) \left[2\left(K_1^2 + q^2/4\right)\left(2\,\mathbf{K}_1 \right.\right.$$

$$\left. +i\,\boldsymbol{\sigma}_1 \times \mathbf{q}\right) + \mathbf{K}_1 \cdot \mathbf{q}\,\left(\mathbf{q} + 2\,i\,\boldsymbol{\sigma}_1 \times \mathbf{K}_1\right)\right]$$

$$-\frac{i\,e}{8\,m_N^3}\left[\mu_{N,1}(q^2) - e_{N,1}(q^2)\right]\left[\mathbf{K}_1 \cdot \mathbf{q}\right.$$

$$\times\left(4\,\boldsymbol{\sigma}_1 \times \mathbf{K}_1 - i\,\mathbf{q}\right) - \left(2\,i\,\mathbf{K}_1 - \boldsymbol{\sigma}_1 \times \mathbf{q}\right)q^2/2$$

$$\left. +2\left(\mathbf{K}_1 \times \mathbf{q}\right)\boldsymbol{\sigma}_1 \cdot \mathbf{K}_1\right] + (1 \rightleftharpoons 2)\,. \tag{222}$$

Finally, the currents at order $e\,Q$ (N3LO) are illustrated diagrammatically in Fig. 14, and consist of: (i) terms generated by minimal substitution in the four-nucleon contact interactions involving two gradients of the nucleon fields as well as by non-minimal couplings to the electromagnetic field (panel (a) of Fig. 14); (ii) OPE terms induced by $\gamma\pi NN$ interactions beyond leading order (panel (b) of Fig. 14); and (iii) one-loop two-pion-exchange (TPE) terms (panels (c)-(k) of Fig. 14). We discuss them below.

The contact minimal and non minimal currents, denoted by the subscripts "min" and "nm" respectively, are written as

$$\mathbf{j}_{a,\text{min}}^{(1)} = \frac{i\,e}{16} G_E^V(q^2)\,(\boldsymbol{\tau}_1 \times \boldsymbol{\tau}_2)_z \left[(C_2 + 3C_4 + C_7)\,\mathbf{k}_1 + (C_2 - C_4 - C_7)\,\mathbf{k}_1\,\boldsymbol{\sigma}_1 \cdot \boldsymbol{\sigma}_2\right.$$

$$\left. +C_7\,\boldsymbol{\sigma}_1 \cdot (\mathbf{k}_1 - \mathbf{k}_2)\,\boldsymbol{\sigma}_2\right] - \frac{i\,e}{4} e_{N,1}(q^2)\,C_5\,(\boldsymbol{\sigma}_1 + \boldsymbol{\sigma}_2) \times \mathbf{k}_1 + (1 \rightleftharpoons 2)\,, \tag{223}$$

$$\mathbf{j}_{a,\text{nm}}^{(1)} = -i\,e\left[G_E^S(q^2)\,C_{15}'\,\boldsymbol{\sigma}_1 + G_E^V(q^2)\,C_{16}'(\tau_{1,z} - \tau_{2,z})\,\boldsymbol{\sigma}_1\right] \times \mathbf{q} + (1 \rightleftharpoons 2)\,. \tag{224}$$

The low-energy constants (LEC's) $C_1, \ldots, C_7$, which also enter the two-nucleon contact potential, have been constrained by fitting np and pp elastic scattering data and the deuteron binding energy. We take their values from the Machleidt and Entem 2011 review paper [5], since the potential discussed in the previous section was developed at a later time. The LEC's C_{15}' and C_{16}' (and d_8', d_9', and d_{21}' below) are determined by fitting photonuclear data of the $A = 2$ and 3 systems, as discussed in Sec. 4.3.

The isovector (IV) OPE current at N3LO (panel (b) of Fig. 14) is given by

$$\mathbf{j}_{b,\text{IV}}^{(1)} = i\,e\,\frac{g_A}{F_\pi^2}\frac{G_{\gamma N\Delta}(q^2)}{\mu_{\gamma N\Delta}}\frac{\boldsymbol{\sigma}_2 \cdot \mathbf{k}_2}{\omega_{k_2}^2}\left[d_8'\tau_{2,z}\,\mathbf{k}_2 - d_{21}'(\boldsymbol{\tau}_1 \times \boldsymbol{\tau}_2)_z\,\boldsymbol{\sigma}_1 \times \mathbf{k}_2\right] \times \mathbf{q} + (1 \rightleftharpoons 2)\,,$$

$$\tag{225}$$

and depends on the two (unknown) LEC's d'_8 and d'_{21}. They can be related [28] to the N-Δ transition axial coupling constant and magnetic moment (denoted as $\mu_{\gamma N \Delta}$) in a resonance saturation picture, which justifies the use of the $\gamma N \Delta$ electromagnetic form factor for this term. It is parametrized as

$$G_{\gamma N \Delta}(q^2) = \frac{\mu_{\gamma N \Delta}}{(1 + q^2/\Lambda_{\Delta,1}^2)^2 \sqrt{1 + q^2/\Lambda_{\Delta,2}^2}} \ , \tag{226}$$

where $\mu_{\gamma N \Delta}$ is taken as $3\,\mu_N$ from an analysis of γN data in the Δ-resonance region [80]. This analysis also gives $\Lambda_{\Delta,1}$=0.84 GeV and $\Lambda_{\Delta,2}$=1.2 GeV. The isoscalar (IS) piece of the OPE current depends on the LEC d'_9 mentioned earlier,

$$\mathbf{j}_{b,IS}^{(1)} = i\,c\,\frac{g_A}{F_\pi^2}\,d'_9\,G_{\gamma \pi \rho}(q^2)\,\boldsymbol{\tau}_1 \cdot \boldsymbol{\tau}_2\,\frac{\boldsymbol{\sigma}_2 \cdot \mathbf{k}_2}{\omega_{k_2}^2}\,\mathbf{k}_2 \times \mathbf{q} + (1 \rightleftharpoons 2) \ , \tag{227}$$

and, again in a resonance saturation picture, this reduces to the well known $\gamma \pi \rho$ current [29]. Accordingly, we have accounted for the q^2 fall-off of the electromagnetic vertex by including a $\gamma \pi \rho$ form factor, which in vector-meson dominance is parametrized as

$$G_{\gamma \pi \rho}(q^2) = \frac{1}{1 + q^2/m_\omega^2} \ , \tag{228}$$

m_ω is the ω-meson mass.

The one-loop TPE currents, diagrams (c)–(g) in Fig. 14, are written [29] as

$$\begin{aligned}
\mathbf{j}_{loop}^{(1)} = {}&-i\,e\,G_E^V(q^2)\,(\boldsymbol{\tau}_1 \times \boldsymbol{\tau}_2)_z\,\boldsymbol{\nabla}_k\,F_1(k) + i\,e\,G_E^V(q^2)\,\tau_{2,z} \\
&\times \left[F_0(k)\,\boldsymbol{\sigma}_1 - F_2(k)\,\frac{\mathbf{k}\,\boldsymbol{\sigma}_1 \cdot \mathbf{k}}{k^2} \right] \times \mathbf{q} + (1 \rightleftharpoons 2) \ ,
\end{aligned} \tag{229}$$

where the functions $F_i(k)$ are

$$\begin{aligned}
F_0(k) = {}&\frac{g_A^2}{8\,\pi^2 F_\pi^4} \left[1 - 2\,g_A^2 + \frac{8\,g_A^2\,m_\pi^2}{k^2 + 4\,m_\pi^2} + G(k) \left[2 - 2\,g_A^2 \right.\right.\\
&\left.\left. - \frac{4\,(1 + g_A^2)\,m_\pi^2}{k^2 + 4\,m_\pi^2} + \frac{16\,g_A^2\,m_\pi^4}{(k^2 + 4\,m_\pi^2)^2} \right] \right] \ ,
\end{aligned} \tag{230}$$

$$\begin{aligned}
F_1(k) = {}&\frac{1}{96\,\pi^2 F_\pi^4}\,G(k) \left[4m_\pi^2(1 + 4g_A^2 - 5g_A^4) \right.\\
&\left. + k^2(1 + 10g_A^2 - 23g_A^4) - \frac{48\,g_A^4 m_\pi^4}{4\,m_\pi^2 + k^2} \right] \ ,
\end{aligned} \tag{231}$$

$$\begin{aligned}
F_2(k) = {}&\frac{g_A^2}{8\,\pi^2 F_\pi^4} \left[2 - 6\,g_A^2 + \frac{8\,g_A^2\,m_\pi^2}{k^2 + 4\,m_\pi^2} + G(k) \left[4\,g_A^2 \right.\right.\\
&\left.\left. - \frac{4\,(1 + 3\,g_A^2)\,m_\pi^2}{k^2 + 4\,m_\pi^2} + \frac{16\,g_A^2\,m_\pi^4}{(k^2 + 4\,m_\pi^2)^2} \right] \right] \ ,
\end{aligned} \tag{232}$$

and the loop function $G(k)$ is defined as

$$G(k) = 2 \frac{\sqrt{4\,m_\pi^2 + k^2}}{k} \ln \frac{\sqrt{4\,m_\pi^2 + k^2} + k}{2\,m_\pi} \ . \tag{233}$$

Finally, we note that the analysis, detailed in Appendix B in Ref. [31], of the loop short-range currents corresponding to diagrams (h) (k) in Fig. 14 shows that they vanish. We also note that the electromagnetic current operator $\mathbf{j}$ up to one loop $(e\,\mathcal{Q})$ satisfies the continuity equation with the potential v_{12} at NLO $(\mathcal{Q}^2)$ such that

$$\mathbf{q} \cdot \mathbf{j} = \left[\frac{\mathbf{p}_1^2}{2\,m_N} + \frac{\mathbf{p}_2^2}{2\,m_N} + v_{12}, \rho \right] \ , \tag{234}$$

where $\mathbf{q}$ is the momentum transfer by the external photon, $\mathbf{p}_i$ is the initial momentum of nucleon i, and the charge operator ρ includes terms up to $e\,\mathcal{Q}^{(-1)}$. In the χEFT formulation, the current is conserved order by order in the power counting. The relations implied by matching powers in Eq. (234) have been verified explicitly in Ref. [28]. Recall that a commutator brings in an additional $\mathcal{Q}^3$ factor in overall power counting.

4.2 CALCULATION

This section is divided in two subsections. The first one deals with the definition of the electromagnetic form factors for $A = 2$ and 3 nuclei, while in the second one we outline the method used to evaluate the matrix elements of the charge and current operator required in the calculation of those form factors.

4.2.1 FEW-NUCLEON FORM FACTORS

Deuterium is a spin-one nucleus and so has three independent form factors: G_C, G_M, and G_Q, respectively charge, magnetic and quadrupole form factors. They are related to the electromagnetic operators in the following way [81]

$$G_C(q) = \frac{1}{3} \sum_{M=\pm 1,0} \langle d; M \mid \rho(q\,\hat{\mathbf{z}}) \mid d; M \rangle \ , \tag{235}$$

$$G_M(q) = \frac{1}{\sqrt{2\,\eta}} \operatorname{Im} \left[\langle d; 1 \mid j_y(q\,\hat{\mathbf{z}}) \mid d; 0 \rangle \right] \ , \tag{236}$$

$$G_Q(q) = \frac{1}{2\,\eta} \big[\langle d; 0 \mid \rho(q\,\hat{\mathbf{z}}) \mid d; 0 \rangle$$
$$- \langle d; 1 \mid \rho(q\,\hat{\mathbf{z}}) \mid d; 1 \rangle \big] \ , \tag{237}$$

where $\mid d; M\rangle$ is the deuteron state with spin projection $J_z = M$, ρ and j_y denote, respectively, the charge operator and y component of the current operator, the momentum transfer $\mathbf{q}$ is taken along the z-axis (the spin quantization axis), and $\eta = (q/2\,m_d)^2$ (m_d is the deuteron mass). They are normalized as

$$G_C(0) = 1 \ , \ G_M(0) = (m_d/m_N)\,\mu_d \ , \ G_Q(0) = m_d^2\,Q_d \ , \tag{238}$$

where μ_d and Q_d are the deuteron magnetic moment (in units of μ_N) and quadrupole moment, respectively. Expressions relating the form factors to the measured structure functions A and B, and tensor polarization T_{20} are given [81]:

$$A(q^2) = G_C^2(q^2) + \frac{2}{3}\,\eta\,G_M^2(q^2) + \frac{8}{9}\,\eta^2\,G_q^2(q^2) \ , \tag{239}$$

$$B(q^2) = \frac{4}{3}\,\eta\,(1+\eta)\,G_M^2(q^2) \ , \tag{240}$$

$$I(q^2,\theta)\,T_{20}(q^2) = -\frac{1}{\sqrt{2}}\left[\frac{8}{3}\,\eta\,G_C(q^2)\,G_Q(q^2) + \frac{8}{9}\,\eta^2\,G_q^2(q^2)\right.$$
$$\left. +\frac{1}{3}\,\eta\,\left[1 + 2\,(1+\eta)\tan^2\theta/2\right]G_M^2(q^2)\right] \tag{241}$$

where $I(q^2,\theta) = A(q^2) + B(q^2)\,\tan^2\theta/2$ with θ being the angle (in the center-of-mass) between the initial and final electron momenta in the elastic scattering process.

The charge and magnetic form factors of the trinucleons are derived from

$$F_C(q) = \frac{1}{Z}\,\langle + \mid \rho(q\,\hat{\mathbf{z}}) \mid +\rangle \ , \tag{242}$$

$$F_M(q) = -\frac{2\,m_N}{q}\,\mathrm{Im}\left[\langle - \mid j_y(q\,\hat{\mathbf{z}}) \mid +\rangle\right] \ , \tag{243}$$

with the normalizations

$$F_C(0) = 1 \ , \qquad F_M(0) = \mu \ , \tag{244}$$

where μ is the magnetic moment (in units of μ_N). Here $\mid \pm\rangle$ represent either the ^{3}He state or ^{3}H state with total $1/2$-spin and spin projections $J_z = \pm 1/2$. Below we also consider the isoscalar and isovector combinations of the trinucleon charge and magnetic form factors, defined as

$$F_C^{S/V}(q) = \frac{1}{2}\left[2\,F_C(q;{}^3\mathrm{He}) \pm F_C(q;{}^3\mathrm{H})\right] \ , \tag{245}$$

$$F_M^{S/V}(q) = \frac{1}{2}\left[F_M(q;{}^3\mathrm{He}) \pm F_M(q;{}^3\mathrm{H})\right] \ . \tag{246}$$

4.2.2 MATRIX ELEMENTS OF THE ELECTROMAGNETIC OPERATORS

The method used to evaluate the matrix elements of the charge and current operator for the $A = 3$ systems is outlined here; a similar prescription is used for $A = 2$. In momentum space, the one-body electromagnetic operators in Sec. 4.1 have the generic form

$$O_{1b}(\mathbf{q}) = \sum_{\text{cyclic } l,m,n} \bar{\delta}(\mathbf{k}_l - \mathbf{q}) \, \bar{\delta}(\mathbf{k}_m) \, \bar{\delta}(\mathbf{k}_n) \, O_{1b}(\mathbf{k}_l, \mathbf{K}_l) \,, \qquad (247)$$

where $\mathbf{k}_l = \mathbf{p}'_l - \mathbf{p}_l$ and $\mathbf{K}_l = (\mathbf{p}'_l + \mathbf{p}_l)/2$ ($\mathbf{p}_l$ and $\mathbf{p}'_l$ are respectively the initial and final momenta of nucleon l). The matrix elements of the operator in Eq. (247) can be written as

$$\begin{aligned}
\langle O_{1b}(\mathbf{q}) \rangle &= \sum_{\text{cyclic } l,m,n} \int_{\mathbf{p}_l, \mathbf{p}_m, \mathbf{p}_n} \psi^\dagger_{M'}(\mathbf{p}_l + \mathbf{q}/2, \mathbf{p}_m, \mathbf{p}_n) \\
&\quad \times O_{1b}(\mathbf{q}, \mathbf{p}_l) \, \psi_M(\mathbf{p}_l - \mathbf{q}/2, \mathbf{p}_m, \mathbf{p}_n) \,,
\end{aligned} \qquad (248)$$

where we have defined

$$\int_{\mathbf{p}_i} = \int \frac{d\mathbf{p}_i}{(2\pi)^3} \quad \text{and} \quad \bar{\delta}(\ldots) = (2\pi)^3 \, \delta(\ldots) \,. \qquad (249)$$

For an assigned configuration $(\mathbf{p}_l, \mathbf{p}_m, \mathbf{p}_n)$, the wave functions are expanded on a basis of 8×3 spin-isospin states for the three nucleons as

$$\psi(\mathbf{p}_l, \mathbf{p}_m, \mathbf{p}_n) = \sum_{a=1}^{24} \psi_a(\mathbf{p}_l, \mathbf{p}_m, \mathbf{p}_n) \, |a\rangle \,, \qquad (250)$$

where the components ψ_a are complex functions and the basis states (for ^{3}H, for example) $|a\rangle = | (p\uparrow)_1, (n\uparrow)_2, (n\uparrow)_3 \rangle$, $| (n\uparrow)_1, (p\uparrow)_2, (n\uparrow)_3 \rangle$, and so on. The spin-isospin algebra for the overlaps

$$\psi^\dagger O \psi = \sum_{a,b=1}^{24} \psi_a^* O_{ab} \psi_b \,, \qquad (251)$$

is carried out with the techniques developed in Ref. [82]. Monte Carlo (MC) methods are used to evaluate the integrations in Eq. (248) by sampling momenta from a

(normalized) probability density $\mid \psi_M(\mathbf{p}_l, \mathbf{p}_m, \mathbf{p}_n) \mid^2$ according to the Metropolis algorithm.

The two-body operators in Sec. 4.1 have the momentum-space representation

$$
\begin{aligned}
O_{2b}(\mathbf{q}) &= \sum_{\text{cyclic } l,m,n} \bar{\delta}(\mathbf{K}_{lm} - \mathbf{q})\, \bar{\delta}(\mathbf{k}_n) \\
&\quad \times O_{2b}(\mathbf{K}_{lm}/2 + \mathbf{k}_{lm}, \mathbf{K}_{lm}/2 - \mathbf{k}_{lm}) ,
\end{aligned}
\tag{252}
$$

where the momenta $\mathbf{K}_{lm} = \mathbf{k}_l + \mathbf{k}_m$ and $\mathbf{k}_{lm} = (\mathbf{k}_l - \mathbf{k}_m)/2$. These operators have power law behavior at large momenta, and need to be regularized. This is accomplished by introducing a momentum cutoff function of the form

$$
C_\Lambda(k_{lm}) = e^{-(k_{lm}/\Lambda)^4} ,
\tag{253}
$$

with the parameter Λ in the range (500–600) MeV (see discussion in Sec. 4.3). The matrix elements are expressed as

$$
\begin{aligned}
\langle O_{2b}(\mathbf{q}) \rangle &= \sum_{\text{cyclic } l,m,n} \int_{\mathbf{k}_{lm}} \int_{\mathbf{p}_l, \mathbf{p}_m, \mathbf{p}_n} \psi_{M'}^\dagger(\mathbf{p}_l + \mathbf{q}/4 + \mathbf{k}_{lm}/2, \mathbf{p}_m + \mathbf{q}/4 - \mathbf{k}_{lm}/2, \mathbf{p}_n) \\
&\quad \times C_\Lambda(k_{lm})\, O_{2b}(\mathbf{q}, \mathbf{k}_{lm})\, \psi_M(\mathbf{p}_l - \mathbf{q}/4 - \mathbf{k}_{lm}/2, \mathbf{p}_m - \mathbf{q}/4 + \mathbf{k}_{lm}/2, \mathbf{p}_n) .
\end{aligned}
\tag{254}
$$

The spin-isospin algebra is handled as above, while the multidimensional integrations are efficiently done by a combination of MC and standard quadratures techniques. We write

$$
\langle O_{2b}(\mathbf{q}) \rangle = \int d\hat{\mathbf{k}} \int_{\mathbf{p}_l, \mathbf{p}_m, \mathbf{p}_n} F(\hat{\mathbf{k}}, \mathbf{p}_l, \mathbf{p}_m, \mathbf{p}_n) \simeq \frac{1}{N_c} \sum_{c=1}^{N_c} \frac{F(c)}{W(c)} ,
\tag{255}
$$

where c denotes configurations $(\hat{\mathbf{k}}, \mathbf{p}_l, \mathbf{p}_m, \mathbf{p}_n)$ (total number N_c) sampled with the Metropolis algorithm from the probability density $W(c) = \mid \psi_M(\mathbf{p}_l, \mathbf{p}_m, \mathbf{p}_n) \mid^2/(4\pi)$, i.e., uniformly over the $\hat{\mathbf{k}}$ directions. For each such configuration c, the function F is obtained by Gaussian integration over the magnitude k_{lm} (as well as the parameters x and y for the case of the charge operators at one loop)

$$
\begin{aligned}
F(c) &= \sum_{\text{cyclic } l,m,n} \frac{1}{(2\pi)^3} \int_0^\infty dk_{lm}\, k_{lm}^2 \sum_{a,b=1}^{24} \psi_a^*(\dots k_{lm}\hat{\mathbf{k}} \dots) \\
&\quad \times O_{2b,ab}(\mathbf{q}, k_{lm}\hat{\mathbf{k}})\, \psi_b(\dots k_{lm}\hat{\mathbf{k}} \dots) .
\end{aligned}
\tag{256}
$$

Convergence in these Gaussian integrations requires of the order of 20-30 points, in the case of k_{lm} distributed over a non-uniform grid up to 2Λ or so, while N_c of the

order of $100,000$ is sufficient to reduce the statistical errors in the MC integrations, which are of the order of a few % at the highest q values (and considerably smaller at lower q). These MC errors are further reduced by taking appropriate linear combinations of the matrix elements of the electromagnetic operators using different $\hat{q}$ directions and different spin projections for the initial and final states. The trinucleons wave functions are obtained with the hyperspherical harmonics (HH) expansion discussed in Refs. [83–86]. This method can be applied in either coordinate- or momentum-space.

4.3 RESULTS

This section consists of three subsections. In the first one, we discuss various strategies for the determination of the unknown LEC's d'_8, d'_9, d'_{21}, C'_{15}, and C'_{16} entering the current operator at N3LO (e Q). In contrast, the charge operator up to N4LO (e Q) only depends on the nucleon axial coupling constant g_A, pion decay amplitude F_π, and nucleon mass and magnetic moments. The two-body operators are regularized via the cutoff function in Eq. (253), and Λ values of 500 MeV and 600 MeV are considered.

In the second and third subsections we present results, respectively, for the deuteron $A(q)$ and $B(q)$ structure functions and tensor polarization $T_{20}(q)$, and for the charge and magnetic form factors of ^{3}H and ^{3}He, along with results for the static properties of these few-nucleon systems including the deuteron quadrupole moment, the deuteron and trinucleons charge and magnetic radii and magnetic moments. The $A = 2$ calculations use either the Argonne v_{18} (AV18) [48] or chiral potentials at order Q^4 with cutoff set at 500 MeV (N3LO) or 600 MeV (N3LO*) [5]. Of course, the $A = 3$ calculations also include three-nucleon potentials—the Urbana-IX model [49] in combination with the AV18, and the chiral N2LO potential [16] in combination with either the N3LO or N3LO*.

The calculations are carried out in momentum space with the methods outlined in Sec. 4.2. The hadronic electromagnetic form factors entering the one- and two-body charge and current operators are those specified in Sec. 4.1. The matrix elements of these operators are evaluated with Monte Carlo methods. The number of sampled configurations is of the order of 10^6 for the deuteron and 10^5 for the $A = 3$ systems. The statistical errors, which are not shown in the results that follow, are typically $\lesssim 1\%$ over the whole momentum-transfer range, and in fact much less than 1% for

TABLE 7: Dimensionless values of the isoscalar LEC's corresponding to cutoffs $\Lambda = 500$ MeV and 600 MeV obtained for the N3LO/N2LO and N3LO*/N2LO* Hamiltonians; the values in parentheses are from the AV18/UIX Hamiltonian.

Λ	d_1^S	$d_2^S \times 10$
500	4.072 (2.522)	2.190 (-1.731)
600	11.38 (5.238)	3.231 (-2.033)

$q \lesssim 2$ fm^{-1}.

4.3.1 DETERMINATION OF THE LEC'S

As already remarked, the LEC's C_i, $i = 1, \ldots, 7$, in the minimal contact current, corresponding to Λ cutoffs of 500 and 600 MeV, are taken from fits to NN scattering data [5]. In reference to the LEC's entering the OPE and non-minimal contact currents at N3LO, it is convenient to introduce the dimensionless set $d_i^{S,V}$ (in units of the cutoff Λ) as

$$C_{15}' = d_1^S/\Lambda^4 , \qquad d_9' = d_2^S/\Lambda^2 ,$$
$$C_{16}' = d_1^V/\Lambda^4 , \qquad d_8' = d_2^V/\Lambda^2 , \qquad d_{21}' = d_3^V/\Lambda^2 , \qquad (257)$$

where the superscript S or V on the $d_i^{S,V}$ characterizes the isospin of the associated operator, i.e., whether it is isoscalar or isovector. The isoscalar d_i^S, listed in Table 7, have been fixed by reproducing the experimental deuteron magnetic moment μ_d and isoscalar combination μ_S of the trinucleon magnetic moments. Invoking the requirement of "naturalness" for the LEC's, we notice that LEC d_1^S multiplying the contact current is rather large, but not unreasonably large, while the LEC d_2^S is quite small.

The isovector LEC d_3^V is taken as $d_2^V/4$ by assuming Δ dominance. The three different sets of remaining LEC's d_1^V and d_2^V reported in Table 8 have been determined in the following way. In set I d_1^V and d_2^V have been constrained to reproduce the experimental values of the np radiative capture cross section σ_{np} at thermal neutron energies ($n+p \rightarrow d+\gamma$) and the isovector combination μ_V of the trinucleons magnetic moments. This procedure, however, leads to large values for both LEC's. This pathology is especially severe in the case of the AV18/UIX Hamiltonian model. In

TABLE 8: Dimensionless values of the isovector LEC's corresponding to cutoffs $\Lambda = 500$ MeV and 600 MeV obtained for the N3LO/N2LO and N3LO*/N2LO* Hamiltonians; the values in parentheses are from the AV18/UIX Hamiltonian. Note that $d_3^V = d_2^V/4$ in all cases; see text for further explanations.

Λ	d_1^V(I)	d_2^V(I)	d_1^V(II)	d_2^V(II)	d_1^V(III)	d_2^V(III)
500	10.36 (45.10)	17.42 (35.57)	13.30 (-9.339)	3.458	-7.981 (-5.187)	3.458
600	41.84 (257.5)	33.14 (75.00)	-22.31 (-11.57)	4.980	-11.69 (-1.025)	4.980

sets II and III d_2^V is assumed to be saturated by the Δ resonance, i.e.

$$d_2^V = \frac{4\,\mu_{\gamma N\Delta}\,h_A\,\Lambda^2}{9\,m_N\,(m_\Delta - m_N)}\,, \tag{258}$$

where $m_\Delta - m_N = 294$ MeV, $h_A/F_\pi = f_{\pi N\Delta}/m_\pi$ with $f_{\pi N\Delta}^2/(4\pi) = 0.35$ as obtained by equating the first-order expression of the Δ-decay width to the experimental value, and the transition magnetic moment $\mu_{\gamma N\Delta} = 3\,\mu_N$, obtained from the analysis of γN data in the Δ-resonace region [80]. A similar strategy has been implemented in a number of calculations, based on the χEFT magnetic moment operator derived in Ref. [27], of the $n + p \to \gamma + d$, $n + d \to \gamma +^3$H, and $n+^3$He$\to \gamma+^4$He radiative captures, and magnetic moments of $A = 2$ and 3 nuclei [87]. On the other hand, the LEC d_1^V multiplying the contact current is fitted to reproduce either σ_{np} in set II or μ_V in set III. Both alternatives still lead to somewhat large values for this LEC, but we find the degree of "unnaturalness" tolerable in this case. There are no three-body currents at N3LO [29], and therefore it is reasonable to fix the strength of the two-nucleon contact operators by fitting a three-nucleon observable such as μ^S and μ^V.

4.3.2 STATIC PROPERTIES AND FORM FACTORS OF THE DEUTERON

The deuteron root-mean-square charge radius and quadrupole moment, obtained with the chiral and AV18 potentials and cutoff parameters $\Lambda = 500$ MeV and 600 MeV, are listed in Table 9. We denote the leading order ($m = -3$ in the notation of Sec. 4.1) term of Eq. (196) with LO, the $m = -1$ relativistic correction of Eq. (198) with N2LO, and the $m = 0$ terms of Eqs. (200) and (201)–(202) with N3LO(OPE) and N3LO(ν), respectively. The remaining charge operators at N4LO ($m = 1$),

TABLE 9: Cumulative contributions to the deuteron root-mean-square charge radius and quadrupole moment corresponding to cutoffs $\Lambda = 500$ and 600 MeV obtained with the N3LO and N3LO* Hamiltonians; results in parentheses are from the AV18 Hamiltonian. The experimental values for r_d and Q_d are 1.9734(44) fm [88] and 0.2859(3) fm^2 [73], respectively.

Λ	r_d (fm)		Q_d (fm^2)	
	500	600	500	600
LO	1.976 (1.969)	1.968 (1.969)	0.2750 (0.2697)	0.2711 (0.2697)
N2LO	1.976 (1.969)	1.968 (1.969)	0.2731 (0.2680)	0.2692 (0.2680)
N3LO(OPE)	1.976 (1.969)	1.968 (1.969)	0.2863 (0.2818)	0.2831 (0.2814)
N3LO($\nu = 1/2$)	1.976 (1.969)	1.968 (1.969)	0.2851 (0.2806)	0.2820 (0.2802)

being isovector, do not contribute to these observables (and corresponding form factors). The N3LO/N3LO* and AV18 potentials neglect non-static corrections in their OPE component, which corresponds to setting $\nu = 1/2$. The N2LO and N3LO corrections to r_d, which is well reproduced by theory, are negligible. The chiral potential predictions for Q_d are within 1% of the experimental value, while the AV18 ones underestimate it by about 2%. Variation of the cutoff in the (500–600) MeV range leads to about 1% (negligible) changes in the N3LO/N3LO* (AV18) results. The LO and N2LO charge operators do not include the cutoff function and the AV18 results are independent of Λ. This is not the case for the results corresponding to the N3LO and N3LO* potentials because of their intrinsic Λ dependence.

The deuteron $A(q)$ structure function and tensor polarization $T_{20}(q)$, obtained at LO and by including corrections up to N3LO in the charge operator, are compared to data in Fig. 15, top panels. In this figure (as well as in those that follow) the momentum-transfer range goes up to $q = 7.5$ fm^{-1}, much beyond the $\simeq$ 3–4 m_π upper limit, where one would naively expect this comparison to be meaningful, given that the present theory retains up to TPE mechanisms.

The $A(q)$ structure function is well reproduced by theory up to $q \simeq 3$ fm^{-1}. At higher momentum transfers, the N3LO results based on the AV18 tend to overestimate the data—a feature also seen in calculations such those of Ref. [81]—while those based on the chiral potentials still provide a good fit to the data. The cutoff dependence is weak at low q, but becomes more pronounced as q
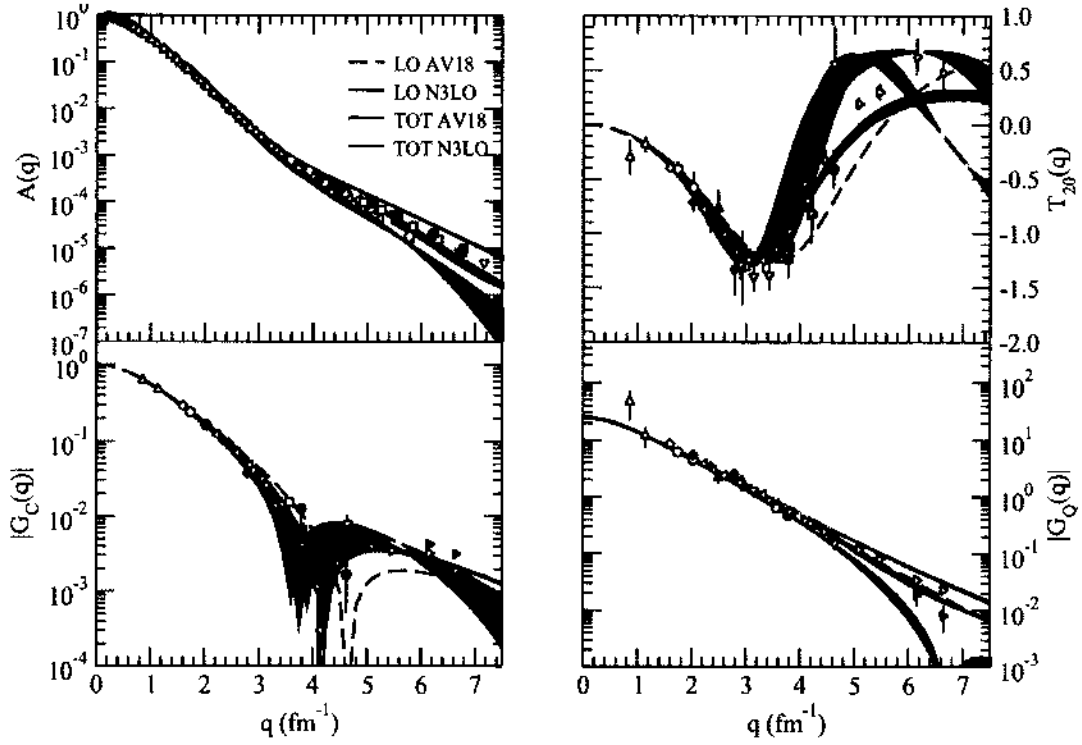
FIG. 15: The deuteron structure function $A(q)$ and tensor polarization $T_{20}(q)$ (top panels), and charge and quadrupole form factors $G_C(q)$ and $G_Q(q)$ (bottom panels), obtained at leading order (LO) and with inclusion of charge operators up to N3LO (TOT), is compared with experimental data from Refs. [89–110]. Predictions corresponding to $\nu = 1/2$ and cutoffs Λ in the range 500–600 MeV are displayed by the bands.

increases. Similar considerations hold for the $T_{20}(q)$ observable, although in this case the N3LO results derived from the chiral potentials overpredict the data for $q \gtrsim 3$ fm^{-1}, while those from the AV18 fit reasonably well the data up to $q \simeq 4.5$ fm^{-1}.

The charge and quadrupole form factors, $G_C(q)$ and $G_Q(q)$ respectively, extracted from the unpolarized and tensor polarized deuteron data are compared to results obtained in LO and by including corrections up to N3LO in Fig. 15, bottom panels. The deuteron magnetic moment is one of the two observables utilized to fix the LEC's entering the isoscalar current operators at N3LO. The structure function $B(q)$ and magnetic form factor $G_M(q)$, obtained with the AV18 and chiral potentials, and currents at LO and by including corrections up to N3LO, are compared to data
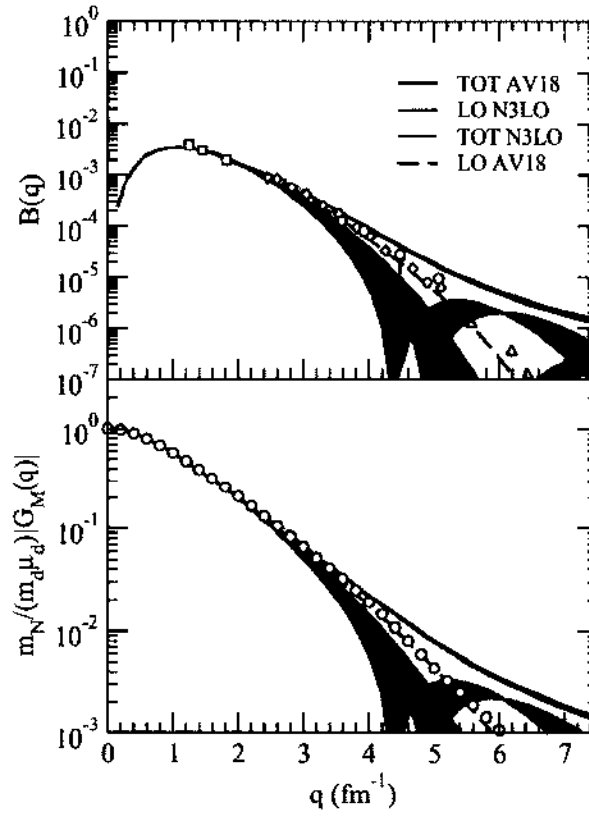
FIG. 16: The deuteron structure function $B(q)$ (top panel) and magnetic form factor $G_M(q)$ (bottom panel), obtained at leading order (LO) and with inclusion of current operators up to N3LO (TOT), is compared with the experimental data from Refs. [89, 95, 96, 111–113]. Predictions corresponding to cutoffs Λ in the range 500–600 MeV are displayed by the bands.

in Fig. 16. There is generally good agreement between theory and experiment for q values up to $\simeq 2$ fm^{-1}. At higher q's, the results corresponding to the chiral (AV18) potential under-predict (over-predict) the data significantly when the current includes up to N3LO corrections. In particular, the diffraction seen in the data at $q \simeq 6.5$ fm^{-1} is absent in the AV18 calculations, and is shifted to lower q values in the N3LO/N3LO* ones. There are large differences between the N3LO/N3LO* and AV18 results with the LO current, which simply reflect differences in the S- and D-wave components of the deuteron wave functions corresponding to these potentials. The cutoff dependence is large for the chiral potentials, while it remains quite modest for the AV18 over the whole momentum transfer range. This is consistent with the rather different sensitivity of the LEC's d_1^S and d_2^S to variations of Λ in the (500–600) MeV range obtained with either the chiral potential or AV18, see Table 7. There is a mismatch in the chiral counting between the potentials of Ref. [5] at order Q^4 and the present current at order $e\,Q$. This becomes obvious when considering current conservation, which for these potentials would require accounting for terms up to order $e\,Q^3$ in the current, well beyond available derivations [29, 32, 33] at this time.

4.3.3 STATIC PROPERTIES AND FORM FACTORS OF THE TRINUCLEONS

The notation for the various components of the charge operator is the same as given at the beginning of Sec. 4.3.2, except that now the one-loop (isovector) corrections at N4LO contribute too, since the ^{3}He and ^{3}H nuclei have predominantly total isospin $T = 1/2$. As a matter of fact, the hyperspherical harmonics wave functions utilized to represent their ground states also include small $T = 3/2$ admixtures due to isospin-symmetry breaking terms induced by the electromagnetic and strong interactions.

There are no unknown LEC's entering the charge operator up to N4LO, and the predicted root-mean-square charge radii of ^{3}He and ^{3}H, obtained with the N3LO/N2LO and AV18/UIX combinations of two- and three-nucleon potentials and cutoffs in the (500–600) MeV range, are listed in Table 10. Corrections at N2LO, N3LO, and N4LO are negligible—the corresponding operators vanish at $q = 0$. The spread between the N3LO/N2LO ($\Lambda = 500$ MeV) and N3LO*/N2LO* ($\Lambda = 600$ MeV) results at LO is about 0.5%, which is much smaller, particularly for ^{3}H, than

FIG. 17: The ^{3}He and ^{3}H charge form factors (top panels), and their isoscalar and isovector combinations (bottom panels), obtained at leading order (LO) and with inclusion of charge operators up to N4LO (TOT), is compared with experimental data [114]. Predictions corresponding to $\nu = 1/2$ and cutoffs Λ in the range (500–600) MeV are displayed by the bands.

TABLE 10: Cumulative contributions in fm to the ^{3}He and ^{3}H root-mean-square charge radii corresponding to $\nu = 1/2$ and cutoffs $\Lambda = 500$ MeV and 600 MeV, obtained with the N3LO/N2LO and N3LO*/N2LO* Hamiltonians; results in parentheses are relative to the AV18/UIX Hamiltonian. The experimental values for the ^{3}He and ^{3}H charge radii are [113] (1.959 ± 0.030) fm and (1.755 ± 0.086) fm, respectively.

	^{3}He		^{3}H	
Λ	500	600	500	600
LO	1.966 (1.950)	1.958 (1.950)	1.762 (1.743)	1.750 (1.743)
N2LO	1.966 (1.950)	1.958 (1.950)	1.762 (1.743)	1.750 (1.743)
N3LO	1.966 (1.950)	1.958 (1.950)	1.762 (1.743)	1.750 (1.743)
N4LO	1.966 (1.950)	1.958 (1.950)	1.762 (1.743)	1.750 (1.743)

the experimental error. The predicted radii for both Hamiltonian models are within 0.5% of the current experimental central values.

The calculated charge form factors of ^{3}He and ^{3}H, and their isoscalar and isovector combinations $F_C^S(q)$ and $F_C^V(q)$, normalized, respectively, to 3/2 and 1/2 at $q = 0$, are compared to data in Fig. 17. The agreement between theory and experiment is excellent for $q \lesssim 2.5$ fm^{-1}. At larger values of the momentum transfer, there is a significant sensitivity to cutoff variations in the results obtained with the chiral potentials. This cutoff dependence is large at LO and is reduced, at least in ^{3}He, when corrections up to N4LO are included. These corrections have opposite sign than the LO, and tend to shift the zeros in the form factors to lower momentum transfers, bringing theory closer to experiment in the diffraction region. As already remarked, the chiral (and realistic) two-nucleon potentials utilized in the present study ignore retardation corrections in their OPE and TPE components, which corresponds to the choice $\nu = 1/2$ in the non-static pieces of the corresponding potentials and accompanying charge operators in Eqs. (202) and (210) [30].

Moving on to the magnetic structure of the trinucleons, we note that the isoscalar combination μ_S of ^{3}He and ^{3}H magnetic moments is used to fix one of the two (isoscalar) LEC's entering the current at N3LO. Both the isovector combination μ_V and the np radiative capture cross section σ_{np} are used to fix the isovector LEC's in

TABLE 11: Cumulative contributions in fm to the ^{3}He and ^{3}H root-mean-square magnetic radii corresponding to cutoffs $\Lambda = 500$ MeV and 600 MeV, obtained with the N3LO/N2LO and N3LO*/N2LO* Hamiltonians; results in parentheses are from the AV18/UIX Hamiltonian. Predictions corresponding to sets I, II, and II of isovector LEC's d_1^V and d_2^V in Table 8 are listed. The experimental values for the ^{3}He and ^{3}H magnetic radii are [113] (1.965 ± 0.153) fm and (1.840 ± 0.181) fm, respectively.

Λ	^{3}He		^{3}H	
	500	600	500	600
LO	2.098 (2.092)	2.090 (2.092)	1.924 (1.918)	1.914 (1.918)
NLO	1.990 (1.981)	1.983 (1.974)	1.854 (1.847)	1.845 (1.841)
N2LO	1.998 (1.992)	1.989 (1.984)	1.865 (1.859)	1.855 (1.854)
N3LO(I)	1.924 (1.931)	1.910 (1.972)	1.808 (1.800)	1.796 (1.819)
N3LO(II)	1.901 (1.890)	1.883 (1.896)	1.789 (1.774)	1.773 (1.778)
N3LO(III)	1.927 (1.915)	1.913 (1.924)	1.808 (1.792)	1.794 (1.797)

set I of the N3LO currents, while in sets II and III one of these LEC's is fixed by Δ dominance, and the other is determined by reproducing σ_{np} (μ_V) in set II (III). By construction, then, the ^{3}He and ^{3}H magnetic moments are exactly reproduced in sets I and III, while in set II they are calculated to be, respectively, -2.186 (-2.196) μ_N and 3.038 (3.048) μ_N with the N3LO/N2LO (N3LO*/N2LO*) Hamiltonian and $\Lambda = 500$ (600) MeV, and similar results with the AV18/UIX Hamiltonian. These should be compared to the experimental values of -2.127 μ_N and 2.979 μ_N.

The ^{3}He and ^{3}H magnetic radii corresponding to sets I-III are given in Table 11. The predicted values are consistent with experiment, although the measurements have rather large errors (10% for ^{3}H). Their spread as Λ varies in the (500–600) MeV range is at the 1% level or less. A recent quantum Monte Carlo study [115], using wave functions derived from realistic two- and three nucleon potentials (the AV18 and Illinois 7 model [116]) and set III of χEFT currents, has led to predictions for magnetic moments and transitions in nuclei with $A \leq 9$ in excellent agreement with the measured values. Therefore in the following, unless stated otherwise, we adopt set III of isovector LEC's. We disregard set I for the reasons already explained in
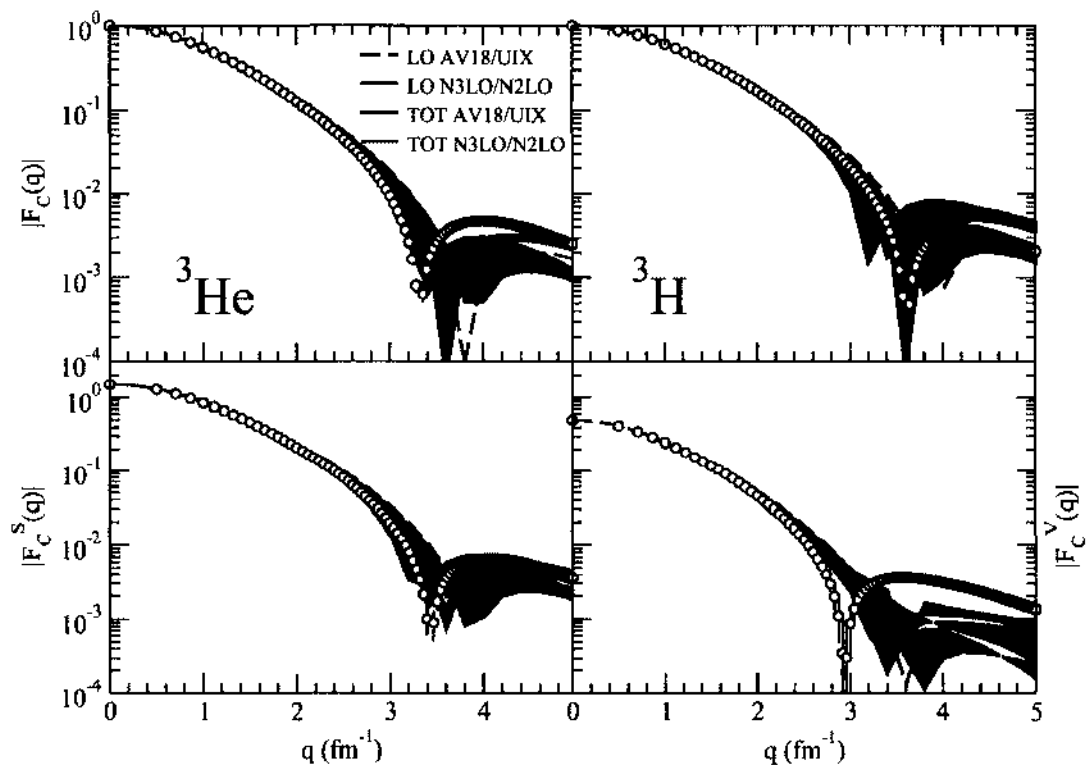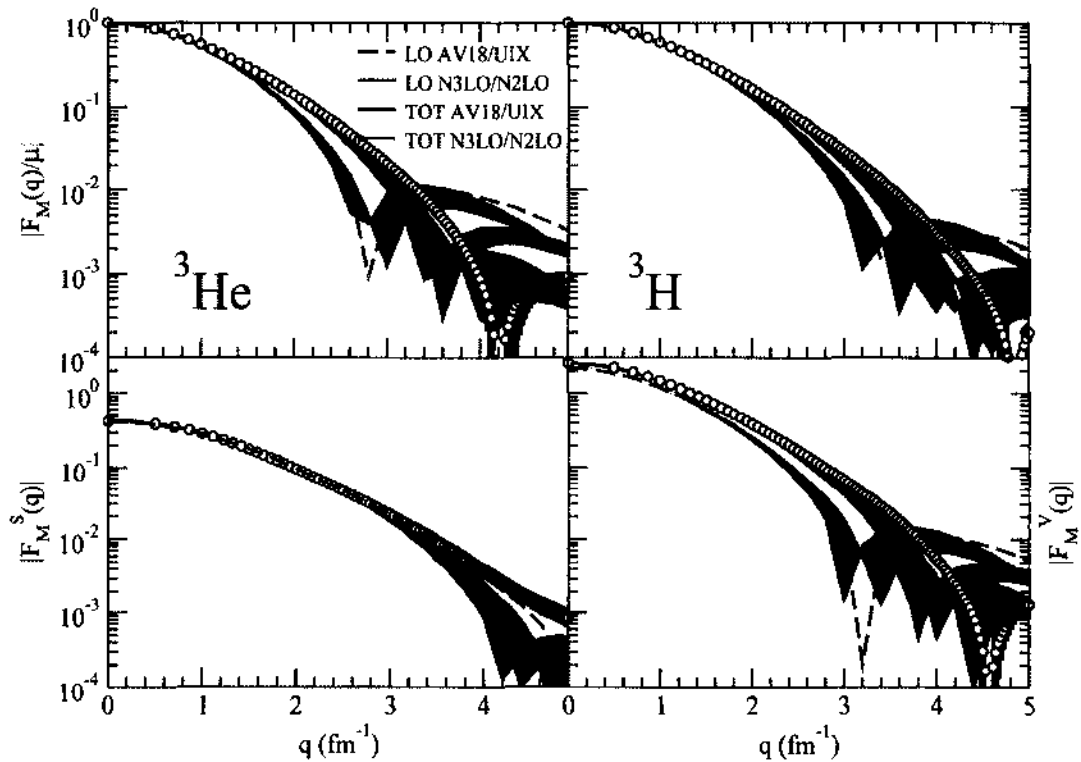
FIG. 18: The ^{3}He and ^{3}H magnetic form factors (top panels), and their isoscalar and isovector combinations (bottom panels), obtained at leading order (LO) and with inclusion of current operators up to N3LO (TOT) corresponding to the LEC's d_1^S and d_2^S in Table 7 and to set III of isovector LEC's d_1^V and d_2^V in Table 8, is compared with experimental data [114]. Predictions relative to cutoffs Λ in the range (500–600) MeV are displayed by the bands.

Sec. 4.3.1.

The magnetic form factors of ^{3}He and ^{3}H and their isoscalar and isovector combinations $F_M^S(q)$ and $F_M^V(q)$, normalized respectively as μ_S and μ_V at $q = 0$, at LO and with inclusion of corrections up to N3LO in the current, are displayed in Fig. 18. Two-body currents are crucial for "filling in" the zeros obtained in the LO calculation. For $q \lesssim 2$ fm^{-1} there is excellent agreement between the present χEFT predictions and experiment. However, as the momentum transfer increases, even after making allowance for the significant cutoff dependence, theory tends to underestimate the data, in particular it predicts the zeros in both form factors occurring at significantly lower values of q than observed.

CHAPTER 5

CONCLUSIONS

The overarching goal of nuclear theory is to understand the structure and reactions of nuclei and nuclear matter. Within this broad goal, the present work investigates the extent to which χEFT correctly describes the strong-interaction dynamics in the few-nucleon systems, and their response to electromagnetic probes.

In the first part of the present study, we have constructed a coordinate-space nucleon-nucleon potential with an electromagnetic interaction component including first and second order Coulomb, Darwin-Foldy, vacuum polarization, and magnetic moment terms, and a strong interaction component characterized by long- and short-range parts. The long-range part includes OPE and TPE terms up to N2LO, derived in the static limit from leading and sub-leading πN and $\pi N \Delta$ chiral Lagrangians. Its strength is fully determined by the nucleon and nucleon-to-Δ axial coupling constants g_A and h_A, the pion decay amplitude F_π, and the sub-leading LEC's c_1, c_2, c_3, c_4, and $b_3 + b_8$, constrained by reproducing πN scattering data (the values adopted for all these couplings are listed in Table 1). In coordinate space, this long-range part is represented by charge-independent central, spin, and tensor components without and with the isospin dependence $\tau_1 \cdot \tau_2$ (the so-called v_6 operator structure), and by charge-dependence-breaking central and tensor components induced by OPE and proportional to the isotensor operator T_{12}.

The short-range part is described by charge-independent contact interactions specified by a total of 24 LEC's (2 at LO, 7 at NLO, and 15 at N3LO) and by charge-dependent ones characterized by 10 LEC's (2 at LO and 8 at NLO), 5 of which multiply charge-symmetry breaking terms proportional to $\tau_{1z} + \tau_{2z}$ and the remaining 5 multiply charge-dependence breaking terms proportional to T_{12}. In the NLO and N3LO contact interactions, Fierz transformations have been used in order to rearrange terms that in coordinate space would otherwise lead to powers of $\mathbf{p}$—the relative momentum operator—higher than two. The resulting charge-independent (coordinate-space) potential contains, in addition to the v_6 operator structure, spin-orbit, $\mathbf{L}^2$, quadratic-spin-orbit, and $\mathbf{p}^2$ components, while the charge-dependent one retains central, tensor, and spin-orbit components.

The 34 LEC's in the short-range potential have been constrained by fitting 5291 pp and np scattering data (including normalizations) up to 300 MeV lab energies, as assembled in the Granada database, and the pp, np, and nn scattering lengths, and the deuteron binding energy. The global $\chi^2(pp + np)$/datum is 1.3 for the three different models we have investigated, each specified by a pair of (coordinate-space) cutoffs, respectively, R_L and R_S for the long- and short-range parts: $(R_L, R_S) = (1.2, 0.8)$ fm for model a, $(1.0, 0.7)$ fm for model b, and $(0.8, 0.6)$ fm for model c. These cutoffs are close to the $1/(2\,m_\pi) \sim 0.7$ fm TPE range. The values of the LEC's corresponding to the three models are given in Table 4.

In the second part of this study, we have provided predictions for the static properties, including charge and magnetic radii and magnetic moments, and elastic form factors of the deuteron and trinucleons, which are among the observables of choice for testing models of nuclear interactions and associated electromagnetic charge and current operators. The wave functions describing these nuclei were derived from either χEFT or realistic two- and three-nucleon potentials. The matrix elements of the χEFT charge and current operators were evaluated in momentum-space with Monte Carlo methods.

The χEFT calculations (based on the chiral Idaho N3LO [5, 6] potential) and the hybrid ones (based on the AV18) reproduce very well the observed electromagnetic structure of the deuteron for momentum transfers q up to 2–3 fm^{-1}. In some cases, as in the $A(q)$ structure function, the agreement between the experimental and χEFT calculated values extends up to $q \lesssim 6$ fm^{-1}, a much higher momentum transfer than one would naively expect the present expansion to be valid for. On the other hand, the measured $B(q)$ structure function is significantly under-predicted (over-predicted) for $q \gtrsim 3$ fm^{-1} in the χEFT (hybrid) calculations. The χEFT results, in contrast to the hybrid ones, have a rather large cutoff dependence. This cutoff dependence originates, in the hybrid calculations, solely from that in the N3LO current, while in the χEFT calculation it also reflects the Λ dependence intrinsic to the potential (the N3LO for $\Lambda = 500$ MeV or N3LO* for $\Lambda = 600$ MeV).

The calculated ^{3}He and ^{3}H charge form factors are in excellent agreement with data up to $q \lesssim 3$ fm^{-1}. However, the observed positions of the zeros are not generally well reproduced by theory, and the measured ^{3}He (^{3}H) form factor in the region of the secondary maximum at $q \simeq 4$ fm^{-1} is underestimated (overestimated) in both χEFT and hybrid calculations. A glance at the $F_C^S(q)$ and $F_C^V(q)$ in Fig. 17 suggests

that two-body isovector contributions to the charge operator should be considerably larger (in magnitude) than presently calculated, in order to shift the zero in $F_C^V(q)$ to smaller q.

The isovector currents at N3LO depend on two LEC's (d_1^V and d_2^V), which have been fixed in one of three different ways: by reproducing the experimental np radiative capture cross section σ_{np} and isovector magnetic moment μ_V of the trinucleons simultaneously (set I); by using Δ dominance to constrain d_2^V and by determining d_1^V so as to fit either σ_{np} (set II) or μ_V (set III). Set I is not considered because of the "unnatural" values of the LEC's. The ^{3}He and ^{3}H magnetic form factors calculated with N3LO currents corresponding to set III, while in excellent agreement with data for $q \lesssim 3$ fm^{-1}, under-predict them at higher momentum transfers.

The NN potential developed in the first part of this work has not yet been utilized in the calculation of the static properties and elastic form factors of $A = 2$ and 3 nuclei since the completion of this program requires one to construct the three-body potential as well as the electromagnetic charge and current operators with explicit inclusion of Δ-isobars degree of freedom. This could be an interesting research project for the future.

Another fascinating line of research would be the implementation of this two-nucleon potential (and accompanying three-nucleon potential) in Quantum Monte Carlo methods which have proved very valuable in computing properties of light nuclei and nucleonic matter.

BIBLIOGRAPHY

[1] S. Weinberg, Phys. Lett. **B251**, 288 (1990); Nucl. Phys. **B363**, 3 (1991); Phys. Lett. **B295**, 114 (1992).

[2] U. van Kolck, Phys. Rev. C **49**, 2932 (1994).

[3] C. Ordónez, L. Ray, and U. van Kolck, Phys. Rev. C **53**, 2086 (1996).

[4] E. Epelbaum, W. Glöckle, and U.-G. Meissner, Nucl. Phys. A637, 107 (1998).

[5] D.R. Entem and R. Machleidt, Phys. Rev. C **68**, 041001(R) (2003).

[6] R. Machleidt and D.R. Entem, Phys. Rep. **503**, 1 (2011).

[7] N. Kaiser, R. Brockmann, and W. Weise, Nucl. Phys. A **625**, 758 (1997).

[8] N. Kaiser, R. Brockmann, and W. Weise, Nucl. Phys. A **637**, 395 (1998).

[9] E. Epelbaum, W. Glöckle, and U.-G. Meißner, Eur. Phys. J. A **19**, 125 (2004).

[10] E. Epelbaum, W. Glöckle, and U.-G. Meissner, Nucl. Phys. A **747**, 362 (2005).

[11] H. Krebs, E. Epelbaum, and Ulf.-G. Meißner, Eur. Phys. J. A **32**, 127 (2007).

[12] E. Epelbaum, H. Krebs, and U.-G. Meissner, arXiv:1412.0142 [nucl-th].

[13] A. Gezerlis *et al.*, Phys. Rev. Lett. **111**, 032501 (2013).

[14] A. Gezerlis *et al.*, Phys. Rev. C **90**, 054323 (2014).

[15] D.R. Entem *et al.*, Phys. Rev. C **91**, 014002 (2015).

[16] P. Navràtil, Few-Body Syst. **41**, 117 (2007).

[17] E. Epelbaum *et al.*, Phys. Rev. C **66**, 064001 (2002).

[18] V. Bernard *et al.*, Phys. Rev. C, **84**, 054001 (2011).

[19] L. Girlanda, A. Kievsky, and M. Viviani, Phys. Rev. C **84**, 014001 (2011).

[20] U. van Kolck *et al.*, Phys. Rev. Lett. **80**, 4386 (1998).

[21] J.L. Friar and U. van Kolck, Phys. Rev. C **60**, 034006 (1999).

[22] E. Epelbaum and U.-G. Meissner, Phys. Lett. B **461**, 287 (1999).

[23] J.L. Friar *et al.*, Phys. Rev. C **70**, 044001 (2004).

[24] J.L. Friar, G.L. Payne, and U. van Kolck, Phys. Rev. C **71**, 024003 (2005).

[25] E. Epelbaum and U.-G. Meissner, Phys. Rev. C **72**, 044001 (2005).

[26] N. Kaiser, Phys. Rev. C **73**, 044001 (2006).

[27] T.-S. Park, D.-P. Min, and M. Rho, Nucl. Phys. A, **596**, 515 (1996).

[28] S. Pastore, R. Schiavilla, and J.L. Goity, Phys. Rev. C **78**, 064002 (2008).

[29] S. Pastore *et al.*, Phys. Rev. C **80**, 034004 (2009).

[30] S. Pastore *et al.*, Phys. Rev. C **84**, 024001 (2011).

[31] M. Piarulli *et al.*, Phys. Rev. C **87**, 014006 (2013).

[32] S. Kölling *et al.*, Phys. Rev. C **80**, 045502 (2009).

[33] S. Kölling *et al.*, Phys. Rev. C **84**, 054008 (2011).

[34] S.S. Schweber, *An Introduction to Relativistic Quantum Field Theory* (Dover Pubblications, 1961).

[35] S. Weinberg, *The Quantum Theory of Fields*, vol.I (Cambridge University Press, 1995).

[36] N. Fettes *et al.*, Ann. Phys. **283**, 273 (2000).

[37] N. Fettes and U.-G. Meissner, Nucl. Phys. **A679**, 629 (2001).

[38] V. Bernard, N. Kaiser, and U.-G. Meissner, Int. J. Mod. Phys. E4, 193 (1995).

[39] L. Girlanda *et al.*, Phys. Rev. C, **81**, 034005 (2010).

[40] M.E. Peskin, D.V. Schroeder, *An Introduction to Quantum Field Theory* (Westview Press, 1995).

[41] F. Gross, *Relativistic Quantum Mechanics and Field Theory* (John Wiley & Sons, Inc., 1993).

[42] R. Schiavilla *et al.*, Phys. Rev. C **45**, 2628 (1992).

[43] M. Viviani, R. Schiavilla, and A. Kievsky, Phys. Rev. C **54**, 534 (1996).

[44] L. Girlanda *et al.*, Phys. Rev. Lett. **105**, 232502 (2010).

[45] L.E. Marcucci *et al.*, Phys. Rev. C **63**, 015801 (2001).

[46] J. Carlson *et al.*, arXiv:1412.3081[nucl-th].

[47] M. Fierz, Z. Phys. **104**, 533 (1937).

[48] R.B. Wiringa, V.G.J. Stoks, and R. Schiavilla, Phys. Rev. C **51**, 38 (1995).

[49] B.S. Pudliner *et al.*, Phys. Rev. Lett. **74**, 4396 (1995).

[50] H. Krebs and E. Epelbaum, Few-Body Syst. **50**, 295 (2011).

[51] A.M. Green, Rep. Prog. Phys. **39**, 1109 (1976).

[52] R.E. Cutkosky *et al.*, Phys. Rev. D **20**, 2839 (1979).

[53] M. Viviani *et al.*, Phys. Rev. C **89**, 064004 (2014).

[54] R.N. Pérez, J.E. Amaro, and E.R. Arriola, Phys. Rev. C **88**, 064002 (2013).

[55] W.H. Press *et al.*, *Numerical Recipes in Fortran 77. The Art of Scientific Computing* (Cambridge University Press, 1992).

[56] J. Bystricky, F. Lehar, and P. Winternitz, J. Phys. **39**, 1 (1978).

[57] J. Bystricky, C. Lechanoine-Leluc, and F. Lehar, J. Phys. **48**, 199 (1987).

[58] V.G.J. Stoks and J.J. de Swart, Phys. Rev. C **42**, 1235 (1990).

[59] F.L. Gross and A. Stadler, Phys. Rev. C **78**, 014005 (2008).

[60] R.N. Pérez, J.E. Amaro, and E.R. Arriola, Phys. Rev. C **89**, 064006 (2014).

[61] M. Kortelainen *et al.*, Phys. Rev. C **82**, 024313 (2010).

[62] R.N. Pérez, J.E. Amaro, and E.R. Arriola, Phys. Rev. C **89**, 024004 (2014).

[63] V.G.J. Stoks *et al.*, Phys. Rev. C **48**, 792 (1993).

[64] V.G.J. Stoks *et al.*, Phys. Rev. C **49**, 2950 (1994).

[65] G.A. Miller, M.K. Nefkens, and I. Slaus, Phys. Rep. **194**, 1 (1990).

[66] R. Machleidt, Phys. Rev. C **63**, 024001 (2001).

[67] D.E. González Trotter *et al.*, Phys. Rev. C **73**, 034001 (2006).

[68] Q. Chen *et al.*, Phys. Rev. C **77**, 054002 (2008).

[69] C. van der Leun and C. Alderlisten, Nucl. Phys. A **380**, 261 (1982).

[70] T.E.O. Ericson and M. Rosa-Clot, Nucl. Phys. A **405**, 497 (1983).

[71] N.L. Rodning and L.D. Knutson, Phys. Rev. C **41**, 898 (1990).

[72] A. Huber *et al.*, Phys. Rev. Lett. **80**, 468 (1998).

[73] D.M. Bishop and L.M. Cheung, Phys. Rev. A **20**, 381 (1979).

[74] R.A. Smith and V.R. Pandharipande, Nucl. Phys. A **256**, 327 (1976).

[75] C.E. Hyde-Wright and K. de Jager, Ann. Rev. Nucl. Part. Sci. **54**, 217 (2004).

[76] G. Höhler *et al.*, Nucl. Phys. B **114**, 505 (1976).

[77] B. Kubis and U.-G. Meissner, Nucl. Phys. A **679**, 698 (2001).

[78] D.R. Phillips, Phys. Lett. B **567**, 12 (2003).

[79] J.L. Friar, Ann. Phys. (N.Y.) **104**, 380 (1977).

[80] C.E. Carlson, Phys. Rev. D **34**, 2704 (1986).

[81] R. Schiavilla and V.R. Pandharipande, Phys. Rev. C **65**, 064009 (2002).

[82] R. Schiavilla, V.R. Pandharipande, and D.O. Riska, Phys. Rev. C **40**, 2294 (1989).

[83] A. Kievsky *et al.*, Few-Body Syst. **22**, 1 (1997).

[84] M. Viviani *et al.*, Few-Body Syst. **39**, 159 (2006).

[85] A. Kievsky *et al.*, J. Phys. G: Nucl. Part. Phys. **35**, 063101 (2008).

[86] L.E. Marcucci *et al.*, Phys. Rev. C **80**, 034003 (2009).

[87] T.-S. Park *et al.*, Phys. Lett. B **472**, 232 (2000); Y.-H. Song *et al.*, Phys. Lett. B **656**, 174 (2007); Y.-H. Song, R. Lazauskas, and T.-S. Park, Phys. Rev. C **79**, 064002 (2009); R. Lazauskas, Y.-H. Song, and T.-S. Park, Phys. Rev. C **83**, 034006 (2011).

[88] P.J. Mohr and B.N. Taylor, Rev. Mod. Phys. **77**, 1 (2005).

[89] C.D. Buchanan and M.R. Yearian, Phys. Rev. Lett. **15**, 303 (1965).

[90] D. Benaksas, D. Drickey, and D. Frèrejacque, Phys. Rev. **148**, 1327 (1966).

[91] J.E. Elias *et al.*, Phys. Rev. **177**, 2075 (1969).

[92] S. Galster *et al.*, Nucl. Phys. B **32**, 221 (1971).

[93] R.W. Berard *et al*, Phys. Lett. B **47**, 355 (1973).

[94] R.G. Arnold *et al.*, Phys. Rev. Lett. **35**, 776 (1975).

[95] G.G. Simon, C. Schmitt, and V.H. Walther, Nucl. Phys. A **364**, 285 (1981).

[96] R. Cramer *et al.*, Z. Phys. C **29**, 513 (1985).

[97] S. Platchkov *et al.*, Nucl. Phys. A **510**, 740 (1990).

[98] D. Abbott *et al.*, Phys. Rev. Lett. **82**, 1379 (1999).

[99] L.C. Alexa *et al.*, Phys. Rev. Lett. **82**, 1374 (1999).

[100] M.E. Schulze *et al.*, Phys. Rev. Lett. **52**, 597 (1984).

[101] I. The *et al.*, Phys. Rev. Lett. **67**, 173 (1991).

[102] C. Zhang *et al.*, Phys. Rev. Lett. **107**, 252501 (2011).

[103] V.F. Dmitriev *et al.*, Phys. Lett. **157B**, 143 (1985).

[104] B.B. Wojtsekhowski *et al.*, Pis'ma Zh. Eksp. Teor. Fiz. **43**, 567 (1986).

[105] R. Gilman *et al.*, Phys. Rev. Lett. **65**, 1733 (1990).

[106] D.M. Nikolenko *et al.*, Phys. Rev. Lett. **90**, 072501 (2003).

[107] B. Boden *et al.*, Z. Phys. C **49**, 175 (1991).

[108] M. Ferro-Luzzi *et al.*, Phys. Rev. Lett. **77**, 2630 (1996).

[109] M. Bouwhuis *et al.*, Phys. Rev. Lett. **82**, 3755 (1999).

[110] D. Abbott *et al.*, Phys. Rev. Lett. **84**, 5053 (2000).

[111] S. Auffret *et al.*, Phys. Rev. Lett. **54**, 649 (1985).

[112] P.E. Bosted *et al.*, Phys. Rev. C **42**, 38 (1990).

[113] I. Sick, Prog. Part. Nucl. Phys. **47**, 245 (2001).

[114] A. Amroun *et al.*, Nucl. Phys. A **579**, 596 (1994).

[115] S. Pastore *et al.*, Phys. Rev. C **87**, 035503 (2013).

[116] S.C. Pieper, AIP Conf. Proc. **1011**, 143 (2008).

[117] J.R. Bergervoet *et al.*, Phys. Rev. C **38**, 15 (1988).

[118] L. Heller, Phys. Rev. **120**, 627 (1960).

[119] W.A. van de Sanden, A.H. Emmen, J.J. de Swart, Report No. THEF-NYM-83.11, Nijmegen (1983), unpublished; quoted in Ref. [117].

APPENDIX A

INTERACTION HAMILTONIANS

In this appendix we define the notation and convention adopted in the present work. We also list the nuclear and electromagnetic interaction Hamiltonians involved in the calculation of the nuclear potential discussed in Chapter 3 and the electromagnetic charge and current operators examined in Chapter 4.

A.1 NOTATION AND CONVENTION

The expressions for the relativistic pion field in the isospin triplet, $\pi_a(\mathbf{r})$, and canonical conjugates, $\Pi_a(\mathbf{r})$, are represented in the Schrödinger picture [34], at position $\mathbf{r}$, as

$$\pi_a(\mathbf{r}) = \sum_{\mathbf{p}} \frac{1}{\sqrt{2\omega_p}} \left[c_{\mathbf{p},a} \, e^{i\mathbf{p}\cdot\mathbf{r}} + \text{h.c.} \right], \qquad (259)$$

$$\Pi_a(\mathbf{r}) = \sum_{\mathbf{p}} -i\sqrt{\frac{\omega_p}{2}} \left[c_{\mathbf{p},a} \, e^{i\mathbf{p}\cdot\mathbf{r}} - \text{h.c.} \right], \qquad (260)$$

where $a = x, y, z$ denotes the Cartesian component in isospin space, $c_{\mathbf{p},a}$ and $c_{\mathbf{p},a}^{\dagger}$ are the annihilation and creation operators for a pion of momentum $\mathbf{p}$ satisfying the standard commutation relations:

$$[c_{\mathbf{p},a}, c_{\mathbf{p}',a'}^{\dagger}] = \delta_{\mathbf{p},\mathbf{p}'}\delta_{a,a'} . \qquad (261)$$

Normalized plane waves $e^{i\mathbf{p}\cdot\mathbf{r}}/L^{3/2}$, satisfying periodic boundary conditions in a cubic box of volume L^3, are used in the above field operators. Since physical observables do not depend upon the normalization volume, we have set $L = 1$. Note that in Eqs. (259)–(261) a limit $L \to \infty$ is implicit; therefore:

$$\sum_{\mathbf{p}} \to \int_{\mathbf{p}} \equiv \int \frac{d\mathbf{p}}{(2\pi)^3} , \qquad (262)$$

$$\delta_{\mathbf{p},\mathbf{p}'} \to (2\pi)^3\delta(\mathbf{p} - \mathbf{p}') \equiv \bar{\delta}(\mathbf{p} - \mathbf{p}') . \qquad (263)$$

The pion energy ω_p is defined as $\omega_p \equiv \sqrt{p^2 + m_\pi^2}$, where in this context $m_\pi = (2\,m_{\pi^+} + m_{\pi^0})/3$ is the averaged pion mass over its states. The annihilation operators

of the charged and neutral pions are related to the Cartesian $c_{\mathbf{p},\alpha}$'s introduced in Eqs. (259)–(260) by

$$c_{\mathbf{p},\pm} = \frac{1}{\sqrt{2}}(c_{\mathbf{p},x} \mp i\, c_{\mathbf{p},y}) \,, \qquad c_{\mathbf{p},0} = c_{\mathbf{p},z} \,, \tag{264}$$

and the charged and neutral pion field operators are defined as

$$\pi_{\pm}(\mathbf{r}) \;=\; \frac{1}{\sqrt{2}}\left[\pi_x(\mathbf{r}) \mp i\,\pi_y(\mathbf{r})\right] = \sum_{\mathbf{p}} \frac{1}{\sqrt{2\omega_p}}\left[c_{\mathbf{p},\pm}\, e^{i\mathbf{p}\cdot\mathbf{r}} + c_{\mathbf{p},\mp}^{\dagger}\, e^{-i\mathbf{p}\cdot\mathbf{r}}\right] \,, \tag{265}$$

$$\pi_0(\mathbf{r}) \;=\; \pi_z(\mathbf{r}) \,, \tag{266}$$

such that $\pi_{+,0,-}(\mathbf{r})$ create $\pi^{-,0,+}$ or annihilate $\pi^{+,0,-}$, respectively.

The nucleon and Δ-isobar fields, $N(\mathbf{r})$ and $\Delta(\mathbf{r})$, with their corresponding canonical conjugates $i\,N^{\dagger}(\mathbf{r})$ and $i\,\Delta^{\dagger}(\mathbf{r})$, are taken in the non-relativistic limit as

$$N(\mathbf{r}) \;=\; \sum_{\mathbf{p},\sigma\tau} b_{\mathbf{p},\sigma\tau}\, e^{i\mathbf{p}\cdot\mathbf{r}}\chi_{\sigma\tau} \,, \tag{267}$$

$$\Delta(\mathbf{r}) \;=\; \sum_{\mathbf{p},\sigma_\Delta\tau_\Delta} d_{\mathbf{p},\sigma_\Delta\tau_\Delta}\, e^{i\mathbf{p}\cdot\mathbf{r}}\chi_{\sigma_\Delta\tau_\Delta} \,, \tag{268}$$

where $b_{\mathbf{p},\sigma\tau}$ and $d_{\mathbf{p},\sigma_\Delta\tau_\Delta}$ are the annihilation operators for a nucleon of momentum $\mathbf{p}$ and spin-isospin state $\chi_{\sigma\tau} = \chi_\sigma\eta_\tau$ and Δ-isobar of momentum $\mathbf{p}$ and spin-isospin state $\chi_{\sigma_\Delta\tau_\Delta} = \chi_{\sigma_\Delta}\eta_{\tau_\Delta}$, respectively. In this case, the operators $b_{\mathbf{p},\sigma\tau}$ and $b_{\mathbf{p},\sigma\tau}^{\dagger}$, and similarly $d_{\mathbf{p},\sigma_\Delta\tau_\Delta}$ and $d_{\mathbf{p},\sigma_\Delta\tau_\Delta}^{\dagger}$, satisfy the standard anticommutation relations for the fermionic fields:

$$\{b_{\mathbf{p},\sigma\tau}, b_{\mathbf{p}',\sigma'\tau'}^{\dagger}\} = \delta_{\mathbf{p},\mathbf{p}'}\delta_{\sigma,\sigma'}\delta_{\tau,\tau'} \,. \tag{269}$$

A.2 STRONG INTERACTION HAMILTONIANS

The interaction Hamiltonians involving pions, nucleons and Δ-isobars fields are derived from the chiral Lagrangiangs $\mathcal{L}_{\pi N}$, $\mathcal{L}_{\pi N\Delta}$, and $\mathcal{L}_{NN}$ in Eq. (2) formulated in Refs. [3, 4, 36–39]. In particular the interaction Hamiltonians implied by πN and $\pi N\Delta$ Lagrangians read as

$$H_{\pi NN} \;=\; \frac{g_A}{F_\pi} \int d\mathbf{r}\, N^{\dagger}(\mathbf{r})\left[\boldsymbol{\sigma}\cdot\boldsymbol{\nabla}\pi_a(\mathbf{r})\right]\tau_a\, N(\mathbf{r}) \,, \tag{270}$$

$$H_{\pi\pi NN} = \frac{1}{F_\pi^2} \int d\mathbf{r}\, N^\dagger(\mathbf{r})\, [\boldsymbol{\pi}(\mathbf{r}) \times \mathbf{\Pi}(\mathbf{r})] \cdot \boldsymbol{\tau}\, N(\mathbf{r}) \ , \tag{271}$$

$$H_{\pi N\Delta} = \frac{h_A}{F_\pi} \int d\mathbf{r}\, \Delta^\dagger(\mathbf{r})\, [\mathbf{S} \cdot \boldsymbol{\nabla}\pi_a(\mathbf{r})]\, T_a\, N(\mathbf{r}) + \text{h.c.} \ , \tag{272}$$

$$H^{(2)}_{\pi\pi NN} = \int d\mathbf{r}\, N^\dagger(\mathbf{r}) \left[c_1 \left(-4\,m_\pi^2 + \frac{8\,m_\pi^2}{F_\pi^2}\,\pi^2(\mathbf{r}) \right) - \frac{4\,c_2}{F_\pi^2}\,\mathbf{\Pi}^2(\mathbf{r}) \right.$$
$$- \frac{4\,c_3}{F_\pi^2}\,\mathbf{\Pi}^2(\mathbf{r}) + \frac{4\,c_3}{F_\pi^2}\,[\boldsymbol{\nabla}\boldsymbol{\pi}(\mathbf{r}) \cdot \boldsymbol{\nabla}\boldsymbol{\pi}(\mathbf{r})]$$
$$\left. + \frac{2\,c_4}{F_\pi^2}\epsilon_{abc}\tau_c\,[\boldsymbol{\nabla}\pi_a(\mathbf{r}) \times \boldsymbol{\nabla}\pi_b(\mathbf{r})] \cdot \boldsymbol{\sigma} \right] N(\mathbf{r}) \ , \tag{273}$$

$$H^{(2)}_{\pi N\Delta} = 2i\,\frac{(b_3 + b_8)}{F_\pi} \int d\mathbf{r}\, \Delta^\dagger(\mathbf{r})\, [\mathbf{S} \cdot \boldsymbol{\nabla}\Pi_a(\mathbf{r})]\, T_a\, N(\mathbf{r}) + \text{h.c.} \ , \tag{274}$$

where σ_a and τ_a are spin and isospin Pauli matrices and S_a and T_a are transition spin and isospin operators, converting a nucleon into a Δ-isobar and satisfying

$$S_a^\dagger S_b = \frac{2}{3}\delta_{ab} - \frac{i}{3}\epsilon_{abc}\sigma_c \ , \tag{275}$$

and similarly for $T_a^\dagger T_b$. The "known" LEC's g_A, F_π, and h_A are the nucleon axial coupling constant, pion decay amplitude, and N-to-Δ axial coupling constant, respectively, while the LEC's, c_i ($i = 1, ..., 4$), are determined by fits to πN scattering data [11] as discussed in Chapter 3. The naive power counting of the interaction Hamiltonians follows by noting that each derivative brings in a factor of Q, where Q is the low-momentum scale. Therefore, Eqs. (270)–(272) give rise to interactions of order Q (panels (a), (b) and (c) of Fig. 19, respectively), while Eqs. (273)–(274) represent their sub-leading corrections of order Q^2 (panels (d) and (e) of Fig. 19, respectively).

The lowest order (LO or Q^0) NN Lagrangian, represented by panel (f) of Fig. (19), has no derivatives of the nucleon fields and reads [1]

$$H_{\text{CT0}} = \frac{1}{2} \int d\mathbf{r} \left[C_S\, [N^\dagger(\mathbf{r})\, N(\mathbf{r})]\, [N^\dagger(\mathbf{r})\, N(\mathbf{r})] + C_T\, [N^\dagger(\mathbf{r})\, \boldsymbol{\sigma}\, N(\mathbf{r})] \cdot [N^\dagger(\mathbf{r})\, \boldsymbol{\sigma}\, N(\mathbf{r})] \right] \ , \tag{276}$$

where the "unknown" LEC's, C_S and C_T, are determined by fit to the NN data.

The second order (Q^2) NN contact interaction, denoted by a solid dot in panel

(g) of Fig. 19, can be stated as follows [3, 4, 39]

$$
\begin{aligned}
H_{\mathrm{CT2}} \;=\; & C_1' \int d\mathbf{r}\Big[[N^\dagger(\mathbf{r})\,\boldsymbol{\nabla} N(\mathbf{r})]^2 + [\boldsymbol{\nabla} N^\dagger(\mathbf{r})\,N(\mathbf{r})]^2\Big] \\
& + C_2' \int d\mathbf{r}\Big[[N^\dagger(\mathbf{r})\,\boldsymbol{\nabla} N(\mathbf{r})]\cdot[\boldsymbol{\nabla} N^\dagger(\mathbf{r})\,N(\mathbf{r})]\Big] \\
& + C_3' \int d\mathbf{r}[N^\dagger(\mathbf{r})\,N(\mathbf{r})]\Big[N^\dagger(\mathbf{r})\,\boldsymbol{\nabla}^2 N(\mathbf{r}) + \boldsymbol{\nabla}^2 N^\dagger(\mathbf{r})\,N(\mathbf{r})\Big] \\
& + i\,C_4' \int d\mathbf{r}\Big[[N^\dagger(\mathbf{r})\,\boldsymbol{\nabla} N(\mathbf{r})]\cdot[\boldsymbol{\nabla} N^\dagger(\mathbf{r})\times\boldsymbol{\sigma}\,N(\mathbf{r})] \\
& \quad + [\boldsymbol{\nabla} N^\dagger(\mathbf{r})\,N(\mathbf{r})]\cdot[N^\dagger(\mathbf{r})\,\boldsymbol{\sigma}\times\boldsymbol{\nabla} N(\mathbf{r})]\Big] \\
& + i\,C_5' \int d\mathbf{r}[N^\dagger(\mathbf{r})\,N(\mathbf{r})][\boldsymbol{\nabla} N^\dagger(\mathbf{r})\cdot\boldsymbol{\sigma}\times N(\mathbf{r})] \\
& + i\,C_6' \int d\mathbf{r}[N^\dagger(\mathbf{r})\,\boldsymbol{\sigma}\,N(\mathbf{r})]\cdot[\boldsymbol{\nabla} N^\dagger(\mathbf{r})\times\boldsymbol{\nabla} N(\mathbf{r})] \\
& + (C_7'\,\delta_{ik}\,\delta_{jl} + C_8'\,\delta_{il}\,\delta_{kj} + C_9'\,\delta_{ij}\,\delta_{kl})\int d\mathbf{r}\Big[[N^\dagger(\mathbf{r})\,\sigma_k\,\partial_i N(\mathbf{r})] \\
& \quad \times[N^\dagger(\mathbf{r})\,\sigma_l\,\partial_j N(\mathbf{r})] + [\partial_i N^\dagger(\mathbf{r})\,\sigma_k\,N(\mathbf{r})][\partial_j N^\dagger(\mathbf{r})\,\sigma_l\,N(\mathbf{r})]\Big] \\
& + (C_{10}'\,\delta_{ik}\,\delta_{jl} + C_{11}'\,\delta_{il}\,\delta_{kj} + C_{12}'\,\delta_{ij}\,\delta_{kl})\int d\mathbf{r}[N^\dagger(\mathbf{r})\,\sigma_k\,\partial_i N(\mathbf{r})] \\
& \quad \times[\partial_j N^\dagger(\mathbf{r})\,\sigma_l\,N(\mathbf{r})] + \left[\tfrac{1}{2}C_{13}'(\delta_{ik}\,\delta_{jl} + \delta_{il}\,\delta_{kj}) + C_{14}'\,\delta_{ij}\,\delta_{kl}\right] \\
& \quad \times \int d\mathbf{r}[\partial_i N^\dagger(\mathbf{r})\,\sigma_k\,\partial_j N(\mathbf{r}) + \partial_j N^\dagger(\mathbf{r})\,\sigma_k\,\partial_i N(\mathbf{r})][N^\dagger(\mathbf{r})\,\sigma_l\,N(\mathbf{r})] \,.(277)
\end{aligned}
$$

The Hamiltonian in Eq. (277) leads (in the center-of-mass frame) to seven independent operator structure in the potential each multiplied by a coefficient named C_i with $i = 1, \ldots 7$ that is a linear combinations of these LEC's C_i'. The Hamiltonian H_{CT4} at order $\mathcal{Q}^4$ (panel (h) of Fig. 19) is not given explicitly. We only list the corresponding contact potential in the center-of-mass (see Chapter 3).

A.3 ELECTROMAGNETIC INTERACTION HAMILTONIANS

In this section we list the electromagnetic interaction Hamiltonians obtained by "minimal" and "non-minimal" substitutions as discussed in Sec. 2.3 of Chapter 2. In the following we distinguish between interactions involved in the construction of the charge operators and those involved in the derivation of the current operators. The electromagnetic operators are obtained up to one loop, $e\,\mathcal{Q}$ in the power counting, and Δ-isobars are not retained in their calculation.
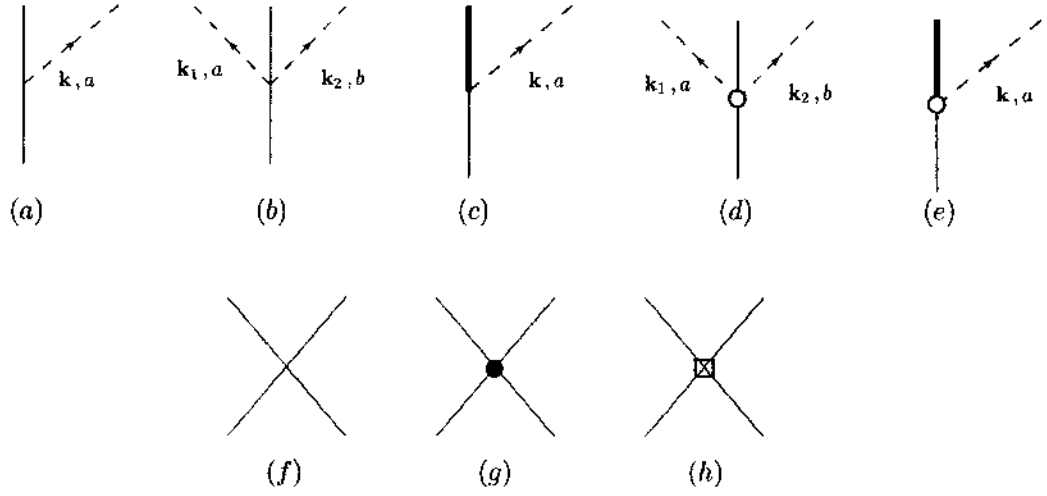
FIG. 19: Schematic representation of the strong interaction Hamiltonians. Pions are represented by dashed lines, nucleons by solid lines and Δ-isobars by solid thick lines. The open circle represents the sub-leading contribution to the corresponding interactions. The solid dot and open square represent the contact interactions at Q^2 and Q^4, respectively.

A.3.1 ELECTROMAGNETIC INTERACTION HAMILTONIANS FOR CHARGE OPERATORS

The relevant interaction Hamiltonians for the derivation of charge operators up to one loop are give by

$$H_{\gamma NN} = e\, e_N \int dr\, N^\dagger(r)\, A^0(r)\, N(r) \ , \tag{278}$$

$$H_{\gamma\pi\pi} = e \int dr\, A^0(r)\, [\pi(r) \times \Pi(r)]_z \ , \tag{279}$$

$$H_{\gamma\pi N} = e\frac{g_A}{2\,F_\pi\,m_N} \int dr\, N^\dagger(r)\, \boldsymbol{\sigma} \cdot \nabla A^0(r)\, [\tau \cdot \pi(r) + \pi_z(r)]\, N(r) \ , \tag{280}$$

$$H_{\gamma NN}^{(2)} = -e\frac{2\,\mu_N - e_N}{8\,m_N^2} \int dr\, N^\dagger(r)\, \left[\nabla^2 A^0(r) + \boldsymbol{\sigma} \times \nabla A^0(r) \cdot \overrightarrow{\nabla}\right.$$

$$\left. - \overleftarrow{\nabla} \cdot \boldsymbol{\sigma} \times \nabla A^0(r)\right] N(r) \ , \tag{281}$$

where m_N is the nucleon mass. The isospin operators e_N and μ_N are defined as

$$e_N = (1 + \tau_z)/2 \ , \quad \kappa_N = (\kappa_S + \kappa_V\, \tau_z)/2 \ , \quad \mu_N = e_N + \kappa_N \ , \tag{282}$$

FIG. 20: Schematic representation of the electromagnetic interaction Hamiltonians involved in the derivation of charge operators. Notation is as in Fig. 19 but for the wavy lines which denotes photons. The full dot in panel (c) represents the $\gamma\pi N$ interaction of order $e\,Q$, and the square in panel (d) denotes the $(Q/m_N)^2$ relativistic correction to the term in panel (a).

and κ_S and κ_V are the isoscalar and isovector combinations of the anomalous magnetic moments of the proton and neutron. The arrow over the gradient specifies whether it acts on the left or right nucleon field. The interaction Hamiltonians in Eqs. (278)–(281) are schematically represented in Fig. 20. They behave, relative to the low-momentum scale Q, in the following way (ignoring the counting Q assumed for the external field): $H_{\gamma NN} \sim e\,Q^0$ (panel (a) of Fig. 20), $H_{\gamma\pi\pi}$ and $H_{\gamma\pi N} \sim e\,Q$ (panel (b) and (c) of Fig. 20), and $H_{\gamma NN}^{(2)} \sim e\,Q^2$ (panel (d) of Fig. 20).

A.3.2 ELECTROMAGNETIC INTERACTION HAMILTONIANS FOR CURRENT OPERATORS

Finally, the relevant interaction Hamiltonians involved in the derivation of current

operators up to one loop read:

$$
H_{\gamma NN} = e \int dr\, N^{\dagger}(\mathbf{r}) \left[i\, \frac{e_N}{2\,m_N}[-\overleftarrow{\nabla} \cdot \mathbf{A}(\mathbf{r}) + \mathbf{A}(\mathbf{r}) \cdot \overrightarrow{\nabla}] \right.
$$
$$
\left. -\frac{\mu_N}{2\,m_N}\, \boldsymbol{\sigma} \cdot \boldsymbol{\nabla} \times \mathbf{A}(\mathbf{r}) \right] N(\mathbf{r})\ , \tag{283}
$$

$$
H_{\gamma\pi\pi} = e \int dr\, \epsilon_{zab}\, \pi_a(\mathbf{r})\, \mathbf{A}(\mathbf{r}) \cdot \left[\boldsymbol{\nabla}\pi_b(\mathbf{r}) \right]\ , \tag{284}
$$

$$
H_{\gamma\pi N} = -e\,\frac{g_A}{F_\pi} \int dr\, N^{\dagger}(\mathbf{r})\, \boldsymbol{\sigma} \cdot \mathbf{A}(\mathbf{r})\, [\boldsymbol{\tau} \times \boldsymbol{\pi}(\mathbf{r})]_z\, N(\mathbf{r})\ , \tag{285}
$$

$$
H^{(2)}_{\gamma\pi N} = \frac{-e}{F_\pi}\frac{g_A}{F_\pi} \int dr\, N^{\dagger}(\mathbf{r}) \left[[d_8'\, \boldsymbol{\nabla}\pi_z(\mathbf{r}) + d_9'\, \tau_a\, \boldsymbol{\nabla}\pi_a(\mathbf{r}) \right.
$$
$$
\left. +d_{21}'\, \epsilon_{zab}\, \tau_b\, \boldsymbol{\sigma} \times \boldsymbol{\nabla}\pi_a(\mathbf{r})] \cdot \boldsymbol{\nabla} \times \boldsymbol{A}(\mathbf{r}) \right] N(\mathbf{r})\ , \tag{286}
$$

where the parameters d_i' are the LEC's discussed in Sec. 4.3. The above Hamiltonians are schematically represented in Fig. 21 and they behave as: $H_{\gamma NN}$ and $H_{\gamma\pi\pi} \sim e\,Q$ (panels (a) and (b) of Fig. 21), $H_{\gamma\pi N} \sim e\,Q^0$ (panel (c) of Fig. 21), and $H^{(2)}_{\gamma\pi N} \sim e\,Q^2$ (panel (d) of Fig. 21). Panel (e) of Fig. 21 represents the $(Q/m_N)^2$ relativistic correction to the one-body operator in panel (a) and scales as $\sim e\,Q^2$.

Minimal substitution in H_{CT2} leads to a contact Hamiltonians which includes the coupling to the EM field and implies a two-nucleon contact operators. These contact interactions, represented by panel (f) of Fig. 21, are listed in [28] and will not be reported here. They depend on the LEC's involved in the strong interaction Hamiltonians H_{CT2} discussed in Sec. A.2.

However non-minimal couplings through the electromagnetic tensor $F_{\mu\nu}$ are also allowed (represented also by panel (f) of Fig. 21). The only two independent operator structure are

$$
H_{CT,\gamma nm} = e \int dr \left[C_{15}' N^{\dagger}(\mathbf{r})\, \boldsymbol{\sigma}\, N(\mathbf{r})\, N^{\dagger}(\mathbf{r})\, N(\mathbf{r}) + C_{16}'[N^{\dagger}(\mathbf{r})\, \boldsymbol{\sigma}\, \tau_z\, N(\mathbf{r})\, N^{\dagger}(\mathbf{r})\, N(\mathbf{r}) \right.
$$
$$
\left. -N^{\dagger}(\mathbf{r})\, \boldsymbol{\sigma}\, N(\mathbf{r})\, N^{\dagger}(\mathbf{r})\, \tau_z\, N(\mathbf{r})] \right] \cdot \boldsymbol{\nabla} \times \boldsymbol{A}\ , \tag{287}
$$

where the isoscalar C_{15}' and the isovector C_{16}' LEC's (as well as the d_i' in Eq. (286) can be determined by fitting data in the few-nucleon systems as discussed in Sec. 4.3.
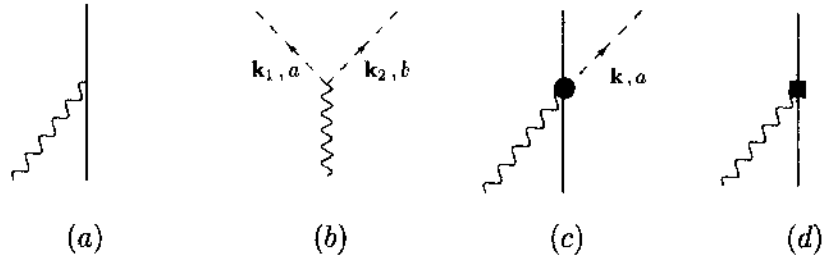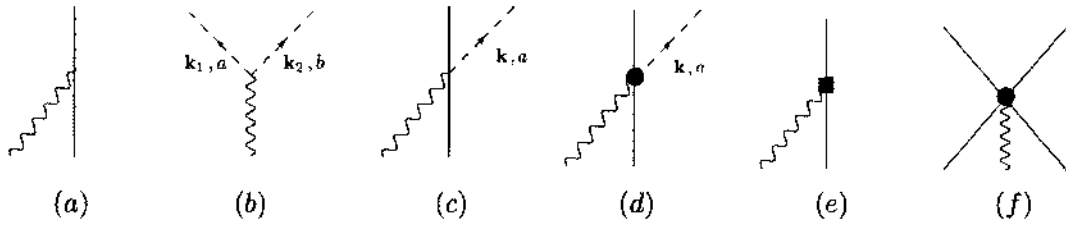
FIG. 21: Schematic representation of the electromagnetic interaction Hamiltonians involved in the derivation of current operators. Notation is as in Fig. 20. The solid dot in panel (d) is associated with the $\gamma\pi N$ current coupling of order $e\,\mathcal{Q}^2$, involving the LEC's d'_8, d'_9, and d''_{21}; the solid dot in panel (f) denote the two-body contact terms of minimal and non-minimal nature, the latter involving the LEC's C'_{15} and C'_{16}. The square in panel (e) denotes the $(\mathcal{Q}/m_N)^2$ relativistic correction to the term in panel (a).

APPENDIX B

DIMENTIONAL REGULARIZATION: LOOP

CORRECTIONS TO THE NN POTENTIAL AT NLO

INCLUDING Δ'S

As discussed in Chapter 3, TPE contributions contain ultraviolet divergencies which need to be removed by a proper regularization scheme. In order to remove these divergencies, loop integrals have been regularized via dimensional regularization (DR) [40, 41]. In practice we evaluate the three momentum loop integrals as follows

$$\int_l = \int \frac{d^3 l}{(2\pi)^3} \rightarrow \int \frac{d^{(3-\epsilon)} l}{(2\pi)^3} \mu^\epsilon \ , \tag{288}$$

where μ is a renormalization scale introduced to preserve physical dimensions. As $d \rightarrow 3$, this integral becomes singular; however its divergent parts are identified by the parameter $\epsilon = 3 - d$. Once the regularization is carried out, the divergencies are absorbed, order by order, by the corresponding LEC's, which are determined from experimental data. In what follows, we discuss DR of the loop integrals involved in the calculation of diagrams (g)-(i) of Fig. 3, given in Eqs. (45) (47), respectively.

B.1 A COLLECTION OF USEFUL FORMULAE

In the following we define

$$\int_l \equiv \int \frac{d^d l}{(2\pi)^d} \tag{289}$$

and

$$I_n^d(A;\alpha) \equiv \int_l \frac{l^n}{(l^2 + A)^\alpha} \ , \qquad \alpha, A > 0 \ , \qquad n \text{ even} \geq 0 \ , \tag{290}$$

where it is understood that the result of the integration is analytically continued to $d = 3$. We find:

$$I_0^d(A;\alpha) = \frac{1}{(4\pi)^{d/2}} \frac{\Gamma(\alpha - d/2)}{\Gamma(\alpha)} A^{-(\alpha - d/2)} \ , \tag{291}$$

$$I_2^d(A;\alpha) = \frac{1}{(4\pi)^{d/2}} \frac{d}{2} \frac{\Gamma(\alpha - d/2 - 1)}{\Gamma(\alpha)} A^{-(\alpha - d/2 - 1)} \ , \tag{292}$$

$$I_4^d(A;\alpha) = \frac{1}{(4\pi)^{d/2}} \frac{d(d+2)}{4} \frac{\Gamma(\alpha - d/2 - 2)}{\Gamma(\alpha)} A^{-(\alpha - d/2 - 2)} \ , \tag{293}$$

where $\Gamma(z)$ is the Γ-function satisfying $z\,\Gamma(z) = \Gamma(z+1)$, with asymptotic behavior for $z \to 0$ given by

$$\Gamma(z) = \frac{1}{z} - \gamma + \left(\frac{\gamma^2}{2} + \frac{\pi^2}{12}\right) z + O(z^2) \,, \tag{294}$$

and $\gamma \approx 0.5772$ is the Euler-Mascheroni constant. Note that a factor μ^{3-d} is understood to multiply the r.h.s. of Eqs. (291)–(293). The following Feynman's parametrizations will also be utilized below:

$$\frac{1}{A^\alpha B^\beta} = \frac{\Gamma(\alpha+\beta)}{\Gamma(\alpha)\,\Gamma(\beta)} \int_0^1 dz \frac{z^{\alpha-1}(1-z)^{\beta-1}}{[z\,A + (1-z)\,B]^{\alpha+\beta}} \,, \tag{295}$$

$$\frac{1}{A\,B\,C} = 2 \int_0^1 dz_1 \int_0^{1-z_1} dz_2 \frac{1}{[z_1\,A + z_2\,B + (1 - z_1 - z_2)\,C]^3} \,. \tag{296}$$

B.2 REGULARIZATION OF "TRIANGLE-LIKE" CONTRIBUTION WITH ONE Δ

The "triangle-like" contribution with one Δ-isobar, given in Eq. (45), can be simplified in the following way

$$v_{\mathrm{tr}}^{2\pi,\mathrm{NLO}}(k; 1\Delta) = \frac{2\,h_A^2}{9\,F_\pi^4}\,\boldsymbol{\tau}_1 \cdot \boldsymbol{\tau}_2 \left[L_0^{\mathrm{tr}}(k)\,k^2 - L_2^{\mathrm{tr}}(k)\right] \,, \tag{297}$$

where $L_0^{\mathrm{tr}}(k)$ and $L_2^{\mathrm{tr}}(k)$ are defined, respectively, as

$$L_0^{\mathrm{tr}}(k) = \frac{2}{\pi} \int_0^\infty d\lambda \frac{\lambda^2}{\lambda^2 + 4\,\Delta^2} \int_l \frac{1}{(\lambda^2 + \omega_+^2)(\lambda^2 + \omega_-^2)} \tag{298}$$

$$L_2^{\mathrm{tr}}(k) = \frac{2}{\pi} \int_0^\infty d\lambda \frac{\lambda^2}{\lambda^2 + 4\,\Delta^2} \int_0^1 dy \int_l \frac{(2\,y - 1)^2\,k^2 + l^2}{[\lambda^2 + l^2 + C(y, k)]^2} \,. \tag{299}$$

Using the Feynman's parametrization given in Eq. (295) and shifting the integration variables, $[\mathbf{l} - (2\,y - 1)\,\mathbf{k}] \to \mathbf{l}$, the term $L_0^{\mathrm{tr}}(k)$ can be written as

$$L_0^{\mathrm{tr}}(k) = \frac{2}{\pi} \int_0^\infty d\lambda \frac{\lambda^2}{\lambda^2 + 4\,\Delta^2} \int_0^1 dy \int_l \frac{1}{[\lambda^2 + l^2 + C(y, k)]^2} \,, \tag{300}$$

where the function $C(y, k)$ has been defined as

$$C(y, k) = 4\left[m_\pi^2 + y\,(1 - y)\,k^2\right] > 0 \qquad y \in [0, 1] \,. \tag{301}$$

The integral over $\mathbf{l}$ is converging; therefore using Eq. (291) we find

$$L_0^{\mathrm{tr}}(k) = \frac{1}{2} \int_0^1 dy \int_\lambda \frac{1}{(\lambda^2 + 4\,\Delta^2)\,[\lambda^2 + C(y, k)]^{1/2}} \,, \tag{302}$$

where we have used

$$\int_0^\infty d\lambda\, \lambda^2 = \frac{(2\pi)^3}{4\pi} \int_\lambda . \tag{303}$$

The integral $L_0^{tr}(k)$ is logarithmically divergent. Using one more time the Eq. (295), we express $L_0^{tr}(k)$ as

$$L_0^{tr}(k) = \frac{1}{4} \int_0^1 dy \int_0^1 dz \frac{1}{\sqrt{z}} \int_\lambda \frac{1}{[\lambda^2 + D(y,z,k)]^{3/2}} , \tag{304}$$

where the function $D(y,z,k)$ has been defined as

$$D(y,z,k) = z\, C(y,k) + 4\,\Delta^2\,(1-z) > 0 \qquad y,z \in [0,1] . \tag{305}$$

The integral over λ is carried out in dimensional regularization ($\epsilon = 3 - d$). Therefore, collecting the results we find that

$$L_0^{tr}(k) = \frac{1}{8\pi^2} \left(\frac{2}{\epsilon} - \gamma + \ln\pi \right) + \overline{L}_0^{tr}(k) , \tag{306}$$

where the finite part of the integral reads as

$$\overline{L}_0^{tr}(k) = -\frac{1}{16\pi^2} \int_0^1 dy \int_0^1 dz \frac{1}{\sqrt{z}} \ln\frac{D(y,z,k)}{4\mu^2} . \tag{307}$$

The integral in Eq. (307) is well defined in the limit $z \to 0$. It can conveniently be calculated numerically.

We now turn our attention to the integral $L_2^{tr}(k)$, which can be written as

$$L_2^{tr}(k) = \frac{2}{\pi} \int_0^\infty d\lambda \frac{\lambda^2}{\lambda^2 + 4\Delta^2} \int_0^1 dy \int_1 \frac{(2y-1)^2 k^2 + l^2}{[\lambda^2 + l^2 + C(y,k)]^2} \equiv L_{2a}^{tr}(k) + L_{2b}^{tr}(k) , \tag{308}$$

and the term $L_{2a}^{tr}(k)$ proportional to $(2y-1)^2 k^2$ can be dealt with as above. Therefore, it reads as

$$L_{2a}^{tr}(k) = \frac{k^2}{24\pi^2} \left(\frac{2}{\epsilon} - \gamma + \ln\pi \right) + \overline{L}_{2a}^{tr}(k) , \tag{309}$$

where

$$\overline{L}_{2a}^{tr}(k) = -\frac{k^2}{16\pi^2} \int_0^1 dy\, (2y-1)^2 \int_0^1 dz \frac{1}{\sqrt{z}} \ln\frac{D(y,z,k)}{4\mu^2} . \tag{310}$$

Instead, the integral $L_{2b}^{tr}(k)$ can be written as

$$L_{2b}^{tr}(k) = \frac{2}{\pi} \int_0^1 dy \int_0^\infty d\lambda \frac{\lambda^2}{\lambda^2 + 4\Delta^2} \int_1 \frac{l^2}{[\lambda^2 + l^2 + C(y,k)]^2} , \tag{311}$$

which can be expressed as the linear combination

$$L_{2b}^{\text{tr}}(k) = L_{2c}^{\text{tr}}(k) - 4\,\Delta^2\, L_{2d}^{\text{tr}}(k) \ , \tag{312}$$

where

$$L_{2c}^{\text{tr}}(k) = \frac{2}{\pi} \int_0^1 \mathrm{d}y \int_0^\infty \mathrm{d}\lambda \int_1 \frac{l^2}{[\lambda^2 + l^2 + C(y,k)]^2} \ , \tag{313}$$

$$L_{2d}^{\text{tr}}(k) = \frac{2}{\pi} \int_0^1 \mathrm{d}y \int_0^\infty \mathrm{d}\lambda \, \frac{1}{\lambda^2 + 4\,\Delta^2} \int_1 \frac{l^2}{[\lambda^2 + l^2 + C(y,k)]^2} \ . \tag{314}$$

In the integral $L_{2c}^{\text{tr}}(k)$ one can first perform the integral in λ obtaining

$$L_{2c}^{\text{tr}}(k) = \frac{1}{2} \int_0^1 \mathrm{d}y \int_1 \frac{l^2}{[l^2 + C(y,k)]^{3/2}} \ , \tag{315}$$

which leads to a quadratic divergent integral. Performing the usual regularization, we find

$$L_{2c}^{\text{tr}}(k) = -\frac{1}{8\,\pi^2} \left(\frac{2}{\epsilon} - \gamma + \ln\pi + \frac{1}{3} \right) \left(6\,m_\pi^2 + k^2 \right) + \overline{L}_{2c}^{\text{tr}}(k) \ , \tag{316}$$

where the finite part of the integral is given by

$$\overline{L}_{2c}^{\text{tr}}(k) = \frac{3}{16\,\pi^2} \int_0^1 \mathrm{d}y \, C(y,k) \ln\frac{C(y,k)}{4\,\mu^2} \ . \tag{317}$$

The remaining integral $L_{2d}^{\text{tr}}(k)$ is decomposed as

$$L_{2d}^{\text{tr}}(k) = L_{2e}^{\text{tr}}(k) - L_{2f}^{\text{tr}}(k) + L_{2g}^{\text{tr}}(k) \ , \tag{318}$$

where

$$L_{2e}^{\text{tr}}(k) = \frac{2}{\pi} \int_0^1 \mathrm{d}y \int_0^\infty \mathrm{d}\lambda \, \frac{1}{\lambda^2 + 4\,\Delta^2} \int_1 \frac{1}{\lambda^2 + l^2 + C(y,k)} \ , \tag{319}$$

$$L_{2f}^{\text{tr}}(k) = \frac{2}{\pi} \int_0^1 \mathrm{d}y \int_0^\infty \mathrm{d}\lambda \int_1 \frac{1}{[\lambda^2 + l^2 + C(y,k)]^2} \ , \tag{320}$$

$$L_{2g}^{\text{tr}}(k) = \frac{2}{\pi} \int_0^1 \mathrm{d}y \, [4\,\Delta^2 - C(y,k)] \int_0^\infty \mathrm{d}\lambda \, \frac{1}{\lambda^2 + 4\,\Delta^2} \int_1 \frac{1}{[\lambda^2 + l^2 + C(y,k)]^2} \ . \tag{321}$$

The integral $L_{2g}^{\text{tr}}(k) \equiv \overline{L}_{2g}^{\text{tr}}(k)$ is finite, and can be easily done. It is convenient to parametrize it as

$$\begin{aligned}
\overline{L}_{2g}^{\text{tr}}(k) &= \frac{1}{8\,\pi^2} \int_0^1 \mathrm{d}y \, [4\,\Delta^2 - C(y,k)] \int_0^1 \mathrm{d}z \, \frac{1}{\sqrt{z}} \int_0^\infty \mathrm{d}\lambda \, \frac{1}{[\lambda^2 + D(y,k)]^2} \\
&= \frac{1}{8\,\pi^2} \int_0^1 \mathrm{d}y \, [4\,\Delta^2 - C(y,k)] \int_0^1 \mathrm{d}z \, \frac{1}{\sqrt{z}} \, \frac{1}{D(y,z,k)} \ ,
\end{aligned} \tag{322}$$

where in the first line the integration in l has been performed and the Feyman's parametrization has been used. The integral $L_{2f}^{tr}(k)$ has a logarithmic divergence; performing first the integral in λ and then using Eq. (291), we find

$$L_{2f}^{tr}(k) = \frac{1}{8\pi^2}\left(\frac{2}{\epsilon} - \gamma + \ln\pi\right) + \overline{L}_{2f}^{tr}(k) \, , \tag{323}$$

where

$$\overline{L}_{2f}^{tr}(k) = -\frac{1}{8\pi^2}\int_0^1 dy \ln\frac{C(y,k)}{4\mu^2} \, . \tag{324}$$

The integral $L_{2e}^{tr}(k)$ is further decomposed as

$$L_{2e}^{tr}(k) = -L_{2h}^{tr}(k) + 4\Delta^2 L_{2i}^{tr}(k) + L_{2j}^{tr}(k) \, , \tag{325}$$

where

$$L_{2h}^{tr}(k) = \frac{2}{\pi}\int_0^1 dy \int_0^\infty d\lambda \int_1 \frac{1}{[\lambda^2 + l^2 + C(y,k)]\,[l^2 + C(y,k)]} \, , \tag{326}$$

$$L_{2i}^{tr}(k) = \frac{2}{\pi}\int_0^1 dy \int_0^\infty d\lambda \frac{1}{\lambda^2 + 4\Delta^2}\int_1 \frac{1}{[\lambda^2 + l^2 + C(y,k)]\,[l^2 + C(y,k)]} \tag{327}$$

$$L_{2j}^{tr}(k) = \frac{2}{\pi}\int_0^1 dy \int_0^\infty d\lambda \frac{1}{\lambda^2 + 4\Delta^2}\int_1 \frac{1}{l^2 + C(y,k)} \, . \tag{328}$$

After integrating over λ, $L_{2h}^{tr}(k)$ can be regularized in $d = 3$ in the usual way as

$$L_{2h}^{tr}(k) = \frac{1}{4\pi^2}\left(\frac{2}{\epsilon} - \gamma + \ln\pi\right) + \overline{L}_{2h}^{tr}(k) \, , \tag{329}$$

where

$$\overline{L}_{2h}^{tr}(k) = -\frac{1}{4\pi^2}\int_0^1 dy \ln\frac{C(y,k)}{4\mu^2} \, . \tag{330}$$

To calculate the (finite) integral $L_{2i}^{tr}(k) \equiv \overline{L}_{2i}^{tr}(k)$, one can use the Feynman's parametrization given in Eq. (296) with $A = \lambda^2 + 4\Delta^2$, $B = l^2 + C$, and $C' = \lambda^2 + l^2 + C$ to obtain

$$\overline{L}_{2i}^{tr}(k) = \frac{1}{4\pi^2}\int_0^1 dy \int_0^1 dz \frac{1 - (1-z)^{1/2}}{z^{3/2}} \frac{1}{D(y,z,k)} \, , \tag{331}$$

where we have rescaled the λ and l integrations as $\sqrt{1-z_2}\,\lambda \to \lambda$ and $\sqrt{1-z_1}\,l \to l$. Also, we have defined $z = 1 - z_1$ and introduced the function $D(y,z,k)$ of Eq. (305). Finally, we have carried out the integrations over z_2, λ, and l, respectively. Note that the singularity at $z = 0$ is integrable. We are left with the linearly divergent integral $L_{2j}^{tr}(k) \equiv \overline{L}_{2j}^{tr}(k)$:

$$\overline{L}_{2j}^{tr}(k) = \frac{1}{2\Delta}\int_0^1 dy \int_1 \frac{1}{l^2 + C(y,k)} = -\frac{1}{4\pi}\int_0^1 dy \sqrt{\frac{C(y,k)}{4\Delta^2}} \, , \tag{332}$$

and the linear divergence does not show up in dimensional regularization. Therefore, the integral $L_{2e}^{tr}(k)$ in Eq. (325) becomes

$$L_{2e}^{tr}(k) = -\frac{1}{4\pi^2} \left(\frac{2}{\epsilon} - \gamma + \ln\pi \right) + \overline{L}_{2e}^{tr}(k) , \tag{333}$$

where

$$\overline{L}_{2e}^{tr}(k) = \frac{1}{4\pi^2} \left[\int_0^1 dy \ln\frac{C(y,k)}{4\mu^2} - \pi \int_0^1 dy \sqrt{\frac{C(y,k)}{4\Delta^2}} \right. $$
$$\left. +4\Delta^2 \int_0^1 dy \int_0^1 dz \frac{1}{D(y,z,k)} \frac{1-(1-z)^{1/2}}{z^{3/2}} \right] , \tag{334}$$

The integral $L_{2d}^{tr}(k)$ in Eq. (318) becomes

$$L_{2d}^{tr}(k) = -\frac{3}{8\pi^2} \left(\frac{2}{\epsilon} - \gamma + \ln\pi \right) + \overline{L}_{2d}^{tr}(k) , \tag{335}$$

where

$$\overline{L}_{2d}^{tr}(k) = \frac{1}{8\pi^2} \left[3 \int_0^1 dy \ln\frac{C(y,k)}{4\mu^2} - 2\pi \int_0^1 dy \sqrt{\frac{C(y,k)}{4\Delta^2}} \right.$$
$$\left. + \int_0^1 dy \int_0^1 dz \frac{1}{\sqrt{z}} \frac{1}{D(y,z,k)} \left[4\Delta^2 \frac{2-2(1-z)^{1/2}+z}{z} - C(y,k) \right] \right] . \tag{336}$$

Finally we find that the integral $L_{2b}^{tr}(k)$ in Eq. (312) is

$$L_{2b}^{tr}(k) = -\frac{1}{16\pi^2} \left[2 \left(\frac{2}{\epsilon} - \gamma + \ln\pi \right) \left(k^2 + 6m_\pi^2 - 12\Delta^2 \right) + \frac{2}{3} \left(k^2 + 6m_\pi^2 \right) \right]$$
$$+ \overline{L}_{2b}^{tr}(k) , \tag{337}$$

where

$$\overline{L}_{2b}^{tr}(k) = -\frac{1}{16\pi^2} \left[3 \int_0^1 dy \left[8\Delta^2 - C(y,k) \right] \ln\frac{C(y,k)}{4\mu^2} \right.$$
$$-16\pi\Delta^2 \int_0^1 dy \sqrt{\frac{C(y,k)}{4\Delta^2}} + 8\Delta^2 \int_0^1 dy \int_0^1 dz \frac{1}{\sqrt{z}} \frac{1}{D(y,z,k)}$$
$$\left. \times \left[4\Delta^2 \frac{2-2(1-z)^{1/2}+z}{z} - C(y,k) \right] \right] . \tag{338}$$

The integral $L_2^{tr}(k)$ in Eq. (308) is given by

$$L_2^{tr}(k) = -\frac{1}{48\pi^2} \left[4 \left(\frac{2}{\epsilon} - \gamma + \ln\pi \right) \left(k^2 + 9m_\pi^2 - 18\Delta^2 \right) + 2 \left(k^2 + 6m_\pi^2 \right) \right] + \overline{L}_2^{tr}(k) , \tag{339}$$

where

$$\overline{L}_2^{\mathrm{tr}}(k) = \overline{L}_{2a}^{\mathrm{tr}}(k) + \overline{L}_{2b}^{\mathrm{tr}}(k) \ , \tag{340}$$

defined in Eq. (310) and Eq. (338), respectively. Combining the results above, we find that the "triangle-like" contribution consists of a polynomial of order 2 in k (with divergent coefficients) and a finite part $\overline{v}_{tr}^{2\pi,\mathrm{NLO}}(k; 1\Delta)$, *i.e.*

$$v_{tr}^{2\pi,\mathrm{NLO}}(k; 1\Delta) = \tau_1 \cdot \tau_2\, P_2^{\mathrm{tr}}(k; 1\Delta) + \overline{v}_{tr}^{2\pi,\mathrm{NLO}}(k; 1\Delta) \ , \tag{341}$$

where the polynomial term is given by

$$
\begin{aligned}
P_2^{\mathrm{tr}}(k; 1\Delta) \;=\;& \frac{1}{216\,\pi^2}\frac{h_A^2}{F_\pi^4}\left[k^2\left[10\left(\frac{2}{\epsilon} - \gamma + \ln\pi - \ln\frac{m_\pi^2}{\mu^2}\right) + 3\right]\right. \\
&+ 18\,m_\pi^2\left[2\left(\frac{2}{\epsilon} - \gamma + \ln\pi - \ln\frac{m_\pi^2}{\mu^2}\right) + 1\right] \\
&\left. - 72\,\Delta^2\left(\frac{2}{\epsilon} - \gamma + \ln\pi - \ln\frac{m_\pi^2}{\mu^2}\right)\right] \ .
\end{aligned}
\tag{342}
$$

The finite part $\overline{v}_{tr}^{2\pi,\mathrm{NLO}}(k; 1\Delta)$ can be defined as

$$\overline{v}_{tr}^{2\pi,\mathrm{NLO}}(k; 1\Delta) = \tau_1 \cdot \tau_2\, v_\tau^{2\pi,\mathrm{tr}}(k; 1\Delta) \tag{343}$$

where

$$
\begin{aligned}
v_\tau^{2\pi,\mathrm{tr}}(k; 1\Delta) \;=\;& \frac{1}{18\,\pi^2}\frac{h_A^2}{F_\pi^4}\left[k^2\int_0^1 \mathrm{d}y\, y\,(y-1)\int_0^1 \mathrm{d}z\, \frac{1}{\sqrt{z}}\ln\frac{D(y,z,k)}{4\,m_\pi^2}\right. \\
&+ 6\,\Delta^2\int_0^1 \mathrm{d}y\, \ln\frac{C(y,k)}{4\,m_\pi^2} - \frac{3}{4}\int_0^1 \mathrm{d}y\, C(y,k)\ln\frac{C(y,k)}{4\,m_\pi^2} \\
&- 4\pi\,\Delta^2\int_0^1 \mathrm{d}y\, \sqrt{\frac{C(y,k)}{4\,\Delta^2}} + 8\,\Delta^4\int_0^1 \mathrm{d}y\int_0^1 \mathrm{d}z\, \frac{2 - 2\sqrt{1-z} + z}{z^{3/2}} \\
&\left.\times\frac{1}{D(y,z,k)} - 2\,\Delta^2\int_0^1 \mathrm{d}y\, C(y,k)\int_0^1 \mathrm{d}z\, \frac{1}{\sqrt{z}}\frac{1}{D(y,z,k)}\right] \ . \tag{344}
\end{aligned}
$$

Note that we have re-expressed the μ-dependent logs in the integrals above as, for example

$$\ln\frac{D}{4\,\mu^2} \longrightarrow \ln\frac{D}{4\,m_\pi^2} + \ln\frac{m_\pi^2}{\mu^2} \ , \tag{345}$$

and have incorporated the resulting polynomials of order two in k (with μ-dependent coefficients) into $P_2^{\mathrm{tr}}(k; 1\Delta)$.

B.3 REGULARIZATION OF BOX CONTRIBUTION WITH ONE Δ

The "box-like" contribution with one Δ given in Eq. (46) can be written as

$$
v_{\text{box}}^{2\pi,\text{NLO}}(\mathbf{k}; 1\Delta) = -\frac{g_A^2 \, h_A^2}{9 \, \Delta \, F_\pi^4} \Bigg[3 \left[L_0^{\text{box}}(k) \, k^4 - 2 \, L_2^{\text{box}}(k) \, k^2 + L_4^{\text{box}}(k) \right]
$$
$$
+ \tau_1 \cdot \tau_2 \left[H_0^{\text{box}}(k) \, k^4 - 2 \, H_2^{\text{box}}(k) \, k^2 + H_4^{\text{box}}(k) \right]
$$
$$
+ 2 \, \tau_1 \cdot \tau_2 \, (\sigma_1 \times \mathbf{k})_\alpha \, (\sigma_2 \times \mathbf{k})_\beta \, L_{\alpha\beta}^{\text{box}}(k)
$$
$$
+ 6 \, (\sigma_1 \times \mathbf{k})_\alpha \, (\sigma_2 \times \mathbf{k})_\beta \, H_{\alpha\beta}^{\text{box}}(k) \Bigg] , \tag{346}
$$

where

$$
L_n^{\text{box}}(k) = \int_l \frac{l^n}{\omega_+^2 \, \omega_-^2} , \tag{347}
$$

$$
L_{\alpha\beta}^{\text{box}}(k) = \int_l \frac{l_\alpha \, l_\beta}{\omega_+^2 \, \omega_-^2} , \tag{348}
$$

and $H_n^{\text{box}}(k)$ and $H_{\alpha\beta}^{\text{box}}(k)$ are defined similarly, but with

$$
\frac{1}{\omega_+^2 \, \omega_-^2} \longrightarrow \frac{2\,\Delta + \omega_+ + \omega_-}{\omega_+ \, \omega_- \, (\omega_+ + 2\,\Delta) \, (\omega_- + 2\,\Delta) \, (\omega_+ + \omega_-)} . \tag{349}
$$

Consider first the integrals $L_n^{\text{box}}(k)$ which can be parametrized as

$$
L_n^{\text{box}}(k) = \int_0^1 dy \int_l \frac{[l + (2\,y - 1)\mathbf{k}]^n}{[l^2 + C(y,k)]^2} . \tag{350}
$$

Using the relevant integrals in Eqs.(291)–(293) we find the following (finite) integrals in dimentional $(d = 3)$ regularization

$$
L_0^{\text{box}}(k) \equiv \overline{L}_0^{\text{box}}(k) = \frac{1}{8\,\pi} \int_0^1 dy \, \frac{1}{\sqrt{C(y,k)}} , \tag{351}
$$

$$
L_2^{\text{box}}(k) \equiv \overline{L}_2^{\text{box}}(k) = -\frac{1}{8\,\pi} \left[3 \int_0^1 dy \, \sqrt{C(y,k)} - k^2 \int_0^1 dy \, (2\,y - 1)^2 \, \frac{1}{\sqrt{C(y,k)}} \right] , \tag{352}
$$

$$
L_4^{\text{box}}(k) \equiv \overline{L}_4^{\text{box}}(k) = \frac{1}{8\,\pi} \Bigg[5 \int_0^1 dy \, [C(y,k)]^{3/2} - 10\,k^2 \int_0^1 dy \, (2\,y - 1)^2 \, \sqrt{C(y,k)}
$$
$$
+ k^4 \int_0^1 dy \, (2\,y - 1)^4 \, \frac{1}{\sqrt{C(y,k)}} \Bigg] . \tag{353}
$$

The integral $L^{\mathrm{box}}_{\alpha\beta}(k)$ can be worked out in a similar way such that

$$
\begin{aligned}
L^{\mathrm{box}}_{\alpha\beta}(k) \equiv \overline{L}^{\mathrm{box}}_{\alpha\beta}(k) &= \int_0^1 \mathrm{d}y \int_1 \frac{[l_\alpha + (2y-1)k_\alpha][l_\beta + (2y-1)k_\beta]}{[l^2 + C(y,k)]^2} \\
&= -\frac{1}{8\pi}\left[\delta_{\alpha\beta} \int_0^1 \mathrm{d}y \sqrt{C(y,k)} - k_\alpha k_\beta \int_0^1 \mathrm{d}y\,(2y-1)^2 \right. \\
&\quad \left. \times \frac{1}{\sqrt{C(y,k)}} \right] ,
\end{aligned}
\tag{354}
$$

and we observe that the tensor term proportional to $k_\alpha k_\beta$ vanishes when contracted with the spin-dependent structure in $v^{2\pi,\mathrm{NLO}}_{\mathrm{box}}(\mathbf{k}; 1\Delta)$. Therefore we have:

$$
\overline{L}^{\mathrm{box}}_{\alpha\beta}(k) = -\frac{1}{8\pi}\, \delta_{\alpha\beta} \int_0^1 \mathrm{d}y\, \sqrt{C(y,k)} .
\tag{355}
$$

The remaining $H^{\mathrm{box}}_n(k)$ integrals can be written as

$$
H^{\mathrm{box}}_n(k) = \frac{4\Delta}{\pi} \int_0^\infty \mathrm{d}\lambda \int_1 \frac{l^n}{(\lambda^2 + 4\Delta^2)(\lambda^2 + \omega_+^2)(\lambda^2 + \omega_-^2)} ,
\tag{356}
$$

and similarly for $H^{\mathrm{box}}_{\alpha\beta}(k)$. The convergent integral $H^{\mathrm{box}}_0(k) \equiv \overline{H}^{\mathrm{box}}_0(k)$ is given by

$$
\overline{H}^{\mathrm{box}}_0(k) = \frac{\Delta}{4\pi^2} \int_0^1 \mathrm{d}y \int_0^1 \mathrm{d}z\, \frac{1}{\sqrt{z}}\, \frac{1}{D(y,z,k)} ,
\tag{357}
$$

where we have used the Feynman's parametrization in Eq. (295) and integrated over λ. The integral $H^{\mathrm{box}}_2(k)$ can be parametrized as

$$
\begin{aligned}
H^{\mathrm{box}}_2(k) &= \frac{4\Delta}{\pi} \int_0^1 \mathrm{d}y \int_0^\infty \mathrm{d}\lambda\, \frac{1}{\lambda^2 + 4\Delta^2} \int_1 \frac{l^2 + (2y-1)^2 k^2}{[\lambda^2 + l^2 + C(y,k)]^2} \\
&= 2\Delta \left[L^{\mathrm{tr}}_{2d}(k) + \frac{k^2}{8\pi^2} \int_0^1 \mathrm{d}y\,(2y-1)^2 \int_0^1 \mathrm{d}z\, \frac{1}{\sqrt{z}}\, \frac{1}{D(y,z,k)} \right] ,
\end{aligned}
\tag{358}
$$

where the integral $L^{\mathrm{tr}}_{2d}(k)$ has been defined in Eq. (314) and solved in Eq. (335). Therefore we have

$$
H^{\mathrm{box}}_2(k) = -\frac{3\Delta}{4\pi^2}\left(\frac{2}{\epsilon} - \gamma + \ln\pi - \ln\frac{m_\pi^2}{\mu^2} \right) + \overline{H}^{\mathrm{box}}_2(k) ,
\tag{359}
$$

where

$$
\overline{H}^{\mathrm{box}}_2(k) = 2\Delta \left[\overline{L}^{\mathrm{tr}}_{2d}(k) + \frac{k^2}{8\pi^2} \int_0^1 \mathrm{d}y\,(2y-1)^2 \int_0^1 \mathrm{d}z\, \frac{1}{\sqrt{z}}\, \frac{1}{D(y,z,k)} \right] ,
\tag{360}
$$

with $\overline{L}_{2d}^{tr}(k)$ defined in Eq. (336) where we already have considered the substitution in Eq. (345). Lastly, $H_4^{box}(k)$ reads as

$$H_4^{box}(k) = \frac{4\Delta}{\pi} \int_0^1 dy \int_0^\infty d\lambda \frac{1}{\lambda^2 + 4\Delta^2}$$
$$\times \int_1 \frac{l^4 + (2y-1)^4 k^4 + 2(2y-1)^2 [k^2 l^2 + 2(1\cdot k)^2]}{[\lambda^2 + l^2 + C(y,k)]^2} . \quad (361)$$

The integral $H_4^{box}(k)$ can be written as

$$H_4^{box}(k) = H_{4a}^{box}(k) + H_{4b}^{box}(k) + H_{4c}^{box,\alpha\beta}(k) + H_{4d}^{box}(k) , \quad (362)$$

where

$$H_{4a}^{box}(k) = \frac{4\Delta}{\pi} \int_0^1 dy \int_0^\infty d\lambda \frac{1}{\lambda^2 + 4\Delta^2} \int_1 \frac{l^4}{[\lambda^2 + l^2 + C(y,k)]^2} , \quad (363)$$

$$H_{4b}^{box}(k) = \frac{4\Delta}{\pi} k^4 \int_0^1 dy (2y-1)^4 \int_0^\infty d\lambda \frac{1}{\lambda^2 + 4\Delta^2}$$
$$\times \int_1 \frac{1}{[\lambda^2 + l^2 + C(y,k)]^2} , \quad (364)$$

$$H_{4c}^{box,\alpha\beta}(k) = \frac{4\Delta}{\pi} k_\alpha k_\beta \int_0^1 dy\, 4(2y-1)^2 \int_0^\infty d\lambda \frac{1}{\lambda^2 + 4\Delta^2}$$
$$\times \int_1 \frac{l_\alpha l_\beta}{[\lambda^2 + l^2 + C(y,k)]^2} , \quad (365)$$

$$H_{4d}^{box}(k) = \frac{4\Delta}{\pi} k^2 \int_0^1 dy\, 2(2y-1)^2 \int_0^\infty d\lambda \frac{1}{\lambda^2 + 4\Delta^2}$$
$$\times \int_1 \frac{l^2}{[\lambda^2 + l^2 + C(y,k)]^2} . \quad (366)$$

In order to proceed for the integral $H_{4a}^{box}(k)$, we need to use the decomposition

$$\frac{p^4}{[\lambda^2 + 4\Delta^2][\lambda^2 + p^2 + C(y,k)]^2} = \frac{p^2}{[\lambda^2 + 4\Delta^2][\lambda^2 + p^2 + C(y,k)]}$$
$$- \frac{p^2}{[\lambda^2 + p^2 + C(y,k)]^2}$$
$$+ \frac{p^2[4\Delta^2 - C(y,k)]}{[\lambda^2 + 4\Delta^2][\lambda^2 + p^2 + C(y,k)]^2} , \quad (367)$$

which is based on Eq. (318). Therefore the integral $H_{4a}^{box}(k)$ can be written as

$$H_{4a}^{box}(k) = H_{4e}^{box}(k) - H_{4f}^{box}(k) + H_{4g}^{box}(k) , \quad (368)$$

where

$$H_{4e}^{\text{box}}(k) = \frac{4\Delta}{\pi} \int_0^1 \mathrm{d}y \int_0^\infty \mathrm{d}\lambda \, \frac{1}{\lambda^2 - 4\Delta^2} \int_1 \frac{l^2}{[\lambda^2 + l^2 + C(y,k)]} \,, \tag{369}$$

$$H_{4f}^{\text{box}}(k) = \frac{4\Delta}{\pi} \int_0^1 \mathrm{d}y \int_0^\infty \mathrm{d}\lambda \int_1 \frac{l^2}{[\lambda^2 + l^2 + C(y,k)]^2} \,, \tag{370}$$

$$H_{4g}^{\text{box}}(k) = \frac{4\Delta}{\pi} \int_0^1 \mathrm{d}y \, [4\Delta^2 - C(y,k)] \int_0^\infty \mathrm{d}\lambda \, \frac{1}{\lambda^2 + 4\Delta^2} \int_1 \frac{l^2}{[\lambda^2 + l^2 + C(y,k)]^2} \,. \tag{371}$$

The integral $H_{4g}^{\text{box}}(k)$ is similar to the integral $L_{2d}^{\text{tr}}(k)$ defined in Eq. (314) and solved in Eq. (335). Therefore, after performing dimensional regularization, we find that

$$H_{4g}^{\text{box}}(k) = \frac{\Delta}{2\pi^2} \left(\frac{2}{\epsilon} - \gamma + \ln\pi - \ln\frac{m_\pi^2}{\mu^2} \right) (k^2 + 6\,m_\pi^2 - 6\,\Delta^2) + \overline{H}_{4g}^{\text{box}}(k) \,, \tag{372}$$

where

$$\begin{aligned}
\overline{H}_{4g}^{\text{box}}(k) &= \frac{\Delta}{4\pi^2} \left[3 \int_0^1 \mathrm{d}y \, [4\Delta^2 - C(y,k)] \ln\frac{C(y,k)}{4\,m_\pi^2} - 2\pi \int_0^1 \mathrm{d}y \, [4\Delta^2 \right. \\
&\quad -C(y,k)] \sqrt{\frac{C(y,k)}{4\Delta^2}} + \int_0^1 \mathrm{d}y \, [4\Delta^2 - C(y,k)] \int_0^1 \mathrm{d}z \, \frac{1}{\sqrt{z}} \frac{1}{D(y,z,k)} \\
&\quad \left. \times \left[4\Delta^2 \frac{2 - 2\,(1-z)^{1/2} + z}{z} - C(y,k) \right] \right] .
\end{aligned} \tag{373}$$

Instead, the integral $H_{4f}^{\text{box}}(k)$ is similar to $L_{2c}^{\text{tr}}(k)$ defined in Eq. (313); therefore in analogy to Eq. (316)

$$H_{4f}^{\text{box}}(k) = -\frac{\Delta}{4\pi^2} \left(\frac{2}{\epsilon} - \gamma + \ln\pi + \frac{1}{3} - \ln\frac{m_\pi^2}{\mu^2} \right) (k^2 + 6\,m_\pi^2) + \overline{H}_{4f}^{\text{box}}(k) \,, \tag{374}$$

where

$$\overline{H}_{4f}^{\text{box}}(k) = \frac{3\Delta}{8\pi^2} \int_0^1 \mathrm{d}y \, C(y,k) \ln\frac{C(y,k)}{4\,m_\pi^2} \,. \tag{375}$$

Finally, the integral $H_{4e}^{\text{box}}(k)$ is considered and the following decomposition is used

$$\frac{p^2}{[\lambda^2 + 4\Delta^2]\,[\lambda^2 + p^2 + C(y,k)]} = \frac{1}{\lambda^2 + 4\Delta^2} - \frac{1}{\lambda^2 + p^2 + C(y,k)} + \frac{4\Delta^2 - C(y,k)}{[\lambda^2 + 4\Delta^2]\,[\lambda^2 + p^2 + C(y,k)]} \,. \tag{376}$$

The integral $H_{4e}^{\text{box}}(k)$ can be written as

$$H_{4e}^{\text{box}}(k) = H_{4h}^{\text{box}}(k) - H_{4i}^{\text{box}}(k) + H_{4j}^{\text{box}}(k) \,, \tag{377}$$

where

$$H_{4h}^{\text{box}}(k) = \frac{4\Delta}{\pi}\int_0^1 dy \int_0^\infty d\lambda \frac{1}{\lambda^2 + 4\Delta^2}\int_1, \tag{378}$$

$$H_{4i}^{\text{box}}(k) = \frac{4\Delta}{\pi}\int_0^1 dy \int_0^\infty d\lambda \int_1 \frac{1}{[\lambda^2 + l^2 + C(y,k)]}, \tag{379}$$

$$H_{4j}^{\text{box}}(k) = \frac{4\Delta}{\pi}\int_0^1 dy \left[4\Delta^2 - C(y,k)\right] \int_0^\infty d\lambda \frac{1}{\lambda^2 + 4\Delta^2}\int_1 \frac{1}{[\lambda^2 + l^2 + C(y,k)]}. \tag{380}$$

The first integral $H_{4h}^{\text{box}}(k)$ gives an infinite constant which we drop. Using the relevant integrals in Eqs.(291)–(293), the integral $H_{4i}^{\text{box}}(k)$ is given by

$$H_{4i}^{\text{box}}(k) = -\frac{\Delta}{6\pi^2}\left(\frac{2}{\epsilon} - \gamma + 1 + \ln\pi - \ln\frac{m_\pi^2}{\mu^2}\right)(k^2 + 6 m_\pi^2) + \overline{H}_{4i}^{\text{box}}(k), \tag{381}$$

where

$$\overline{H}_{4i}^{\text{box}}(k) = \frac{\Delta}{4\pi^2}\int_0^1 dy\, C(y,k)\ln\frac{C(y,k)}{4 m_\pi^2}. \tag{382}$$

The integral $H_{4j}^{\text{box}}(k)$ is similar to $L_{2e}^{\text{tr}}(k)$ defined in Eq. (319) and solved in Eq. (333). Therefore we find

$$H_{4j}^{\text{box}}(k) = \frac{\Delta}{3\pi^2}\left(\frac{2}{\epsilon} - \gamma + \ln\pi - \ln\frac{m_\pi^2}{\mu^2}\right)(k^2 + 6 m_\pi^2 - 6\Delta^2) + \overline{H}_{4j}^{\text{box}}(k), \tag{383}$$

where

$$\begin{aligned}\overline{H}_{4j}^{\text{box}}(k) &= \frac{\Delta}{2\pi^2}\Bigg[\int_0^1 dy\,[4\Delta^2 - C(y,k)]\ln\frac{C(y,k)}{4 m_\pi^2} - \pi\int_0^1 dy\,[4\Delta^2 - C(y,k)]\\ &\quad\times\sqrt{\frac{C(y,k)}{4\Delta^2}} + 4\Delta^2\int_0^1 dy\,[4\Delta^2 - C(y,k)]\int_0^1 dz\frac{1}{D(y,z,k)}\\ &\quad\times\frac{1 - (1-z)^{1/2}}{z^{3/2}}\Bigg].\end{aligned} \tag{384}$$

Finally, the integral $H_{4e}^{\text{box}}(k)$ in Eq. (377) is given by

$$\begin{aligned}H_{4e}^{\text{box}}(k) &= \frac{\Delta}{6\pi^2}\Bigg[3\left(\frac{2}{\epsilon} - \gamma + \ln\pi - \ln\frac{m_\pi^2}{\mu^2}\right)(k^2 + 6 m_\pi^2 - 4\Delta^2) + k^2 + 6 m_\pi^2\Bigg]\\ &\quad + \overline{H}_{4e}^{\text{box}}(k), \end{aligned} \tag{385}$$

where

$$
\overline{H}_{4e}^{\text{box}}(k) = \frac{\Delta}{4\pi^2}\left[\int_0^1 dy\,\left[8\Delta^2 - 3\,C(y,k)\right]\ln\frac{C(y,k)}{4\,m_\pi^2} - 2\pi\int_0^1 dy\,\left[4\Delta^2 - C(y,k)\right]\right.
$$
$$
\times\sqrt{\frac{C(y,k)}{4\Delta^2}} + 8\Delta^2\int_0^1 dy\,\left[4\Delta^2 - C(y,k)\right]\int_0^1 dz\,\frac{1}{D(y,z,k)}
$$
$$
\left.\times\frac{1-(1-z)^{1/2}}{z^{3/2}}\right]\,.
\tag{386}
$$

The integral $H_{4a}^{\text{box}}(k)$ in Eq. (368) is given by

$$
H_{4a}^{\text{box}}(k)z = \frac{\Delta}{4\pi^2}\left[5\left(\frac{2}{\epsilon} - \gamma + \ln\pi - \ln\frac{m_\pi^2}{\mu^2}\right)(k^2 + 6\,m_\pi^2 - 4\,\Delta^2)\right.
$$
$$
\left. + (k^2 + 6\,m_\pi^2)\right] + \overline{H}_{4a}^{\text{box}}(k)\,,
\tag{387}
$$

where

$$
\overline{H}_{4a}^{\text{box}}(k) = \frac{\Delta}{8\pi^2}\left[5\int_0^1 dy\,\left[8\Delta^2 - 3\,C(y,k)\right]\ln\frac{C(y,k)}{4\,m_\pi^2} - 8\pi\int_0^1 dy\,[4\,\Delta^2\right.
$$
$$
\left. - C(y,k)]\,\sqrt{\frac{C(y,k)}{4\Delta^2}} + \int_0^1 dy\,\left[4\Delta^2 - C(y,k)\right]\int_0^1 dz\,\frac{1}{\sqrt{z}}\frac{1}{D(y,z,k)}\right.
$$
$$
\left.\times\left[8\Delta^2\frac{4 - 4\,(1-z)^{1/2} + z}{z} - 2\,C(y,k)\right]\right]\,.
\tag{388}
$$

Now we consider the finite integral $H_{4b}^{\text{box}}(k) \equiv \overline{H}_{4b}^{\text{box}}(k)$ in Eq. (364) which is similar to $L_{2g}^{\text{tr}}(k)$ in Eq. (322). Therefore we have

$$
\overline{H}_{4b}^{\text{box}}(k) = \frac{\Delta}{4\pi^2}k^4\int_0^1 dy\,(2y-1)^4\int_0^1 dz\,\frac{1}{\sqrt{z}}\frac{1}{D(y,z,k)}\,.
\tag{389}
$$

Lastly, the integrals $H_{4c}^{\text{box},\alpha\beta}(k)$ and $H_{4d}^{\text{box}}(k)$ in Eqs. (365)–(366) can be combined together such that

$$
H_{4(c+d)}^{\text{box}}(k) \equiv H_{4c}^{\text{box},\alpha\beta}(k) + H_{4d}^{\text{box}}(k)
$$
$$
= \frac{4\Delta}{\pi}\frac{10}{3}k^2\int_0^1 dy\,(2y-1)^2\int_0^\infty d\lambda\,\frac{1}{\lambda^2 + 4\Delta^2}\int_1\frac{l^2}{[\lambda^2 + l^2 + C(y,k)]^2}\,.
\tag{390}
$$

This integral $H_{4(c+d)}^{\text{box}}(k)$ is similar to $H_{4g}^{\text{box}}(k)$ defined in Eq. (371) and solved in Eq. (372). Therefore

$$
H_{4(c+d)}^{\text{box}}(k) = -\frac{5\,\Delta}{6}k^2\left(\frac{2}{\epsilon} - \gamma + \ln\pi - \ln\frac{m_\pi^2}{\mu^2}\right) + \overline{H}_{4(c+d)}^{\text{box}}(k)\,,
\tag{391}
$$

where

$$\overline{H}^{\text{box}}_{4(c+d)}(k) = \frac{5\,\Delta}{6\,\pi^2}\,k^2\left[3\int_0^1 dy\,(2\,y-1)^2\,\ln\frac{C(y,k)}{4\,m_\pi^2} - 2\,\pi\int_0^1 dy\,(2\,y-1)^2\right.$$
$$\times\sqrt{\frac{C(y,k)}{4\,\Delta^2}} + \int_0^1 dy\,(2\,y-1)^2\int_0^1 dz\,\frac{1}{\sqrt{z}}\frac{1}{D(y,z,k)}$$
$$\left.\left[4\,\Delta^2\,\frac{2-2\,(1-z)^{1/2}+z}{z} - 2\,C(y,k)\right]\right]. \tag{392}$$

The integral $H^{\text{box}}_4(k)$ therefore becomes:

$$H^{\text{box}}_4(k) = \frac{\Delta}{24\,\pi^2}\left[10\left(\frac{2}{\epsilon}-\gamma+\ln\pi-\ln\frac{m_\pi^2}{\mu^2}\right)\left(k^2+18\,m_\pi^2-12\,\Delta^2\right)+\left(k^2+6\,m_\pi^2\right)\right]$$
$$+\overline{H}^{\text{box}}_4(k), \tag{393}$$

with

$$\overline{H}^{\text{box}}_4(k) = \overline{H}^{\text{box}}_{4a}(k) + \overline{H}^{\text{box}}_{4b}(k) + \overline{H}^{\text{box}}_{4(c+d)}(k), \tag{394}$$

where the integrals $\overline{H}^{\text{box}}_{4a}(k)$, $\overline{H}^{\text{box}}_{4b}(k)$ and $\overline{H}^{\text{box}}_{4(c+d)}(k)$ have been defined in Eqs. (388)–(389) and (392), respectively. Finally, we need to calculate $H^{\text{box}}_{\alpha\beta}(k)$. When you apply Feynman's parametrization you need to substitute $l_\alpha \to l_\alpha - k_\alpha\,(2\,y-1)$. The term proportional to $k_\alpha\,k_\beta$ vanishes as in the case $L^{\text{box}}_{\alpha\beta}(k)$. Therefore we have

$$H^{\text{box}}_{\alpha\beta}(k) = \frac{2\,\Delta}{3}\,\delta_{\alpha\beta}L^{\text{tr}}_{2d}(k)$$
$$= -\frac{\Delta}{4\,\pi^2}\,\delta_{\alpha\beta}\left(\frac{2}{\epsilon}-\gamma+\ln\pi-\ln\frac{m_\pi^2}{\mu^2}\right)+\overline{H}^{\text{box}}_{\alpha\beta}(k), \tag{395}$$

where

$$\overline{H}^{\text{box}}_{\alpha\beta}(k) = \frac{2\,\Delta}{3}\,\delta_{\alpha\beta}\overline{L}^{\text{tr}}_{2d}(k), \tag{396}$$

with $\overline{L}^{\text{tr}}_{2d}(k)$ defined in Eq. (336) where the substitution in Eq. (345) has been performed. Finally the "box-like" contribution with one Δ can be written

$$v^{2\pi,\text{NLO}}_{\text{box}}(\mathbf{k};1\Delta) = \overline{v}^{2\pi,\text{NLO}}_{\text{box}}(\mathbf{k};1\Delta) + \boldsymbol{\tau}_1\cdot\boldsymbol{\tau}_2\,P^{\text{box}}_2(k;1\Delta)$$
$$+(k^2\,\boldsymbol{\sigma}_1\cdot\boldsymbol{\sigma}_2 - \boldsymbol{\sigma}_1\cdot\mathbf{k}\,\boldsymbol{\sigma}_2\cdot\mathbf{k})\,P^{\text{box}}_0(k;1\Delta), \tag{397}$$

111

where

$$P_0^{\text{box}}(k; 1\Delta) = \frac{g_A^2 h_A^2}{F_\pi^4} \frac{1}{6\pi^2} \left(\frac{2}{\epsilon} - \gamma + \ln\pi - \ln\frac{m_\pi^2}{\mu^2} \right) , \qquad (398)$$

$$P_2^{\text{box}}(k; 1\Delta) = -\frac{g_A^2 h_A^2}{F_\pi^4} \frac{1}{216\pi^2} \left[k^2 \left[46 \left(\frac{2}{\epsilon} - \gamma + \ln\pi - \ln\frac{m_\pi^2}{\mu^2} \right) + 1 \right] \right.$$
$$+ 6 m_\pi^2 \left[30 \left(\frac{2}{\epsilon} - \gamma + \ln\pi - \ln\frac{m_\pi^2}{\mu^2} \right) + 1 \right]$$
$$\left. - 120 \Delta^2 \left(\frac{2}{\epsilon} - \gamma + \ln\pi - \ln\frac{m_\pi^2}{\mu^2} \right) \right] , \qquad (399)$$

and

$$\bar{v}_{\text{box}}^{2\pi,\text{NLO}}(\mathbf{k}; 1\Delta) = v_{c,\text{box}}^{2\pi,\text{NLO}}(k; 1\Delta) + v_{\sigma,\text{box}}^{2\pi,\text{NLO}}(k; 1\Delta) \boldsymbol{\sigma}_1 \cdot \boldsymbol{\sigma}_2$$
$$+ v_{t,\text{box}}^{2\pi,\text{NLO}}(k; 1\Delta) S_{12}(\mathbf{k}) + [v_{\tau,\text{box}}^{2\pi,\text{NLO}}(k; 1\Delta)$$
$$+ v_{\sigma\tau,\text{box}}^{2\pi,\text{NLO}}(k; 1\Delta) \boldsymbol{\sigma}_1 \cdot \boldsymbol{\sigma}_2 + v_{t\tau,\text{box}}^{2\pi,\text{NLO}}(k; 1\Delta) S_{12}(\mathbf{k})] \boldsymbol{\tau}_1 \cdot \boldsymbol{\tau}_2 , \qquad (400)$$

with

$$v_{c,\text{box}}^{2\pi,\text{NLO}}(k; 1\Delta) = -\frac{g_A^2 h_A^2}{24\Delta F_\pi^4 \pi} \left[k^4 \int_0^1 dy \left[1 - 2(2y-1)^2 + (2y-1)^4 \right] \right.$$
$$\times \frac{1}{\sqrt{C(y,k)}} + 2k^2 \int_0^1 dy \left[3 - 5(2y-1)^2 \right] \sqrt{C(y,k)}$$
$$\left. + 5 \int_0^1 dy \left[C(y,k) \right]^{3/2} \right] , \qquad (401)$$

$$v_{\sigma,\text{box}}^{2\pi,\text{NLO}}(k; 1\Delta) = -\frac{g_A^2 h_A^2}{27 F_\pi^4 \pi^2} k^2 \left[3 \int_0^1 dy \ln\frac{C(y,k)}{4 m_\pi^2} - 2\pi \int_0^1 dy \sqrt{\frac{C(y,k)}{4\Delta^2}} \right.$$
$$+ \int_0^1 dy \int_0^1 dz \frac{1}{\sqrt{z}} \frac{1}{D(y,z,k)} \left[4\Delta^2 \frac{2 - 2(1-z)^{1/2} + z}{z} \right.$$
$$\left. \left. - C(y,k) \right] \right] , \qquad (402)$$

$$v_{t,\text{box}}^{2\pi,\text{NLO}}(k; 1\Delta) = \frac{g_A^2 h_A^2}{54 F_\pi^4 \pi^2} \left[3 \int_0^1 dy \ln\frac{C(y,k)}{4 m_\pi^2} - 2\pi \int_0^1 dy \sqrt{\frac{C(y,k)}{4\Delta^2}} \right.$$
$$+ \int_0^1 dy \int_0^1 dz \frac{1}{\sqrt{z}} \frac{1}{D(y,z,k)} \left[4\Delta^2 \frac{2 - 2(1-z)^{1/2} + z}{z} \right.$$
$$\left. \left. - C(y,k) \right] \right] , \qquad (403)$$

$$v_{\tau,\text{box}}^{2\pi,\text{NLO}}(k;1\Delta) = -\frac{g_A^2\,h_A^2}{216\,F_\pi^4\pi^2}\left[6\,k^4\int_0^1 dy\,\left[1-2\,(2\,y-1)^2+(2\,y-1)^4\right]\right.$$

$$\times\int_0^1 dz\frac{1}{\sqrt{z}}\frac{1}{D(y,z,k)}-4\,k^2\left[3\int_0^1 dy\,\left[3-5\,(2\,y-1)^2\right]\right.$$

$$\times\ln\frac{C(y,k)}{4\,m_\pi^2}-2\,\pi\int_0^1 dy\,\left[3-5\,(2\,y-1)^2\right]\,\sqrt{\frac{C(y,k)}{4\,\Delta^2}}$$

$$+\int_0^1 dy\,\left[3-5\,(2\,y-1)^2\right]\int_0^1 dz\frac{1}{\sqrt{z}}\frac{1}{D(y,z,k)}$$

$$\times\left[4\,\Delta^2\frac{2-2\,(1-z)^{1/2}+z}{z}-C(y,k)\right]\right]+3\left[5\int_0^1 dy\right.$$

$$\times\left[8\,\Delta^2-3\,C(y,k)\right]\,\ln\frac{C(y,k)}{4\,m_\pi^2}-8\,\pi\int_0^1 dy\,[4\,\Delta^2$$

$$\left.-C(y,k)]\,\sqrt{\frac{C(y,k)}{4\,\Delta^2}}+\int_0^1 dy\,\left[4\,\Delta^2-C(y,k)\right]\int_0^1 dz\frac{1}{\sqrt{z}}\right.$$

$$\left.\left.\times\frac{1}{D(y,z,k)}\left[8\,\Delta^2\frac{4-4\,(1-z)^{1/2}+z}{z}-2\,C(y,k)\right]\right]\right]\;,\quad (404)$$

$$v_{\sigma\tau,\text{box}}^{2\pi,\text{NLO}}(k;1\Delta) = \frac{g_A^2\,h_A^2}{54\,\Delta\,F_\pi^4\,\pi}\,k^2\int_0^1 dy\,\sqrt{C(y,k)}\;,\quad (405)$$

$$v_{t\tau,\text{box}}^{2\pi,\text{NLO}}(k;1\Delta) = -\frac{g_A^2\,h_A^2}{108\,\Delta\,F_\pi^4\,\pi}\int_0^1 dy\,\sqrt{C(y,k)}\;.\quad (406)$$

B.4 REGULARIZATION OF BOX CONTRIBUTION WITH TWO INTERMEDIATE Δ'S

The "box-like" contribution with two intermediate Δ's given in Eq. (47) can be written in the following way

$$v_{\text{box}}^{2\pi,\text{NLO}}(\mathbf{k};2\Delta) = -\frac{h_A^4}{81\,F_\pi^4}\left[(6+\boldsymbol{\tau}_1\cdot\boldsymbol{\tau}_2)\left[\widetilde{L}_0^{\text{box}}(k)\,k^4-2\,\widetilde{L}_2^{\text{box}}(k)\,k^2+\widetilde{L}_4^{\text{box}}(k)\right.\right.$$

$$\left.+(\boldsymbol{\sigma}_1\times\mathbf{k})_\alpha\,(\boldsymbol{\sigma}_2\times\mathbf{k})_\beta\,\widetilde{L}_{\alpha\beta}^{\text{box}}(k)\right]$$

$$+(6-\boldsymbol{\tau}_1\cdot\boldsymbol{\tau}_2)\left[\widetilde{H}_0^{\text{box}}(k)\,k^4-2\,\widetilde{H}_2^{\text{box}}(k)\,k^2+\widetilde{H}_4^{\text{box}}(k)\right.$$

$$\left.\left.-(\boldsymbol{\sigma}_1\times\mathbf{k})_\alpha\,(\boldsymbol{\sigma}_2\times\mathbf{k})_\beta\,\widetilde{H}_{\alpha\beta}^{\text{box}}(k)\right]\right]\;,\quad (407)$$

where

$$\widetilde{L}_n^{\text{box}}(k) = \int_1 \frac{\omega_+^2 + \omega_-^2 + \omega_+\omega_- + 4\Delta\left(\omega_+ + \omega_- + \Delta\right)}{\omega_+\omega_-\left(\omega_+ + 2\Delta\right)^2\left(\omega_- + 2\Delta\right)^2\left(\omega_+ + \omega_-\right)} l^n , \qquad (408)$$

$$\widetilde{L}_{\alpha\beta}^{\text{box}}(k) = \int_1 \frac{\omega_+^2 + \omega_-^2 + \omega_+\omega_- + 4\Delta\left(\omega_+ + \omega_- + \Delta\right)}{\omega_+\omega_-\left(\omega_+ + 2\Delta\right)^2\left(\omega_- + 2\Delta\right)^2\left(\omega_+ + \omega_-\right)} l_\alpha l_\beta , \qquad (409)$$

and

$$\widetilde{H}_n^{\text{box}}(k) = \frac{1}{2\Delta} H_n^{\text{box}}(k) , \qquad \widetilde{H}_{\alpha\beta}^{\text{box}}(k) = \frac{1}{2\Delta} H_{\alpha\beta}^{\text{box}}(k) , \qquad (410)$$

with $H_n^{\text{box}}(k)$ and $H_{\alpha\beta}^{\text{box}}(k)$ defined as in the previous section. Note that

$$\frac{\omega_+^2 + \omega_-^2 + \omega_+\omega_- + 2a\left(\omega_+ + \omega_- + a/2\right)}{\left(\omega_+ + a\right)^2\left(\omega_- + a\right)^2\left(\omega_+ + \omega_-\right)} = -\frac{d}{da}\frac{a + \omega_+ + \omega_-}{\left(\omega_+ + a\right)\left(\omega_- + a\right)\left(\omega_+ + \omega_-\right)} , \qquad (411)$$

with $a = 2\Delta$. Therefore the Eqs. (408)-(409) can be written as

$$\widetilde{L}_n^{\text{box}}(k) = -\frac{d}{da} H_n^{\text{box}}(k) , \qquad \widetilde{L}_{\alpha\beta}^{\text{box}}(k) = -\frac{d}{da} H_{\alpha\beta}^{\text{box}}(k) . \qquad (412)$$

The finite integral $\widetilde{L}_0^{\text{box}}(k) \equiv \overline{\widetilde{L}}_0^{\text{box}}(k)$ is given by

$$\overline{\widetilde{L}}_0^{\text{box}}(k) = -\frac{1}{8\pi^2}\int_0^1 dy \int_0^1 dz \frac{1}{\sqrt{z}}\left[\frac{D(y,z,k) - 8\Delta^2(1-z)}{D(y,z,k)^2}\right] , \qquad (413)$$

where we used the definitions of $H_0^{\text{box}}(k)$ in Eq. (357) and $D(y,z,k) = zC(y,z) + a^2(1-z)$. Note that $C(y,z)$ does not depend on a. The integral $\widetilde{L}_2^{\text{box}}(k)$ reads as follow

$$\widetilde{L}_2^{\text{box}}(k) = \frac{3}{8\pi^2}\left(\frac{2}{\epsilon} - \gamma + \ln\pi - \ln\frac{m_\pi^2}{\mu^2}\right) + \overline{\widetilde{L}}_2^{\text{box}}(k) , \qquad (414)$$

with

$$\overline{\widetilde{L}}_2^{\text{box}}(k) = -\frac{1}{8\pi^2}\left[3\int_0^1 dy \ln\frac{C(y,k)}{4m_\pi^2} + \int_0^1 dy \int_0^1 dz \frac{1}{\sqrt{z}}\frac{1}{D(y,z,k)^2}\right.$$
$$\times\left[4\Delta^2\frac{2 - 2(1-z)^{1/2} + z}{z}\left[3D(y,z,k) - 8\Delta^2(1-z)\right]\right.$$
$$\left.-C(y,k)\left[D(y,z,k) - 8\Delta^2(1-z)\right]\right] + k^2\int_0^1 dy\,(2y-1)^2$$
$$\left.\times\int_0^1 dz \frac{1}{\sqrt{z}}\frac{D(y,z,k) - 8\Delta^2(1-z)}{D(y,z,k)^2}\right] . \qquad (415)$$

where we used the definition of $H_2^{\text{box}}(k)$ in Eq. (359). Finally the integral $\widetilde{L}_4^{\text{box}}(k)$ is given by

$$
\widetilde{L}_4^{\text{box}}(k) \;=\; -\frac{1}{48\,\pi^2}\left[10\left(\frac{2}{\epsilon}-\gamma+\ln\pi-\ln\frac{m_\pi^2}{\mu^2}\right)\left(k^2+18\,m_\pi^2-36\,\Delta^2\right)+\left(k^2+6\,m_\pi^2\right)\right]
$$
$$
+\overline{\widetilde{L}}_4^{\text{box}}(k)\,,
\tag{416}
$$

with

$$
\overline{\widetilde{L}}_4^{\text{box}}(k) \;=\; -\frac{1}{8\,\pi^2}\,k^4\int_0^1 dy\,(2\,y-1)^4\int_0^1 dz\,\frac{1}{\sqrt{z}}\,\frac{1}{D(y,z,k)^2}[D(y,z,k)-8\,\Delta^2
$$
$$
\times(1-z)]-\frac{5}{12\,\pi^2}\,k^2\left[3\int_0^1 dy\,(2\,y-1)^2\ln\frac{C(y,k)}{4\,m_\pi^2}+\int_0^1 dy\,(2\,y-1)^2
$$
$$
\times\int_0^1 dz\,\frac{1}{\sqrt{z}}\,\frac{1}{D(y,z,k)^2}\left[4\,\Delta^2\,\frac{2-2\,(1-z)^{1/2}+z}{z}[3\,D(y,z,k)-8\,\Delta^2
$$
$$
\times(1-z)]-C(y,k)\left[D(y,z,k)-8\,\Delta^2(1-z)\right]\right]\right]-\frac{1}{16\,\pi^2}\left[5\int_0^1 dy\right.
$$
$$
\times\left[24\,\Delta^2-3\,C(y,k)\right]\ln\frac{C(y,k)}{4\,m_\pi^2}-64\,\pi\Delta^2\int_0^1 dy\,\sqrt{\frac{C(y,k)}{4\,\Delta^2}}
$$
$$
+\int_0^1 dy\int_0^1 dz\,\frac{1}{\sqrt{z}}\,\frac{1}{D(y,z,k)^2}\left[8\,\Delta^2\frac{4-4\,(1-z)^{1/2}+z}{z}\right.
$$
$$
\times\left[\,\left[20\,\Delta^2-3\,C(y,k)\right]\,D(y,z,k)-8\,\Delta^2\left[4\,\Delta^2-C(y,k)\right](1-z)\right]
$$
$$
-2\,C(y,k)\left[\,\left[12\,\Delta^2-C(y,k)\right]\,D(y,z,k)-8\,\Delta^2\left[4\,\Delta^2-C(y,k)\right]\right.
$$
$$
\left.\left.\left.\times(1-z)\right]\right]\right]\,,
\tag{417}
$$

where we used the definition of $H_4^{\text{box}}(k)$ in Eq. (393). The integral $\widetilde{L}_{\alpha\beta}^{\text{box}}(k)$ reads as

$$
\widetilde{L}_{\alpha\beta}^{\text{box}}(k) \;=\; \frac{1}{8\,\pi^2}\,\delta_{\alpha\beta}\left(\frac{2}{\epsilon}-\gamma+\ln\pi-\ln\frac{m_\pi^2}{\mu^2}\right)+\overline{\widetilde{L}}_{\alpha\beta}^{\text{box}}(k)\,,
\tag{418}
$$

with

$$
\overline{\widetilde{L}}_{\alpha\beta}^{\text{box}}(k) \;=\; -\frac{1}{24\,\pi^2}\,\delta_{\alpha\beta}\left[3\int_0^1 dy\ln\frac{C(y,k)}{4\,m_\pi^2}+\int_0^1 dy\int_0^1 dz\,\frac{1}{\sqrt{z}}\,\frac{1}{D(y,z,k)^2}\right.
$$
$$
\times\left[4\,\Delta^2\,\frac{2-2\,(1-z)^{1/2}+z}{z}\left[3\,D(y,z,k)-8\,\Delta^2\,(1-z)\right]\right.
$$
$$
\left.\left.-C(y,k)\left[D(y,z,k)-8\,\Delta^2\,(1-z)\right]\right]\right]\,,
\tag{419}
$$

where the definition of $H_{\alpha\beta}^{\mathrm{box}}(k)$ in Eq. (395) has been used. Finally the "box-like" contribution with two intermediate Δ's can be written

$$
\begin{aligned}
v_{\mathrm{box}}^{2\pi,\mathrm{NLO}}(\mathbf{k};2\Delta) &= \widetilde{v}_{\mathrm{box}}^{2\pi,\mathrm{NLO}}(\mathbf{k};2\Delta) + \widetilde{P}_0'^{\,\mathrm{box}}(k;2\Delta) + \boldsymbol{\tau}_1\cdot\boldsymbol{\tau}_2\,\widetilde{P}_2^{\,\mathrm{box}}(k;2\Delta) \\
&\quad + (k^2\,\boldsymbol{\sigma}_1\cdot\boldsymbol{\sigma}_2 - \boldsymbol{\sigma}_1\cdot\mathbf{k}\,\boldsymbol{\sigma}_2\cdot\mathbf{k})\,\widetilde{P}_0^{\,\mathrm{box}}(k;2\Delta)\ ,
\end{aligned}
\tag{420}
$$

where the polymonial pieces are defined as

$$
\begin{aligned}
\widetilde{P}_0'^{\,\mathrm{box}}(k;2\Delta) &= -\frac{h_A^4}{F_\pi^4}\frac{10}{27\,\pi^2}\,\Delta^2\left(\frac{2}{\epsilon} - \gamma + \ln\pi - \ln\frac{m_\pi^2}{\mu^2}\right)\ , \\
\widetilde{P}_0^{\,\mathrm{box}}(k;2\Delta) &= -\frac{h_A^4}{F_\pi^4}\frac{1}{54\,\pi^2}\left(\frac{2}{\epsilon} - \gamma + \ln\pi - \ln\frac{m_\pi^2}{\mu^2}\right)\ , \\
\widetilde{P}_2^{\,\mathrm{box}}(k;2\Delta) &= \frac{h_A^4}{F_\pi^4}\frac{1}{1944\,\pi^2}\left[k^2\left[46\left(\frac{2}{\epsilon} - \gamma + \ln\pi - \ln\frac{m_\pi^2}{\mu^2}\right) + 1\right]\right. \\
&\quad + 6\,m_\pi^2\left[30\left(\frac{2}{\epsilon} - \gamma + \ln\pi - \ln\frac{m_\pi^2}{\mu^2}\right) + 1\right] \\
&\quad \left. - 240\,\Delta^2\left(\frac{2}{\epsilon} - \gamma + \ln\pi - \ln\frac{m_\pi^2}{\mu^2}\right)\right]\ .
\end{aligned}
$$

$$\tag{421}$$
$$\tag{422}$$

The finite part $\widetilde{v}_{\mathrm{box}}^{2\pi,\mathrm{NLO}}(\mathbf{k};2\Delta)$ can be written as

$$
\begin{aligned}
\widetilde{v}_{\mathrm{box}}^{2\pi,\mathrm{NLO}}(\mathbf{k};2\Delta) &= v_{c,\mathrm{box}}^{2\pi,\mathrm{NLO}}(k;2\Delta) + v_{\sigma,\mathrm{box}}^{2\pi,\mathrm{NLO}}(k;2\Delta)\,\boldsymbol{\sigma}_1\cdot\boldsymbol{\sigma}_2 \\
&\quad + v_{t,\mathrm{box}}^{2\pi,\mathrm{NLO}}(k;2\Delta)\,S_{12}(\mathbf{k}) + [v_{\tau,\mathrm{box}}^{2\pi,\mathrm{NLO}}(k;2\Delta) \\
&\quad + v_{\sigma\tau,\mathrm{box}}^{2\pi,\mathrm{NLO}}(k;2\Delta) + v_{t\tau,\mathrm{box}}^{2\pi,\mathrm{NLO}}(k;2\Delta)\,S_{12}(\mathbf{k})]\boldsymbol{\tau}_1\cdot\boldsymbol{\tau}_2\ ,
\end{aligned}
\tag{423}
$$

where

$$
\begin{aligned}
v_{c,\text{box}}^{2\pi,\text{NLO}}(k;2\Delta) \;=\; & -\frac{h_A^4}{324\,F_\pi^4\,\pi^2}\left[24\,\Delta^2\,k^4\int_0^1 dy\left[1-2\,(2\,y-1)^2+(2\,y-1)^4\right]\right.\\
& \times\int_0^1 dz\,\frac{1}{\sqrt{z}}\,\frac{(1-z)}{D(y,z,k)^2}+4\,k^2\left[\pi\int_0^1 dy\left[3-5\,(2\,y-1)^2\right]\right.\\
& \times\sqrt{\frac{C(y,k)}{4\,\Delta^2}}+\int_0^1 dy\left[3-5\,(2\,y-1)^2\right]\int_0^1 dz\,\frac{1}{\sqrt{z}}\,\frac{1}{D(y,z,k)^2}\\
& \times\left[4\,\Delta^2\,\frac{2-2\,(1-z)^{1/2}+z}{z}\left[D(y,z,k)-4\,\Delta^2(1-z)\right]\right.\\
& \left.+4\,\Delta^2\,C(y,k)\,(1-z)\right]\right]-3\left[5\int_0^1 dy\,8\,\Delta^2\ln\frac{C(y,k)}{4\,m_\pi^2}\right.\\
& -4\,\pi\int_0^1 dy\left[4\,\Delta^2+C(y,k)\right]\sqrt{\frac{C(y,k)}{4\,\Delta^2}}\\
& +\int_0^1 dy\int_0^1 dz\,\frac{1}{\sqrt{z}}\,\frac{1}{D(y,z,k)^2}\left[8\,\Delta^2\frac{4-4\,(1-z)^{1/2}+z}{z}\right.\\
& \times\left[\left[8\,\Delta^2-C(y,k)\right]\,D(y,z,k)-4\,\Delta^2\left[4\,\Delta^2-C(y,k)\right](1-z)\right]\\
& \left.\left.\left.-8\,\Delta^2\,C(y,k)\left[D(y,z,k)-\left[4\,\Delta^2-C(y,k)\right](1-z)\right]\right]\right]\right] \quad (424)
\end{aligned}
$$

$$
\begin{aligned}
v_{\sigma,\text{box}}^{2\pi,\text{NLO}}(k;2\Delta) \;=\; & \frac{h_A^4}{243\,F_\pi^4\pi^2}\,k^2\left[3\int_0^1 dy\,\ln\frac{C(y,k)}{4\,m_\pi^2}-\pi\int_0^1 dy\,\sqrt{\frac{C(y,k)}{4\,\Delta^2}}\right.\\
& +\int_0^1 dy\int_0^1 dz\,\frac{1}{\sqrt{z}}\,\frac{1}{D(y,z,k)^2}\left[4\,\Delta^2\,\frac{2-2\,(1-z)^{1/2}+z}{z}\right.\\
& \times\left[2\,D(y,z,k)-4\,\Delta^2(1-z)\right]-C(y,k)\left[D(y,z,k)\right.\\
& \left.\left.\left.-4\,\Delta^2(1-z)\right]\right]\right], \quad (425)
\end{aligned}
$$

$$
\begin{aligned}
v_{t,\text{box}}^{2\pi,\text{NLO}}(k;2\Delta) \;=\; & -\frac{h_A^4}{486\,F_\pi^4\pi^2}\left[3\int_0^1 dy\,\ln\frac{C(y,k)}{4\,m_\pi^2}-\pi\int_0^1 dy\,\sqrt{\frac{C(y,k)}{4\,\Delta^2}}\right.\\
& +\int_0^1 dy\int_0^1 dz\,\frac{1}{\sqrt{z}}\,\frac{1}{D(y,z,k)^2}\left[4\,\Delta^2\,\frac{2-2\,(1-z)^{1/2}+z}{z}\right.\\
& \times\left[2\,D(y,z,k)-4\,\Delta^2(1-z)\right]-C(y,k)\left[D(y,z,k)\right.\\
& \left.\left.\left.-4\,\Delta^2(1-z)\right]\right]\right], \quad (426)
\end{aligned}
$$

$$v_{\tau,\text{box}}^{2\pi,\text{NLO}}(k;2\Delta) \;=\; \frac{h_A^4}{1944\,F_\pi^4\,\pi^2}\left[6\,k^4\int_0^1 dy\left[1-2\left(2\,y-1\right)^2+\left(2\,y-1\right)^4\right]\right.$$

$$\times\int_0^1 dz\,\frac{1}{\sqrt{z}}\,\frac{D(y,z,k)-4\,\Delta^2(1-z)}{D(y,z,k)^2}-4\,k^2\left[3\int_0^1 dy\right.$$

$$\times\left[3-5\left(2\,y-1\right)^2\right]\ln\frac{C(y,k)}{4\,m_\pi^2}-\pi\int_0^1 dy\left[3-5\left(2\,y-1\right)^2\right]$$

$$\times\sqrt{\frac{C(y,k)}{4\,\Delta^2}}+\int_0^1 dy\left[3-5\left(2\,y-1\right)^2\right]\int_0^1 dz\,\frac{1}{\sqrt{z}}\,\frac{1}{D(y,z,k)^2}$$

$$\times\left[4\,\Delta^2\,\frac{2-2\,(1-z)^{1/2}+z}{z}\left[2\,D(y,z,k)-4\,\Delta^2(1-z)\right]\right.$$

$$\left.-C(y,k)\left[D(y,z,k)-4\,\Delta^2(1-z)\right]\right]\right]+3\left[5\int_0^1 dy\left[16\,\Delta^2\right.\right.$$

$$-3\,C(y,k)\right]\ln\frac{C(y,k)}{4\,m_\pi^2}-4\,\pi\int_0^1 dy\left[12\,\Delta^2-C(y,k)\right]\sqrt{\frac{C(y,k)}{4\,\Delta^2}}$$

$$+\int_0^1 dy\int_0^1 dz\,\frac{1}{\sqrt{z}}\,\frac{1}{D(y,z,k)^2}\left[8\,\Delta^2\,\frac{4-4\,(1-z)^{1/2}+z}{z}\right.$$

$$\times\left[\left[12\,\Delta^2-2\,C(y,k)\right]D(y,z,k)-4\,\Delta^2\left[4\,\Delta^2-C(y,k)\right](1-z)\right]$$

$$-2\,C(y,k)\left[\left[8\,\Delta^2-C(y,k)\right]D(y,z,k)-4\,\Delta^2\left[4\,\Delta^2-C(y,k)\right]\right.$$

$$\left.\left.\left.\left.\times(1-z)\right]\right]\right]\right]\,,\tag{427}$$

$$v_{\sigma\tau,\text{box}}^{2\pi,\text{NLO}}(k;2\Delta) \;=\; \frac{h_A^4}{1458\,F_\pi^4\pi^2}\,k^2\left[\pi\int_0^1 dy\,\sqrt{\frac{C(y,k)}{4\,\Delta^2}}+\int_0^1 dy\int_0^1 dz\,\frac{1}{\sqrt{z}}\,\frac{1}{D(y,z,k)^2}\right.$$

$$\times\left[4\,\Delta^2\,\frac{2-2\,(1-z)^{1/2}+z}{z}\left[D(y,z,k)-4\,\Delta^2(1-z)\right]\right.$$

$$\left.\left.+4\,\Delta^2\,C(y,k)\,(1-z)\right]\right]\,,\tag{428}$$

$$v_{t\tau,\text{box}}^{2\pi,\text{NLO}}(k;2\Delta) \;=\; -\frac{h_A^4}{2916\,F_\pi^4\pi^2}\left[\pi\int_0^1 dy\,\sqrt{\frac{C(y,k)}{4\,\Delta^2}}+\int_0^1 dy\int_0^1 dz\,\frac{1}{\sqrt{z}}\,\frac{1}{D(y,z,k)^2}\right.$$

$$\times\left[4\,\Delta^2\,\frac{2-2\,(1-z)^{1/2}+z}{z}\left[D(y,z,k)-4\,\Delta^2(1-z)\right]\right.$$

$$\left.\left.+4\,\Delta^2\,C(y,k)\,(1-z)\right]\right]\,.\tag{429}$$

APPENDIX C

RELEVANT EXPRESSIONS FOR THE

COORDINATE-SPACE REPRESENTATION OF TPE

AND CONTACT INTERACTIONS

In this appendix we list the relevant expressions for the coordinate-space representation of TPE and contact interaction radial functions introduced in Eqs. (128)–(141), respectively.

C.1 TWO-PION-EXCHANGE

The coordinate-space representation of the TPE radial functions at NLO and N2LO are summarized here. The NLO terms corresponding to diagrams (d)–(f) read as

$$v_\sigma^{2\pi,\mathrm{NLO}}(r;\Lambda) = \frac{1}{2\pi^3 r^4} \frac{g_A^4}{F_\pi^4} m_\pi \left[3x\, K_0(2x) + (3+2x^2)K_1(2x) \right] , \qquad (430)$$

$$v_t^{2\pi,\mathrm{NLO}}(r;\Lambda) = -\frac{1}{8\pi^3 r^4} \frac{g_A^4}{F_\pi^4} m_\pi \left[12x\, K_0(2x) + (15+4x^2)K_1(2x) \right] , \qquad (431)$$

$$v_\tau^{2\pi,\mathrm{NLO}}(r;\Lambda) = \frac{1}{8\pi^3 r^4} \frac{m_\pi}{F_\pi^4} \left[x \left[1 + 10g_A^2 - g_A^4(23+4x^2) \right] K_0(2x) \right.$$
$$\left. + \left[1 + 2g_A^2(5+2x^2) - g_A^4(23+12x^2) \right] K_1(2x) \right] , \qquad (432)$$

where $x = m_\pi r$ (m_π is the average pion mass) and K_n are modified Bessel functions of the second kind. The NLO terms corresponding to diagrams (e)–(f) with a single

Δ intermediate state are given by

$$v_c^{2\pi,\mathrm{NLO}}(r;1\Delta) = -\frac{1}{6\pi^2 r^5}\frac{g_A^2 h_A^2}{y}\frac{1}{F_\pi^4}e^{-2x}\left(6 + 12x + 10x^2 + 4x^3 + x^4\right), \tag{433}$$

$$v_\sigma^{2\pi,\mathrm{NLO}}(r;1\Delta) = -\frac{1}{72\pi^3 r^5}\frac{g_A^2 h_A^2}{F_\pi^4}\left[2\int_0^\infty d\mu\,\frac{\mu^2}{\sqrt{\mu^2 + 4x^2}}e^{-\sqrt{\mu^2+4x^2}}(\mu^2 + 4x^2)\right.$$

$$-\frac{1}{y}\int_0^\infty d\mu\,\frac{\mu}{\sqrt{\mu^2 + 4x^2}}e^{-\sqrt{\mu^2+4x^2}}(\mu^2 + 4x^2)$$

$$\left.\times(\mu^2 + 4y^2)\arctan\frac{\mu}{2y}\right], \tag{434}$$

$$v_t^{2\pi,\mathrm{NLO}}(r;1\Delta) = \frac{1}{144\pi^3 r^5}\frac{g_A^2 h_A^2}{F_\pi^4}\left[2\int_0^\infty d\mu\,\frac{\mu^2}{\sqrt{\mu^2 + 4x^2}}e^{-\sqrt{\mu^2+4x^2}}(3 + 3\sqrt{\mu^2 + 4x^2}\right.$$

$$+\mu^2 + 4x^2) - \frac{1}{y}\int_0^\infty d\mu\,\frac{\mu}{\sqrt{\mu^2 + 4x^2}}e^{-\sqrt{\mu^2+4x^2}}(\mu^2 + 4y^2)$$

$$\left.\times(3 + 3\sqrt{\mu^2 + 4x^2} + \mu^2 + 4x^2)\arctan\frac{\mu}{2y}\right], \tag{435}$$

$$v_\tau^{2\pi,\mathrm{NLO}}(r;1\Delta) = -\frac{1}{216\pi^3 r^5}\frac{h_A^2}{F_\pi^4}\left[\int_0^\infty d\mu\,\frac{\mu^2}{\sqrt{\mu^2 + 4x^2}}e^{-\sqrt{\mu^2+4x^2}}(12x^2 + 5\mu^2 + 12y^2)\right.$$

$$\left.-12y\int_0^\infty d\mu\,\frac{\mu}{\sqrt{\mu^2 + 4x^2}}e^{-\sqrt{\mu^2+4x^2}}(2x^2 + \mu^2 + 2y^2)\arctan\frac{\mu}{2y}\right]$$

$$-\frac{1}{216\pi^3 r^5}\frac{g_A^2 h_A^2}{F_\pi^4}\left[-\int_0^\infty d\mu\,\frac{\mu^2}{\sqrt{\mu^2 + 4x^2}}e^{-\sqrt{\mu^2+4x^2}}\right.$$

$$\times(24x^2 + 11\mu^2 + 12y^2) + \frac{6}{y}\int_0^\infty d\mu\,\frac{\mu}{\sqrt{\mu^2 + 4x^2}}e^{-\sqrt{\mu^2+4x^2}}$$

$$\left.\times(2x^2 + \mu^2 + 2y^2)^2\arctan\frac{\mu}{2y}\right], \tag{436}$$

$$v_{\sigma\tau}^{2\pi,\mathrm{NLO}}(r;1\Delta) = \frac{1}{54\pi^2 r^5}\frac{g_A^2 h_A^2}{y}\frac{1}{F_\pi^4}e^{-2x}\left(1 + x\right)\left(3 + 3x + x^2\right), \tag{437}$$

$$v_{t\tau}^{2\pi,\mathrm{NLO}}(r;1\Delta) = -\frac{1}{54\pi^2 r^5}\frac{g_A^2 h_A^2}{y}\frac{1}{F_\pi^4}e^{-2x}\left(1 + x\right)\left(3 + 3x + 2x^2\right), \tag{438}$$

where $y = \Delta r$ (Δ is the Δ-nucleon mass difference) and the parametric integral over μ is carried out numerically. The NLO terms corresponding to diagram (g) with 2 Δ

intermediate states are

$$
v_c^{2\pi,\mathrm{NLO}}(r;2\Delta) = -\frac{1}{108\pi^3 r^5}\frac{h_A^4}{F_\pi^4}\left[\int_0^\infty d\mu\frac{\mu^2}{\sqrt{\mu^2+4x^2}}e^{-\sqrt{\mu^2+4x^2}}\left[4y^2\right.\right.
$$
$$
\left.+2\frac{(2x^2+\mu^2+2y^2)^2}{(\mu^2+4y^2)}\right]+\frac{1}{y}\int_0^\infty d\mu\frac{\mu}{\sqrt{\mu^2+4x^2}}e^{-\sqrt{\mu^2+4x^2}}
$$
$$
\left.\times(2x^2+\mu^2+2y^2)(2x^2+\mu^2-6y^2)\arctan\frac{\mu}{2y}\right], \tag{439}
$$

$$
v_\sigma^{2\pi,\mathrm{NLO}}(r;2\Delta) = -\frac{1}{1296\pi^3 r^5}\frac{h_A^4}{F_\pi^4}\left[-6\int_0^\infty d\mu\frac{\mu^2}{\sqrt{\mu^2+4x^2}}e^{-\sqrt{\mu^2+4x^2}}(\mu^2+4x^2)\right.
$$
$$
+\frac{1}{y}\int_0^\infty d\mu\frac{\mu}{\sqrt{\mu^2+4x^2}}e^{-\sqrt{\mu^2+4x^2}}(\mu^2+4x^2)(\mu^2+12y^2)
$$
$$
\left.\times\arctan\frac{\mu}{2y}\right], \tag{440}
$$

$$
v_t^{2\pi,\mathrm{NLO}}(r;2\Delta) = \frac{1}{2592\pi^3 r^5}\frac{h_A^4}{F_\pi^4}\left[-6\int_0^\infty d\mu\frac{\mu^2}{\sqrt{\mu^2+4x^2}}e^{-\sqrt{\mu^2+4x^2}}(3+3\sqrt{\mu^2+4x^2}\right.
$$
$$
+\mu^2+4x^2)+\frac{1}{y}\int_0^\infty d\mu\frac{\mu}{\sqrt{\mu^2+4x^2}}e^{-\sqrt{\mu^2+4x^2}}(3+3\sqrt{\mu^2+4x^2}
$$
$$
\left.+\mu^2+4x^2)(\mu^2+12y^2)\arctan\frac{\mu}{2y}\right], \tag{441}
$$

$$
v_\tau^{2\pi,\mathrm{NLO}}(r;2\Delta) = -\frac{1}{1944\pi^3 r^5}\frac{h_A^4}{F_\pi^4}\left[\int_0^\infty d\mu\frac{\mu^2}{\sqrt{\mu^2+4x^2}}e^{-\sqrt{\mu^2+4x^2}}\left[(24x^2+11\mu^2\right.\right.
$$
$$
\left.+24y^2)+6\frac{(2x^2+\mu^2+2y^2)^2}{(\mu^2+4y^2)}\right]-\frac{3}{y}\int_0^\infty d\mu\frac{\mu}{\sqrt{\mu^2+4x^2}}e^{-\sqrt{\mu^2+4x^2}}
$$
$$
\left.\times(2x^2+\mu^2+2y^2)(2x^2+\mu^2+10y^2)\arctan\frac{\mu}{2y}\right], \tag{442}
$$

$$
v_{\sigma\tau}^{2\pi,\mathrm{NLO}}(r;2\Delta) = -\frac{1}{7776\pi^3 r^5}\frac{h_A^4}{F_\pi^4}\left[-2\int_0^\infty d\mu\frac{\mu^2}{\sqrt{\mu^2+4x^2}}e^{-\sqrt{\mu^2+4x^2}}(\mu^2+4x^2)\right.
$$
$$
+\frac{1}{y}\int_0^\infty d\mu\frac{\mu}{\sqrt{\mu^2+4x^2}}e^{-\sqrt{\mu^2+4x^2}}(\mu^2+4x^2)(-\mu^2+4y^2)
$$
$$
\left.\times\arctan\frac{\mu}{2y}\right], \tag{443}
$$

$$v_{tr}^{2\pi,\text{NLO}}(r; 2\Delta) = \frac{1}{15552\pi^3 r^5} \frac{h_A^4}{F_\pi^4} \left[-2 \int_0^\infty d\mu \frac{\mu^2}{\sqrt{\mu^2 + 4x^2}} e^{-\sqrt{\mu^2 + 4x^2}} (3 + 3\sqrt{\mu^2 + 4x^2} \right.$$

$$+\mu^2 + 4x^2) + \frac{1}{y} \int_0^\infty d\mu \frac{\mu}{\sqrt{\mu^2 + 4x^2}} e^{-\sqrt{\mu^2 + 4x^2}} (3 + 3\sqrt{\mu^2 + 4x^2}$$

$$\left. +\mu^2 + 4x^2)(-\mu^2 + 4y^2) \arctan \frac{\mu}{2y} \right] . \tag{444}$$

Moving on to the loop corrections at N2LO, the terms corresponding to diagrams (j)–(m) are given by

$$v_c^{2\pi,\text{N2LO}}(r; \Delta) = \frac{3}{2\pi^2 r^6} \frac{g_A^2}{F_\pi^4} e^{-2x} [2c_1 x^2 (1+x)^2 + c_3 (6 + 12x + 10x^2$$

$$+4x^3 + x^4)] , \tag{445}$$

$$v_{\sigma\tau}^{2\pi,\text{N2LO}}(r; \Delta) = \frac{1}{3\pi^2 r^6} \frac{g_A^2}{F_\pi^4} c_4 e^{-2x} (1+x) (3 + 3x + 2x^2) , \tag{446}$$

$$v_{t\tau}^{2\pi,\text{N2LO}}(r; \Delta) = -\frac{1}{3\pi^2 r^6} \frac{g_A^2}{F_\pi^4} c_4 e^{-2x} (1+x) (3 + 3x + x^2) , \tag{447}$$

while those corresponding to diagrams (l)–(o) are given by

$$v_c^{2\pi,\text{N2LO}}(r; 1\Delta) = \frac{1}{18\pi^3 r^6} \frac{h_A^2 y}{F_\pi^4} \left[\int_0^\infty d\mu \frac{\mu^2}{\sqrt{\mu^2 + 4x^2}} e^{-\sqrt{\mu^2 + 4x^2}} [-24c_1 x^2 \right.$$

$$+c_2 (5\mu^2 + 12x^2 + 12y^2) - 6c_3 (\mu^2 + 2x^2)]$$

$$+\frac{6}{y} \int_0^\infty d\mu \frac{\mu}{\sqrt{\mu^2 + 4x^2}} e^{-\sqrt{\mu^2 + 4x^2}} (\mu^2 + 2x^2 + 2y^2)$$

$$\left. \times [4c_1 x^2 - 2c_2 y^2 + c_3 (\mu^2 + 2x^2)] \arctan \frac{\mu}{2y} \right] , \tag{448}$$

$$v_\sigma^{2\pi,\text{N2LO}}(r; 1\Delta) = -\frac{1}{18\pi^3 r^6} \frac{(b_3 + b_8) h_A g_A^2 y}{F_\pi^4} \left[2 \int_0^\infty d\mu \frac{\mu^2}{\sqrt{\mu^2 + 4x^2}} e^{-\sqrt{\mu^2 + 4x^2}} \right.$$

$$\times (\mu^2 + 4x^2) - \frac{1}{y} \int_0^\infty d\mu \frac{\mu}{\sqrt{\mu^2 + 4x^2}} e^{-\sqrt{\mu^2 + 4x^2}} (\mu^2 + 4x^2)$$

$$\left. \times (\mu^2 + 4y^2) \arctan \frac{\mu}{2y} \right] , \tag{449}$$

$$v_t^{2\pi,\text{N2LO}}(r;1\Delta) = \frac{1}{36\pi^3 r^6}\frac{(b_3+b_8)\,h_A\,g_A^2\,y}{F_\pi^4}\left[2\int_0^\infty d\mu\frac{\mu^2}{\sqrt{\mu^2+4x^2}}e^{-\sqrt{\mu^2+4x^2}}\right.$$

$$(3+3\sqrt{\mu^2+4x^2}+\mu^2+4x^2)-\frac{1}{y}\int_0^\infty d\mu\frac{\mu}{\sqrt{\mu^2+4x^2}}$$

$$e^{-\sqrt{\mu^2+4x^2}}(3+3\sqrt{\mu^2+4x^2}+\mu^2+4x^2)$$

$$\left.\times(\mu^2+4y^2)\arctan\frac{\mu}{2y}\right], \tag{450}$$

$$v_\tau^{2\pi,\text{N2LO}}(r;1\Delta) = -\frac{1}{54\pi^3 r^6}\frac{(b_3+b_8)\,h_A\,y}{F_\pi^4}\left[+\int_0^\infty d\mu\frac{\mu^2}{\sqrt{\mu^2+4x^2}}e^{-\sqrt{\mu^2+4x^2}}\right.$$

$$\times(5\mu^2+12x^2+12y^2)-12\,y\int_0^\infty d\mu\frac{\mu}{\sqrt{\mu^2+4x^2}}e^{-\sqrt{\mu^2+4x^2}}$$

$$\left.\times(\mu^2+2x^2+2y^2)\arctan\frac{\mu}{2y}\right]-\frac{1}{54\pi^3 r^6}\frac{(b_3+b_8)\,h_A\,g_A^2\,y}{F_\pi^4}$$

$$\times\left[-\int_0^\infty d\mu\frac{\mu^2}{\sqrt{\mu^2+4x^2}}e^{-\sqrt{\mu^2+4x^2}}(11\mu^2+24x^2+12y^2)\right.$$

$$+\frac{6}{y}\int_0^\infty d\mu\frac{\mu}{\sqrt{\mu^2+4x^2}}e^{-\sqrt{\mu^2+4x^2}}\left(\mu^2+2x^2+2y^2\right)^2$$

$$\left.\times\arctan\frac{\mu}{2y}\right], \tag{451}$$

$$v_{\sigma\tau}^{2\pi,\text{N2LO}}(r;1\Delta) = -\frac{1}{108\pi^3 r^6}\frac{c_4\,h_A^2\,y}{F_\pi^4}\left[2\int_0^\infty d\mu\frac{\mu^2}{\sqrt{\mu^2+4x^2}}e^{-\sqrt{\mu^2+4x^2}}(\mu^2+4x^2)\right.$$

$$-\frac{1}{y}\int_0^\infty d\mu\frac{\mu}{\sqrt{\mu^2+4x^2}}e^{-\sqrt{\mu^2+4x^2}}(\mu^2+4x^2)(\mu^2+4y^2)$$

$$\left.\times\arctan\frac{\mu}{2y}\right], \tag{452}$$

$$v_{t\tau}^{2\pi,\text{N2LO}}(r;1\Delta) = \frac{1}{216\pi^3 r^6}\frac{c_4\,h_A^2\,y}{F_\pi^4}\left[2\int_0^\infty d\mu\frac{\mu^2}{\sqrt{\mu^2+4x^2}}e^{-\sqrt{\mu^2+4x^2}}(3+3\sqrt{\mu^2+4x^2}\right.$$

$$+\mu^2+4x^2)-\frac{1}{y}\int_0^\infty d\mu\frac{\mu}{\sqrt{\mu^2+4x^2}}e^{-\sqrt{\mu^2+4x^2}}(3+3\sqrt{\mu^2+4x^2}$$

$$\left.+\mu^2+4x^2)(\mu^2+4y^2)\arctan\frac{\mu}{2y}\right]. \tag{453}$$

Lastly, the contributions corresponding to diagram (p) read

$$
v_c^{2\pi,\text{N2LO}}(r;2\Delta) = -\frac{2}{81\pi^3 r^6}\frac{(b_3+b_8)h_A^3\, y}{F_\pi^4}\left[\int_0^\infty d\mu \frac{\mu^2}{\sqrt{\mu^2+4x^2}}e^{-\sqrt{\mu^2+4x^2}}\right.
$$

$$
\times[6\frac{(\mu^2+2x^2+2y^2)^2}{\mu^2+4y^2}+11\mu^2+24x^2+12y^2]
$$

$$
-\frac{3}{y}\int_0^\infty d\mu \frac{\mu}{\sqrt{\mu^2+4x^2}}e^{-\sqrt{\mu^2+4x^2}}(\mu^2+2x^2+10y^2)
$$

$$
\left.\times(\mu^2+2x^2+2y^2)\arctan\frac{\mu}{2y}\right], \tag{454}
$$

$$
v_{\sigma\tau}^{2\pi,\text{N2LO}}(r;2\Delta) = -\frac{1}{972\pi^3 r^6}\frac{(b_3+b_8)h_A^3\, y}{F_\pi^4}\left[-6\int_0^\infty d\mu \frac{\mu^2}{\sqrt{\mu^2+4x^2}}e^{-\sqrt{\mu^2+4x^2}}\right.
$$

$$
\times(\mu^2+4x^2)+\frac{1}{y}\int_0^\infty d\mu \frac{\mu}{\sqrt{\mu^2+4x^2}}e^{-\sqrt{\mu^2+4x^2}}(\mu^2+4x^2)
$$

$$
\left.\times(\mu^2+12y^2)\arctan\frac{\mu}{2y}\right], \tag{455}
$$

$$
v_t^{2\pi,\text{N2LO}}(r;2\Delta) = \frac{1}{324\pi^3 r^6}\frac{(b_3+b_8)h_A^3\, y}{F_\pi^4}\left[-6\int_0^\infty d\mu \frac{\mu^2}{\sqrt{\mu^2+4x^2}}e^{-\sqrt{\mu^2+4x^2}}\right.
$$

$$
\times(3+3\sqrt{\mu^2+4x^2}+\mu^2+4x^2)+\frac{1}{y}\int_0^\infty d\mu \frac{\mu}{\sqrt{\mu^2+4x^2}}e^{-\sqrt{\mu^2+4x^2}}
$$

$$
\left.\times(3+3\sqrt{\mu^2+4x^2}+\mu^2+4x^2)(\mu^2+12y^2)\arctan\frac{\mu}{2y}\right], \tag{456}
$$

$$
v_\tau^{2\pi,\text{N2LO}}(r;2\Delta) = -\frac{1}{243\pi^3 r^6}\frac{(b_3+b_8)h_A^3\, y}{F_\pi^4}\left[\int_0^\infty d\mu \frac{\mu^2}{\sqrt{\mu^2+4x^2}}e^{-\sqrt{\mu^2+4x^2}}\right.
$$

$$
\times[6\frac{(\mu^2+2x^2+2y^2)^2}{\mu^2+4y^2}+11\mu^2+24x^2+12y^2]
$$

$$
-\frac{3}{y}\int_0^\infty d\mu \frac{\mu}{\sqrt{\mu^2+4x^2}}e^{-\sqrt{\mu^2+4x^2}}(\mu^2+2x^2+10y^2)
$$

$$
\left.\times(\mu^2+2x^2+2y^2)\arctan\frac{\mu}{2y}\right], \tag{457}
$$

$$
v_\sigma^{2\pi,\text{N2LO}}(r;2\Delta) = -\frac{1}{162\pi^3 r^6}\frac{(b_3+b_8)h_A^3\, y}{F_\pi^4}\left[-6\int_0^\infty d\mu \frac{\mu^2}{\sqrt{\mu^2+4x^2}}e^{-\sqrt{\mu^2+4x^2}}\right.
$$

$$
\times(\mu^2+4x^2)+\frac{1}{y}\int_0^\infty d\mu \frac{\mu}{\sqrt{\mu^2+4x^2}}e^{-\sqrt{\mu^2+4x^2}}(\mu^2+4x^2)
$$

$$
\left.\times(\mu^2+12y^2)\arctan\frac{\mu}{2y}\right], \tag{458}
$$

$$
\begin{aligned}
v_{tr}^{2\pi,\text{N2LO}}(r;2\Delta) &= \frac{1}{1944\pi^3 r^6}\frac{(b_3+b_8)\,h_A^3\,y}{F_\pi^4}\left[\,-6\int_0^\infty d\mu\,\frac{\mu^2}{\sqrt{\mu^2+4x^2}}e^{-\sqrt{\mu^2+4x^2}}\right.\\
&\quad \times(3+3\sqrt{\mu^2+4x^2}+\mu^2+4x^2)+\frac{1}{y}\int_0^\infty d\mu\,\frac{\mu}{\sqrt{\mu^2+4x^2}}e^{-\sqrt{\mu^2+4x^2}}\\
&\quad \left. \times(3+3\sqrt{\mu^2+4x^2}+\mu^2+4x^2)(\mu^2+12y^2)\arctan\frac{\mu}{2y}\right]\,. \quad (459)
\end{aligned}
$$

The radial functions of the charge-independent part of the potential $v_{12}^{\rm L}$ in Eq. (128) are defined as

$$
\begin{aligned}
v_{\rm L}^c(r) &= v_c^{2\pi,\text{NLO}}(r;1\Delta)+v_c^{2\pi,\text{NLO}}(r;2\Delta)+v_c^{2\pi,\text{N2LO}}(r;\not\!\Delta)+v_c^{2\pi,\text{N2LO}}(r;1\Delta)\\
&\quad +v_c^{2\pi,\text{N2LO}}(r;2\Delta)\,, \qquad (460)\\
v_{\rm L}^\sigma(r) &= v_\sigma^{2\pi,\text{NLO}}(r;\not\!\Delta)+v_\sigma^{2\pi,\text{NLO}}(r;1\Delta)+v_\sigma^{2\pi,\text{NLO}}(r;2\Delta)+v_\sigma^{2\pi,\text{N2LO}}(r;1\Delta)\\
&\quad +v_\sigma^{2\pi,\text{N2LO}}(r;2\Delta)\,, \qquad (461)\\
v_{\rm L}^t(r) &= v_t^{2\pi,\text{NLO}}(r;\not\!\Delta)+v_t^{2\pi,\text{NLO}}(r;1\Delta)+v_t^{2\pi,\text{NLO}}(r;2\Delta)+v_t^{2\pi,\text{N2LO}}(r;1\Delta)\\
&\quad +v_t^{2\pi,\text{N2LO}}(r;2\Delta)\,, \qquad (462)\\
v_{\rm L}^\tau(r) &= v_\tau^{2\pi,\text{NLO}}(r;\not\!\Delta)+v_\tau^{2\pi,\text{NLO}}(r;1\Delta)+v_\tau^{2\pi,\text{NLO}}(r;2\Delta)+v_\tau^{2\pi,\text{N2LO}}(r;1\Delta)\\
&\quad +v_\tau^{2\pi,\text{N2LO}}(r;2\Delta)\,, \qquad (463)\\
v_{\rm L}^{\sigma\tau}(r) &= v_{\sigma\tau}^{\pi,\text{LO}}(r)+v_{\sigma\tau}^{2\pi,\text{NLO}}(r;1\Delta)+v_{\sigma\tau}^{2\pi,\text{NLO}}(r;2\Delta)+v_{\sigma\tau}^{2\pi,\text{N2LO}}(r;\not\!\Delta)\\
&\quad +v_{\sigma\tau}^{2\pi,\text{N2LO}}(r;1\Delta)+v_{\sigma\tau}^{2\pi,\text{N2LO}}(r;2\Delta)\,, \qquad (464)\\
v_{\rm L}^{t\tau}(r) &= v_{t\tau}^{\pi,\text{LO}}(r)+v_{t\tau}^{2\pi,\text{NLO}}(r;1\Delta)+v_{t\tau}^{2\pi,\text{NLO}}(r;2\Delta)+v_{t\tau}^{2\pi,\text{N2LO}}(r;\not\!\Delta)\\
&\quad +v_{t\tau}^{2\pi,\text{N2LO}}(r;1\Delta)+v_{t\tau}^{2\pi,\text{N2LO}}(r;2\Delta)\,, \qquad (465)
\end{aligned}
$$

Each is multiplied by the cutoff $C_{R_{\rm L}}(r)$ (see Sec. 3.2 of Chapter 3),

$$
v_{\rm L}^l(r)\longrightarrow C_{R_{\rm L}}(r)\,v_{\rm L}^l(r)\,, \qquad (466)
$$

with $l=c,\tau,\sigma,\sigma\tau,t,t\tau,\sigma T,tT$.

C.2 CONTACT TERMS

Using the expressions in Eqs. (133)–(139), the functions $v_{\rm S}^l(r)$ in Eq. (141) are

obtained as

$$v_S^c(r) = C_S\, C_{R_S}(r) + C_1\left[-C_{R_S}^{(2)}(r) - \frac{2}{r}\,C_{R_S}^{(1)}(r)\right] + D_1\left[C_{R_S}^{(4)}(r) + \frac{4}{r}\,C_{R_S}^{(3)}(r)\right],$$
(467)

$$v_S^\tau(r) = C_2\left[-C_{R_S}^{(2)}(r) - \frac{2}{r}\,C_{R_S}^{(1)}(r)\right] + D_2\left[C_{R_S}^{(4)}(r) + \frac{4}{r}\,C_{R_S}^{(3)}(r)\right],$$
(468)

$$v_S^\sigma(r) = C_T\, C_{R_S}(r) + C_3\left[-C_{R_S}^{(2)}(r) - \frac{2}{r}\,C_{R_S}^{(1)}(r)\right] + D_3\left[C_{R_S}^{(4)}(r) + \frac{4}{r}\,C_{R_S}^{(3)}(r)\right],$$
(469)

$$v_S^{\sigma\tau}(r) = C_4\left[-C_{R_S}^{(2)}(r) - \frac{2}{r}\,C_{R_S}^{(1)}(r)\right] + D_4\left[C_{R_S}^{(4)}(r) + \frac{4}{r}\,C_{R_S}^{(3)}(r)\right],$$
(470)

$$v_S^t(r) = -C_5\left[C_{R_S}^{(2)}(r) - \frac{1}{r}\,C_{R_S}^{(1)}(r)\right] + D_5\left[C_{R_S}^{(4)}(r) + \frac{1}{r}C_{R_S}^{(3)}(r) - \frac{6}{r^2}C_{R_S}^{(2)}(r)\right.$$
$$\left. + \frac{6}{r^3}C_{R_S}^{(1)}(r)\right],$$
(471)

$$v_S^{t\tau}(r) = -C_6\left[C_{R_S}^{(2)}(r) - \frac{1}{r}\,C_{R_S}^{(1)}(r)\right] + D_6\left[C_{R_S}^{(4)}(r) + \frac{1}{r}C_{R_S}^{(3)}(r) - \frac{6}{r^2}C_{R_S}^{(2)}(r)\right.$$
$$\left. + \frac{6}{r^3}C_{R_S}^{(1)}(r)\right],$$
(472)

$$v_S^b(r) = -C_7\frac{1}{r}C_{R_S}^{(1)}(r) + D_7\left[\frac{1}{r}C_{R_S}^{(3)}(r) + 2\frac{1}{r^2}C_{R_S}^{(2)}(r) - \frac{2}{r^3}C_{R_S}^{(1)}(r)\right],$$
(473)

$$v_S^{b\tau}(r) = D_8\left[\frac{1}{r}C_{R_S}^{(3)}(r) + 2\frac{1}{r^2}C_{R_S}^{(2)}(r) - \frac{2}{r^3}C_{R_S}^{(1)}(r)\right],$$
(474)

$$v_S^{bb}(r) = -D_9\frac{1}{r^2}\left[C_{R_S}^{(2)}(r) - \frac{1}{r}\,C_{R_S}^{(1)}(r)\right],$$
(475)

$$v_S^q(r) = -D_{10}\frac{1}{r^2}\left[C_{R_S}^{(2)}(r) - \frac{1}{r}\,C_{R_S}^{(1)}(r)\right],$$
(476)

$$v_S^{q\sigma}(r) = -D_{11}\frac{1}{r^2}\left[C_{R_S}^{(2)}(r) - \frac{1}{r}\,C_{R_S}^{(1)}(r)\right],$$
(477)

$$v_S^p(r) = D_{12}\left[-C_{R_S}^{(2)}(r) - \frac{2}{r}\,C_{R_S}^{(1)}(r)\right],$$
(478)

$$v_S^{p\sigma}(r) = D_{13}\left[-C_{R_S}^{(2)}(r) - \frac{2}{r}\,C_{R_S}^{(1)}(r)\right],$$
(479)

$$v_S^{pt}(r) = -D_{14}\left[C_{R_S}^{(2)}(r) - \frac{1}{r}\,C_{R_S}^{(1)}(r)\right],$$
(480)

$$v_S^{pt\tau}(r) = -D_{15}\left[C_{R_S}^{(2)}(r) - \frac{1}{r}\,C_{R_S}^{(1)}(r)\right],$$
(481)

$$v_S^T(r) = C_0^{\text{IT}} C_{R_S}(r) + C_1^{\text{IT}} \left[-C_{R_S}^{(2)}(r) - \frac{2}{r} C_{R_S}^{(1)}(r) \right] , \qquad (482)$$

$$v_S^{\tau z}(r) = C_0^{\text{IV}} C_{R_S}(r) + C_1^{\text{IV}} \left[-C_{R_S}^{(2)}(r) - \frac{2}{r} C_{R_S}^{(1)}(r) \right] , \qquad (483)$$

$$v_S^{\sigma T}(r) = C_2^{\text{IT}} \left[-C_{R_S}^{(2)}(r) - \frac{2}{r} C_{R_S}^{(1)}(r) \right] , \qquad (484)$$

$$v_S^{\sigma \tau z}(r) = C_2^{\text{IV}} \left[-C_{R_S}^{(2)}(r) - \frac{2}{r} C_{R_S}^{(1)}(r) \right] , \qquad (485)$$

$$v_S^{tT}(r) = -C_3^{\text{IT}} \left[C_{R_S}^{(2)}(r) - \frac{1}{r} C_{R_S}^{(1)}(r) \right] , \qquad (486)$$

$$v_S^{t\tau z}(r) = -C_3^{\text{IV}} \left[C_{R_S}^{(2)}(r) - \frac{1}{r} C_{R_S}^{(1)}(r) \right] , \qquad (487)$$

$$v_S^{bT}(r) = -C_4^{\text{IT}} \frac{1}{r} C_{R_S}^{(1)}(r) , \qquad (488)$$

$$v_S^{b\tau z}(r) = -C_4^{\text{IV}} \frac{1}{r} C_{R_S}^{(1)}(r) . \qquad (489)$$

Note that in Eqs. (138) and (139) only the terms proportional to $\mathbf{L}^2$ and $(\mathbf{L} \cdot \mathbf{S})^2$ are retained.

APPENDIX D

PROTON-PROTON PHASE SHIFTS AND EFFECTIVE

RANGE EXPANSION

We discuss briefly the calculation of the *pp* phase shifts and effective range expansion with inclusion of the full electromagnetic potential $v_{12}^{\rm EM}$ [48]. Radial wave functions behave in the asymptotic region $(r \gtrsim 30 \text{ fm})$ as

$$\frac{u_L(r)}{r} \simeq \frac{1}{2}\left[\overline{h}_L^{(2)}(kr;\eta') + e^{2i\delta_L^{\rm EM}}\,\overline{h}_L^{(1)}(kr;\eta')\right] \,, \qquad (490)$$

where $L = J$ for single channels or $L = L' = J \mp 1$ for coupled channels (the pair isospin and spin subscripts T and S have been dropped for simplicity), $\overline{h}_L^{(1,2)}(kr;\eta')$ are defined in terms of regular, $\overline{F}_L(kr;\eta')$, and irregular, $\overline{G}_L(kr;\eta')$, electromagnetic (EM) functions as

$$\overline{h}_L^{(1,2)}(kr) = \frac{\overline{F}_L(kr;\eta')}{kr} \mp i\,\frac{\overline{G}_L(kr;\eta')}{kr} \,, \qquad (491)$$

$\delta_L^{\rm EM}$ are the EM phase shifts shown in Sec. 3.4, and the Coulomb parameter η' is defined [117] as

$$\eta' = \frac{\alpha M_p}{2\,k}\frac{1 + 2\,k^2/M_p^2}{\sqrt{1 + k^2/M_p^2}} \,. \qquad (492)$$

The EM functions, generically denoted as $X_L(kr;\eta')$, are solutions of the radial equation

$$\left[\frac{d^2}{dr^2} + k^2 - \frac{L(L+1)}{r^2} - M_p\left[V_{C1}(r) + V_{C2}(r) + V_{VP}(r)\right]\right] X_L(kr;\eta') = 0 \,, \qquad (493)$$

where V_{C1} (V_{C2}) and V_{VP} are respectively the first-order (second-order) Coulomb and vacuum polarization terms. These terms include form factors to remove singularities in the $r = 0$ limit [48]. Note that the Darwin-Foldy and magnetic moment corrections are not included above, since at large r the former falls off exponentially and the latter behaves as $1/r^3$.

Following Ref. [118] and treating the $V_{C2}(r)$ and $V_{VP}(r)$ corrections in first order perturbation theory, one finds that $\overline{F}_L(kr;\eta'$ and $\overline{G}_L(kr;\eta')$ can be expressed as

$$
\begin{aligned}
\overline{F}_L(kr;\eta') &= F_L(kr;\eta') \left[1 - \int_r^\infty dr'\, G_L(kr';\eta')\, V(r')\, F_L(kr';\eta')\right] \\
&\quad + G_L(kr;\eta') \left[\tan(\rho_L + \tau_L) + \int_r^\infty dr'\, F_L(kr';\eta')\, V(r')\, F_L(kr';\eta')\right] ,
\end{aligned}
\tag{494}
$$

$$
\begin{aligned}
\overline{G}_L(kr;\eta') &= G_L(kr;\eta') \left[1 + \int_r^\infty dr'\, G_L(kr';\eta')\, V(r')\, F_L(kr';\eta')\right] \\
&\quad - F_L(kr;\eta') \left[\tan(\rho_L + \tau_L) + \int_r^\infty dr'\, G_L(kr';\eta')\, V(r')\, G_L(kr';\eta')\right] ,
\end{aligned}
\tag{495}
$$

where the F_L and G_L are standard Coulomb functions, the function $V(r)$ is proportional to $V_{C2}(r)$ and $V_{VP}(r)$,

$$
V(r) = \frac{M_p}{k}\left[V_{C2}(r) + V_{VP}(r)\right] ,
\tag{496}
$$

and the phase shifts ρ_L and τ_L corresponding, respectively, to V_{C2} and V_{VP} are given (in first order perturbation theory) by

$$
\tan(\rho_L + \tau_L) \simeq \rho_L + \tau_L = -\int_0^\infty dr\, F_L(kr;\eta')\, V(r)\, F_L(kr;\eta') .
\tag{497}
$$

In the absence of V_{C2} and V_{VP}, the solutions $\overline{F}_L$ and $\overline{G}_L$ reduce to the regular and irregular Coulomb functions. In the computer programs Eqs. (494)–(495) are used to construct the EM functions and Eq. (497) to obtain the phase shifts ρ_L and τ_L.

The effective range expansion in the $^1S_0$ channel is obtained as [117–119]

$$
F_{\rm EM}(k^2) = -\frac{1}{a_{\rm EM}} + \frac{1}{2} r_{\rm EM}\, k^2 + \dots ,
\tag{498}
$$

with

$$
\begin{aligned}
F_{\rm EM}(k^2) &= k\, C_0^2(\eta')\, \frac{(1+\chi_0)\cot\delta_0^{\rm EM} - \tan\tau_0}{(1+A_1)(1-\chi_0)} + 2\,k\,\eta'\,h(\eta')\,(1-A_2) \\
&\quad + k^2\, d\left[C_0^4(\eta') - 1\right] + k\,\widetilde{l}_0 ,
\end{aligned}
\tag{499}
$$

where

$$C_0^2(\eta') = \frac{2\pi\,\eta'}{e^{2\pi\eta'} - 1} \,, \qquad h(\eta') = -\gamma - \ln\eta' + \sum_{n=1}^{\infty} \frac{\eta'^2}{n\,(n^2 + \eta'^2)} \,, \qquad (500)$$

$$\chi_o = -\frac{4\alpha}{3\pi}\,\eta' \int_0^{\infty} dr\, \frac{I(r)}{r}\, F_0(kr;\eta')\, G_0(kr;\eta') \,,$$

$$\tilde{l}_0 = -\frac{4\,\alpha}{3\pi}\,\eta' \int_0^{\infty} dr\, \frac{I(r)}{r}\left[C_0^2(\eta')\, G_0^2(kr;\eta') - 1 \right] \,, \qquad (501)$$

$$d = \frac{\alpha}{M_p} \,, \qquad A_1 = 4\,d\,k\,\eta'\left[\ln\left(2\,d\,k\,\eta'\right) + h(\eta') + 2\,\gamma - 1\right] \,,$$

$$A_2 = 2\,d\,k\,\eta'\left(2\ln\alpha + 2\,\gamma - 1\right) + \frac{A_1}{2} \,, \qquad (502)$$

γ is Euler's constant, and the function $I(r)$ entering the vacuum polarization potential $V_{VP}(r)$ is defined as in Ref. [118],

$$I(r) = \int_1^{\infty} dx\, e^{2m_e rx}\left(1 + \frac{1}{2\,x^2}\right) \frac{\sqrt{x^2 - 1}}{x^2} \,. \qquad (503)$$
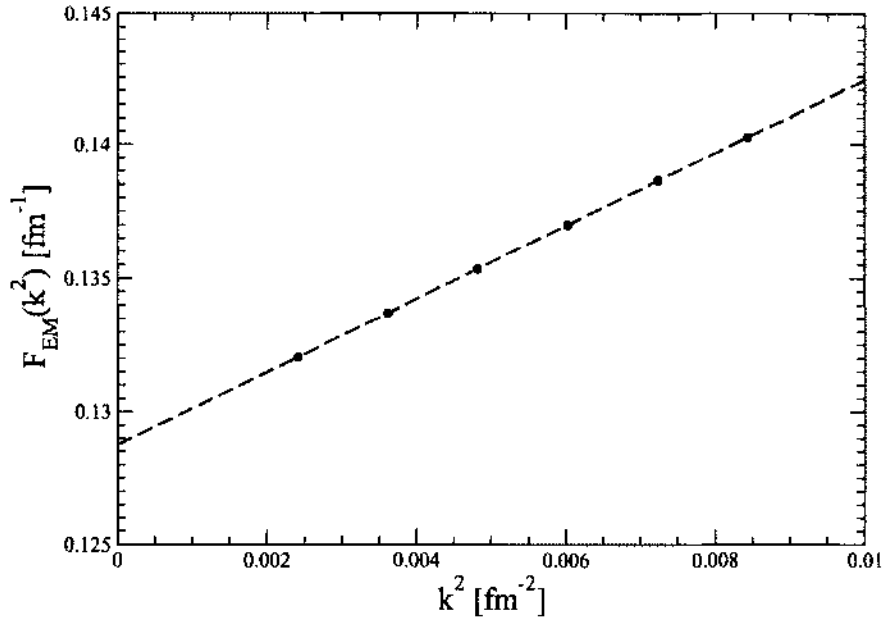

FIG. 22: The effective range function of Eq. (499) for the potential model b with $(R_{\mathrm{L}}, R_{\mathrm{S}}) = (1.0, 0.7)$ fm. The dashed line is a straight line fit.

The effective range function $F_{\mathrm{EM}}(k^2)$ corresponding to model b is shown in Fig. 22. The numerical methods are stable down to lab energies of 1 keV.

APPENDIX E

TABLES OF PHASE SHIFTS AND FIGURES OF

POTENTIAL COMPONENTS

The pp and np phase shifts calculated with model b are listed in Tables 12-14, while the various components of the long-range (v_{12}^{L}) and short-range $(v_{12}^{S,CI})$ potentials corresponding to models a, b, and c and projected out in pair spin and isospin $S = 0, 1$ and $T = 0, 1$, are shown in Figs. 23 30.

TABLE 12: pp phase shifts in degrees for potential model b with $(R_{L}, R_{S}) = (1.0, 0.7)$ fm. The phases are relative to electromagnetic functions.

E_{lab}	$^1S_0$	$^1D_2$	$^1G_4$	$^3P_0$	$^3P_1$	$^3F_3$	$^3P_2$	ϵ_2	$^3F_2$	$^3F_4$
1	32.69	0.00	0.00	0.14	-0.08	-0.00	0.02	-0.00	-0.00	0.00
5	55.00	0.04	0.00	1.64	-0.90	-0.00	0.22	-0.05	-0.01	0.01
10	55.49	0.17	0.00	3.90	-2.06	-0.03	0.64	-0.19	-0.01	0.02
25	49.13	0.69	0.04	9.21	-4.95	-0.23	2.42	-0.80	0.06	0.04
50	39.52	1.68	0.16	12.77	-8.38	-0.70	5.73	-1.71	0.27	0.14
100	25.66	3.77	0.43	11.21	-13.42	-1.58	11.02	-2.73	0.73	0.47
150	15.44	5.75	0.71	6.21	-17.63	-2.28	14.16	-3.05	1.10	0.97
200	7.20	7.38	1.01	0.50	-21.38	-2.90	15.90	-2.97	1.30	1.55
250	0.22	8.59	1.33	-5.18	-24.68	-3.52	16.89	-2.65	1.27	2.16
300	-5.88	9.36	1.66	-10.62	-27.55	-4.20	17.45	-2.19	0.98	2.76

TABLE 13: $T = 1$ np phase shifts in degrees for potential model b with $(R_L, R_S) = (1.0, 0.7)$ fm. The phases are relative to spherical Bessel functions.

E_{lab}	$^1S_0$	$^1D_2$	$^1G_4$	$^3P_0$	$^3P_1$	$^3F_3$	$^3P_2$	ϵ_2	$^3F_2$	$^3F_4$
1	62.10	0.00	0.00	0.18	-0.11	-0.00	0.02	-0.00	0.00	0.00
5	63.65	0.04	0.00	1.67	-0.92	-0.00	0.24	-0.05	0.01	0.00
10	60.00	0.16	0.00	3.80	-2.02	-0.03	0.68	-0.19	0.02	0.00
25	50.83	0.67	0.03	8.71	-4.72	-0.20	2.53	-0.76	0.11	0.01
50	40.22	1.69	0.14	11.90	-7.88	-0.63	5.95	-1.63	0.33	0.08
100	25.84	3.86	0.40	10.06	-12.42	-1.46	11.35	-2.58	0.81	0.38
150	15.46	5.90	0.69	4.97	-16.17	-2.12	14.49	-2.81	1.20	0.84
200	7.13	7.58	1.00	-0.77	-19.50	-2.70	16.17	-2.64	1.44	1.41
250	0.09	8.81	1.33	-6.48	-22.43	-3.27	17.05	-2.24	1.45	2.01
300	-6.04	9.59	1.67	-11.93	-24.96	-3.89	17.49	-1.72	1.21	2.60

TABLE 14: Same as in Table 13 but for $T = 0$ np phase shifts.

| E_{lab}	$^1P_1$	$^1F_3$	$^3D_2$	$^3G_4$	$^3S_1$	ϵ_1	$^3D_1$	$^3D_3$	ϵ_3	$^3G_3$
1	-0.19	-0.00	0.01	0.00	147.81	0.10	-0.00	0.00	0.00	-0.00
5	-1.53	-0.01	0.22	0.00	118.32	0.63	-0.17	0.00	0.01	-0.00
10	-3.15	-0.07	0.85	0.01	102.80	1.06	-0.65	0.00	0.08	-0.00
25	-6.55	-0.43	3.70	0.17	80.86	1.53	-2.77	0.00	0.55	-0.04
50	-9.87	-1.16	8.89	0.73	63.00	1.62	-6.42	0.18	1.62	-0.25
100	-14.05	-2.33	17.21	2.20	43.53	1.67	-12.31	1.16	3.54	-0.97
150	-17.48	-3.12	22.33	3.71	31.32	1.92	-16.61	2.34	4.87	-1.88
200	-20.78	-3.69	25.02	5.10	22.35	2.34	-19.83	3.17	5.72	-2.83
250	-24.04	-4.14	26.09	6.36	15.26	2.84	-22.27	3.40	6.23	-3.76
300	-27.23	-4.56	26.10	7.46	9.40	3.39	-24.11	3.01	6.52	-4.62
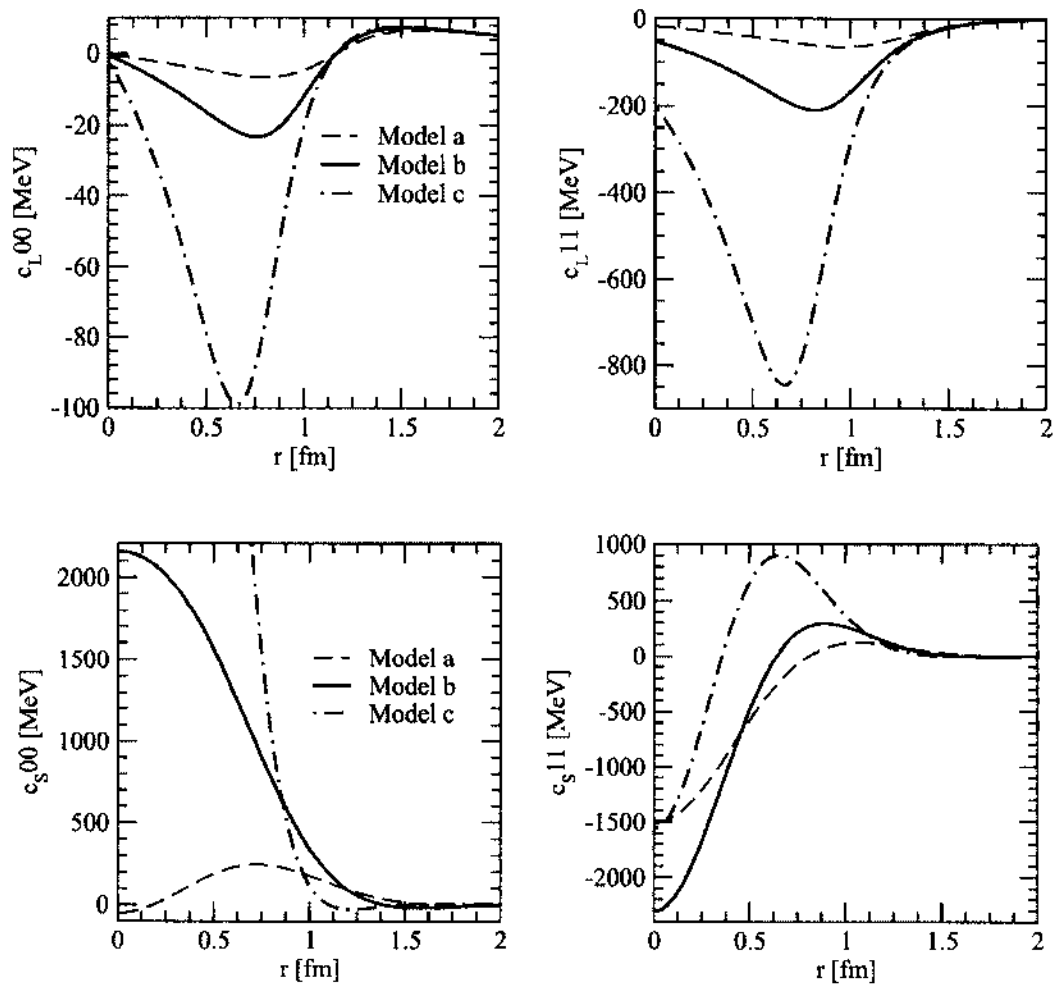
FIG. 23: Central components of the long-range potential v_{12}^L (top panels) and for the short-range charge-independent potential $v_{12}^{S,CI}$ (bottom panels) in pair spin-isospin channels $ST = 00$ and 11.
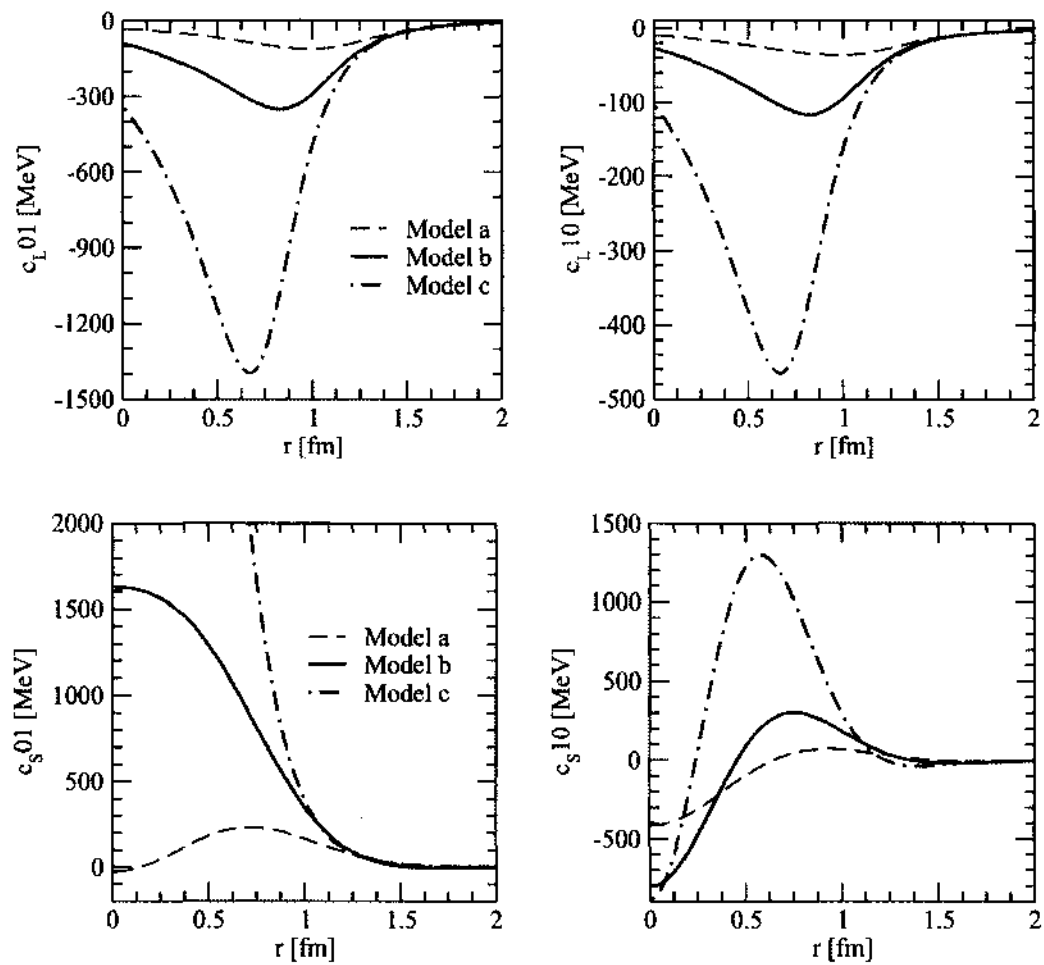
FIG. 24: Same as in Fig. 23 but in pair spin-isospin channels $ST = 01$ and 10.

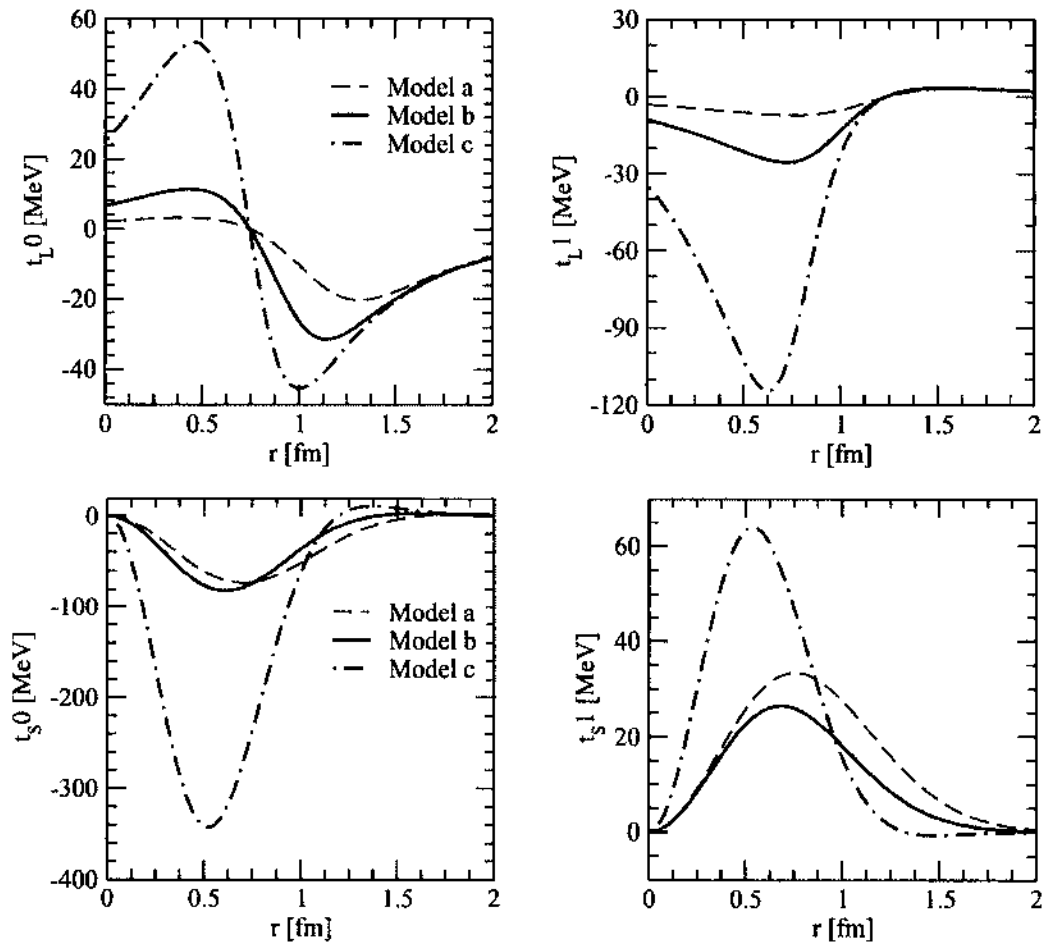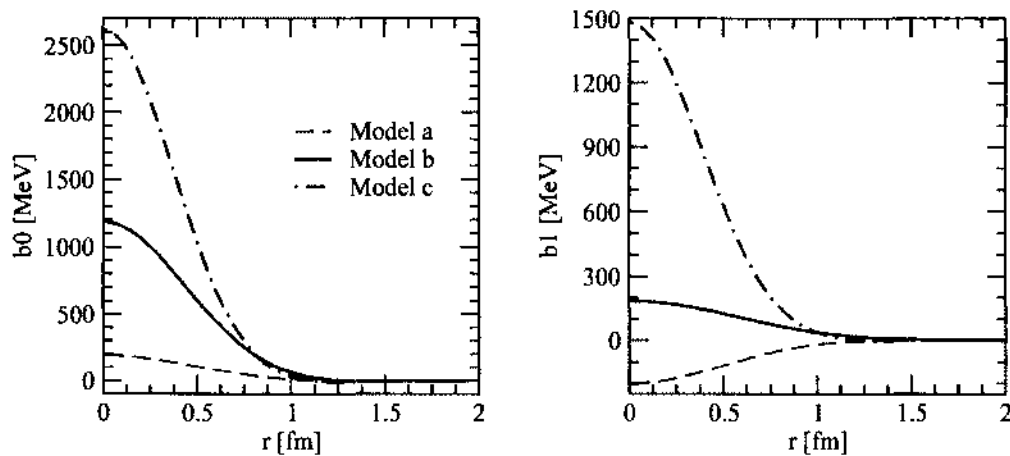FIG. 25: Tensor components of the long-range potential v_{12}^{L} (top pannels) and the short-range charge-independent potential $v_{12}^{S,CI}$ (bottom pannels) in pair isospin channels $T = 0$ and 1.

FIG. 26: Spin-orbit components of the short-range charge-independent potential $v_{12}^{S,CI}$ in pair isospin channels $T = 0$ and 1.
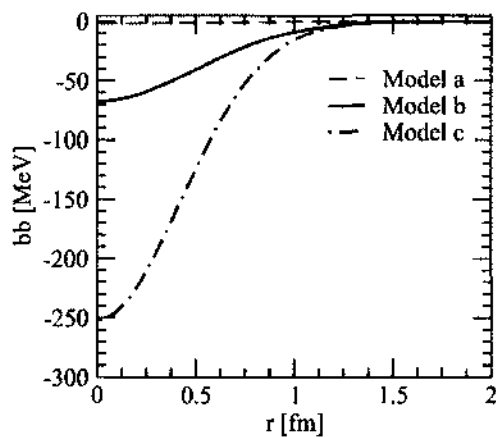

FIG. 27: Spin and isospin independent quadratic spin-orbit components of the short-range charge-independent potential $v_{12}^{S,CI}$.
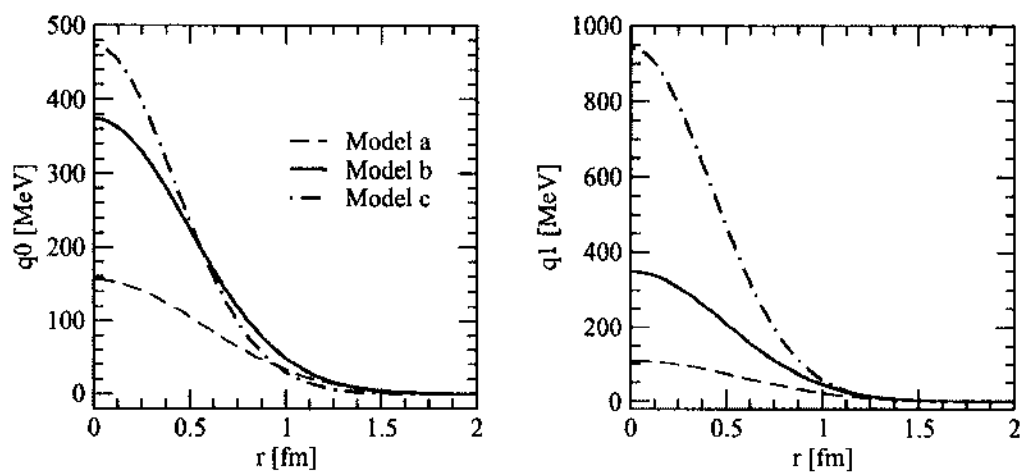
FIG. 28: Quadratic orbital angular momentum components of the short-range charge-independent potential $v_{12}^{S,CI}$ in pair spin channels $S = 0$ and 1.
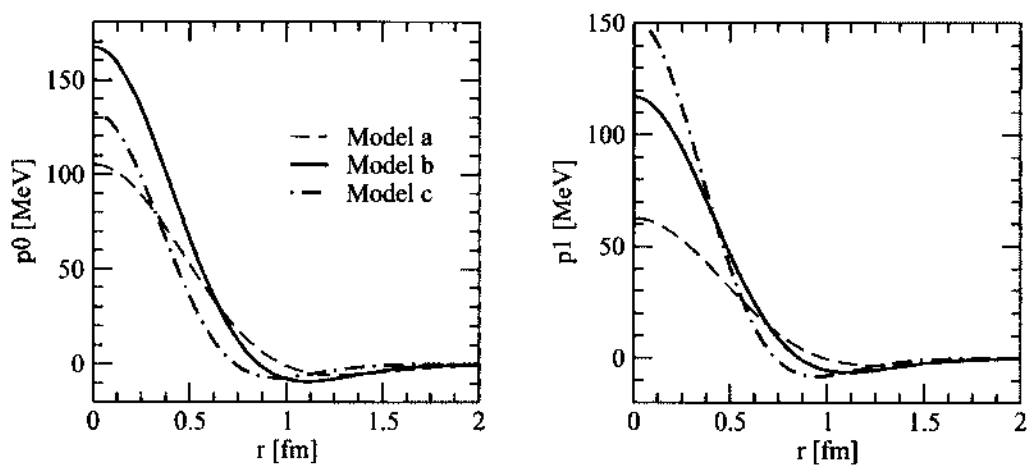

FIG. 29: Quadratic relative momentum components of the short-range charge-independent potential $v_{12}^{S,CI}$ in pair spin channels $S = 0$ and 1.
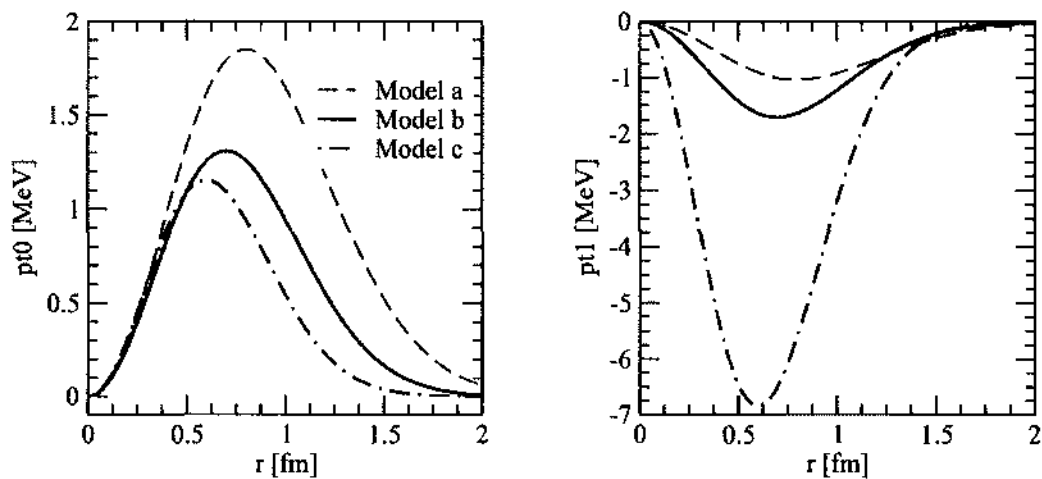
FIG. 30: Quadratic relative momentum tensor components of the short-range charge-independent potential $v_{12}^{S,CI}$ in pair isospin channels $T = 0$ and 1.

APPENDIX F

LOOP INTEGRATIONS

In this appendix, we outline the derivation of the two-body charge operators at one loop, listed in Sec. 4.1.1. For the sake of illustration, we consider the contribution in Fig. 14, given by [30]

$$
\begin{aligned}
\rho_f^{(1)} = -e \frac{2 g_A^4}{F_\pi^4} \int_{\mathbf{q}_1,\mathbf{q}_2,\mathbf{q}_3} & \vec{\delta}(\mathbf{q}_2 + \mathbf{q}_3 - \mathbf{k}_2)\vec{\delta}(\mathbf{q}_1 - \mathbf{q}_2 - \mathbf{k}_1) \\
& \times \vec{\delta}(\mathbf{q}_1 + \mathbf{q}_3 - \mathbf{q}) \frac{1}{\omega_1^2 \omega_2^2 \omega_3^2} \Big[2\, \tau_{1,z} \, (\mathbf{q}_2 \cdot \mathbf{q}_1 \; \mathbf{q}_2 \cdot \mathbf{q}_3 \\
& - \boldsymbol{\sigma}_1 \cdot \mathbf{q}_2 \times \mathbf{q}_1 \; \boldsymbol{\sigma}_2 \cdot \mathbf{q}_3 \times \mathbf{q}_2) - (\boldsymbol{\tau}_1 \times \boldsymbol{\tau}_2)_z \; \mathbf{q}_1 \cdot \mathbf{q}_2 \\
& \times \boldsymbol{\sigma}_2 \cdot \mathbf{q}_3 \times \mathbf{q}_2 \Big] + 1 \rightleftharpoons 2 \, ,
\end{aligned}
\tag{504}
$$

which can conveniently be written as

$$
\rho_f^{(1)} = -e \frac{2 g_A^4}{F_\pi^4} \int_{\mathbf{p}} \frac{N(\mathbf{q}, \mathbf{k}, \mathbf{p})}{\omega_{\mathbf{q}/2+\mathbf{p}}^2 \; \omega_{\mathbf{q}/2-\mathbf{p}}^2 \; \omega_{\mathbf{p}-\mathbf{k}}^2} + 1 \rightleftharpoons 2 \, ,
\tag{505}
$$

with

$$
\begin{aligned}
N(\mathbf{q}, \mathbf{k}, \mathbf{p}) = \; & 2\, \tau_{1,z} \big[(\mathbf{p}-\mathbf{k}) \cdot (\mathbf{q}/2+\mathbf{p}) \; (\mathbf{p}-\mathbf{k}) \cdot (\mathbf{q}/2-\mathbf{p}) - \boldsymbol{\sigma}_1 \cdot (\mathbf{p}-\mathbf{k}) \\
& \times (\mathbf{q}/2+\mathbf{p}) \; \boldsymbol{\sigma}_2 \cdot (\mathbf{q}/2-\mathbf{p}) \times (\mathbf{p}-\mathbf{k}) \big] \\
& - (\boldsymbol{\tau}_1 \times \boldsymbol{\tau}_2)_z \; (\mathbf{q}/2+\mathbf{p}) \cdot (\mathbf{p}-\mathbf{k}) \; \boldsymbol{\sigma}_2 \cdot (\mathbf{q}/2-\mathbf{p}) \times (\mathbf{p}-\mathbf{k}) \, ,
\end{aligned}
\tag{506}
$$

and the momentum $\mathbf{k}$ defined as in Eq. (194). We now use standard techniques given in Eq. (296) to express the product of energy denominators in the following way

$$
\begin{aligned}
\frac{1}{\omega_{\mathbf{q}/2+\mathbf{p}}^2 \; \omega_{\mathbf{q}/2-\mathbf{p}}^2 \; \omega_{\mathbf{p}-\mathbf{k}}^2} = \; & 2 \int_0^1 dz_1 \int_0^{1-z_1} dz_2 \\
& \times \Big[\left[(\mathbf{q}/2+\mathbf{p})^2 + m_\pi^2\right] z_1 + \left[(\mathbf{q}/2-\mathbf{p})^2 + m_\pi^2\right] z_2 \\
& + \left[(\mathbf{p}-\mathbf{k})^2 + m_\pi^2\right] (1 - z_1 - z_2) \Big]^{-3} \, ,
\end{aligned}
\tag{507}
$$

which, in terms of

$$
\mathbf{p}' = \mathbf{p} + (z_1 - z_2)\, \mathbf{q}/2 - (1 - z_1 - z_2)\, \mathbf{k} \, ,
\tag{508}
$$

FIG. 31: Example of two-body charge operators at one loop (eQ or N4LO). The labels "1", "2", and "3" denotes the internal loop momenta q_1, q_2, and q_3, respectively.

simply reads

$$\frac{1}{\omega^2_{q/2+p}\,\omega^2_{q/2-p}\,\omega^2_{p-k}} = 2 \int_0^1 dz_1 \int_0^{1-z_1} dz_2 \left[p'^2 + \lambda^2(z_1,z_2) \right]^{-3} , \quad (509)$$

where

$$\lambda^2(z_1, z_2) = (z_1 + z_2)\,q^2/4 - \left[(z_1 - z_2)\,q/2 - (1 - z_1 \right.$$
$$\left. -z_2)\,k \right]^2 + (1 - z_1 - z_2)\,k^2 + m_\pi^2 . \quad (510)$$

After these manipulations, the charge operator can finally be written as

$$\rho_t^{(1)} = -e\frac{4\,g_A^4}{F_\pi^4} \int_0^1 dx\,x \int_{-1/2}^{1/2} dy \int_{p'} N'(q,k,p')$$
$$\times \left[p'^2 + \lambda^2(x,y) \right]^{-3} + 1 \rightleftharpoons 2 , \quad (511)$$

where the function N' is obtained from N by expressing p in terms of p' via Eq. (508). We have also changed variables in the parametric integrals by introducing [41]

$$x = z_1 + z_2 , \qquad x\,y = (z_1 - z_2)/2 , \quad (512)$$

such that

$$\int_0^1 dz_1 \int_0^{1-z_1} dz_2 \longrightarrow \int_0^1 dx\,x \int_{-1/2}^{1/2} dy . \quad (513)$$

The function N' is a polynomial in p', and the p'-integrations are carried out in dimensional regularization as in Appendix B. They are finite and lead to the charge operator given in Eq. (211).

VITA

Maria Piarulli
Department of Physics
Old Dominion University
Norfolk, VA 23529

Education:

Old Dominion University, Norfolk, Virginia,
M.S., December 2011.

M.S., *summa cum laude*, March 2009,
Thesis: *Muon Capture on Deuteron*,
Advisor: Dr. L. E. Marcucci.

Università di Pisa, Pisa, Italy,
B.S., February 2006.

Typeset using LaTeX.